ADSORPTION, CATALYTIC AND PHOTOCATALYTIC PROPERTIES OF METAL ION EXCHANGED ZEOLITES

THESIS

Submitted to

BHAVNAGAR UNIVERSITY

for the degree of

DOCTOR OF PHILOSOPHY

in

CHEMISTRY

by

JINCE SEBASTIAN

Silicates and Catalysis Discipline

Central Salt and Marine Chemicals Research Institute

Bhavnagar-364002, India

2004

22 December 2004

Candidate's Statement

I hereby declare that the work incorporated in the thesis entitled **"Adsorption, Catalytic and Photocatalytic Properties of Metal Ion Exchanged Zeolites"** is original and has not been submitted to any university / institution for the award of any diploma / degree.

I further declare that the results presented in the thesis and the considerations made therein, contribute in general to the advancement of knowledge in chemistry and in particular to adsorption, catalytic and photocatalytic properties of metal ion exchanged zeolites.

(Jince Sebastian)

Jince Sebastian
Senior Research Fellow
CSMCRI, Bhavnagar

Dir.☎(0278) 2471793

Dr. R. V. Jasra

Deputy Director

22 December 2004

Certificate by the Ph.D. Supervisor

This is to certify that the contents of this thesis entitled **"Adsorption, Catalytic and Photocatalytic Properties of Metal Ion Exchanged Zeolites"** is the original research work of **Mr. Jince Sebastian** carried out under my supervision at Silicates and Catalysis Discipline, Central Salt and Marine Chemicals Research Institute, Bhavnagar.

I further certify that the work has not been submitted either partly or fully to any university / institution for the award of any diploma / degree.

(R. V. Jasra)

ACKNOWLEDGEMENT

It is said that four conditions are essential to complete a doctoral thesis: an interesting topic, sufficient financial funding, an insightful supervisor and patient, understanding and loving near and dear. I have been lucky to have all of them working under my beloved guide **Dr. Raksh Vir Jasra,** who led me from the front with his inspiring and invaluable guidance, insights and advice over the years, as well as for demonstrating an unending supply of patience and spirited discussions. His supportive critics made me feel worthy and joyful throughout the period of my work at Silicates and Catalysis Discipline, CSMCRI, Bhavnagar that paved a lot in presenting this mammoth piece of work which is just a drop in the ocean of knowledge.

I am indebted to **Dr. Pushpito K. Ghosh**, Director, CSMCRI, for providing me his kind permission to carry out this research work at CSMCRI, Bhavnagar.

I express my sincere thanks to Dr. Chintansinh D. Chudasama, for his support in paving an easy way to carry out this research work.

My special heart felt thanks to Mr. Rajesh J. Tayade, Mr. Mukesh Yadav, Mr. Shobhit Singh Chauhan and Mr. Sunil A. P. for their constant support, encouragement and creating a great piece of work atmosphere.

I would like to place my respect and deep sense of gratitude to Dr. H. C. Bajaj, Dr. R. S. Shukla, Dr. S.H.R. Abdi, Dr. S. D. Bhatt, Dr. R. I. Kureshy, Dr. S. Kannan, Dr. R. S. Somani, Dr. N. H. Khan, Dr. H. M. Mody, Dr. Beena Tyagi, Dr. A. B. Boricha, Dr. D. B. Shukla, Dr. E. Suresh, Dr. J. V. Prasad, Dr. A. Hussein, Dr. Amitava Das, Dr. P. Dastidar, Dr. S. Muthusamy and Dr. P. S. Subramanian for their encouraging and supportive words.

I render my thankfulness to Mr. Chandrakanth CK, for his prompt help in many occasions, especially during the drafting of my first patent.

I am grateful to Dr. P. Paul, DC, Analytical Science Discipline, for providing various instrumental facilities.

I am thankful to Mr. S. T. Talreja and Mr. Pradeep Parmar, for upkeep of the instruments and providing liquid nitrogen and Mr. Vinod P. Boricha, Dr. Pragnya Bhatt, for their support in the characterisation of my samples.

I am also thankful to Dr. Priti. H. Pandya, Dr. Yogi. M. Badheka, Dr. Atintra. D. Shukla, Dr. S. A. Babu, Dr. Amit Dubey, Dr. C. Gunanathan, Mr. Vivek K. Srivastava and Mr. Dharmesh U. Parmar, for their valuable suggestions and support in many difficult situations.

I like to extend my special regards to Mr. Surendra Singh, Mr. Irshad Ahmed, Mr. Prabhash R. Prasad and Mr. J. Krishna Mohan for their support.

I am thankful to Mr. P. G. Mohanan Pillai, Mr. K. Rajagopalan, Mr. P. Balakrishnan, Mr. V. C. Zala, Mr. M. L. Bhatt and Mr. V. M. Rajan for the support and I also acknowledge Mr. Chimanbhai. D. Gohil, Mr. Bharat B. Parmar, Mr. Jayanthi M. Parmar, Mr. Ali H. Lakhani, Mr. Bahadur M. Vaghela, for their prompt help rendered during this period

I am very much gratified to the staff from canteen, library, I. T. cell, BDIM, electrical, mechanical, carpentry, refrigeration, store & purchase, administration, finance & accounts and watch & ward sections for their co-operation during this period.

I convey my words of appreciation to Mr. Pramod Makwana, Mr. Sanjay Jani and Mr. H. S. Vasudevan for their assistance in various problems related to PC and software during this period.

I would also like to acknowledge the support of my friends and colleagues Mr. D. Krishna Kumar, Mr. Darsak R. Trivedi, Mr. Amar Ballabh, Mr. Amilan Jose, Dr. Kishor Dasari, Mr. Manish Mishra, Mr. M. S. Reddy, Dr. Jagan Mohan, Mr. Prashant Bhatt, Mr. Dharmesh Bhatt, Mr. Kartik S. Patel, Miss Kavita Pathak, Mr. Achyut P. Bhatt, Mr. Devendra L. Ghelani, Mr. Hasmukh Patel, Mr. Sumeet Sharma, Mr. Kalpesh Sidhpuria, Mr. Vishal J. Mayani, Mr. Mallikarjun V. Patil, Mr. Kiran S. Patil, Mr. Arvind Chaudhary, Miss Chitraleka Khatri, Mr. Praveen K. Suroliya, Mr. Afsar Ali, Mr. Rajkumar, Mr. Shubhankar K. Bose and Mr. Munir D. Khokhar for providing a good friendly working atmosphere.

Last but not least, I would also like to express my sincere thanks to all the staff members of CSMCRI for their cooperation and assistance through out my tenure directly or indirectly.

I feel it worthwhile to mention at this juncture about the 'ASAP 2010' Adsorption System from Micromeritics Instrument Corporation, USA, which made the adsorption measurements easy and I really enjoyed by working with it.

The financial assistance from the Department of Science and Technology, Govt. of India and Council of Scientific and Industrial Research, New Delhi, in the forms of sponsored project and Senior Research Fellowship are greatly acknowledged.

I express my sincere gratitude to my mother, sisters, brothers, teachers and friends for their moral support to complete this work successfully. Finally I place my regards to all those who helped me knowingly or unknowingly.

(Jince Sebastian)

Table of Contents

Aim and Scope of the Present Work

Zeolites are crystalline aluminosilicates with crystallographically well-defined channels and cavities. The fundamental building units in zeolites are the SiO_4 and AlO_4 tetrahedra. These units are joined together by sharing oxygen atoms of the tetrahedra, resulting in the three dimensional anionic framework with channels and cavities. The negative charge of the framework was neutralised by charge compensating cations present inside the cavities and channels. The framework is sufficiently open to accommodate neutral guest molecules and cations. The charge compensating cations are easily replaceable with other cations. Zeolites are of great interest due to their unique properties such as ion exchange, adsorption and catalysis. These extra framework cations are largely responsible for the adsorption and catalytic properties of these materials. Synthetic zeolites A, X and mordenite having alkali and alkaline earth metals as the extra framework cations are used as nitrogen selective adsorbents for the air separation based on difference in the interactions of oxygen and nitrogen molecules with the zeolite surface. Adsorbents like carbon molecular sieves, pore engineered zeolites and titanosilicates with adjustable pores are reported for the size/shape selective separation of air. Nitrogen selective zeolites NaCaA, NaX, LiX and LSLiX are the widely used adsorbents for the oxygen enrichment of air. Among these zeolite based adsorbents, LSLiX having more than 95% of the extra framework cations exchanged with lithium ions is reported to be the best adsorbent known for oxygen production due to its high nitrogen adsorption capacity (~30cc g^{-1} at 101.3kPa and 303.0K) and nitrogen/oxygen selectivity (~10). The three important limitations with the currently used adsorbents for nitrogen and oxygen separation from air, which confine their applications, are as follows,

1. The maximum attainable purity by adsorption processes is around 95%, with separation of 0.934-mole percent argon present in the air being a limiting factor to achieve 100% oxygen purity.
2. The adsorption-based air separation processes are not commercially viable when compared to cryogenic fractionation of air for production levels more than 200-ton oxygen and 50-ton nitrogen per day.
3. The recovery of oxygen is at the best around 35% and simultaneous recovery of high purity nitrogen is also not practicable.

The main objective of the present study was to develop superior molecular sieve adsorbents to overcome some of the above limitations with special thrust to (i) development of adsorbent with higher adsorption capacity and selectivity by ion exchange of zeolites with various transition metal cations, (ii) development of adsorbent having nitrogen as well as argon selectivity over oxygen, to overcome the present limitation of 95% oxygen purity by adsorption process, (iii) investigative exploration of the factors contributing towards the adsorption of N_2, O_2 and Ar in these porous solids, (iv) study of the O_2 activation properties of cobalt ion exchanged zeolites and its use in the catalytic epoxidation of styrene to styrene oxide using molecular oxygen and (v) the photochemical oxidation of bromide to bromine using aqueous dispersion of silver exchanged zeolites. The details of the approaches followed during the studies are as follows:

(i). Silver ions incorporated Zeolites for the Selective Adsorption of Nitrogen and Argon

Most of earlier studies use alkali and alkaline earth cations for post synthesis modification of zeolites to enhance interaction of nitrogen with zeolite surface. Ag^+ is the only noble monopositive cation that forms mononuclear species with appreciable stability in aqueous solution. No hydrolysis occurs. Of the all noble metals, only Ag^+ can be exchanged easily and completely into zeolites from aqueous solution. Stoichimetric ion exchange, which is impossible to achieve for most cations, is frequently observed for Ag^+. Ag^+ is also known to have strong influence on the adsorption properties of some zeolites. In the present work, silver cations are introduced in to the cavities of various types of zeolites by the conventional cation exchange methods from aqueous solution. Initially, adsorption of N_2, O_2 and Ar on low silica zeolites of type A and X was investigated. Encouraged by the results, adsorption studies were extended onto other commercially available zeolite species viz., zeolite Y, L, beta, mordenite and ZSM-5. On proper vacuum dehydration at high temperature co-ordinately unsaturated silver cations were generated in the zeolite cavities. These co-ordinately unsaturated silver ions tend to interact very strongly with the nitrogen molecules via π-complexation. These silver exchanged zeolites are also useful for the selective adsorption of argon over oxygen.

(ii). Post Synthesis Modifications of the Zeolites using Transition Metal Cations

Very less literature is available on transition metal ion exchanged zeolites used for adsorption of air components. This may be due to the fact that though electrostatic interactions between individual multivalent cation and the nitrogen molecules increases, with multivalent cations the total number of extra framework cations inside the zeolite cavity decreases which might result into reduced overall interactions between zeolite surface and adsorbate molecules. It has earlier been observed that locations of cations also play significant role during adsorbate-zeolite interactions. Zeolites containing co-ordinately unsaturated transition metal ions are known to form complexes with a variety of guest molecules. Inert molecules having lone pair or π-electrons are capable to interact with transition metals ions with completely filled d-orbitals through back donation of π-in addition to the usual σ-donation, resulting in a very strong interaction. In the present study, post synthesis modification of the zeolites by ion exchanging with various transition metal cations such as cobalt, manganese, nickel, copper, zinc and cadmium are carried out to study the effects of these cations in the adsorption properties of zeolites towards the air components.

Interestingly, during the adsorption studies it was found that some of the transition metal ion exchanged zeolites are capable to activate small molecules like nitrogen and oxygen towards chemical reactions. It was also found that the silver ions in zeolite cavities undergo reversible oxidation-reduction reactions. Against the backdrop of this observation some industrially important oxidation processes were further investigated.

(iii). Cobalt Exchanged Zeolite X as catalyst for Styrene Epoxidation Reaction Using Molecular Oxygen

Epoxidation of styrene-to-styrene oxide is practically very important reaction, since styrene oxide is an important organic intermediate in the synthesis of fine chemicals and pharmaceuticals. Conventional production of styrene oxide is based on the dehydrochlorination of styrene chlorohydrin with a base or by using organic peracids. However, peracids are very expensive, hazardous to handle, non-selective for the epoxide formation and also lead to formation of

undesirable products, creating a lot of waste. Homogeneous catalysis using transition metal complexes for the epoxidation also lead to a large volume of waste because of their separation problem. Molecular oxygen is the most desirable oxidant for the epoxidation of alkenes with respect to environmental and economic consideration. However, little success has been achieved for the selective epoxidation of alkenes with O_2. In the present study, the oxygen activation properties of cobalt-exchanged zeolites were successfully used for the catalytic epoxidation of styrene-to-styrene oxide using molecular oxygen in presence of Co^{2+} exchanged zeolite X. Effect of water molecules in the reaction mixture on the conversion and selectivity is also studied. In order to increase the styrene conversion and styrene oxide selectivity in the reaction, various alkali and alkaline earth metal promoters are also used.

(iv). Photochemical Oxidation of Bromide to Bromine in Aqueous Dispersion of Silver Exchanged Zeolites

Hydrated silver zeolites are light sensitive materials and undergo reversible redox reaction in the presence of light. This reversible oxidation-reduction of silver in the zeolites is an excellent model to study the photocatalytic oxidation reactions. In the early reports the efficiency of silver exchanged zeolites for the photocatalytic splitting of water and reduction of chloride ions to chlorine. Silver containing zeolites have been tested for the removal of NO_x from air. In the present work, this redox property of the silver exchanged zeolites is successfully used for the oxidation of bromide to bromine in an acidic aqueous solution containing bromide ions and silver exchanged zeolites. Silver zeolites should be excellent catalysts for the production of bromine from seawater and solar light conversion.

Chapter-1

Adsorbents for Air Separation

1.1. INTRODUCTION

Separation of oxygen, nitrogen and argon from air is one of the commercially very important separation processes. Nitrogen and oxygen, respectively second and third most abundantly produced chemicals today, are mainly produced from air, which is rich in nitrogen (78.08 mol%) and oxygen (20.94 mol%). In fact, air is the only source used for the production of these gases ever since Linde achieved large-scale liquefaction of air in 1895. The various physical properties of oxygen, nitrogen and argon, are given in Table-1.1 and form the basis of separation of these gases from air. Gaseous oxygen, nitrogen and argon required for commercial applications is obtained predominantly using cryogenic fractionation due to difference in the liquefaction temperature of these gases.

Table-1.1. Physical Properties of Oxygen, Nitrogen and Argon

Property	Value		
	Nitrogen	Oxygen	Argon
Atomic weight	28.01	32.00	39.95
Boiling point, °C at 101.3kPa	-195.8	-182.9	-185.9
Quadrupole moment	0.31	<0.11	0.00
Polarizability, $cm^3 \times 10^{24}$	1.76	1.60	1.64
Lennerad-Jones force constant, ε/k, K	95	118	121
Lennerad-Jones force constant, σ, Å	3.7	3.5	3.4
Molecular length, Å	2.1	2.0	1.92
Molecular width, Å	1.5	1.4	1.92
Kinetic diameter, Å	2.67	2.49	3.42
Critical diameter, Å	3.0	2.8	3.8
Vander wall radii, Å	1.54	1.40	1.91

Combustion of hydrocarbons in air to produce nitrogen was an accepted method in the 1850s. This gave relatively pure nitrogen the only impurities being carbon dioxide and moisture. In early 1900s, cryogenics based processes came into practice for production of highly pure and dry nitrogen. Cryogenic industries, today, has become the predominant source for nitrogen supply to many industries. The late 1970s and early 1980s saw the advent of membrane and adsorption technology for air separation and made their niche for the separation of oxygen and nitrogen from air. Mid 1990s

saw the invention of chemical and ion transport membrane processes for the air separation.

The physical properties of nitrogen, oxygen and argon are nearly same (Table-1.1) and are non-polar. These molecules adsorb nearly the same in all adsorbents except zeolites. In 1938 Barrer observed that zeolites showed distinct adsorption isotherms for nitrogen and oxygen and could therefore distinguish between nitrogen and oxygen molecules and the heat of adsorption of N_2 on chabazite as high was as 8 kcal mol^{-1} [1-2]. These high heats of adsorption values were subsequently explained in terms of the quadrupole-electric field gradient interaction [3-4]. Nitrogen molecules having higher quadrupole moment (0.31) will have higher interactions compared to oxygen molecules of quadrupole moment <0.11). The invention of synthetic zeolites of type A and X by Milton in 1959 [5] and the pressure swing adsorption cycles by Skarstrom in 1960 [6] and by Guerin de Montrareuil and Domine in 1964 [7] opened up the possibility of separating air at ambient temperature by adsorption. NaCaA (5A) and NaX (13X) were used as nitrogen selective adsorbents for oxygen production in those days.

The typical adsorption processes used for the separation of oxygen and nitrogen from air in its simplest form consists of two adsorption beds, which are alternately pressurised and depressurised. The feed gas, at a pressure of 3-7 atmospheres is passed into an adsorbent bed through the feed end; the strongly adsorbing gas will get adsorbed on the adsorbent, i.e., nitrogen in the case of oxygen enrichment process and oxygen in the case of nitrogen enrichment process. The high purity product is being withdrawn from the product end continuously, while keeping constant feed flow, until the adsorbate breakthrough into the product stream. When the adsorbent bed gets saturated with adsorbate, feed flow will be stopped and the bed pressure will reduce to atmospheric pressure. During this step, adsorbed gas is largely desorbed into the gas phase and gets released as a waste stream. To complete the regeneration, adsorbent bed is further purged with product quality gas from the product end at low-pressure, counter current to the feed flow. The adsorption and desorption steps are interchanged within the two adsorbent beds in order to make the process cyclic and get a continuous product stream. The total cycle time may vary from a few seconds to minutes depending on the feed throughput and adsorption capacity and size of the adsorbent bed.

1.2. ADSORBENTS FOR AIR SEPARATION

Adsorption processes for the separation of oxygen and nitrogen from air are being increasingly used for commercial purposes for the last three decades [8-28]. Adsorption processes are less complex and more passive than cryogenic technology and are operating at ambient temperatures. Adsorption process will continue to improve in both cost and energy efficiency through ongoing research and development of adsorbent materials. Adsorptive separation or concentration of nitrogen or oxygen from air can be achieved either by adsorbing oxygen or by adsorbing nitrogen. Thus the adsorbents used for the air separation can be classified into oxygen selective and nitrogen selective depending on the gas that is getting adsorbed on it. The adsorbents, which selectively adsorb oxygen, are called oxygen selective adsorbents and that selectively adsorbs nitrogen are called nitrogen selective adsorbents. There are few adsorbents, which are capable of adsorbing both nitrogen and argon selectively over oxygen and are termed as nitrogen-argon selective adsorbents. During the last four decades, the demand for oxygen-free nitrogen for inert gas atmosphere led to the development of nitrogen generation plants. The use of N_2 as an inert gas for blanketing started gaining ground in the 1950s. The use for purging the tanks and vessels that store hydrocarbons and corrosive liquids gave an impetus to N_2 applications in chemical industries. Another growing application for nitrogen is for maintaining dust free and inert atmosphere in the electronic industry. Nitrogen gas production, during last 4-5 decades, has become a major industry as a consequence of these diverse applications. Adsorptive separation of nitrogen can be achieved by using oxygen selective adsorbents. These systems are useful to produce 99+% pure nitrogen by adsorption process.

Oxygen requirements in sewage treatment, fermentation, cutting and welding, fish breeding, electric furnaces, pulp bleaching, glass blowing, medical purposes and in the steel industries particularly when the required oxygen purity is only up to 95% is being largely met by adsorption based pressure swing or vacuum swing processes or in combination. In fact it is estimated that at present, around 20% of the world's oxygen demand is met by adsorptive separation of air. However, the maximum attainable purity by adsorption processes is around 95%, with separation of 0.934-mole percent argon present in the air being a limiting factor to achieve 100% oxygen purity. Adsorption systems produce by-product nitrogen containing significant

amounts of oxygen. If high purity nitrogen is required from the by-product, an add-on deoxo or other purification system must be employed to upgrade the quality of the nitrogen. Furthermore, the adsorption-based air separation processes are economically not competitive to cryogenic fractionation of air for production levels more than 200-ton oxygen and 50-ton nitrogen per day. Of the total cost of the oxygen production by adsorption processes, it is estimated that capital cost of equipment and power consumption are the two major factors influencing the overall cost with their share being 50% and 40% respectively. Along with the factors like process and system design, the adsorbent is the key component, which can bring down the cost of oxygen production by adsorption. The adsorbent selectivity and capacity are important parameters for determining the size of the adsorption vessels, compressors or vacuum pumps. It is desirable to have an adsorbent, which shows a high adsorption capacity as well as selectivity for nitrogen compared to oxygen. The improvement in these properties of the adsorbent directly results in lowering the adsorbent inventory of a system and hence the size and power consumption of the air compressor or vacuum pump. Furthermore, adsorbent having a high nitrogen capacity and selectivity can also be used to produce reasonably pure nitrogen along with oxygen by evacuating nitrogen adsorbed on the adsorbent bed. Furthermore, adsorbents having both nitrogen and argon selectivity over oxygen can be used for producing high purity oxygen from air.

Molecular sieving action of the adsorbents results due to steric effect, kinetic effect and equilibrium effects, singly or in combination. In zeolites and carbon molecular sieves, the pore size distribution is in molecular size range, i.e. 3-10Å. In the case of steric selectivity, only small and properly shaped molecules can diffuse into the adsorbent, where as other molecules are totally excluded. The size difference among the molecules can be exploited for the separation of molecules based on the difference in their size. Kinetic selectivity results if one of the components diffuses faster than the others inside the pores of the molecular sieves. If the micropore diameter of the molecular sieve and the molecular diameter of the adsorbate are nearly the same, steric-kinetic effect can occur. Equilibrium effects are observed when one of the components interacts strongly with the adsorbent surface than the other components. Highly polar molecular sieves like zeolite A, X and Y will preferentially adsorb polar molecules, where as silicate with a nonpolar surface will prefer non-polar molecules.

1.3. NITROGEN SELECTIVE ADSORBENTS

Nitrogen molecule possesses a quadrupole moment (0.31) higher than oxygen molecule (<0.11) and is expected to interact strongly with polar surfaces. This difference in adsorption affinities with polar surface forms the basis for separation of these gases from air wherein nitrogen is retained on the adsorbent surface and oxygen enriched air is recovered as a product. In principle, nitrogen can interact more strongly then O_2 with all polar adsorbents such as alumina, silica gel and zeolite molecular sieve. However, zeolite based adsorbents shows the maximum difference in the interaction and are used as nitrogen selective adsorbents for oxygen production by adsorptive separation of air. The different zeolites used for O_2 enrichment by adsorption methods include, alkali and alkaline earth metal ion exchanged zeolite A and X, mordenite, chabazite and erionite. The nitrogen adsorption selectivity mainly depends on the equilibrium effects. In the case of these adsorbents, the positively charged centres are the principal sites for selective adsorption of the adsorbate molecules, which can have higher electrostatic interaction with these adsorbates. Thus, for air mixture, nitrogen molecules more strongly adsorbs in these adsorbents than oxygen and argon molecules due to its higher quadrupole moment. As air is passed through a bed of these adsorbent materials, nitrogen is retained and an oxygen rich stream exits the bed.

1.3.1. ZEOLITES

Zeolites are a class of materials, which have crystallographically well defined channels and cavities [29-30]. The framework structure of zeolites are composed of a three dimensional network of basic structural units consisting SiO_4 and AlO_4 tetrahedrons linked to each other by sharing apical oxygen atoms. The resulting alumino-silicate structure, which is generally highly porous, possesses three-dimensional pores the access to which is through molecular sized windows. Most zeolites contain exchangeable extra framework cations in their channels and cavities, as needed to balance the anionic charge of their frameworks. They may also contain easily replaceable guest molecules such as water or organic molecules. Zeolites can show high selectivity towards adsorbates and can be used as selective sorbents for gas and liquid phase separations. A general chemical formula of zeolites are represented as

$$M_{2/n}O.Al_2O_3.xSiO_2.yH_2O$$

where M is the exchangeable cation with a valancy n, the value of x is equal to or greater than 2 because Al^{3+} does not occupy adjacent tetrahedral sites and y is the number of water molecules adsorbed on the zeolite. Mainly alkali and alkaline earth cations are present in the zeolites in the form of exchangeable cations. The structure of the crystal framework contains voids (cavities, pores) and channels of molecular dimensions. The pore or channel openings range from 3 to 10Å, depending on the zeolite type. Framework structures of zeolite of type A, X, mordenite and chabazite, commonly used as adsorbents in air separation are given in Figure-1.1.

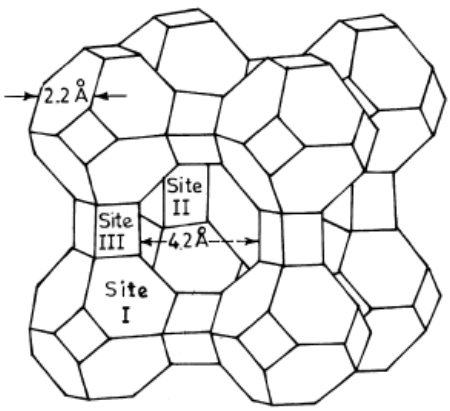

(a) Zeolite A

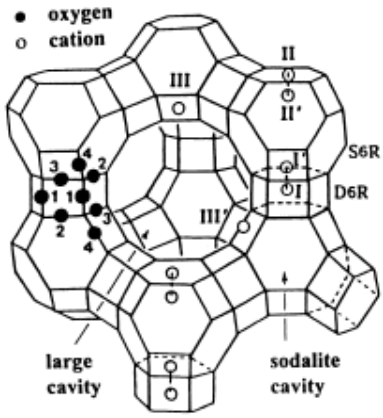

(b) Zeolite X

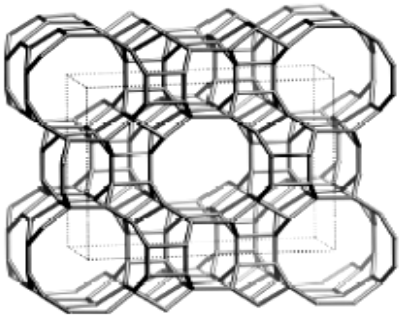

(c) Mordenite

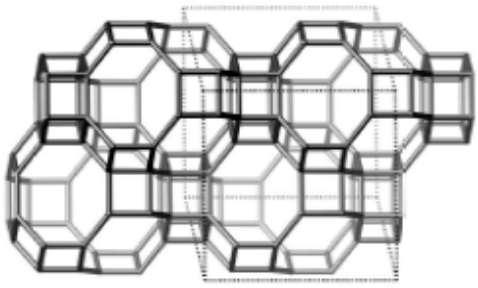

(d) Chabazite

Figure-1.1. Framework structures of zeolite A, X, mordenite and chabazite

Synthetic zeolites of the type A, X and mordenite having alkali and alkaline earth metals as the extra framework cations are used for the oxygen enrichment, based on the difference in the interactions of oxygen and nitrogen molecules with the zeolite surface. Nitrogen selective zeolites such as NaCaA (5A), NaX (13X), LiX and LSLiX are the most commercially used adsorbents for the oxygen enrichment of air. The efforts to enhance the adsorption capacity and selectivity have been reported by

increasing the number of exchangeable cations into the zeolite structure by modifying the chemical composition of the zeolite. The adsorption selectivity for nitrogen has also been substantially enhanced by exchanging the zeolite with cations like lithium and / or calcium in zeolites.

1.3.1.1. Zeolite A Based Adsorbents

Zeolite A (Figure-1.1a) may be viewed as an assemblage of truncated octahedra, each composed of 24 tetrahedra ($12AlO_4$ and $12SiO_4$) [29-30]. These are also referred to as cuboctahedra, sodalite cavities or β-cages. These cuboctahedra are octahedrally joined at 4-rings by four bridging oxygen atoms and results into a central cavity also known as super in diameter separated from one another similar cage by an 8-ring opening or window which has a diameter of 4.2Å. Each supercage is surrounded by eight smaller cavities of 6.6Å diameters, which have pore openings of 2.2Å. It is only supercages those are accessible to nitrogen, oxygen and argon molecules for adsorption. However, for water molecules, even the smaller cavities are accessible for adsorption. There are 12 negative charges that are balanced by cations in each unit cell. For $Na_{12}A$, 8 Na^+ ions are located at Site I at the centre of the six-member ring, 3 at site II at the eight-member aperture directly obstructing the entrance and 1 at site III near the four-member ring inside the cavity (Figure-1.1a). The sodium ions can be replaced by other cations. However, the cation location varies with the nature of the cation depending on its size and charge. On partially replacing (around 50%) Na^+ (0.95Å) with K^+ (1.33Å) ions in NaA, molecular sieve 3A zeolite is formed resulting in a smaller effective pore opening size of 3Å due to the occupation of larger potassium ions at site II. On replacing sodium ions with divalent cations such as calcium or magnesium, one Ca^{2+} or Mg^{2+} replaces two Na^+ ions; therefore half the cations are present in the zeolite. The occupancy of site II is reduced as seen below on exchanging Ca^{2+} into NaA resulting into the decrease in obstruction of 8-ring pore opening to the cavities. Consequently, NaCaA with at least 75% sodium exchange results into a molecular sieve with larger pore opening (4.8Å).

Zeolite NaCaA (5A) has been the most commonly used adsorbents for air separation [31-34]. The adsorption capacity and nitrogen oxygen selectivity of 5A depends on the extent of cation exchange on zeolite 4A (NaA). In typical 5A zeolite used for air separation is made by exchanging more than 70% of the extra framework sodium cations with calcium ions. NaCaA shows equilibrium nitrogen adsorption capacity

14cc g^{-1} and nitrogen/oxygen selectivity of 3.5 at STP. The oxygen adsorption capacity is slightly higher than argon adsorption capacity at the same pressure.

Magnesium exchanged zeolite A shows high nitrogen adsorption capacity and nitrogen–oxygen selectivity [35]. MgNaA shows a nitrogen adsorption capacity value of 28cc g^{-1} at 22^{o}C and 1 atm pressure. Nitrogen–oxygen selectivity values increased with the level of magnesium exchange with a maximum value of 8.6 on 81% magnesium exchanged zeolite A. However, it is known that the magnesium-exchanged zeolite is not stable because the framework structure tends to collapse upon calcination, due to the formation of MgO. It is also not possible to obtain more than 81% magnesium exchange for magnesium-exchanged zeolite A.

1.3.1.2. Zeolite X Based Adsorbents

Zeolite X (Figure-1.1b) is a synthetic aluminium rich analogue of the naturally occurring mineral faujasite [29-30, 36]. The 14-hedron with 24 vertices known as the sodalite cavity or β-cage may be viewed as its principal building block. These β-cages are connected tetrahedrally at six-rings by bridging oxygen to give double six-rings (D6Rs, hexagonal prisms) and concomitantly, an interconnected set of even larger cavities (supercage) accessible in three dimensions through 12-ring (24-membered) windows. The Si and Al atoms occupy the vertices of these polyhedra. The oxygen atoms lie approximately midway between each pair of Si and Al atoms but are displaced from those points to give near-tetrahedral angles about Si and Al. Single six-rings (S6Rs) are shared by sodalite and supercage, and may be viewed as the entrances to the sodalite units. Each unit cell has eight sodalite units, eight supercage, 16 D6Rs, 16 12-rings, and 32 S6Rs. Exchangeable cations that balance the negative charge of the aluminosilicate framework are found within the zeolite cavities. They are usually found at the six different sites: site I at the centre of the D6R, I′ in the sodalite cavity on the opposite side of one of the D6Rs six-rings from site I, II′ inside the sodalite cavity near a S6R, II at the centre of the S6R or displaced from this point into a supercage, III in the supercage on a twofold axis opposite a four-ring between two 12-rings, and III′ somewhat or substantially off III (off the twofold axis) on the inner surface of the supercage (Figure-1.1b).

Zeolite NaX (13X) has been commercially used as the adsorbent for the adsorptive separation of air. The adsorption of nitrogen and oxygen on ion exchanged zeolite X

was studied, independently, by McKee [37], Habgood [38-39] and Berlin [40]. Commercial zeolite X with Si/Al ratio closer to 1.25 was used for the ion exchange with alkali and alkaline earth metal ions. The adsorption studies were performed at 1 atm pressure and the nitrogen-oxygen selectivity were obtained in the order $Ba^{2+}>Sr^{2+}>Li^{+}$. The work of McKee and Habgood showed that zeolite X with divalent cations shows the highest nitrogen adsorption capacity and nitrogen-oxygen selectivity. Most of the sorbents developed in 1980's followed this line of thinking. Coe and Kuznicki [41] showed that CaX followed by SrX shows the highest nitrogen adsorption capacity nitrogen-oxygen selectivity at STP. Sircar et al [42] showed that mixed SrCaX having about 90% Sr^{2+} cations and 10% Ca^{2+} cations exhibited higher nitrogen adsorption capacity at 3 atm compared to CaX and SrX, without effecting the nitrogen-oxygen selectivity. The oxygen adsorption capacity also increases on the cation exchange with divalent cations. Several studies on the adsorption properties of calcium exchanged zeolite X [43-46] containing various amount of calcium and other co-cations. Among the transition metal ions, yttrium (III) exchanged zeolite X was reported as a nitrogen selective adsorbent over oxygen and argon [47]. 90% yttrium (III) exchanged zeolite X shows nitrogen/oxygen selectivity 8.6 and nitrogen/argon selectivity 10.2 in the Henry's region.

The true potential of LiX for air separation was not understood until the investigation of Chao [48]. The synthesis of low silica zeolite X (LSX, Si/Al=1) was accomplished in the early 1980's [49]. Figure-1.2 represents the graph showing a comparison of the nitrogen isotherms at about 23°C on LSLiX (SiO_2/Al_2O_3 = 2.0), LiX (SiO_2/Al_2O_3 = 2.5) and NaX (SiO_2/Al_2O_3 = 2.5) [49].

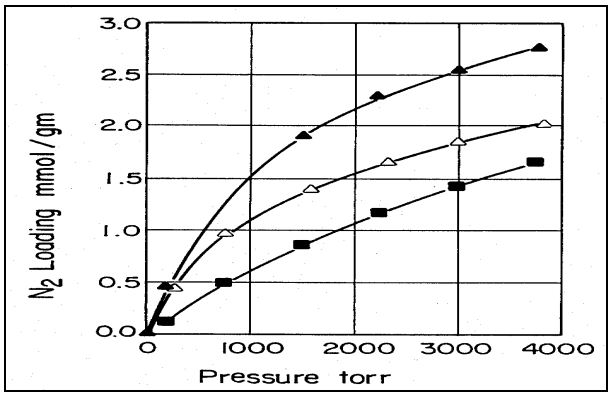

Figure 1.2. N_2 adsorption isotherms on ▲ LSLiX (SiO_2/Al_2O_3, Δ LiX (SiO_2/Al_2O_3 = 2.5) and ■ NaX (SiO_2/Al_2O_3 = 2.5) at 23°C

Chao found that the nitrogen adsorption capacity significantly increases when the Si/Al ratio decreases to one and a threshold of ~80% lithium exchange for zeolite X and ~70% lithium exchange for LSX must be reached for increase nitrogen adsorption capacity, beyond which the amount of nitrogen increased linearly with lithium content. Several studies on LiX with different silica alumina ratios [50-51] and containing various amounts of Al^{3+}, alkali, alkaline earth and transition metal ions were reported [52-66]. LiX containing small amount of silver ions shows higher nitrogen adsorption capacities than the pure LiX [67-71]. Silver is known to have very strong effects on the adsorption properties of some zeolites. The addition of very small amounts of Ag and the proper dehydration conditions resulted in the enhanced adsorptive characteristics and increased energetic heterogeneity as compared to those of the near fully exchanged lithium zeolites [70]. The silver ion modified LSLiX provides a significantly higher (>10%) product throughput, at the same product purity and recovery, when compared to that of the near fully lithium exchanged low silica zeolite X. ab initio molecular orbital calculations showed that the enhanced nitrogen adsorption was due to the complexation of the N_2 molecules with the non-framework silver ions present in the zeolite cavities [71].

The adsorption isotherms of nitrogen and argon on LSLiX and CaA at 298K are shown in Figure-1.3. The oxygen sorption capacity on CaA at higher pressures is higher than that on LSLiX, where as capacity of nitrogen on CaA is by ~40% lower than that in the LSLiX [100].

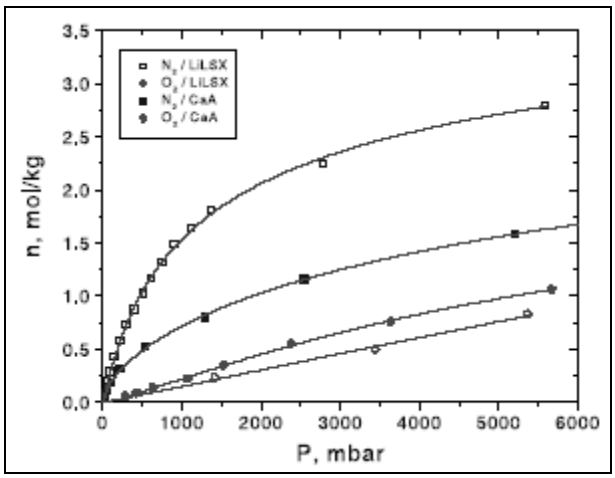

Figure 1.3. Sorption isotherms for N_2 and O_2 on LSLiX and CaA zeolites at 298K

1.3.1.3. Other Zeolites Based Adsorbents

Other zeolites and zeolite type microporous solids also hold potential for new adsorbent for this application. Natural zeolites such as chabazite, mordenite, clinoptilolite etc. suitable for air separation are reported in the literature [72-75]. For example, Itado mordenite from Japan shows nitrogen adsorption capacity about 30cc g^{-1} at STP. Oxygen generator using this zeolite has also been reported [73]. However, natural zeolites have problems of purity and availability. In addition, the adsorptions of N_2, O_2 and Ar on their high purity synthetic forms are also reported [76-91]. The sorption of nitrogen, oxygen and argon on various alkali and alkaline earth metal ion exchanged synthetic mordenite samples were also reported [76-81]. The synthetic sodium mordenite shows nitrogen adsorption capacity 21cc g^{-1} and nitrogen / oxygen selectivity 4.2 at STP. Polyvalent ion exchanged chabazite was reported for the selective removal of trace nitrogen from argon [82]. Coe et al. [83] have reported that synthetic Lithium exchanged chabazite (Si/Al= 2.6) exhibits N_2 and O_2 adsorption capacity 26.5 and 6.7cc g^{-1} respectively and N_2/O_2 selectivity of 5.9 at STP.

Lithium exchanged zeolites such as low silica EMT-containing metallosilicates [92], chabazite, offretite, erionite, levyne, mordenite, gmelinite, zeolite T, EMC-2, ZSM-3, ZSM-18, ZK-5, zeolite L, and beta are also reported for the selective adsorption of nitrogen from other gases [93]. Faujasite adsorbent with non-uniform aluminium distribution [92] is also reported for selective nitrogen adsorption. Copper exchanged ZSM-5 type zeolite shows very strong interaction with N_2 molecules at room temperature [95-98]. During the vacuum dehydration process, the Cu^{2+} ions undergo auto reduction and forms Cu^{+} in the zeolite cavities. These Cu^{+} ions in the zeolite cavities interact very strongly with the nitrogen molecules. The IR band obtained at 2295 cm^{-1} indicating the existence of strong interaction between the monovalent copper ions and N_2 molecules [97]. The strong interaction of the Cu^{+} with N_2 was further confirmed from the high heat of adsorption (85 kJ mol^{-1}) of N_2 on the Cu^{+} species [97-98].

1.3.2. FORCES CONTRIBUTING TO THE ENERGY OF ADSORPTION ON ZEOLITES

The total energy of physical adsorption between nitrogen/oxygen/argon molecules and zeolite surface is comprised of dispersion ϕ_D, polarization ϕ_P, field-dipole

interactions $\phi_{F\mu}$, field-quadrupole interactions ϕ_{FQ}, close-range repulsion ϕ_R, and sorbate-sorbate interactions ϕ_{SP} [30]. Thus, ϕ is given as

$$\phi = -(\phi_D-\phi_P) - \phi_{P-} \phi_{FD} - \phi_{FQ} - \phi_{SP}$$

The adsorbate nitrogen and oxygen being nonpolar and also adsorption coverage being small, the term $\phi_{F\mu}$ and ϕ_{SP} can be ignored while calculating interaction energy. Hence the above equation for total energy becomes

$$\phi = -(\phi_D-\phi_P) - \phi_P - \phi_{FQ}$$

Substituting the terms for various interactions the equation becomes

$$\phi = -\,{}^1/_4\, Q(\phi_F/\phi_R) - \tfrac{1}{2}\,(\phi_S/k)\, F2 - \Sigma A/r^6 + \Sigma B/r^{12}$$

where Q is quadrupole moment, k is a constant (in SI units, $k=9 \times 10^9$), F is the field, and ϕ_s is the polarizability of an adsorbate molecule. The values of the constants A and B are calculated by the method described by Barrer [30].

As, in zeolites Al and Si atoms are buried inside the centre of the tetrahedral and are not directly exposed to nitrogen / oxygen molecules and also possess small polarizability values, their interactions with the adsorbates molecules can be ignored. Therefore, the principle interactions of oxygen and nitrogen molecules with the zeolite structure are through the lattice oxygen atoms and accessible extra framework cations.

1.3.3. FACTORS EFFECTING ADSORPTION CAPACITY AND SELECTIVITY OF ZEOLITES

The factors like zeolite type, Si/Al ratio, number, location and nature of the extra framework cations, extent of cation exchange, residual water content and extent of dehydration influence strongly on the adsorption properties of the zeolites as shown below:

1.3.3.1. Type of Zeolite and Si/Al Ratio

Both natural and synthetic zeolites have been reportedly used for oxygen enrichment of air using adsorption. Most of adsorbent development research has been confined to post synthesis modification particularly of zeolite A and X. Other zeolites and zeolite type microporous solids also hold potential for new adsorbent for this application.

Natural zeolite reported [72-75] suitable for this includes chabazite, mordenite, clinoptilolite etc. For example, Itado mordenite from Japan adsorbs 30cc g^{-1} nitrogen at STP. Oxygen generator using this zeolite has also been reported [73]. However, natural zeolites have problems of purity and availability. Coe et al. [83] have reported that synthetic lithium exchanged chabazite (Si/Al = 2.6) exhibits 26.5 and 6.7cc g^{-1} at STP nitrogen and oxygen adsorption capacity respectively and nitrogen oxygen selectivity of 5.9. With suitable isotherm shape at ambient conditions to increase the working adsorption productivity beyond the standard zeolites used for air separation, this adsorbent is reported to hold potential for oxygen enrichment. Most of the present commercial PSA units employ synthetic zeolites with NaCaA, NaX, CaX, LiX and mordenite for oxygen enrichment. The isosteric heat of adsorption and N_2 /O_2 selectivity on various types of zeolites are given in Table-1.2.

Table-1.2. Heat of adsorption and N_2 /O_2 Selectivity in different types of zeolites

Zeolite Type	Si/Al ratio	Isosteric Heat of Adsorption in kJ mol^{-1}		N_2 /O_2 Selectivity	Reference
		Nitrogen	Oxygen		
Zeolite A	1.0	19.6	13.8	3.1	[99]
Zeolite X	1.25	18.5	12.0	3.4	[98]
LSX	1.0	22.1	12.2	3.5	[11]
Zeolite Y	5.5	19.8	15.8	3.5	[11]
Mordenite	5.5	25.6	17.0	4.1	[76]
Mordenite	10.0	18.9	16.8	1.1	[76]
Chabazite	Natural	32.0	19.0	-	[4]

The adsorption capacity of an adsorbent depends on the zeolite Si/Al ratio and number of extra framework cations. However, the strength of the cation-sorbate interaction is relatively independent of the number of the cations present [85]. Hence, the adsorption capacity for weakly interacting adsorbates such as nitrogen is directly related to the number of sorbate-accessible cations in a zeolite. Therefore, it can be increased if the numbers of cations are increased in a given zeolite. Further, the number of cations in a zeolite depends on its Si/Al ratio. Coe et al. [86] have developed an interesting way of increasing aluminium content in the form of low silica X zeolite (LSX) with Si/Al ratio equal to 1 (the typical value being 1.25).

LSCaX contains about 18.5% more accessible cations over CaX having Si/Al as 1.25. This results in a 20% increase in the nitrogen adsorption capacity. It is claimed that LSX possesses air separation properties superior to other nitrogen selective adsorbent [86]. In a similar manner, a low silica zeolite X in which more than 95% of cations can be exchanged with lithium is patented [97], which exhibits an extraordinarily high adsorption capacity and selectivity towards nitrogen from its mixture with oxygen. For example, at 700torr, the nitrogen adsorption capacity of 99% Li exchanged LSX (Si/Al =1)) is 32% higher than the 94% lithium exchanged zeolite X (Si/Al =1.25). The adsorption data for binary mixtures of oxygen and nitrogen [97] also show that LiX (1.0) has higher nitrogen selectivity than LiX (1.25) with the same exchange level has. It has been shown [97] that at room temperature and at 1atm. N_2/O_2 separation factor of LiX (Si/Al = 1.0) is 11 compared to 6.4 of LiX (Si/Al = 1.25) and 3.2 of NaX.

1.3.3.2. Nature and Locations of Cations

In general, in a given zeolite the interaction energy and the adsorption capacity for nitrogen are expected to increase with the charge density of the cation [98-117]. There are factors other than cation charge density, which play significant role in adsorbate-adsorbent interactions. Figure-1.4 represents the nitrogen heats of adsorption on charge density of the extra framework cations of the zeolite.

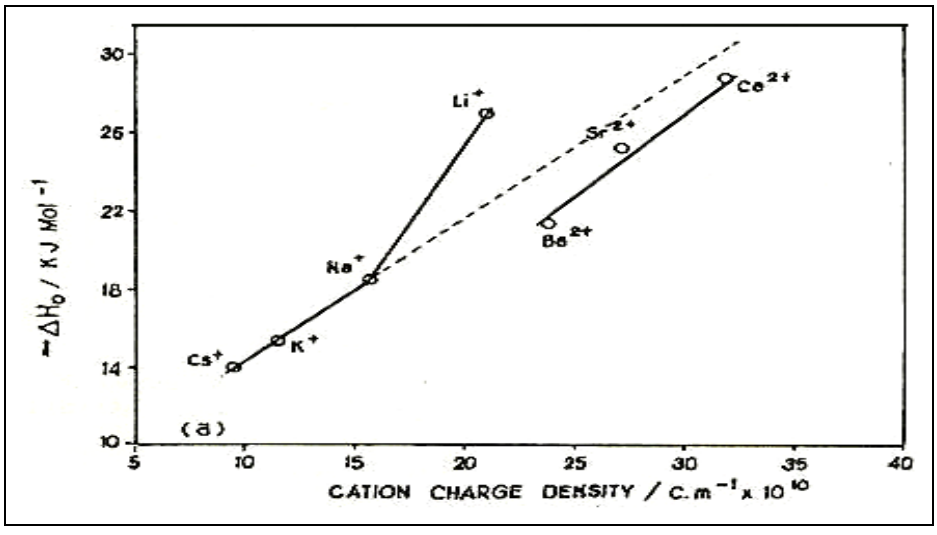

Figure-1.4. Dependence of N_2 heats of adsorption on extra framework cation charge density

It was found that the isosteric heat of adsorption increases with increase in the charge density of the cations. For example, among monovalent cations, lithium shows

abnormally high values for heats of adsorption, specific retention volume and adsorption selectivity. Furthermore, bivalent cations show values lower that that expected by extending the heats of adsorption versus cation charge density plot for monovalent cations. These observations have been attributed in terms of different sites these cations occupy inside zeolite structure. The isosteric heat of adsorption for nitrogen on various cationic forms of zeolite X at zero coverage is given in Table-1.3.

Table-1.3. Heat of Adsorption on various cationic forms of zeolite X at zero coverage

Cations	Isosteric Heat of Adsorption in kJ mol^{-1}		Reference
	Nitrogen	Oxygen	
Lithium	27.0	13.4	[98]
Sodium	18.5	12.0	[98]
Potassium	15.4	11.9	[98]
Caesium	14.1	12.2	[98]
Calcium	28.8	15.3	[98]
Strontium	25.2	13.9	[98]
Silver	33.5	15.5	[11]
Cerium	13.9	71.8	[182]

Location of the extra framework cations in relation to the alumino silicate framework has primary importance for elucidating the effect on the adsorption properties of the zeolite. The distribution of cations in NaX is of 4 type I sites, 32 type I′ sites, 31 type II sites and 8 type III sites with 6 ions unlocated. However, the cations, which are accessible and interact with the adsorbate nitrogen/oxygen/argon molecules, are site II and site III cations only. Lithium are reported [118-123] to preferentially occupy sites I′ and II in zeolite X. Li^+ ion due to its smaller size (0.68Å) reside almost in the plane of the six member ring, while the larger Na^+ cation (0.95Å) is held above the plane in trigonal-pyramidal coordination to the O_2 molecules. As a result, site II Li^+ cations are less accessible to adsorbate molecules than site Na^+ ions and show weaker interactions and heats of adsorption. Once the entire Na^+ cations of site II are replaced, Na^+ ions from site III or unlocated positions are replaced by Li^+ ions and increase in heats of adsorption is observed. It has been reported [122-123] that the sharp rise in the heat value observed above 90% Li exchange is due Li^+ ions occupying accessible site III at the expense of Na^+ ions from site I or unlocated

position. On the basis of Li-NMR spectra [120], it has been shown that for zeolite LiNaX [$Na_{14.3}$ $Li_{67.4}$ $(AlO_2)_{81.7}$ $(SiO_2)_{110.3}$], 32 Li^+ ions/unit cell are in site I′, 32 Li^+ ions are in the site II position and 4 Li^+ ions with 14 Na^+ ions/unit cell are in site III in the super cage. NMR lines corresponding to Li^+ ions at site III are only observed when Li^+ exchange is higher than 64 Li^+ ions/unit cell. This clearly shows that site III Na^+ are replaced with Li^+ at about 80 % Li^+ exchange. This means that the increase in the sorption properties of nitrogen and oxygen observed nearly this exchange level is due to the site III Li^+ ion interaction with sorbate molecules. However, the sharp rise in sorption properties at lithium exchange above 90% indicates that, at those Li^+ exchange values, the four site I or six unallocated Na^+ ions start getting removed. However, as the site I position is energetically unfavourable [119-125] the in comings Li^+ ions occupy site III instead of site I. Thus, there is an increase in the number of accessible site III Li^+ ions equal to those Na^+ ions, which are removed from site I/unallocated site. The abnormally high values of sorption properties observed for LiX-98 compared to NaX, NaKX and NaCsX could be explained in terms of the availability of these additional sites III Li^+ ions compared to other monovalent ions. The lower heats of adsorption observed for bivalent Ca, Ba and Sr cation in zeolite X compared to values extrapolated from monovalent cations is also resulting from the fact that bivalent cations occupy site II only [74, 125] where monovalent cations occupy sites II and III. Site III is more accessible to adsorbate molecules and show higher interaction.

Similar conclusions have been made about the effect of cation locations on the adsorption of nitrogen/oxygen in zeolite A [99] particularly in calcium exchanged zeolite A where abnormally high adsorption capacity and selectivity was observed with calcium exchange of >90%. This has been attributed to the highly accessible site near the pore opening of the zeolite A occupied by calcium cations at this exchange level. Far IR studies [106,126] have shown that at higher than 90% calcium exchange in zeolite A, a major part of Ca^{2+} ions are located at site I, i.e., in the six-ring but displaced into the α-cage and hence more accessible to adsorbate molecules. The remaining cations are located at the inaccessible site I′, in the six-ring displaced in the β-cage. However, at calcium exchange level, less than 75%, Ca^{2+} ions are located at site I′, i.e., in the plane of the six-ring. Therefore, it is highly significant to understand cation locations in the zeolite structure to develop the desired adsorbent. It

has been demonstrated [99, 105, 127] that the adsorption capacities for zeolites having multivalent cations are more sensitive to the activation procedure followed.

1.3.3.3. Degree of Cation Exchange

In general, the nitrogen adsorption capacity and selectivity increase with the increase in the degree of cation exchange [105-106]. The high N_2 adsorption capacity and N_2 heat of adsorption were observed only at higher cation ion exchange levels. For example, Henry constant for N_2, which is indicative of adsorption capacity, increases with calcium exchange with steep rise at 90% exchange level. However, Henry's constants for oxygen are not affected significantly by calcium exchange. Similarly, heats of adsorption data for N_2 increases form 18 to 25kJ mol^{-1} as the percent calcium exchange increase to 97 whereas heat of adsorption for O_2 remains at 14-15kJ mol^{-1}. In the case of zeolite X, the effect of calcium exchange on N_2 adsorption capacity and selectivity is more pronounced than in zeolite A. Three fold increase in nitrogen selectivity as calcium exchange increases from 0 to 95% level was observed in zeolite A. The dependence of heat of adsorption measured in Henry region on calcium content of zeolite A given in Figure-1.5 shows that the N_2 heat of adsorption increases from 18 to 25kJmol^{-1} as percentage of calcium exchange increases from 0-97 [99]. The N_2 heat of adsorption increases with the percentage of calcium exchange, after reaching the calcium exchange level beyond 70%, sharp increase in the N_2 heat of adsorption value is observed. Far IR spectroscopic studies [105, 127] have shown that sharp rise in the N_2 heat of adsorption at higher calcium exchange is essentially due to Ca^{2+} ions located in site I′ i.e., in the six ring but displaced into the alpha cage, which are early accessible to nitrogen molecules. At lower exchange level, Ca^{2+} ions are located at site I, i.e., in the six ring on the plane of the ring.

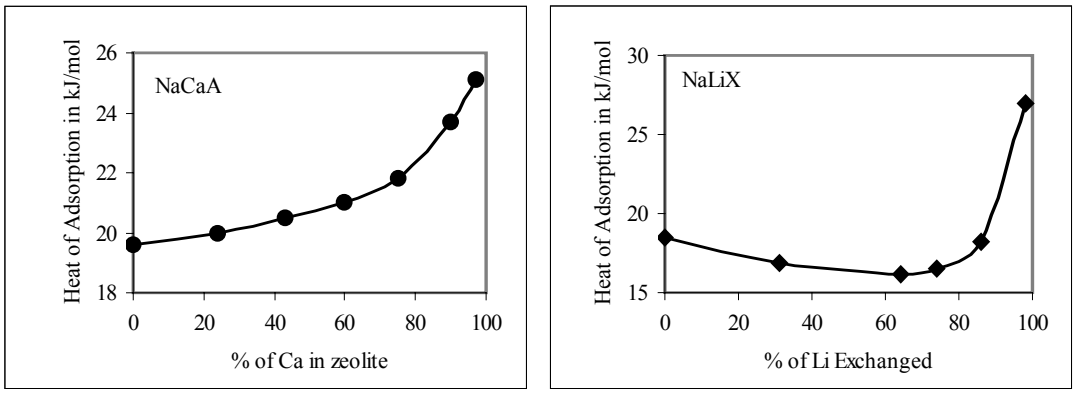

Figure 1.5. Variation of N_2 heat of adsorption with percentage of cation exchange

The N_2 heat of adsorption is plotted against percentage of lithium exchange given in Figure-1.5 shows sharp increase in heats of adsorption value at lithium exchange higher than 90% [98]. In fact, at lower lithium exchange levels, there is small decrease in the value of N_2 heat of adsorption. This variation of N_2 heat of adsorption with lithium content is due to different sites Na^+/Li^+ cations occupy in zeolite structure. The distribution of Na^+ ions is of 4 type I sites, 32 type I′ sites, 31 type II sites and 8 type III sites, with 6 ions unallocated. The ions, which are accessible to sorbate molecules, are 31 (site II) and 8 (site III).

1.3.3.4. Activation of Adsorbent and Pre-sorbed Moisture

In any application of zeolites for adsorption purposes, the first step is to activate / regenerate the adsorbent in order to drive off the residual water. This activation generally being carried out by heating the adsorbent at an elevated temperature (up to 450^{o}C. The effects of presorbed moisture on the adsorption properties of zeolites are well studied in the literature. Both for zeolite A [99] and X [105, 106, 127], it has been shown that an activation procedure has an influence on the adsorption behaviour of calcium exchanged zeolites. It has further been emphasized that in the case of polyvalent cation exchanged zeolites, thermal activation step should be carefully controlled failing which zeolite undergoes substantial degree of hydroxylation. Studies [99] in zeolite A has demonstrated that the presence of moisture and CO_2 in the air from which N_2 is adsorbed has also negative effect on the adsorption capacity and selectivity. This effect is more pronounced even with less than 1mmol g^{-1} of adsorbed water for highly calcium-exchanged zeolite A is given in Table-1.4.

Effect of CO_2 is more pronounced than moisture. CO_2 may be physisorbed or chemisorbed in NaCaA zeolites and thus effecting the adsorption behaviour [99]. Effect of pre-sorbed water can be explained in terms of hydroxylation of the bivalent cations. Hydration is an equilibrium reaction represented by

$$M^{n+}.xH_2O \longrightarrow M(OH)^{(n-e)+} + eH^+ + (x-e)H_2O$$

where M is a cation having valancy n (usually 2 or 3), x is 1 to 6 and e is 1 or 2. Products on the right hand side of the equation are detrimental to the zeolite capacity and stability. Hydroxylated multivalent cations, such as $Ca(OH)^+$, are known to be ineffective sites for the selective adsorption especially for nitrogen. Additionally, the zeolite framework is unstable towards H^+. The equilibrium may be shifted towards

left by minimising the amount of water present at any given temperature particularly above 150^{o}C during activation.

Table-1.4. Effect of Pre-sorbed Water on ΔHo of N_2 and O_2 in Different Adsorbent Samples

ΔHo, kJ/mol, for pre-sorbed water, mmol/g of zeolite				
Adsorbate	0.0	0.9	1.6	3.5
NaA				
N_2	19.6	11.7	-	-
O_2	13.8	8.5	-	-
NaCaA-24				
N_2	20.0	19.7	19.5	16.5
O_2	14.3	14.0	13.4	13.1
NaCaA-43				
N_2	20.5	20.0	19.7	16.6
O_2	14.3	13.5	13.4	13.0
NaCaA-60				
N_2	21.0	20.6	20.4	19.8
O_2	14.0	14.4	13.5	14.1
NaCaA-75				
N_2	21.8	21.5	21.1	20.0
O_2	14.0	13.8	13.8	14.5
NaCaA-90				
N_2	23.7	21.9	21.7	19.3
O_2	14.0	13.7	14.1	14.3
NaCaA-97				
N_2	25.1	23.7	21.8	21.3
O_2	141	14.8	13.9	14.6

Hutson et al. [128] measured the room temperature equilibrium adsorption isotherms for N_2, O_2 and Ar on LSLiX after varied degree of dehydration. The effect of residual water on the adsorption of these gases was then simulated using Monte Carlo methods. It was observed that a very small amounts of water in the LSLiX zeolite have a significant effect on the adsorptive capacity of these atmospheric gases with the capacity of N_2 dropping from 17.4 molecules of N_2 adsorbed per unit cell for the fully dehydrated zeolite to <2 molecules of N_2 adsorbed per unit cell when the sample

contain 32 residual water molecules per unit cell, an indication that the N_2 molecules only interact with the supercage Li^+ cations [128-129].

1.3.4. NITROGEN BINDING METAL COMPLEXES

It was reported that some organometallic complexes [130-133] of some transition metals absorbs nitrogen from nitrogen containing gas mixtures. These complexes can be used for gas separation process as dispersion in a solvent or on solids such as polymers or porous inorganic solids. A dilute solution in the range of 0.1M is generally used for the N_2 adsorption process. Generally speaking, polar and hydrophilic liquids or liquid mixtures are used as solvents for dispersing these metal complexes, although non-polar liquids may be useful in some cases. Organometallic complex of the transition metals of Groups 7, 8 and 9, such as the early and third row transition metals Mo (0), W (0), Re (I), Re (II), Ru (II), Fe (I), Fe (II), Co (0), Co (I), Os (II), Ir (I), Rh (I) and Mn (I), having at least one ligands capable of providing five or six coordinate absorbs nitrogen from a nitrogen containing gas mixtures. The organometallic complex is preferably penta-coordinate, with bound nitrogen occupying the sixth coordination site. When the bound nitrogen displaces one of the ligands, the organometallic complex may be hexa-coordinate. The dinitrogen complexes of the metals in Groups 3 through 6 are generally less preferred for the gas separation, as they tend to be susceptible to chemical reaction (such as protonation) at the coordinated dinitrogen, which may lead to loss of nitrogen-binding capability of the organometallic complex. The typical nitrogen adsorption isotherms on ruthenium and iron complex at ambient temperature and nitrogen partial pressures up to 760 psi are given in Figure-1.6.

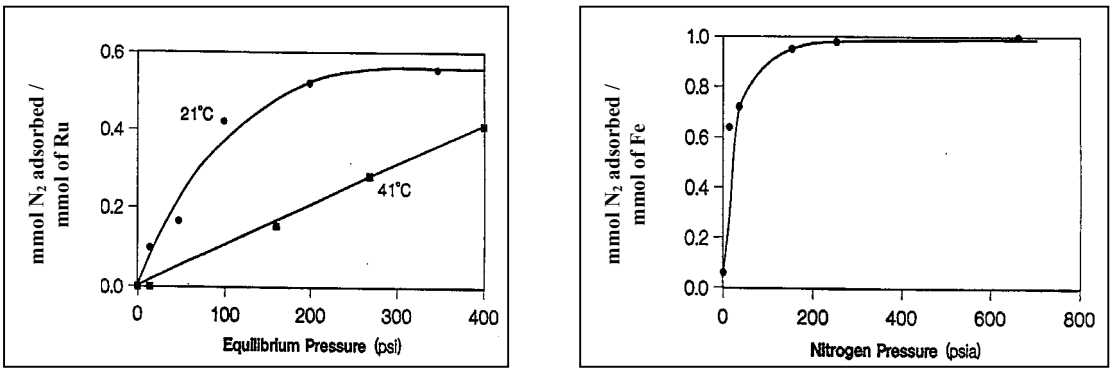

Figure-1.6. N_2 Adsorption isotherms of Ru and Fe metal Complexes at ambient temperature [130 - 131]

Typically 0^oC to 40^oC and 2-30 atm nitrogen partial pressure was used for the reversible binding of nitrogen using these metal complexes. The increase in the temperature and / or decrease in the pressure will leads to the decrease in the N_2 adsorption capacity and selectivity.

Reversible nitrogen-binding transition metal complexes form 1:1 M: N_2 or 1:2 M: N_2 complexes with dinitrogen. However, transition metal complexes, which form 2:1 M: N_2 complexes or other metal-rich stoichiometries may also lead to an efficient nitrogen-removal process. Transition metal complexes, which form metal-rich/dinitrogen complexes, i.e., 2:1 M: N_2 complexes may be modified to prevent the binding of two or more transition metals to one molecule of nitrogen. An exemplary method that may be used to prevent the formation of metal-rich/dinitrogen complexes is the addition of sterically hindering substituents to one or more of the ligands on the metal. This addition of steric hindrance to the ligand environment in some cases prevent more than one transition metal complex from binding to one dinitrogen molecule. Another method that may be used to prevent the formation of metal-rich/dinitrogen complexes is to prepare electrostatically charged nitrogen-binding transition metal complexes. The electronic charge on the transition metal complexes will then repulse other similarly charged transition metal complexes, thereby preventing aggregation of the transition metal complexes around a single dinitrogen molecule. Figure-1.7 is illustrating the nitrogen-binding capacity of iron based a sorption material as a function of pressure.

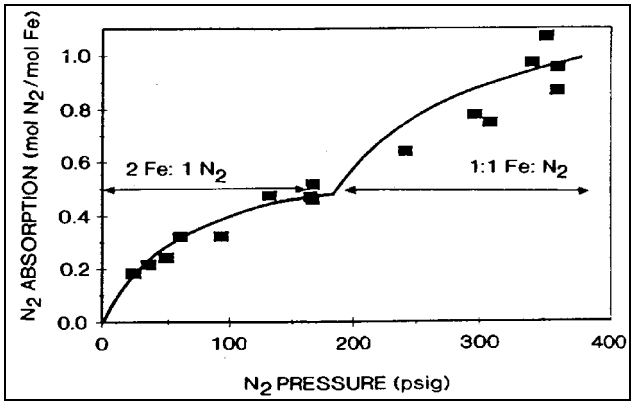

Figure-1.7. N_2 Adsorption isotherms of Fe metal Complexes at ambient temperature [132-133]

These nitrogen binding organometallic complexes are mainly used for the removal of nitrogen from natural gas. The use of such nitrogen selective organometallic complexes for the air separation process is yet not in practice.

1.4. NITROGEN AND ARGON SELECTIVE ADSORBENTS

Silver is known to have very strong effect on the adsorption of N_2 molecules on some zeolites. It is also known that during the vacuum dehydration at higher temperatures, the silver ions in the zeolites undergo auto reduction to form charged silver clusters with in the zeolite cavities. These silver clusters are capable to interact with small molecules by σ-donation and π-back donation, resulting in a very strong interaction. Silver exchanged zeolites of type X and mordenite shows nitrogen and argon selectivity over oxygen [134-137]. These adsorbents are useful to overcome the present oxygen purity limit of 95%. Silver mordenite [136] containing about 12% by mass silver was used as the adsorbent for the production of 99.7% pure oxygen by pressure swing adsorption method at 60°C. The adsorption isotherms for oxygen and argon on silver mordenite upto pressure of 1900Torr are given in Figure-1.8. The adsorption isotherms show the clear selectivity of argon over oxygen. The argon selectivity over oxygen increases with increase in the pressure. In the very low-pressure region, the silver exchanged mordenite is not capable to distinguish oxygen and argon.

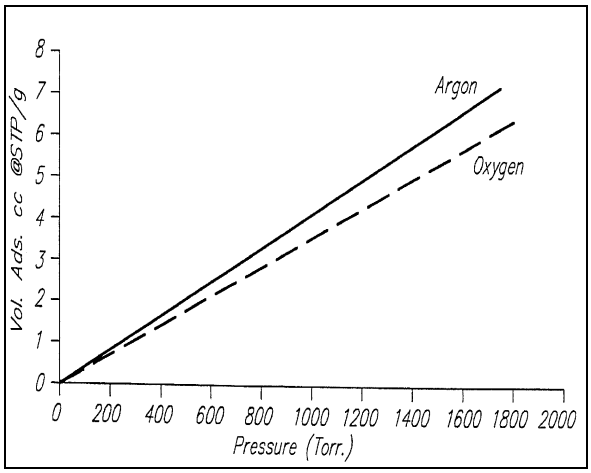

Figure-1.8. Ar and O_2 adsorption isotherms on silver mordenite [134]

The argon/oxygen selectivity observed is a typical property of the silver exchanged zeolites. This argon/oxygen selectivity is generally not observed for other cationic forms of the zeolites. The dependence of argon/oxygen selectivity on the extra framework cation in zeolite X is shown in Figure-1.9. The parent sodium form of the zeolite X shows little selectivity towards oxygen over argon. When the sodium ions are replaced with cations having high charge density, such as lithium or calcium, the

oxygen/argon selectivity increases. Replacement of sodium ions with lower charge density cations like potassium shows no selectivity towards oxygen or argon. But the complete replacement of the extra framework cations of the zeolite with silver cations results in clear selectivity of argon over oxygen.

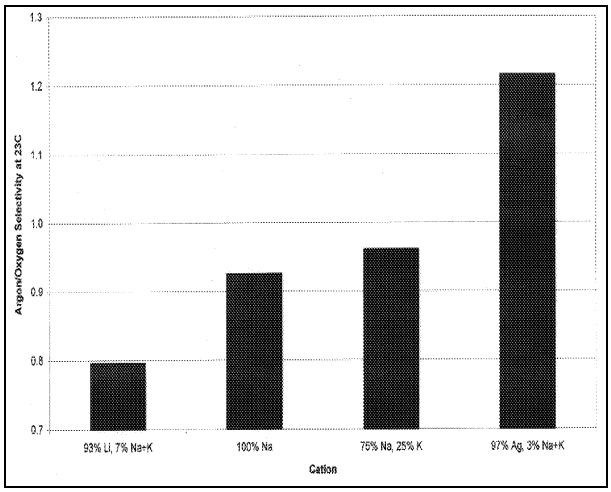

Figure-1.9. Ar/O_2 Selectivity Dependence on Cation [137]

Silver exchanged zeolite X having at least 80% of the extra framework cations are exchanged with silver ions is used for the production of high purity oxygen [134-135]. Zeolite X having a silver exchange level of 20-70% was used for the production of oxygen at purities above 97% by pressure swing / vacuum swing adsorption process [137]. The value of the argon/oxygen selectivity depends on the type of zeolite, extent of cation exchange, etc. The dependence of argon/oxygen selectivity on silver loading on zeolite X is shown in Figure-1.10.

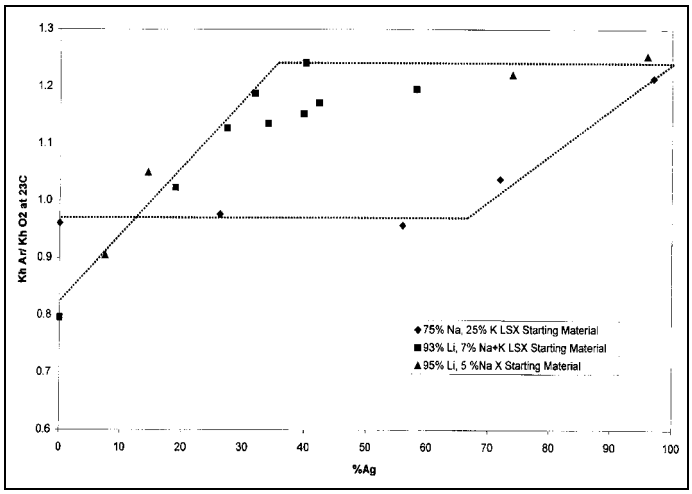

Figure-1.10. Ar/O_2 Selectivity vs Silver loading on Zeolite X [137]

1.5. OXYGEN SELECTIVE ADSORBENTS

The nitrogen/oxygen ratio in air is approximately 4, therefore, much less work will be needed to separate air by using oxygen selective adsorbent. The oxygen selective adsorbent selectively removes oxygen from the feed gas. The oxygen adsorption selectivity can be due to the combination of kinetic and steric factors or equilibrium effects. A carbon molecular sieve has been widely used for the nitrogen production by PSA. Zeolite A has also been used for the nitrogen production. O_2-binding transition metal complexes are also developed for the selective adsorption and separation of oxygen from air.

1.5.1. CARBON MOLECULAR SIEVES

Carbon molecular sieves (CMS) are a highly porous special type of activated carbons having uniform sized pores of molecular size range. The activated carbons separate molecules through differences in their adsorption equilibrium constants. In contrast, the most essential feature of the carbon molecular sieves is that they provide molecular separations based on rate of adsorption rather than on the differences in adsorption capacity. This behaviour is clearly evident in pressure swing adsorption (PSA) where gas dynamics dominate. The separation of nitrogen from air by PSA is the single most important application of CMS [138-167]. At the same conditions, the rate of adsorption is made up of atleast two important factors, the equilibrium uptake or capacity of the sieve, and the diffusivity, or rate of diffusion in the porous material. The relative diffusivity determines the degree of molecular sieving. In a mixture of two gases, when one molecule is excluded from entering a pore, the diffusivity is zero for that molecule and the degree of sieving is infinite for the other molecule. The extent of molecular sieving can be defined as the ratio of the rate of adsorption of one molecule to another.

The molecular sieving properties of CMS were derived from their unique pore structure. The basis of the kinetic oxygen selectivity is the more rapid diffusion of the smaller O_2 molecule through pore openings that are comparable in size to the molecular widths of O_2, N_2, and Ar (2.8Å, 3.0Å, and 3.84Å respectively). The difference in the kinetic diameters of oxygen and nitrogen is 0.2Å. The kinetic diameters of O_2, N_2 and Ar (3.46Å 3.64Å and 3.4Å) are often used to explain the kinetic selectivity of carbon molecular sieves. These values do not correlate to the

observed order of adsorption rates (O_2>N_2>Ar). Therefore, minimum molecular width is likely to be a better gauge of the rate-limiting dimension for adsorption into the 'slit-like' pore openings of carbon. The kinetic selectivity of the adsorbent is imparted or enhanced by nanowing the pore-mouth openings of the carbon micropores.

The production of nitrogen from air by PSA is largely based on the kinetic separation for oxygen due to the faster diffusion of the latter in carbon molecular sieve. Various types of carbon molecular sieves (CMS) have been prepared from the carbonaceous sources, such as coal [144], ligninocellulosic materials and biomass [145–148]. Tan et al utilised the palm shell to prepare carbon molecular sieve (CMS) by carbonisation for air separation [149]. They investigated the effect of different carbonisation temperatures on the pore structures and adsorptive properties for oxygen and nitrogen and their results showed that within 1min of time, one of the samples had shown excellent separation capability and very high O_2/N_2 selectivity. Oxygen and nitrogen adsorption uptake curves on palm shell-CMS samples after the carbonisation at 900^{o}C and 1000^{o}C are given in Figure-1.11.

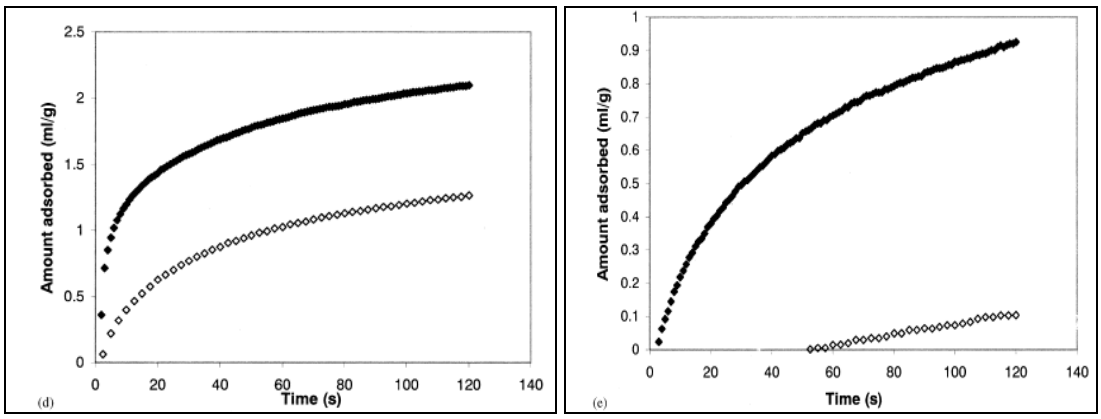

Figure-1.11. Oxygen and Nitrogen adsorption uptake curves on palm shell-CMS samples: (d) C900 and (e) C1000. Filled Symbol O_2; Unfilled N_2 [149]**.**

From the sorption uptake curves for oxygen and nitrogen, it is observed that oxygen is adsorbed to its equilibrium value much faster than nitrogen [138]. This is because oxygen molecule that is smaller in size (kinetic diameter 3.46 Å) diffuses much faster in carbon molecular sieve than nitrogen (kinetic diameter 3.64 Å). The diffusion time constant (D/r^2) for oxygen and nitrogen in carbon molecular sieve, as calculated from sorption uptake, are reported [138-143] to be 1.7×10^{-4} s^{-1} and 7×10^{-6} s^{-1}, respectively. Hence, oxygen gets selectively adsorbed in carbon molecular sieve adsorbent and nitrogen is collected as the high-pressure product.

Carbon molecular sieves used for air separation are made from activated carbon by post treatment that narrows the pore size distribution so that predominant pores are 3-4Å [10, 11, 19]. These sieves are able to distinguish the 0.2Å difference in molecular width between O_2 and N_2. Unlike zeolites, there are no cations present in carbon molecular sieves. Adsorption mainly occurs on defect sites and/or along the edges of basal planes of graphitic arrays. Carbon molecular sieves differ from activated carbon not only in terms of narrower and precise pore size distribution but also in actual surface compositions. Surface functionality like ketonic, carboxylic, phenolic groups normally observed on activated carbon surfaces is not detectable in carbon molecular sieves [19, 160].

The surface of CMS is non-polar or only slightly polar as a result of the surface oxide and inorganic impurities and does not contain any cations or charged centres for interacting with the adsorbate molecules. The heat of adsorption in CMS is lower compared to other adsorbents. There fore only the non-specific van der Waals forces are available as the force for adsorption. Thus the regeneration of the sorbent requires relatively lower energy. CMS are hydrophobic and are used for the separation of wet gas stream without dehydration.

General methods of manufacturing carbon molecular sieves involve [145-167] carbonisation of coal or nut hulls in inert atmosphere. Carbonised solids are activated in a reactive atmosphere like air or steam to generate porosity. Controlled deposition of carbonaceous material on pore entrance does further control the pore size of thus produced porous material. This is the key step in production of carbon molecular sieves and is mainly done by pyrolysis of benzene or furfuryl alcohol or olefins near the pore mouth.

Carbon molecular sieves based adsorption process has established [149] itself in the nitrogen separation area with more than 1500 commercial units operating world wide for producing nitrogen from a few litres per minute to 3000 Nm^3 per hour with a purity range of 95 to 99.999% by volume. Especially for uses requiring moderately pure nitrogen (>99.9%), PSA is most competitive. Presently 46% of the nitrogen produced is used in inerting of storage tanks, process lines, vessels etc. It is also being increasingly used in creating modified atmosphere to prolong storage life in food storage area. In fact, it can be an environmentally accepted replacement for food grain fumigants such as ethylene bromide. The nitrogen purity achieved with PSA is

of 99.9%. To obtain a higher purity, the residual oxygen is reacted with hydrogen on a palladium catalyst.

1.5.2. ZEOLITE MOLECULAR SIEVES

In the recent years, attempts are in progress to develop oxygen selective zeolites through molecular engineering of the starting zeolites [168-171]. Zeolite 4A is modified [172] by incorporating divalent iron and further by partly exchanging sodium with potassium cations. The Fe in the NaA forms terminal bonding such as -Si-O-Fe-, -Al-O-Fe-, etc. These types of bonding leads to a partial pore closure, which in turn results in a slower diffusion of nitrogen. It has been observed that incorporation of 0.5% of Fe as Fe (II) ion decreases the rate of nitrogen adsorption, simultaneously increasing the capacity of oxygen adsorption from 2.2cc g^{-1} to 3cc g^{-1} and to 3.8cc g^{-1} in the case of 1 % Fe containing NaA. The difference in the rates of adsorption increases with lowering temperature. If the Na^+ ions are replaced by K^+ ions the oxygen selectivity is further enhanced. Efforts are being made to improve the processes for air separation [168-173] using oxygen selective zeolites based on the different diffusivities for nitrogen and oxygen. In the sodium form of zeolite A (4A), the 8-membered windows of the zeolite are partially blocked by Na^+ cation, which reduces the free diameter to about 3.9Å. At ambient temperature, both nitrogen and oxygen are able to penetrate the 4A lattice at a rate, which is controlled by the intracrystalline diffusion. Intracrystalline diffusion in 4A is an activated process. Correlation of the diffusion energies of the small molecules in molecular sieve adsorbents with the van der Waals radius shows that the diffusion kinetics is largely controlled by the repulsive energy involved in during the passing of the molecules through the pores. Nitrogen and oxygen molecules have difference of 0.2Å in their van der Waals radii. It is interesting to observe that such a small difference in size is sufficient to cause an appreciable difference in the activation energies (23 and 18.5kJ mol^{-1} for N_2 and O_2 respectively) [174] and thus in diffusion coefficients.

The diffusivities for nitrogen, oxygen and argon in 4A at 30^oC as reported [175] are 3.6×10^{-9}, 3.8×10^{-11} and $8 \times 10^{-11} cm^2 s^{-1}$ respectively. The characteristic diffusion time for nitrogen and argon is 2-3 orders of magnitude longer than that of oxygen. In zeolite crystals, the diffusion time is in seconds for oxygen and in minutes for nitrogen. The characteristic diffusion time for oxygen in crystals is also much shorter than that of oxygen in pellets. This shows that the diffusion of oxygen in crystals is

the dominant step in the kinetic separation cycle. The equilibrium isotherms for nitrogen and oxygen in 4A zeolite at 25^{o}C show that the thermodynamic equilibrium is not favourable for kinetic separation because nitrogen, which is strongly adsorbed, has a lower diffusivity [175]. The equilibrium adsorption isotherms of N_2, O_2 and Ar on NaA at 288.2K are given in Figure-1.12 (a).

It has been reported widely that by calcination of NaA zeolites the adsorption preference towards oxygen over nitrogen is enhanced many folds, which can be attributed mostly to pore size shrinkage [176]. The calcined zeolite A pellets showed oxygen selectivity below 213K, while the powder form becomes oxygen selective only below 163K. This higher oxygen selectivity may also be due to the migration of cations from the binder during the calcination [177], which also prohibits the diffusion of N_2 molecules into the zeolite pores. By substitution of K over Na in A type zeolites forming Na-K-A the similar preferential adsorption of oxygen over nitrogen is again observed. The conventional theory suggests that the window diameter is reduced from 4Å to 3Å by the exchange of Na^+ at the 8-membered ring with K^+. Thus as the K^+ exchanged window would be anticipated not to allow both nitrogen and oxygen to enter into the pores of zeolite A, but the experimental results were quite surprising. The K^+ cations located at 8 membered rings get relocated to 6 membered ring [175] resulting into steric hindrance to nitrogen thereby facilitating adsorption of oxygen by a pressure swing operation. It is possible to increase the adsorption selectivity of oxygen over nitrogen by reducing the operating temperature below room temperature [179]. Partially zinc ion exchanged KA zeolite also shows oxygen selectivity over nitrogen at ambient temperatures. The oxygen adsorption capacity on ZnKA was greater than that of nitrogen and both amounts increased with increasing adsorption temperature [180]. The ZnKA with zinc ion exchange levels above 70% shows opposite adsorption behaviour, which is similar to those of NaA and CaA.

Nitrogen selective zeolite A was also converted to oxygen selective, without affecting the oxygen adsorption capacity, by depositing inert species like silica on the external surface of the zeolite to control the pore opening size. Liquid phase deposition [181-182] and chemical vapour deposition technique were used for controlling the pore opening size of the zeolites by the depositing silicon alkoxide [183-187]. The silicon alkoxide deposited on the external surface was converted into silica by thermal

treatment. Pore size controlled zeolite A adsorbs oxygen in preference to nitrogen and argon because of the decrease in the pore opening size. The nitrogen and argon adsorption capacities decreases on silica deposition, while that of oxygen remained unchanged on the pore size controlled zeolite A and separation of gas based on molecular size was obtained. The oxygen selectivity observed in silica deposited zeolites is kinetic selectivity not equilibrium selectivity. The observed adsorption selectivity of oxygen over nitrogen or argon are due to the difference in their adsorption rates which follow the order O_2>N_2>Ar, in consonance with order in their molecular sizes. The decreases in the nitrogen and argon adsorption capacities were proportional to the amount of silica deposited. The adsorption isotherms of nitrogen, oxygen and argon on zeolite NaA and 0.2% TEOS deposited NaA [181] is given in Figure-1.12.

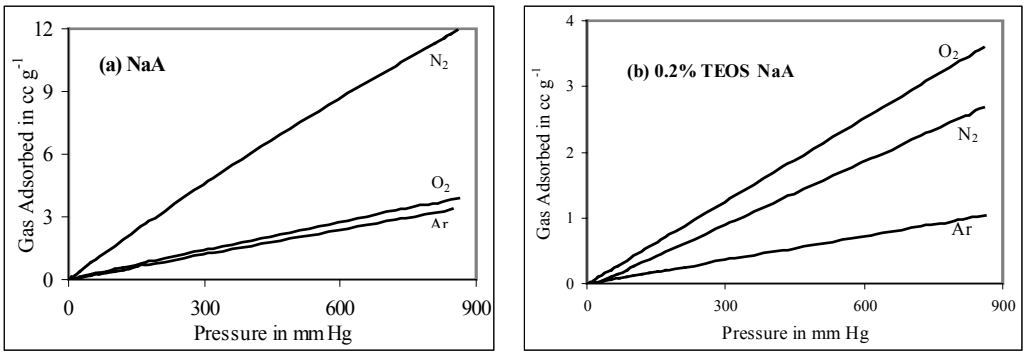

Figure-1.12. Adsorption isotherms on (a) NaA and (b) 0.2% TEOS deposited NaA at 288.2K

The framework of the titanosilicate molecular sieve, ETS-4 can be systematically contracted through dehydration at elevated temperature to tune the effective size of the pores giving access to the interior of the crystal. This molecular gate effect can be used to tailor the adsorption properties of the material to give size selective adsorbents [188-190] suitable for separation of gas mixture Ar/O_2 and N_2/O_2 [188]. This size shape selectivity is due to the contraction of the unit cell, which is associated with the loss of water molecules that are coordinated with the extra-framework cations. The cations have substantial effect on the temperature range over which shrinkage occurs. ETS-4 dehydrated at 270^oC allows N_2 molecules to adsorb inside the pores. Dehydration at 300^oC results in pore contraction to show the signs of nitrogen exclusion while smaller oxygen molecules can still penetrate into the crystal, resulting in an oxygen selective adsorbent. The typical dehydration behaviour of ETS-4 framework is shown in Figure-1.13.

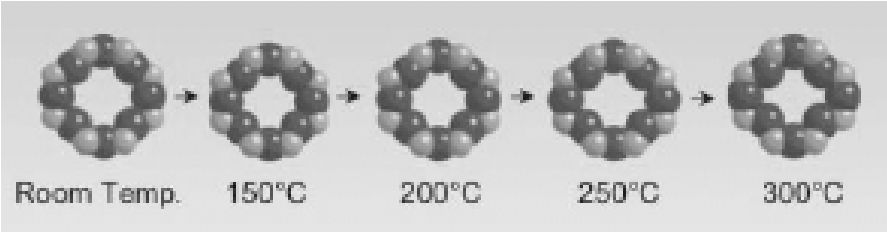

Figure-1.13. Size of the eight-ring pore opening in ETS-4 as a function of dehydration temperature [188]

Contraction of the eight-ring opening of ETS-4 as a function of dehydration temperature is given in Table-1.5. Distances are the pore-openings separating van der Waals radii between opposite O5 (D1), O1 (D2) and O2 (D3) atom pairs.

Table 1.5. Eight-ring opening as a function of dehydration temperature

Dehydration Temperature, °C	van der Waals opening (Å)		
	D1	D2	D3
RT	4.27	4.43	3.61
150	3.97	4.02	3.28
200	3.95	1.09	3.29
250	3.94	4.57	3.27
300	3.90	4.57	2.77

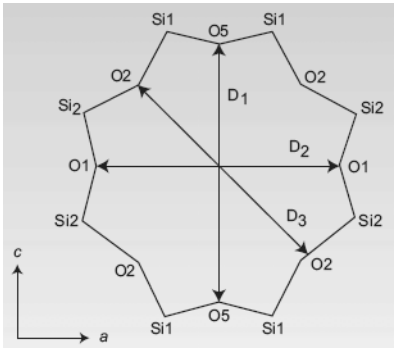

The proof that dehydration indeed does change the pore access is demonstrated by adsorption isotherms shown in Figure 1.14. The separation shown in the top of this figure, between O_2 and N_2, shows how precisely the pore sizes can be adjusted [188].

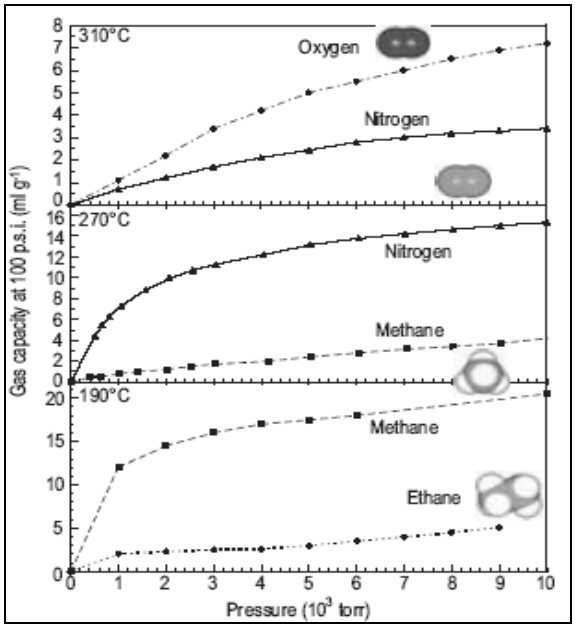

Figure-1.14. Adsorption of selected molecules as a function of dehydration temperature

Zeolite X containing cerium cations shows oxygen adsorption selectivity over nitrogen and argon [191]. But the selectivity is only in the low-pressure region [192]. The cerium-exchanged zeolite X shows very strong interaction with oxygen molecules and the isosteric heat of adsorption is as high as 60kJ mol^{-1} at zero coverage. The selective adsorption of oxygen in NaCeX over nitrogen and argon is due to the interaction of oxygen molecules with the non-stoichimetric cerium oxide formed between the cerium ions and the framework oxygen atoms during the vacuum dehydration process [182]. Oxygen selectivity for cerium exchanged zeolite X is better appreciated from the adsorption data at low equilibrium pressures shown in Figure-1.15. Rectilinear shape of the adsorption isotherm for oxygen indicates very strong interaction of oxygen molecules with zeolite surface in Henry region. Heat of adsorption for oxygen is substantially higher than that of nitrogen and argon confirming stronger interaction of oxygen with adsorbent surface.

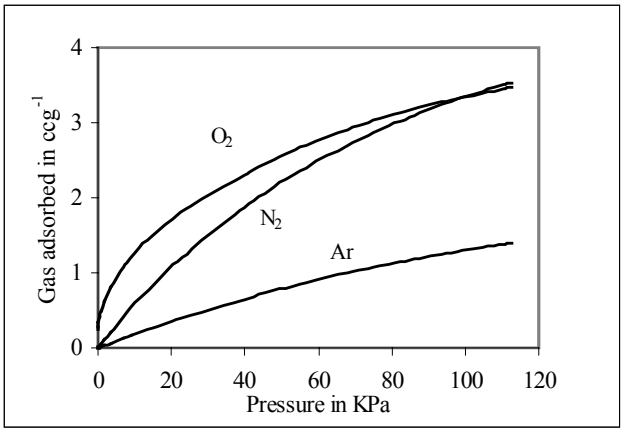

Figure-1.15. Adsorption isotherms on NaCeX at 288.2K [182]

During activation of the adsorbent under vacuum at higher temperature, CeO_{2-x} is formed as oxygen deficient atmosphere prevails inside zeolite cavities. On oxygen adsorption, the interaction of oxygen with CeO_{2-x} occurs to drive the reaction for forming CeO_2. The typical oxygen binding reversible reaction of CeO_{2-x} is as shown below:

$$CeO_{2-x} + \tfrac{1}{2}\, xO_2 \rightleftharpoons CeO_2$$

The very high heats of adsorption observed for oxygen show that the possibility of chemisorptions type interaction stated above taking place. As oxygen interacts strongly with CeO_{2-x}, even stronger than nitrogen molecules interaction with cerium cations, oxygen selective adsorption is observed at low coverage. However, following

the complete interaction of oxygen molecules with CeO_{2-x}, further interaction of oxygen and nitrogen occurs with Ce^{3+} or Ce^{4+} cations only and we know that nitrogen interacts strongly with these cations compared to oxygen and we observe reversal in adsorption selectivity from oxygen to nitrogen [182].

1.5.3. OXYGEN BINDING METAL COMPLEXES

Natural dioxygen complexes play a significant role in the absorption, transport and storage of dioxygen for respiration in biological systems. Natural dioxygen carriers can be divided into two main types: (i) the heme-containing proteins such as hemoglobin and myoglobin and (ii) the non-heme proteins such as hemerythrins and hemocyanins. These dioxygen carriers are generally dioxygen complexes in which dioxygen is coordinated to a metal ion firmly bound in a multidentate ligand. The oxygen free metal complex is named as prosthetic group. Hemoglobin and myoglobin consist of an iron (II) protoporphyrin prosthetic group associated with a protein part called globin. All vertebrates have hemoglobin in their blood cells and myoglobin in muscular tissue. Hemoglobin is also found in the root nodules of leguminous plants. Hemerythrins and hemocyanins, which are non-heme dioxygen carrying proteins containing iron and copper, respectively, in their corresponding prosthetic groups, are found in various types of terrestrial and marine invertebrates.

The chemistry of transition-metal complexes capable of reacting reversibly with the dioxygen molecule is now a fast developing area of science, with numerous families of oxygen binding species having been developed [193-196]. However, despite this enormous effort, the practical utility of synthetic dioxygen carriers has been very limited, primarily due to the occurrence of rapid, irreversible decomposition reactions that lead to short working lifetimes for the complexes, making commercial development economically nonviable. It has been shown that the lifetime of the dioxygen adducts may be increased dramatically by removing them from solution and binding them to a support in the solid state. This is not a new idea – the first identification of a synthetic dioxygen carrier based on iron was reported by Wang as long ago as 1958, when he supported a mixture of the diethyl ester of iron (II) protoporphyrin and ethyl imidazole in a polystyrene matrix [197]. Since then, there have been many other reports concerning supported complexes, using both organic polymers and functionalised silica as supports [198]. The study of the synthetic reversible oxygen carrier complexes is important to biological system and industrial

processes. The reversible binding of the dioxygen with protein complexes are of critical importance to advanced and primitive forms of animal life because these proteins can bind, transport, store and release dioxygen. The structures and properties of these proteins are of interest to chemists who design and study the metal complexes as models for oxygen transport. Synthetic oxygen binding complexes have promising application for separation of oxygen from air. The success of dioxygen complexes for oxygen separation depends on several critical factors, which includes, (i) long-term reversibility of oxygen uptake, (ii) fast complexation and regeneration of the complex, (iii) stability in the presence of moisture, (iv) high equilibrium capacity for oxygen uptake and (v) capability for the ligand to be synthesised easily from low-cost precursors, which impact the cost of the dioxygen complex.

There are several transition metal complexes of transition metals like cobalt [218-275], manganese [276-312], iron [313-330], copper [331-345], nickel [346], ruthenium [347], chromium [348], molybdenum [350-354], etc. known to be reversibly bind oxygen in solution or solid form. These metal complexes bind dioxygen molecules in solution or solid form at or above room temperature. The synthesis of adsorbents using these complexes are also done by ship-in-a-bottle concept wherein oxygen selective metal complexes are synthesised inside the cavities / pores of microporous solids like zeolites. It is known that certain metal complexes with appropriate ligands reversibly bind oxygen [194] as shown in equation below:

$$nM(L) + O_2 \rightleftharpoons [M(L)_n]O_2$$

$$n = 1 \text{ or } 2$$

To make use of such complexes for oxygen separation, metal complex-oxygen adduct reaction needs to be reversed by increasing the temperature of the adduct or by lowering the partial pressure of oxygen or by the addition of a ligand capable of replacing the bound oxygen. The absorption by these complexes is reversible with changes in temperature and pressure so that it is theoretically possible to achieve separation or concentration of oxygen by means of a temperature swing or a pressure swing cycle of the air.

Binding of oxygen molecule to metal centre may form two types of species namely superoxo (I) and peroxo (II) as shown below.

(1:1) (2:1) (1:1) (2:1)

I **II**

Monomeric (1:1) and dimeric (2:1) metal-oxygen adduct form with both superoxo and peroxo binding. However monomeric adducts are found to be more active for reversible binding of oxygen. Examples for these superoxo and peroxo types of metal-oxygen adduct are shown in Table-1.6.

Table-1.6. Oxygen Adduct of some Metal Complexes

Name of Complex	Type of Complex	M: O
Co(bzacen)(py)(O_2)	Superoxide-like	1:1
Fe(TpivPP)(1-Melm)(O_2)	-do-	-do-
Cr(TPP)(py)(O_2)	-do-	-do-
$[Co_2(NH_3)_{10}(O_2)]^{5+}$	-do-	1:2
$[Co_2(CN)_{10}(O_2)]^{5-}$	-do-	-do-
Ir(CO)(PPh_3)$_2$(Cl)(O_2)	Peroxide-like	1:1
Ti(OEP)(O_2)	-do-	-do
$[Co_2(NH_3)_{10}(O_2)]^{+}$	-do-	1:2
$[Co_2(CN)_{10}(O_2)]^{6-}$	-do-	-do-

The reversible uptake of oxygen by cobalt complexes in solutions, aqueous as well non-aqueous, has been extensively studied with a view to understanding the binding and activation of oxygen. However, the synthesis of these complexes in the porous cavities of microporous solids like zeolites and the use of such systems for air separation is an area of recent interest. The three-dimensional pore structure of zeolites provides the possibility of site isolation; stabilize complexes by anchoring them to the lattice by co-ordination to framework oxygen. Synthesizing these complex inside the cavities of a zeolite inhibits the dimerisation and irreversible oxidation of the complex, which occurs in the solutions. The typical adsorption isotherms of

nitrogen and oxygen on zeolite NaY and metal complex encapsulated zeolite Y at ambient temperature are shown in Figure-1.16.

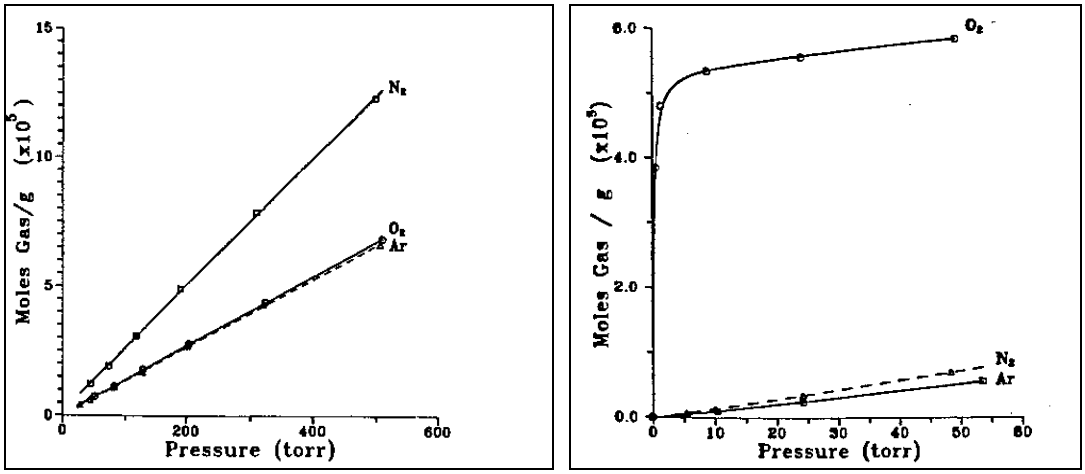

Figure-1.16. Adsorption isotherms on zeolite NaY and metal complex encapsulated zeolite Y

It has been observed that to synthesise reversible oxygen adduct, it is necessary to have metal ions that have oxidation potential lying in a certain range so that there is some donation of electron to the oxygen molecules but not enough to cause irreversible oxidation of the metal. This shows that the metal like Cr (II) that are readily oxidized react with oxygen irreversibly and the metal like Ni (II) that are difficult to oxides do not react with oxygen. However, metal like Co (II) having redox potential lying between the two limiting redox potentials react reversibly with oxygen. This is the reason that Co (II) complexes are most studied for reversible oxygen binding. Four coordinate Co (II) complexes are poor oxygen absorbers whereas five coordinate chelates readily bind oxygen at ambient pressure of oxygen.

1.5.3.1. Metal Complexes of Cobalt

Co (II) complexes are the most extensively studied metal complexes both in solution and solid state. The binding of dioxygen to cobalt (II) chelate complexes of Schiff base and cyclidene lacunar has been studied extensively. The oxygen binding characteristics of these complexes are very dependant upon the preparation and pre-treatment of the sample, as well as the purity of the starting material. Cobalt (II) Schiff base complexes are classified into two types; type A and B, based on the oxygen binding property. Complexes of type A absorb up to 0.5 mol of O_2/mol of cobalt, the oxygenated complex forming μ–peroxo dimeric species with the dioxygen

being peroxo-like. Type B complexes can absorb up to 1.0 mol of O_2/mol of cobalt, the oxygenated complex being monomeric and the dioxygen moiety superoxo like. Both type A and B complexes are paramagnetic in the unoxygenated state. On oxygenation, type A complexes become diamagnetic and type B complexes reduce their paramagnetism from three unpaired electron to one.

The use of Co (II) metal complexes with ligands like amines, cyanide and bi- or ter-pyridine dispersed in zeolites has been encouraging and has led to some perspective on metal complexes based oxygen selective adsorbent development. These complexes have enhanced reversible oxygen binding, as the active species are mono dispersed in the zeolite cavities and thus retarding binuclear complexes formation. However, these systems have a major disadvantage, as the number of mono or bidentate ligands surrounding the Co (II) cation is not easily controlled. The use of polydentate ligands like salen and tetren was reported to overcome this problem. D. E. De Vos et al. [237-238] has studied tetravalent as well pentavalent ligands in zeolite Y and in EMT. With the use of tetradentate salen and acacen ligand in zeolites CoNaY, low concentration of oxygen binding Co (II) species is reported. Incorporation of nitrogen base into these schiff bases results in the pentadentate ligands smdpt and amdpt, which has enhanced concentration of oxygen binding Co (II) species. Co (II) Schiff base complexes have also been immobilized in porous organic hosts and have been found to bind oxygen at room temperature.

In the last few years, the subject of polymer-supported dioxygen carriers has grown in importance largely due to advances in the area of membrane technology as applied to gas separation because such systems offer the potential of a selective extraction mechanism for O_2 from the atmosphere [218]. Several groups have reported work in the area [219], with the extensive work of Tsuchida et al., using cobalt (R) porphyrin complexes being particularly noteworthy [220]. Recently studies on the reversible binding of dioxygen to the 'lacunar' family of complexes supported on various copolymer matrices [221]. The lacunar complexes were originally developed by Busch and co-workers and are excellent species to use in studies of stability to autoxidation because it is possible to vary systematically the steric and electronic properties of the ligand by varying the nature of the groups on the ligand periphery [222]. The ease of structural variation allows fine-tuning of the complex to achieve the desired physical properties for the carrier molecule. A wealth of data exists

concerning the oxidative stability and the dioxygen affinity of various cobalt (R) lacunar complexes in solution and found that the copolymer- supported dioxygen adducts of these species show particularly good stability to oxidation, in favourable cases with half-lives of the order of 30days at room temperature [222]. Figure-1.17 represents the oxygen and nitrogen adsorption isotherms on Co (3,5-di-tert-BusalDAP) measured at 0^oC [210].

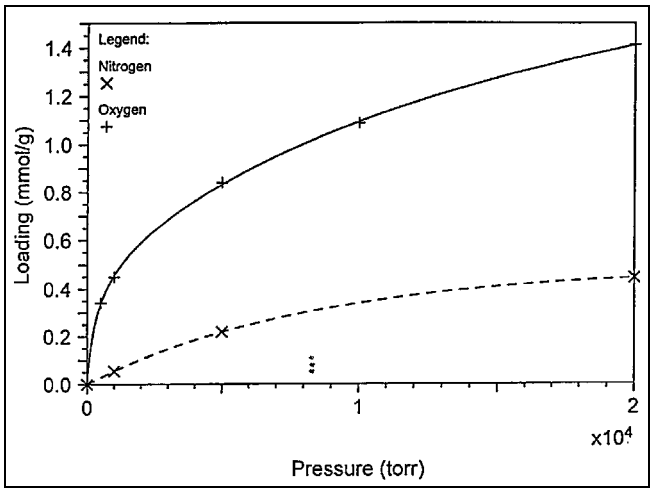

Figure-1.17. O_2 and N_2 adsorption isotherms on Co (3,5-di-tert-BusalDAP) at 0^oC

Several studies [214-215, 225-228] have been carried out for modifying oxygen-binding capacity of Co (II) complexes by attaching suitable ligands to the metal inside the zeolite. Five coordinated Co (II)-amine complexes $[Co(II)L_x]$-Y with L= ammonia, methylamine, and n-propylamine in zeolite-Y formed six coordinated oxygen adducts $[Co(III)\ LxO_2^-]^{2+}$. Both with ammonia and methylamine, monomeric (1:1) and also dimeric (2:1) Co-oxygen adduct can be formed whereas with n-propylamine only 1:1 adduct is observed [225]. With ethylenediamine (en) monomeric 1:1 oxygen adducts $[Co\ (III)\ (en)_2O_2^-]^{2+}$ formed are found sufficiently stable in the presence of O_2 up to 70ºC in zeolite X and Y [214]. The mixed-ligand bipyridine-terpyridine complex in zeolite Y formed the oxygen adduct $[Co\ (III)\ (bpy)(tpy)O_2^-]^{2+}$ in the presence of 30 Torr of O_2 which was found to be completely reversible at 298K and was thermally stable in the presence of O_2 up to 343K [226]. In partially Co-exchanged LiY, this mixed complex can be obtained in higher concentration [227]. These complexes have been characterized by EPR spectroscopy. The close similarity between the EPR parameters of 1:1 adducts of CoY and in frozen solution or the solid state suggests that the structure is the same. The monomeric 1:1

oxygen adducts are superoxo species where the unpaired electron is largely localised on the oxygen molecule [215, 225].

These Co (II) complexes involve neutral ligands and though effective for separating oxygen from air, coordination of water as a sixth ligand or oxidation of the ligand limits their utility [227]. Drago and coworkers [222-224] overcame these problems by reporting an anionic, oxygen selective Co-cyanide complex, $[Co(CN)_5]^{3-}$ within zeolite Y. This adsorbent is stable to repeated cycling in air. Even at low concentration of complex loading in the zeolite, adsorbent was observed to increase the amount of oxygen adsorbed by more than twice over argon at 100Torr. It has shown that by exchanging Cs^+ ion into Co-Na-Y prior to the addition of cyanide, the active $Co(CN)_5^{3-}$ complex is formed inside the zeolite at higher concentration. An equilibrium constant for oxygen binding of 18 ± 2$Torr^{-1}$, with an oxygen binding cobalt species concentration of 43 ± 4micro mol g^{-1} material was reported [223]. Very high oxygen affinity of these complexes results in a high oxygen adsorption capacity and very high oxygen/nitrogen selectivity value of 5000. Air products Inc. has reported [268-275] the synthesis of lithium cyanocobaltate which when used as such has highest reported oxygen capacity (55cc g^{-1}) for any solid adsorbent at ambient temperature. Polymeric cyanocobaltate, $Li_3Co(CN)_5.4DMF$ was observed to bind O_2 reversibly at ambient temperature. Dioxygen equilibrium absorption isotherms on $Li_3Co(CN)_5$ .1.42 DMF. 0.48 DMAC and $Li_3Co(CN)_5$ .2.0 DMF at 25°C are given in Figure-1.18.

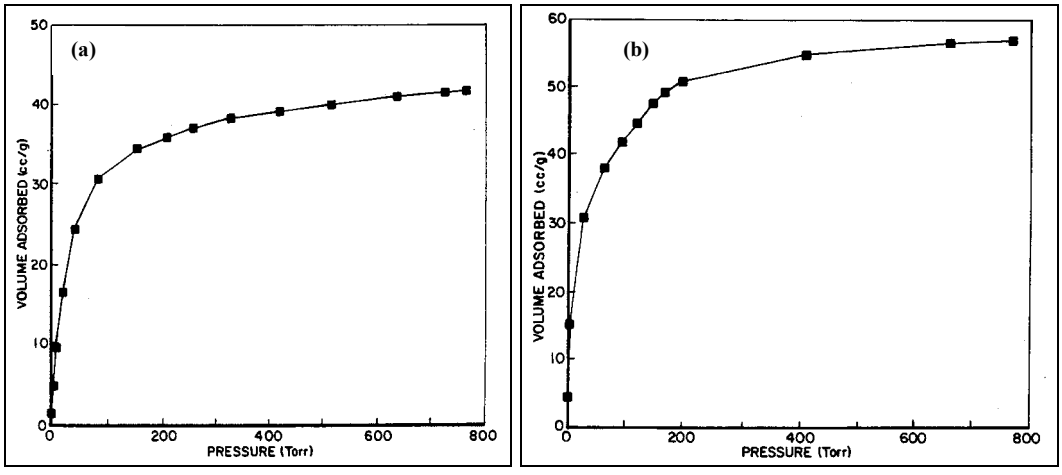

Figure 1.18. Dioxygen equilibrium absorption isotherms at 25°C for (a) $Li_3Co(CN)_5$ .1.42 DMF. 0.48 DMAC and (b) $Li_3Co(CN)_5$ .2.0 DMF [273]

This complex loses two DMF molecules on heating up to 160^{o}C to produce a complex $Li_3Co(CN)_5$.2DMF. This complex was found to have higher capacity for oxygen than the one with four DMF molecules and was also reported to bind O_2 at a faster rate. For example, $Li_3Co(CN)_5$.2DMF sorbs about 7 wt% O_2 in 10 minutes and purging with N_2 releases more than 90% of the adsorbed oxygen in 30 minutes. However, there are two drawbacks of this material, which do not make these complexes attractive for commercial application. For example, its capacity is sensitive to moisture and on repeated cycling use; there is a loss in its activity.

1.5.3.2. Metal Complexes of Manganese

The interaction of manganese with dioxygen has been considered to be important in a number of processes of biological and industrial importance. Therefore model manganese compounds have been employed in order to study their interaction with dioxygen and these studies have led to the discovery of many dioxygen carriers. The chemistry of tetra dentate Schiff base manganese (II) complexes and their interaction with dioxygen have been extensively studied [276-279]. Titus et al. prepared a series of manganese (II) complexes with different number of CH_2 groups in the ligand bridge and found the oxygenation reaction to be a function of the methylene carbon chin [280] length so that only C_6-C_{10} derivatives react with dioxygen both in solution and solid state, while all others react only when moist, dissolved in pyridine or suspended in dimethyl sulphoxide. Coleman and Taylor [281-283] reported the preparation and characterisation of some manganese (II) complexes employing a series of Schiff base pentadentate O_2N_3 ligands. These complexes quickly reacted with dioxygen or air when dissolved or suspended in a solvent. Heating these oxygenated complexes in vacuum at 110^{o}C librated the oxygen with the generation of the manganese (II) precursors. The manganese complexes of other potentially pentadentate ligands with donor sets of O_2N_3, O_3N_2 and O_2SN_2 derived from substituted aldehydes and polyamines have also been studied [283].

The first manganese system that involves solely oxygen donor groups from the ligand is believed to be tris (3,5-di-tert-butylcatecholato) manganese (III), [Mn(III) $(dtbc)_3^{3-}$], an oxidation product of which Mn (III) $(cat)_2$ $(semiquinone)_2$ $(OH)^{3-}$ was reported to bind dioxygen reversibly in dimethyl sulphoxide solution [284]. At room temperature, similar results are obtained in N, N-dimethylformamide and N, N-dimethylacetamide,

but the reversibility is optimal in acetonitrile. Magers et al. has investigated this interesting system and found that this reaction was affected by concentration, acidity, dioxygen partial pressure, moisture and light [285]. Cooper and Hartman claimed that [Mn (IV) $(dtbc)_3^{2-}$] does not bind dioxygen reversibly. This result has been reconfirmed by more spectroscopic results by Chin and Sawyer. The Mn (IV)-dtbc complex represents an interesting new category of dioxygen carriers in which electron transfer from the catecholato ligand to molecular oxygen is necessary for binding.

The phthalocyanine complexes of manganese have been studied for many years. Barrett et al. first reported that a pyridine solution of Mn (II) phthalocyanine absorbed dioxygen, the colour changing from olive green to dark blue [286]. Boiling the solution regenerated the olive green colour and the cold solution absorbs further amounts of dioxygen and becomes dark blue. Lever et al established the formation of a superoxo complex on oxygenation of MnPc in N, N-dimethylacetamide solution [287], and a similar result has been obtained for a tetrasulphonated phthalocyanine derivative [288]. The solution of the dioxygen adduct can be converted into the μ-oxo species by the addition of either imidazole or N-methylimidazole.

The oxygen binding properties of a series of manganese porphyrins complexes are studied and have shown that these complexes act as reversible oxygen carriers at low temperatures [311]. The structure of the oxygen adduct was studied by spectroscopic methods and showed the Griffith mode of coordination for the O_2 molecule [289-392].

A large number of manganese (II) tertiary phosphine complexes of general formula $MnLX_2$ (L = tertiary phosphine, but not PPh_3 and X=Cl, Br, I, NCS) have prepared and characterised [293-299]. These compounds can bind dioxygen reversibly in a manner that resembles the properties of hemoglobin and myoglobin. The $MnLX_2$ complexes are pale in colour, but on exposure to dioxygen they rapidly become deeply coloured. In addition to the $MnLX_2$ complexes, complexes with the general formula MnL_2X_2 have been prepared. These complexes were also shown to bind dioxygen reversibly in both the solid state and in solution, and the reactivity towards oxygen appears to be dependent on the phosphine. Solid-state isotherms for the $MnLX_2$ complexes have a remarkable similarity to those of the natural dioxygen carriers, hemoglobin and myoglobin.

The hindered ligand, $HB(3,5\text{-}iPr_2pz)^{3-}$, is useful in preparing manganese complexes modelling the active sites of manganese proteins. Di-p-hydroxo manganese complex $[Mn(HB(3,54Pr_2pz)_3)](OH)_2$ synthesised by Kitajima et al. might serve as a model for the reduced states of ribonucleotide reductase and catalase; both proteins are known to have a dimanganese site. Such a unit may exist in the poly manganese site in the oxygen-evolving centre (OEC) in photosynthetic system I1 (PSII).

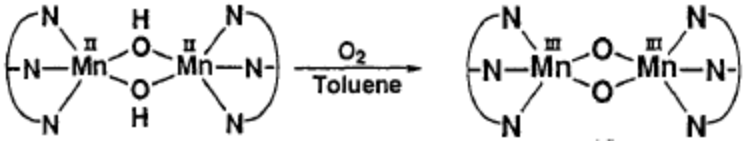

The complex reacts with dioxygen giving two main products, a five-coordinate di-p-oxo dimanganese(II1) complex, $[Mn(HB(3,5\text{-}iPr_2pz)_3)](O)$ and a dimanganese (III) complex**,** where one of the isopropyl groups in each tris(pyrazoly1)borate ligand is first hydroxylated and then coordinated as an alkoxo ligand [300-301].

1.5.3.3. Metal Complexes of Copper

Copper-dioxygen interactions are important and essential in biological and industrial processes. Multidentate ligands with N-donor atoms are known to impart O_2-reactivity to the resulting Cu (I) complexes. Besides the μ–1,2 (end-on Cu--Cu ≅ 4.3Å) and the $\mu\text{-}\eta^2\text{:}\eta^2$ (side on Cu--Cu ≅ 3.6Å) dicopper (II)- peroxo complexes, Cu_n/O_2 reactions can also be lead to Cu (III)-bis-μ-oxo species ($Cu_n\text{-}(O)_2$, n = 2 or 3). Spectroscopic and structural studies show that a diversity of $Cu_n\text{-}O_2$ binding modes exists. The different types of $Cu_n\text{-}O_2$ binding modes are as shown below.

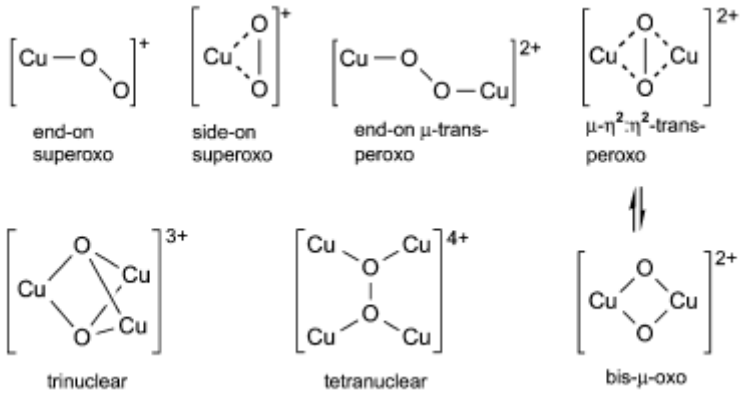

Research group of Tolman [302-303] and Stack [304-305] have demonstrated that using different tridentate or bidentate alkyl amine ligands, and depending on conditions (i.e. solvent, counter anion) a given Cu (I) compound can react with O_2 to form both the μ-η^2:η^2 peroxo- or the bis-μ-oxo-dicopper (III) cores (Cu--Cu $\cong$ 2.7Å) and these species may be in rapid equilibrium [305]. Liang et al. studied the copper (I) complexes of tridentate ligands AN (3,3′-iminobis (N, N-dinethylpropylamine)) and MeAN (N, N, N', N', N"-penta methyl dipropyl amine)) [316]. Two complexes, namely $[Cu^{I}\ (MeAN)]^{+}$ and $[Cu^{I}\ (AN)]^{+}$ formed differ drastically in their dioxygen adducts. The first one, i.e. $[Cu^{I}\ (MeAN)]^{+}$ reacts with dioxygen at 193K giving essentially only the μ-η^2:η^2 side on complex $[(Cu^{II}\ (MeAN))_2(O_2)]^{2+}$. While only the μ-oxo species $[(Cu^{III}\ (AN))_2\ (O)_2]^{2+}$ is obtained with $[Cu^{I}\ (AN)]^{+}$.

Hemocyanin (Hc) is a dioxygen carrier for arthropods and molluscs and its active site is composed of a pair of copper ions to which dioxygen is bound symmetrically as a peroxide ion. Oxy-Hc has been characterized by abnormally low ν(O-O) frequency (ca. 750 cm^{-l}), two absorption bands at ca. 350nm (-20000/2Cu) and ca. 580nm (-1000) and diamagnetism due to the strong magnetic coupling between two copper (I1) ions. On the basis of magnetism, it has been long believed that an endogenous bridging ligand (X) other than dioxygen exists between two copper ions and dioxygen is bound in a cis-coordination mode as shown below [313].

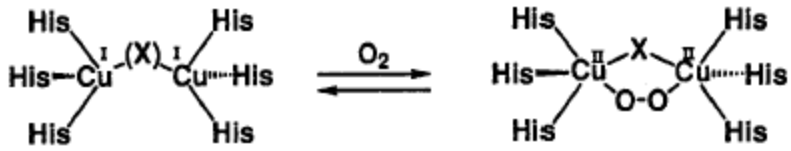

1.5.3.4. Metal Complexes of Iron

Hemoglobin (Hb) and myoglobin (Mb) are heme proteins responsible for dioxygen storage and transport in biological systems. In the deoxy forms of both Hb and Mb the heme iron is bound to a single, 'proximal', axial imidazole resulting in a five-coordinate high-spin (S = 2) Fe^{II}; upon oxygenation at the opposite 'distal' face, a diamagnetic $Fe^{III}O_2^{-}$complex forms reversibly. The protein superstructure is responsible for the kinetic stabilization of the oxygenated form. The controlled interaction of dioxygen with iron (II) complexes in a reversible manner analogous to

that of the hemoproteins, myoglobin and hemoglobin has been an elusive goal for transition metal co-ordination chemist for many years.

Since the earliest claim of Kunz and Kress in 1927 [331] until 1973 no confirmed examples of reversible dioxygen binding by a synthetic iron (II) system existed, despite considerable activity in the area. In 1973, two groups succeeded in their pioneering work on the generation and characterisation of iron (II) dioxygen complexes [332-333]. Baldwin's group made use of sterically restricted iron (II) complex of a 14-membered unsaturated macrocycle in the belief that the steric bulk attached to the macrocycle periphery would serve the function of the globin portion of myoglobin and prevent irreversible oxidation of the metal ion occurring via μ–peroxo dimmer formation [332]. The approach proved moderately successful in that the complex appeared to reversibly bind dioxygen in dry toluene at –80^{o}C. However, at -50^{o}C the complex irreversibly oxidised with a half-life of minutes. Following the same approach, Collman's and other groups [333] developed sterically encumbered porphyrin complexes, which functionalised as excellent reversible O_2 carriers even at room temperature, although only in non-aqueous solvents. In light of the relative success of these two approaches to oxygen binding, porphyrins-based model systems have been developed for dioxygen binding [334].

Iron (II) dimethylglyoxime [335] is the first synthetic oxygen carrying chelate reported that do not have cobalt as the co-ordinating atom. It dissolves in 50% aqueous dioxane solutions containing added bases such as pyridine, ammonia, histidine or imidazole. In the pH range of 7-11, the reaction with oxygen proceeds. The reaction can be reversed readily by bubbling nitrogen through the solution.

Herron et al. [336] synthesised a wide range of non-porphyrin iron dioxygen carriers having lacunar macrobicyclic ligands and they have been shown to be remarkable reversible dioxygen carriers. One heavily substituted complex reversibly binds dioxygen at 20^{o}C and even at 37^{o}C considerable reversibility persists.

As the structural analogue of nonheme iron oxygen carrier, hemerythrin (Hr), a five-coordinate carboxylato iron (II) complex Fe(PhCOO)(HB(3,5-iPr_2pz)$_3$) was prepared using hydrotris (3,5-diisopropyl- 1-pyrazolyl) borate. The complex reacts with a variety of o-donor such as pyridine to form a stable adduct, whereas it does not interact with CO as just like Hr. It was found that this complex binds dioxygen reversibly at -20^{o}C in toluene [337].

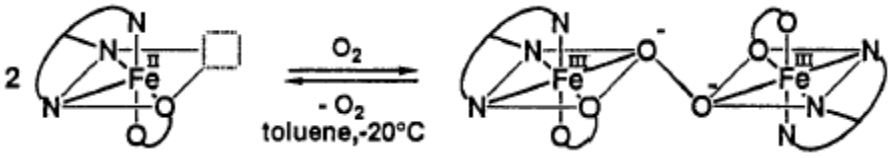

The dioxygen adduct was characterized by dioxygen consumption stoichiometry and by spectroscopic methods, UV-Vis, resonance Raman and EXAFS, by which the adduct was identified as a peroxo diiron (III) complex.

1.5.3.5. Metal Complexes of Others Transition Metals

Strong alkaline solution of nickel (II) dimethylglyoxime reversibly binds oxygen. This was the first nickel oxygen carrier appeared in the literature [346]. Desorption of oxygen was accomplished by either increasing the temperature, decreasing the pressure or flushing with argon.

The reversible binding of dioxygen at room temperature to tetraphenylporphinato- and octaethylporphinatoruthenium (II) complexes have been reported [347]. Solutions of $Ru(OEP)(CH_3CN)_2$ in DMA, DMF or pyrrole are observed to absorb 1.0mol of O2 for each ruthenium metal centre at room temperature and 1 atm O_2. At constant pressures, the reaction follow pseudo-first order behaviour with the value of $t_{½}$ being reported as ~1min (DMA), ~7min (pyrrole) and ~30 min (DMF). However, solutions of $Ru^{II}(OEP)(B)_2$, where B= pyridine or 1-methylimidazole in presence of oxygen, result only in irreversible oxidation of ruthenium centre to a Ru(III) species.

The synthesis of chromium dioxygen adduct, $Cr(TPP)(py)(O_2)$ from solid five co-ordinate $Cr^{II}(TPP)(py)$ represents a logical extension of metalloporphyrin complexes containing bivalent first row transition metal ions [348]. Chromous porphyrins bind oxygen strongly and irreversibly and the co-ordinated oxygen has a superoxide like structure.

The catalytic oxygenation reactions involving molybdenum have produced some complexes having dioxygen ligand [349]. Several such reactions of molybdenum porphyrins complexes with dioxygen species (O_2^- or O_2^{2-}) have been studied. Rohbock and Buchler reported that the paramagnetic μ–oxo dimmer of [$\{Mo^{IV}O$ $(oep)\}_2$ (μ-O)] was eventually formed by the reaction of $[Mo^{IV}O$ (oep)] with O_2 [350]. Hoshino et al. reported that a paramagnetic dioxygen complex was formed in the

reaction of [$Mo^{IV}O$ (tpp)] with O_2 at room temperature [351]. Diamagnetic dioxygen complexes are detected by studying the reaction of [$Mo^{IV}O$ (tpp)] with O_2 at temperatures around –70^oC [352]. Tachibana et al. prepared a molybdenum (VI) 5,10,15,20-tetramesitylporphyrin dioxygen complex at room temperature. Desorption of the dioxygen was achieved either by photo irradiation of the toluene solution with visible light or by heating the solid sample at 40-90^oC [353]. The crystal structure of the reversible molecular oxygen carrying molybdenum porphyrins complex $Mo^{IV}O$ (tmp) (O_2) was determined by Fujihara et al. [354] and found that the oxo and dioxygen ligands are co-ordinated with cis conformation, which leads to a saddle like distortion of the porphyrin ring.

1.6. REFERENCES

[1] R. M. Barrer, *Proc. Roy. Soc. A*, 1937, **161**, 476.

[2] R. M. Barrer, *Proc. Roy. Soc. A*, 1938, **167**, 393.

[3] L. E. Drain, *Trans Faraday Soc.* 1953, **49**, 650.

[4] G. L. Kington and A. C. Macleod, *Trans Faraday Soc.* 1959, **55**, 1799.

[5] R. M. Milton, *U. S. Pat. No. 2,882,243*, 1959.

[6] C. W. Skarstrom, *U. S. Pat. No. 2,944,627*, 1960.

[7] P. Guerin de Montgareuil and D. Domine, *U. S. Pat. No. 3,155,468*, 1964.

[8] R. V. Jasra, N. V. Choudary and S. G. T. Bhatt, *Sep. Sic. Tech.,* 1991, **26**, 885.

[9] R. V. Jasra and S. G. T. Bhatt, *Chemical Industry Digest,* 1995, **3**, 89.

[10] R. T. Yang, *Gas Separation by Adsorption Process*, Imperial College Press, 1997.

[11] R. T. Yang, *Adsorbents: Fundamentals and Applications*, Wiley Interscience, New York, 2003.

[12] D. M. Ruthven, *Principles of adsorption and adsorption Processes,* John Wiley and Sons Inc, New York, 1984

[13] G. Reiβ, *Gas Sep. Purif*. 1994, **8**, 95.

[14] B. Tyagi, C. D. Chudasama and R. V. Jasra, *Indian chemical society*, 2001, **78**, 551.

[15] S. Sircar, *Ind. Eng. Chem. Res*., 2002, **41**, 1389.

[16] S. U. Rege and R. T. Yang, *Ind. Eng. Chem. Res*., 1997, **36**, 5358.

[17] R. Kumar, *Separation Science and Technology*, 1996, **31**, 877.

[18] A. R. Smith and J. Klosek, *Fuel processing technology*, 2001, **70**, 115.

[19] T. R. Gaffney, *Current Option in Solid State and Material Science*, 1996, **1**, 69.

[20] J. O. Hirschfelder, C. F. Curtiss and R. B. Bird, *Molecular Theory of Gases and Liquids*, John Wiley and Sons, New York, 1954.

[21] F. Notaro: *"Advances in Ambient Temperature Air Separation",* Munich Meeting on Air Separation Technology, Oct. 10–11, 1996, 227.

[22] C. H. Simpson, *Chemicals from the Atmosphere,* Doubleday and Co., Garden City, New York 1969. (Chemical process).

[23] F. Notaro, M. W. Ackley and J. Smolarek, *Chemical Engineering*, 1999, 104.

[24] A. M. M. Mendes, C. A. V. Costa and A. E. Rodrigues, *Separation and Purification Technology* 2001, **24**, 173.

[25] D. Bathen, *Separation and Purification Technology* 2003, **33**, 163.

[26] D. T. Kearns and P. A. Webley, *Chemical Engineering Scienc*e 2004, **59**, 3537.

[27] R. W. Triebe and F. H. Tezel, *Gas Separation and Purification* 1995, **9**, 223.

[28] W. H. Isalski: *Separation of Gases,* Clarendon Press, Oxford, 1989.

[29] D. W. Breck, *Zeolite Molecular Sieves,* Wiley-Inter Science, New York, 1978.

[30] R. M. Barrer, *Zeolites and Clay Minerals as Sorbents and Molecular Sieves*, Academic Press, London, 1978.

[31] L. Puppe and G. Reiss, *U. S. Pat. No. 4,950,312*, 1990.

[32] G. Reiss, *U. S. Pat. No. 5,114,440,* 1992.

[33] L. B. Batta, *U. S. Pat. No. 3,564,816*, 1971.

[34] J .J. Collins, *U. S. Pat. No. 4,026,680*, 1977.

[35] C. G. Coe, J. E. MacDougall and S.J. Weigel, *U. S. Pat. No. 5,354,360*, 1994.

[36] D. H. Olson, *Zeolites*, 1995, **15**, 439.

[37] D. W. McKee, *U. S. Pat. No. 3,140,933*, 1964.

[38] H. W. Habgood, *U. S. Pat. No. 2,843,219*, 1958.

[39] H. W. Habgood, *Canadian J. Chem.* 1964, **42**, 2340.

[40] N. H. Berlin, *U. S. Pat. No. 3,313,091*, 1967.

[41] C. G. Coe and S. M. Kuznicki, *U. S. Pat. No., 4,481,018*, 1984.

[42] S. Sircar, R. R. Conrad and W. J. Ambs, *U. S. Pat. No. 4,557,736*, 1985.

[43] C. C. Chao, *U. S. Pat. No. 5,454,857*, 1995.

[44] G. Reiss, L. Puppe and B. Hees, *U. S. Pat. No. 5,656,066*, 1997.

[45] C. C. Chao, *U. S. Pat. No. 5,698,013*, 1997.

[46] C. G. Coe and S. M. Kuznicki, *U. S. Pat. No. 4,544,378*, 1985.

[47] N. V. Choudary, R. V. Jasra and S. G. T. Bhat, *U. S. Pat. No. 6,030,916*, 2000.

[48] C. C. Chao, *U. S. Pat. No. 4,859,217*, 1989.

[49] S. A. Butter and S. M. Kuznicki, *U. S. Pat. No. 4,606,899*, 1986.

[50] J. F. Kirner, *U. S. Pat. No. 5,268,023*, 1993.

[51] J. T. Mullhaupt and P. C. Stephenson, *U. S. Pat. No. 5,441,557*, 1995.

[52] A. J. Caglione, T. R. Cannan, N. Greenlay and R. J. Hinchey, U. *S. Pat. No. 5,366,720*, 1993.

[53] G. H. Khul and H.S. Sherry, *UK Pat. No. GB 1,580,928*, 1980.

[54] G. H. Khul, *Zeolites*, 1987, **7**, 451.

[55] F. W. Leavitt, *U. S. Pat. No. 5,074,892*, 1991.

[56] S. Yoshida, S. Hirano, A. Haeada and M. Nakana, *Microporous and Mesoporous Materials* 2001, **46**, 203.

[57] C. C. Chao, J. D. Sherman, J. T. Mullhaupt and C. M. Bolinger, *U. S. Pat. No. 5,174,979*, 1992.

[58] C. G. Coe, J. F. Kirner, R. Pierantozzi and T. R. White, *U. S. Pat. No. 5,152,813*, 1992.

[59] C. G. Coe, J. F. Kirner, R. Pierantozzi and T. R. White, *U. S. Pat. No. 5,258,058*, 1993.

[60] C. C. Chao; Chien, J. D. Sherman, J. T. Mullhaupt and C. M. Bolinger, *U. S. Pat. No. 5,413,625*, 1995.

[61] C. G. Coe, J. F. Kirner, R. Pierantozzi and T. R. White, *U. S. Pat. No. 5,417,957*, 1995.

[62] C. G. Coe, J. F. Kirner, R. Pierantozzi and T. R. White, *U. S. Pat. No. 5,419,891*, 1995.

[63] F. R. Fitch, M. Bulow and A. F. Ojo, *U. S. Pat. No. 5,464,467*, 1995.

[64] N. Ogawa, S. Hirano and K. Itabashi, *U. S. Pat. No. 5,868,818*, 1999.

[65] C. C. Chao and S. J. Pontonio, *U. S. Pat. No. 6,425,940*, 2002.

[66] J. B. Kim, H. Jo, H. Yoshioka and H. Kiyama U. S. Pat. No. 6,761,754, 2004.

[67] R. T. Yang, Y. D. Chen, J.D. Peck and N. Chen, *Ind. Eng. Chem. Res.*, 1996, **35**, 3093.

[68] N. Chen and R. T. Yang, *Ind. Eng. Chem. Res.* 1996, **35**, 4020.

[69] R. T. Yang and N. D. Hutson, *PCT Pat. No. WO 00/40332*, 2000.

[70] N. D. Hutson, D. A. Reisner, R. T. Yang and B.H. Toby, *Chem. Matter*, 2000, **12**, 3020.

[71] N. D. Hutson, S.U. Rege and R. T. Yang, *AIChE Journal*, 1999, **45**, 724.

[72] M. W. Ackley, S. U. Rege and H. Saxena, *Microporous and Mesoporous Materials,* 2003, **61**, 25.

[73] W. N. Chen, and R. T. Yang, in *Recent Developments in Separation Science*, (N. N. Li and J. M. Calo, eds.), 1984, Vol. IX, CRC Press, Boca Raton, Florida.

[74] H. Minato and T. Tamura in *Natural Zeolites, Occurrence, Properties, Use,* L. B. Sand and F. A. Mumpton (ed), Pergamon Press, Oxford, 1978, 509.

[75] L. J. Smith, H. Eckert and A. K. Cheetham, *J. Am. Chem. Soc.* 2000, **122**, 1700.

[76] N. V. Choudary, R. V. Jasra and S. G. T. Bhat, *Indian Journal of Chem.*, 1999, **39A**, 34.

[77] A. D. Stefanis, G. Perez, E. Semprini, F. Stefani and A.A.G. Tomlinson, *Microporous and Mesoporous Materials* 2004, **71**, 103.

[78] S. Furuyama and K. Sato, *J. Phys. Chem*. 1984, **88**, 1735.

[79] S. Furuyama and M. Nagato, *J. Phys. Chem.* 1982, **86**, 2498.

[80] C. G. Coe and D. A. Roberts, *U. S. Pat. No. 4,732,584*, 1988.

[81] C. G. Coe, T. R. Gaffney and R. S. Srinivasan, *U. S. Pat. No. 4,925,460*, 1990.

[82] C. G. Coe, T. R. Gaffney, R. Srinivasan and T. Naheiri, *Separation Technology*, E. F. Vansnat (ed.), 1994, 267.

[83] P. J. Maroulis, C. G. Coe, S. M. Kuznicki, P. J. Clark and D. A. Roberts, *U. S. Pat. No. 4,744,805*, 1988.

[84] P. J. Maroulis, C. G. Coe, S. M. Kuznicki and D. A. Roberts, *U. S. Pat. No. 4,747,854*, 1988.

[85] R. J. Neddenriep, *J. Colloid Interface Sci.*, 1968, **28**, 293.

[86] C. G. Coe, S. M. Kuznicki, R. Srinivasan, and R. J. Jenkins, R. J., in *Perspectives in Molecular Sieve Sciences*, W. H. Flank, and T. E. Whyte, Jr., eds. *ACS Symp. Series*, 1988, 368, 478.

[87] B. L. Su, M. Bulow, J. L. Blin, A. F. Ojo, S. Jale, D. Shen, Q. M. Wang and F. R. Fitch, *U. S. Pat. No. 6,350,298*, 2002.

[88] C. C. Chao, *U. S. Pat. No., 4,964, 889*, 1990.

[89] G. Aguilar-Armenta, G. Hernandez-Ramirez, E. Flores-Loyola, A. Ugarte-Castaneda, R. Silva-Gonzalez, C. Tabares-Munoz, A. Jimenez-Lopez and E. Rodriguez-Castellon, *J. Phys. Chem. B.*, 2001, **105**, 1313.

[90] C. G. Coe, T. R. Gaffney, H. X. Li, Y. Xiong, J. A. Martens and P. A. Jacobs, *U. S. Pat. No. 5,562,756*, 1996.

[91] A. F. Ojo, F. R. Fitch and M. Bulow, *U. S. Pat. No. 5,616,170*, 1997

[92] J. E. Mac Dougall, T. A. Braymer, C. G. Coe, T. R. Gaffney and B. K. Peterson, *U. S. Pat. No. 5,882,625*, 1999.

[93] Y. Kuroda, R. Kumashiro, A. Itadani, M. Nagao and H. Kobayashi, *Phys. Chem. Chem. Phys.* 2001, **3**, 1383.

[94] Y. Kuroda, T.Okamoto, R. Kumashiro, Y. Yoshikawa and M. Nagao, *Chemical Communications,* 2002, 1758.

[95] Y. Kuroda, A. Itadani, R. Kumashiro, T. Fujimoto and M. Nagao, *Phys. Chem. Chem. Phys.* 2004, **6**, 2534.

[96] A. Itadani, R. Kumashiro, Y. Kuroda and M. Nagao, *Thermochimica Acta,* 2004, **416**, 99.

[97] C. C. Chao, *European Pat. No. 0,297,542*, 1989.

[98] R. V. Jasra, N. V. Choudary, and S. G. T. Bhat, *Ind. Eng. Chem. Res.*, 1996, **35**, 4221.

[99] N. V. Choudary, R. V. Jasra and S. G. T. Bhat, *Ind. Eng. Chem. Res.,* 1993, **32**, 548.

[100] D. Shen, M. Bulow, S. R. Jale, F. R. Fitch and A. F. Ojo, *Microporous and Mesoporous Materials*, 2001, **48**, 211.

[101] M. Bülow, *Studies in Surface Science and Catalysis,* 1994, **83**, 209

[102] D. Shen and M. Bülow, *Microporous and Mesoporous Materials,* 1998, **22**, 237.

[103] S. Savitz, A.L. Myers and R.J. Gorte, *Microporous and Mesoporous Materials* 2000, **37**, 33.

[104] H. W. McRobbie, *U. S. Pat. No. 3,140,931*, 1964.

[105] R. V. Jasra, N. V. Choudary and S. G. T. Bhat, *Indian J. Chem.*, 1995, **34A**, 15.

[106] N. V. Choudary, R. V. Jasra and S. G. T. Bhat, *Studies in Surface Science and Catalysis*, 1994, **84B**, 1247.

[107] R. V. Jasra, N. V. Choudary, K. V. Rao, G. C. Pandey, and S. G. T. Bhat, *Chem. Phys. Lett.*, 1993, **211**, 214.

[108] D.Shen, M.Bülow and N.O Lemcoff, *Adsorption,* 2003, **9**, 295.

[109] D. Shen, M. Bülow, F. Siperstein, M. Engelhard and A. L. Myers, *Adsorption,* 2000, **6**, 275.

[110] M. Bülow and F. R. Fitch, *Filtration and Separation,* 1997, **34**, 839.

[111] M. Bülow, D. Shen and S. Jale, *Applied Surface Science,* 2002, **196**, 157.

[112] M. Bülow, *Adsorption,* 2002, **8**, 9.

[113] O. Talu, J. Li, R. Kumar, P. M. Mathias, J. D. Moyer Jr. and J. M. Schork, *Gas. Sep. Purif.* 1996, **10**, 149.

[114] S. R Jale, D. Shen, M. Bülow, and F. R. Fitch, *Studies in Surface Science and Catalysis,* 2002, **142B**, 1995-2002

[115] Y. Lü and M. Bülow, *Adsorption,* 2000, **6**, 125.

[116] Y. Lü, S. J. Doong and M. Bülow, *Adsorption,* 2003, **9**, 337.

[117] V. B Kazansky, M. Bülow and E. Tichomirova, *Adsorption,* 2001, **7**, 291.

[118] H. Herden, W. D. Einicke, R. Schollner, W. J.Morter, L. R. Gellens and J. B. Uytterhoeven, *Zeolites*, 1982, **2**, 131.

[119] H. Herden, W. D. Einicke, R. Schollner and A. Dayer, *J. Inorg. Nucl. Chem.*, 1981, **43**, 2533.

[120] H. Herden, W. D. Einicke and R. Schollner, *Inorganic Chem.,* 1987, **43**, 2538.

[121] M. Feuerrstein, G. Engelhardt, P. L. McDaniel, J. E. Dougall and T.R. Gaffney, *Microporous and Mesoporous Materials,* 1998, **26**, 27.

[122] M. Feuerstein and R.F. Lobo, *Chem. Matter*, 1998, **10**, 2197.

[123] M. Feuerstein and R. F. Lobo, *Chem. Commun*. 1998, 1647.

[124] W. J. Mortier, H. J. Bosmans and J. B. Uytterhoeven, *J. Phys. Chem.,* 1972, **76**, 650.

[125] W. J. Mortier, *Compilation of Extra framework Sites in Zeolites,* Butterworths, Surrey, 1982.

[126] M. D. Baker, J. Godber, K. Helwing and G. A. Ozin, *J. Phys. Chem.,* 1988, **92**, 6017.

[127] C. G. Coe and S. M. Kuznicki, *European Pat. No. 109,063*, 1984.

[128] N. D. Hutson, S. C. Zajic and R. T. Yang, *Ind. Eng. Chem. Res.* 2000, **39**, 1775.

[129] J. Hua, Z. Bi-Ying and X. You-Chang, *Acta Physico - Chimica Sinica*, 2002, **18**, 577.

[130] D. T. Friesen, W. C. Babcock, D. J. Edlund and W. K. Miller, *U. S. Pat. No. 5,225,174*, 1993.

[131] D. T. Friesen, W. C. Babcock, D. J. Edlund, D. K. Lyon and W. K. Miller, *U. S. Pat. No. 5,516,745*, 1996.

[132] D. T. Friesen, W. C. Babcock, D. J. Edlund, D. K. Lyon and W. K. Miller, *U. S. Pat. No. 6,136,222*, 2000.

[133] D. T. Friesen, W. C. Babcock, D. J. Edlund, D. K. Lyon and W. K. Miller, *U. S. Pat. No.* 6,077,457, 2000.

[134] A. I. Kandybin, Anderson and D. L. Reichley, *U. S. Pat. No. 5,470,378*, 1995.

[135] A. I. Kandybin, Anderson and D. L. Reichley, *PCT Pat. No. WO 94/06541*, 1994.

[136] K. S. Knaebel and A. I. Kandybin, *U. S. Pat. No. 5,226,933*, 1993.

[137] R. L. Chiang, R. D. Whitley, J. E. Ostroski and D. P. Dee, *U. S. Pat. No. 6,432,170*, 2002.

[138] F. Wolf and P. Koenig, *Z. Chem.*, 1974, **14**, 320.

[139] K. Knoblauch, *Chem. Eng.*, 1978, **85**, 87.

[140] K. Knoblauch, *German Pat. No. 3,168,426*.

[141] K. Knoblauch and H. Heimbach, *Ger. Offen. 2,932,333*, 1981.

[142] K. Knoblauch, H. Juntgen, K. Knoblauch and K. Harder, *Fuel*, 1981, **60**,817.

[143] K. Knoblauch, F. Tarnow and H. Heimbach, *U. S. Pat. No. 4,880,765*, 1989.

[144] K. Miura and J. Hayashi, *Carbon*, 1991, **29**, 653.

[145] Z. Hu and E.F. Vansant, *Carbon*, 1995, **33**, 561.

[146] C. Nguyen and D.D. Do, *Carbon*, 1995, **33**, 1717.

[147] J. Hayashi, *Carbon,* 1999, **37**, 524.

[148] T. S. Farris, C. G. Coe, J. N. Armor and J. M. Schork, *U. S. Pat. No. 5164355*, 1992.

[149] J. S. Tan and F. N. Ani, *Separation and Purification Technology*, 2004,**35**, 47.

[150] H. Juntgen, *Carbon*, 1977, **15**, 273.

[151] C. Marumo, E. Hayata and N. Shiomi, *U. S. Pat. No. 4,933,314*, 1990.

[152] S. Moreau, B. Sardan and P. Ehrburger *U. S. Pat. No. 5,411,577*, 1995.

[153] T. C. Golden, W.C. Kratz and M. N. Mead, *U. S. Pat. No. 5,447,557*, 1995.

[154] T. R. Gaffney, T.S. Farris, A. L. Cabrera and J. N. Armor, *U. S. Pat. No. 5,098,880*, 1992.

[155] T. S. Farris, C. G. Coe, J. N. Armor and J. M. Schork, *U. S. Pat. No. 5,164,355*, 1992.

[156] T. Yamamoto, A. Endo, T. Ohmori and M. Nakaiwa, *Carbon,* 2004, **42**, 1671.

[157] T. C. Golden, P. J. Battavio, Y. Chen, T. S. Farris and J. N. Armor, *U. S. Pat. No. 5,135,548*, 1992.

[158] S. Sircar, T. C. Golden and M. B. Rao, *Carbon,* 1996, **34**, l.

[159] Z. Hu and E. F. Vasant, *Carbon*, 1995, **33**, 561.

[160] H. C. Foley, *Microporous Materials*, 1995, **4**, 407.

[161] J. S. Tan and F. N. Ani, *Separation and Purification Technology,* 2004, **35**, 47.

[162] J. C. Tao, *Gas Separation by Adsorption Technology*, edited by E. F. Vasant 1994, Elesevier Science B.V.

[163] S. Villar-Rodil, A. Martınez-Alonso and J. M. D. Tascon, *Journal of Colloid and Interface Science*, 2002, **254**, 414.

[164] S. U. Rege and R. T. Yang, *Adsorption*, 2000, **6**, 15.

[165] Y. D. Chen, R. T. Yang and P. Uawithya, *AIChE Journal*, 1994, **40**, 577.

[166] Y. D. Chen and R. T. Yang, *Ind. Eng. Chem. Res.* 1994, **33**, 3146.

[167] Y. D. Chen and R. T. Yang, *Chemical Engineering Science*, 1992, **47**, 3895.

[168] D. G. Schalles and R. P. Danner, *AIChE Symposium Series*, 1988, **84**, 83.

[169] N. Haq and D. M. Ruthven, *J. Colloid Interface Sci.*, 1986, **112**, 154.

[170] Z. J. Pan, R. T. Yang and J.A. Ritter in *New Directions in Sorption Technology*, (G. E. Keller and R. T. Yang, eds.), Butterworths, 1989.

[171] D. M. Ruthven, in *Gas Separation Technology*, (E. F. Vansant and R. Dewolfs, eds.), Elesevier, Amsterdam, 1990.

[172] J. Izumi, *European Pat. No. 0,040,935*, 1981.

[173] H. S. Shin and K. S. Kneabel, *AIChE Journal*, 1988, **34**, 1409.

[174] G. E. Keller and C. A. Kuo, *U. S. Pat. No. 4,354,859,* 1982.

[175] N. Oka, J. Izumi and M. Suzuki, *Adsorption*, 2000, **6**, 149.

[176] J. Izumi and M. Suzuki, *Adsorption*, 2000, **6**, 23.

[177] J. Izumi and M. Suzuki, *Adsorption*, 2001, **7**, 27.

[178] R. V. Jasra, B. Tyagi, Y. M. Badheka, N.V. Choudary and S. G.T. Bhatt, *Ind. Eng. Chem. Res.,* 2003, **42**, 3263.

[179] J. Izumi, H. Tsutaya, T. Amitani, M. Kubo and K. Maehara, *U. S. Pat. No. 4,453,952*, 1984.

[180] M. Iwamoto, K. Yamaguchi, Y. Akutagawa and S, Kagawa, *J. Phys. Chem.* 1984, **88**, 4195.

[181] R. V. Jasra, C. D. Chudasama, J. Sebastian, *U.S. Pat. Published Appn. No. 20040192537*, 2004.

[182] C. D. Chudasama, *Ph. D. Thesis*, Bhavnagar University, 2003.

[183] M. Niwa, K. Yamazaki and Y. Murakami, *Ind. Eng. Chem. Res*., 1991, **30**, 38.

[184] M. Niwa, K. Yamazaki and Y. Murakami, *Chemistry Letters*, 1989, 441.

[185] M. Niwa, M. Kato, T. Hattori and Y. Murakami, *J. Phys. Chem.* 1986, **90**, 6233.

[186] M. Niwa, S. Kato, T. Hattori and Y. Murakami, *JCS Faraday Trans. I*, 1984, **80**, 3135.

[187] D. Ohayon, R. L. V. Mao, D. Ciaravino, H. Hazel, A. Cochennec and N. Rolland, *Applied Catalysis A: General*, 2001, **217**, 241.

[188] S. M. Kuznicki, V. A. Bell, S. Nair, H. W. Hillhouse, R. M. Jacubinas, C. M. Braunbarth, B. M. Toby and M. Tsapatsls, *Nature,* 2001, **412**, 720.

[189] G. Guan, K. Kusakabe and S. Morooka, *Separation Science and Technology*, 2002, **37**, 1031.

[190] S. M. Kuznicki, V. A. Bell, I. Petrovic and B. T. Desai, *U. S. Pat. No. 6,068,682*, 2000.

[191] N. V. Choudary, R. V. Jasra and S. G. T. Bhatt, *U. S. Pat. No. 6,087,289*, 2000.

[192] A. Jayraman, R. T. Yang, S. H. Cho, S. G. T. Bhat and N. V. Choudary, *Adsorption*, 2002, *8*, 271.

[193] G. Q. Li and R. Govind, *Ind. Eng. Chem. Res.,* 1994, **33**, 755.

[194] R. D. Jones, D. A. Summerville and F. Basolo, *Chemical Reviews*, 1979, **79**, 139.

[195] L. H. Vogt, Jr., H. M. Faigenbaum and S. E. Wiberly, *Chem. Rev*., 1963, **63**, 269.

[196] R. A. Friesner, M. H. Baik, B. F. Gherman, V. Guallar, M. Wirstam, R. B. Murphy and S. J. Lippard, *Coordination Chemistry Review*s 2003, **238-/239**, 267.

[197] J. H. Wang, *J. Am. Chem. Soc*., 1958, **80**, 3168.

[198] O. Leal, D. L. Anderson, R. G. Bowman, F. Basolo and R. L. Burwell, *J. Am. Chem. Soc.* 1975, **97**, 5125.

[199] S. E. Watkins, D. C. Craig and S. B. Colbran, *J. Chem. Soc*., *Dalton Trans*., 2002, 2423.

[200] A. L. Cabrera and J. N. Armor, *U. S. Pat. No. 5,071,450*, 1991.

[201] D. T. Friesen, W. K. Miller, B. M. Johnson and D. J.Edlund, *U. S. Pat. No. 5,266,283*, 1993.

[202] D. L Roberts and R. M. Laine, *U. S. Pat. No. 4,605,475*, 1986.

[203] F. A. Walker, *J. Am. Chem. Soc*., 1970, **92**, 4235.

[204] J. T. F. Wong, *U. S. Pat. No. 4,064,118*, 1977.

[205] J. T. Mullhaupt, N. A. Stephenson and P. C. Stephenson, *U. S. Pat. No. 5,945,079*, 1999.

[206] J. Bonaventura and C. Bonaventura, *U. S. Pat. No. 4,343,715*, 1982.

[207] K. Sugie, *U. S. Pat. No. 4,985,053*, 1991

[208] K. C Morris, P. Bonsen and M. B. Laver, *U. S. Pat. No. 4,061,736*, 1977.

[209] M. G. Simmons and L. J. Wilson, *J. Chem. Soc. Chem. Commun*, 1978, 634.

[210] N. A. Stephenson and P. M. C. Stephenson, *U. S. Pat. No.6,183,709*, 2001.

[211] P. Bonsen, M. B. Laver and K. C. Morris, *U. S. Pat. No. 4,001,200*, 1977.

[212] P. Bonsen, M. B. Laver and K. C. Morris, *U. S. Pat. No. 4,001,401*, 1977.

[213] Q. M. Wang, D. Shen, M. L. Lau, M. Bulow, F. R. Fitch, N. O. Lemcoff and P. Connolly, *U. S. Pat. No. 6,436,171*, 2002.

[214] R. F. Howe and J. H. Lunsford, J. *Phy. Chem.*, 1975, **79**, 1836.

[215] R. W. Triebe and F. H. Tezel, *Gas. Sep. Purif.* 1995, **9**, 223.

[216] S. Imamuro and J. H. Lunsford, *Langmuir*, 1985, **1**, 326.

[217] S. Moreau and C. Barbe, *U. S. Pat. No. 5,672,195*, 1997.

[218] P. Meares, in: *Membranes in Gas Separation and Enrichment*, Royal Society of Chemistry, London, 1986.

[219] M. S. Delaney, D. Reddy and R.A. Wessling, *J. Membrane Sci*., 1990, **49**, 15.

[220] H. Nishide, T. Suzuki, Y. Soejima and E. Tsuchida, *Macromol. Symp*. 1994, **80**, 145.

[221] J.H. Cameron, H.B. Harvey and A. McKee, *Transition Met. Chem.* 1996, **21**, 85.

[222] D.H. Busch, S.C. Jackels, R.C. Callahan, J.J. Grzybowski, L.L. Zimmer, M. Kojima, D.J. Olszanski, W.P. Schammel, J.C. Stevens, K.A. Holter and J. Mccak, *Inorg. Chem.* 1981, **20,** 2834.

[223] R. J. Taylor, R. S. Drago and J. E. George, *J. Am. Chem. Soc.* 1989, **111**, 6610.

[224] R. S. Drago, I. Bresinska, J. E. George, K. Balkus, Jr., and R. J. Taylor, *J. Am. Chem. Soc.* 1988, **110**, 304.

[225] R. F. Howe and J. H. Lunsford, J. *Am. Chem. Soc.*, 1975, **97**, 5156.

[226] D. E. De Vos, F. Thibault-Starzyk and P. A. Jacobs, *Angew. Chem. Int. Ed. Engl.* 1994, **33**, 431.

[227] R. J. Taylor, R. S. Drago and J. P. Hage, *Inorg. Chem*. 1992, **31**, 253.

[228] K. Mizuno, S. Imamuro and J. H. Lunsford, *Inorg. Chem.* 1984, **223**, 3510.

[229] N. Herron, *Inorg. Chem*., 1986, **25**, 4714.

[230] C. Bazzicalupi, A, Bencini, E. Berni, A. Bianchi, C. Giorgi, P. Paoletti and B. Valtancoli, *Ind. Eng. Chem. Res*. 2000, **39**, 3484.

[231] M. Shinoura, S. Kita, M. Ohba, H. Okawa, H. Furutachi and M. Suzuki, *Inorg. Chem.* 2000, **39**, 4520.

[232] A. C. Sharma and A.S. Borovik, *J. Am. Chem. Soc.*, 2000, **122**, 6946.

[233] C. Comuzzi, A. Melchior, P. Polese, R. Portanova and M. Tolazzi, *Inorg. Chem.* 2003, **42**, 8214.

[234] A. G. Kolchinski, B. K. Daszkiewicz, E. V. R. Akimova, D. H. Busch, N. W. Alcock and H. J. Clase, *J. Am. Chem. Soc.*, 1997, **119**, 4160.

[235] J. F. Krebs and A. S. Borovik, *Chem. Commun*. 1998, 553.

[236] D. E. De Vos, E. J. P. Feijen, R. A. Schoonheydt and P. A. Jacobs, *J. Am. Chem. Soc.*, 1994, **116**, 4746.

[237] S. Imamuro and J. H. Lunsford, *Langmuir*, 1985, **1**, 326.

[238] E. V. Rybak-Akimova, K. Marek, M. Masarwa and D. H. Busch, *Inorganica Chemica Acta*, 1998, **270**, 151.

[239] P. K. Dutta and C. Bowers, *Langmuir*, 1991, **7**, 937.

[240] H. Chen, A. Matsumoto, N. Nishimiya, T. Takeichi, and K. Tsutsumi, *Microporous and Mesoporous Materials* 2000, **40**, 289.

[241] M. Huber, L. Bubacco, M. Beltramini, B. Salvato, H. Elias, J. Peisach, E. Larsen, S. E. Harnung and W. Haase, *Inorganic Chemistry*, 1996, **35**, 7482.

[242] J. H. Bowen, N. V. Shokhirev, A. M. Raitsimring, D. H. Buttlaire and F. A. Walker, *J. Phys. Chem. B.* 1997, **101**, 8683.

[243] A. G. Kolchinski, N. W. Alcock and D. H. Busch, *Inorganic Chemistry*, **36**, 2754.

[244] E. V. Rybak-Akimova, W. Otto, P. Deardorf, R. Roesner and D. H. Busch, *Inorganic Chemistry*, **36**, 2746.

[245] H. Furutachi and H. Okawa, *Bull. Chem. Soc. Jpn.* 1998, **71**, 671.

[246] K. Yamanari, T. Kawamoto, Y. Kushi, T. Komorita and A. Fuyuhiro, *Bull. Chem. Soc. Jpn.* 1998, **71**, 2635.

[247] B. Steiger, J. S. Baskin, F. C. Anson and A. H. Zewail, *Angew. Chem. Int. Ed.* 2000, **39**, 257.

[248] M. J. Barnes, R. S. Drago and K. J. Balkus Jr. *J. Am. Chem. Soc.* 1988, **110**, 6780.

[249] Y. Inaba and Y. Kobuke, *Tetrahedron,* 2004, **60**, 3097.

[250] J. Gao, R.A. Zingaro and M. Z. Gao, *Polyhedron,* 2004, **23**, 59.

[251] S. Cabani, *Reactive and Functional Polymers,* 1996, **28**, 167.

[252] N. Ceccanti, R. Pardini , F. Secco, M. R. Tine, M. Venturini, A. Bianchi and P. Paoletti, *Polyhedron,* 2000, **19**, 2447.

[253] A. Bencini, A. Bianchi, C. Giorgi, P. Paoletti, B. Valtancoli, N. Ceccanti and R. Pardini, *Polyhedron,* 2000, **19**, 2441.

[254] C. Bazzicalupi, A. Bencini, A. Bianchi, C. Duce, P. Fornasari, C. Giorgi, P. Paoletti, R. Pardini, M. R. Tinè and B. Valtancoli, *Dalton Trans.* 2004, 463.

[255] J. H. Cameron, S. Graham, H. B. Harvey, J. J. Liggat, A. McKee, I. Soutar and E. L. Scott, *Reactive and Functional Polymers,* 1998, **36**, 173.

[256] J. F. Krebs and A. S. Borovik, *Chem. Commun.*, 1998, 553.

[257] E. V. Rybak-Akimova, K. Marek, M. Masarwa and D. H. Busch, *Inorganica Chemica Acta*, 1998, **270**, 151.

[258] S. Bhattacharyya, D. Ghosh, S. Mukhopadhyay, W. P. Jensen, E. R. T. Tiekink and M. Chaudhary, *J. Chem. Soc., Dalton Trans.* 2000, 4677.

[259] J. M. Barbe, G. Canard, S. Brandès, F. Jérôme, G. Dubois and R. Guilard, *Dalton Trans.* 2004, 1208.

[260] S. D. Piero, A. Melchior, P. Polese, R. Portanova and M. Tolazzi, *Dalton Trans*. 2004, 1358.

[261] H. Chen, A. Matsumoto, N. Nishimiya, T. Takeichi and K. Tsutsumi, *Microporous and Mesoporous Materials,* 2000, **40**, 289.

[262] T. Tanase, T. Onaka, M. Nakagoshi, I. Kinoshita, K. Shibata, M. Doe, J. Fujiib and S. Yano, *Chem. Commun*. 1997, 2115.

[263] R. Boca, H. Elias, W. Haase, M. Huber, R. Klement, L. Muller, H. Paulus, I. Svoboda and M. Valko, *Inorganic Chemica Acta* 1998, 127.

[264] S. Djebbar-Sid, O. Benali-Baitich and J. P. Deloume, *J. Molecular Structure*, 2001, **569**, 121.

[265] S. Cabani, N. Ceccanti, R. Pardini and M. R. Tine, *Polyhedron* 1999, **18**, 3295.

[266] A. Vishnyakov, P. I. Ravikovitch, A. V. Neimark, M. Bülow and Q. M. Wang, *Nano Letters, 2003,* **3**, 713

[267] S. K. Cheung, C. J. Grimes, J. Wong and C. A. Reed, *J. Am. Chem. Soc.,* 1976, **98**, 5028.

[268] D. Ramprasad, T. J. Markley and G. P. Pez, *Journal of Molecular Catalysis A: Chemical,* 1997, **117**, 273.

[269] D. Ramprasad, I. K. Meier, R. M. Pearlstein and G. P. Pez, U. *S. Pat. No. 5,294,418*, 1994.

[270] D. Ramprasad, G. P. Pez, R. M. Pearlstein and I. K. Meier, *U. S. Pat. No. 5,126,466*, 1992.

[271] D. Ramprasad, G. P. Pez, R. M. Pearlstein and I. K. Meier, *U. S. Pat. No. 5,141,725*, 1992.

[272] D. Ramprasad, G. P. Pez, R. M. Pearlstein and I. K. Meier, *U. S. Pat. No. 5,208,335*, 1993.

[273] D. Ramprasad, U. *S. Pat. No. 5,239,098*, 1993.

[274] I. K. Meirer, R. M. Pearlstein, D. Ramprasad and G. P. Pez, *Inorg. Chem.* 1997, **36**, 1707.

[275] D. Ramprasad, G. P. Pez, B. H. Toby, T. J. Markley and R. M. Pearlstein, *J. Am. Chem. Soc.* 1995, **117**, 10694.

[276] W. M. Coleman and L. T. Taylor, *Coord. Chem. Rev*. 1980, **32**, 1.

[277] S. J. Ebbs and L. T. Taylor, *Inorg. Nucl. Chem. Lett*. 1974, **10**, 1137.

[278] G. Wilkinson, R. D. Galliard and J. A. McCleverty, *Comprehensive Coordination Chemistry*, Pergamon, London, 1987.

[279] S. J. E. Titus, W. M. Barr and L. T. Taylor, *Inorg. Chem. Acta*, 1979, **32**, 103.

[280] W. M. Coleman and L. T. Taylor, *Inorg. Chem*. 1977, **16**, 1114.

[281] W. M. Coleman and L. T. Taylor, *Inog. Chem. Acta*, 1978, **30**, L291.

[282] W. M. Coleman, R. K. Boggess, J. W. Hughes, and L. T. Taylor, *Inog. Chem.* 1981, **61**, 13.

[283] W. M. Coleman and L. T. Taylor, *Inog. Chem. Acta*, 1982, **62**, 123.

[284] K. D. Magers, C. G. Smith and D. T. Sawyer, *J. Am. Chem. Soc*., 1978, **100**, 989.

[285] K. D. Magers, C. G. Smith and D. T. Sawyer, *Inorg. Chem*. 1980, **19**, 492.

[286] J. Barrett, T. Dent and P. Linsyead, *J. Chem. Soc.* 1936, 1719.

[287] J. A. Elvidge and A. B. P. Lever, *Proc. Chem. Soc. Lond*. 1959, 195.

[288] L. H. Vogt, A. Zalkin and D. H. Templeton, *Inorg. Chem*. 1967, **6**, 1725.

[289] L. K. Hanson and B. M. Hoffman, *J. Am. Chem. Soc*. 1980, **102**, 4602.

[290] J. E. Newton and M. B. Hall, *Inorg. Chem*. 1985, **24**, 2573.

[291] M. W. Urban, K. Nagamoto and F. Basolo, *Inorg. Chem*. 1982, **21**, 3406.

[292] R. D. Jones, J. R. Budge, P. E. Ellis and J. E. Linerd, *J. Organometallic Chem*. 1979, **181**, 151.

[293] C. A. McAuliffe, *Mol. Catal*. 1988, **44**, 35.

[294] C. A. McAuliffe and H. F. Al-Khateeb, *Inorg. Chem. Acta,* 1980, **45**, L195.

[295] C. A. McAuliffe, H. F. Al-Khateeb, M. H. Jones, W. Levason, K. Minten and F. P. McClullough, *J. Chem. Soc. Chem. Commun*. 1979, 736.

[296] C. A. McAuliffe, H. F. Al-Khateeb, D. S. Barret, J. C. Briggs, A. Challita, A. Hosseiny, M. G. Little, A. G. Mackie and K. Minten, *J. Chem. Soc. Dalton Trans.* 1983, 2147.

[297] C. A. McAuliffe, S. M. Godferry, A. G. Mackie and R. G. Pritchard, *J. Chem. Soc. Chem. Commun*. 1992, 483.

[298] R. M. Brown, R. E. Bull, M. L. H. Green, P. D. Grebenik, J. J. Martin-Polo and D. M. P. Mingos, *J. Organometallic Chem*. 1980, **201**, 4371.

[299] M. L. H. Green, *J. Organometallic Chem*. 1982, **228**, 263.

[300] N. Kitajima, U. P. Singh, H. Amagai, M. Osawa, and Y. Moro-oka, *J. Am. Chem. Soc.*, 1991, **113**, 7757.

[301] N. Kitajima, M. Osawa, M. Tanaka, and Y. Moro-oka, *J. Am. Chem. Soc.*, 1991, **113**, 8952.

[302] W. M. Coleman and L. T. Taylor, *Inorg. Chem*. 1977, **16**, 1114.

[303] D. De Vos and T. Bein, *J. Am. Chem. Soc.* 1997, **119**, 9460.

[304] J. A. Halfen, S, Mahapatra, E. C. Wilkinson, S. Kaderli, V. G. Young Jr., L. Que, Jr., A. D. Zuberbiihler and W. B. Tolman, *Science*, 1996, **271**, 1397.

[305] P. L. Holland and W. B. Tolman, *Coord. Chem. Rev*. 1999, **190-192**, 855.

[306] V. Madhavan, Z. Hou, A. P. Cole, D. E. Root, T. K. Lal, E. I. Solomon and T. D. P. Stack, *J. Am. Chem. Soc.* 1997, **119**, 11996.

[307] V. Madhavan, M. J. Henson, E. I. Solomon and T. D. P. Stack *J. Am. Chem. Soc*., 2000, **122**, 10249.

[308] A. E. Meier, M. M. Whittaker and J. W. Whittaker, *Biochemistry*, 1996, **35**, 348.

[309] M. Ghisletta, L. Hausherr-Primo, K. Gajda-Schrantz, G. Machula, L. Nagy, H. W. Schmalle, G. Rihs, F. Endres and K. Hegetschweiler, *Inorganic Chemistry*, 1998, **37**, 997.

[310] C. J. Weschler, B. M. Hoffman and F. Basolo, *J. Am. Chem. Soc.,* 1975, **97**, 5278.

[311] B. M. Hoffman, C. J. Weschler and F. Basolo, *J. Am. Chem. Soc.,* 1976, **98**, 5473.

[312] T. Nakamura, K. Niwa, S. Usugi, H. Asada, M. Fujiwara and T. Matsushita, *Polyhedron,* 2001, **20**, 191.

[313] N. Kitajima, T. Koda, S. Hashimoto, T. Kitagawa, and Y. Moro-oka, *J. Chem. Soc., Chem. Commun,* 1988, 151.

[314] K. D. Karlin, W. B. Tolman, S. Kaderli, A. D. Zuberbiihler, *Journal of Molecular Catalysis A: Chemical,* 1997, **117**, 215.

[315] H. C. Liang, C. X. Zhang, M. J. Henson, R. D. Sommer, K. R. Hatwell, S. Kaderli, A. D. Zuberbuhler, A. L. Rheingold, E. I. Solomon and K. D. Karlin, *J. Am. Chem. Soc*. 2002, **124**, 4170.

[316] H. C. Liang, K. D. Karlin, R. Dyson, S. Kaderli, B. Jung and A. D. Zuberbuhler, *Inorg. Chem.* 2000, **39**, 5884.

[317] T. Osako, Y. Tachi, M. Tachi, S. Fukuzumi and S. Itoh, *Inorg. Chem*. 2001, **40**, 6604.

[318] M. Metz and E. I. Solomon, *J. Am. Chem. Soc.*, 2001, **123**, 4938.

[319] Z. Hu, R. D. Williams, D. Tran, T. G. Spiro and S. M. Gorun, *J. Am. Chem. Soc*. 2000, **122**, 3556.

[320] Y. Tachi, K. Aita, S. Teramae, F. Tani, Y. Naruta, S. Fukuzumi and S. Itoh, *Inorg. Chem.* 2004, **43**, 4558.

[321] T. J. Hubin, N. W. Alcock, L. L.Seib and D. H. Busch, *Inorg. Chem.* 2002, **41**, 7006.

[322] R. A. Ghiladi, R. M. Kertzer, I. Guzei, A. L. Rheingold, Y. M. Neuhold, K. R. Hatwell, A. D. Zuberbuhler and K. D. Karlin, *Inorg. Chem.* 2001, **40**, 5754.

[323] G. C. Wagner and R. J. Kassner, *J. Am. Chem. Soc,* 1974, **96**, 5593.

[324] H.C. Fry, D.V. Scaltrito, K. D. Karlin and G. J. Meyer, *J. Am. Chem. Soc.*, 2003, **125**, 11866.

[325] R. Koerner, M. M. Olmstead, A. Ozarowski, S. L. Phillips, P. M. V. Calcar, K. Winkler and A. L. Balch, *J. Am. Chem. Soc.*, 1998, **120**, 1274.

[326] B. S. Lim and R. H. Holm, *Inorganic Chemistry*, 1998, **37**, 4898.

[327] J. E. Bol, W. L. Driessen, R. Y. N. Ho, B. Maase, L. Que Jr. and J. Reedijk, *Angew. Chem. Int. Ed. Engl.* 1997, **36**, 998.

[328] M. Beltramini, E. Borghi, P. D. Muro, A. L. Monaca, B. Salvato and C. Santini, *Journal of Molecular Structure,* 1996, **383**, 237.

[329] L. M. Berreau, J. A. Halfen, V. G. Young Jr. and W. B. Tolman, *Inorganica Chimica Acta,* 2000, **297**, 115.

[330] K. D. Karlin, W. B. Tolman, S. Kaderli and A. D. Zuberbiihler, *Journal of Molecular Catalysis A: Chemical,* 1997, **117**, 215.

[331] K. Kunz and A. J. Kress, *Chem. Ber*. 1927, **60**, 367.

[332] J. E. Baldwin and J. Huff, *J. Am. Chem. Soc.* 1973, **95**, 5257.

[333] J. P. Collman, R. R. Gagne, T. R. Halbert, J. C. Marchon and C.A. Reed, *J. Am. Chem. Soc.*, 1973, **95**, 7868.

[334] J. Almong, J. E. Baldwin and J. Huff, *J. Am. Chem. Soc.* 1975, **97**, 227.

[335] J. F. Drake and R. J. P. Williams, *Nature*, 1958, **182**, 1084.

[336] N. Herron, L. L. Zimmer, J. J. Grzybowski, D. J. Olszanski, S. C. Jackels, R. W. Callahan, J. H. Cameron, G. G. Christoph and D. H. Busch, *J. Am. Chem. Soc.* 1983, **105**, 6585.

[337] N. Kitajima, H. Fukui, Y. Moro-oka, Y. Mizutani, and T. Kitagawa, *J. Am. Chem. Soc.*, 1990, **112**, 6402.

[338] Y. S. Yang, J. Baldwin, B. A. Ley, J. M. Bollinger Jr. and E. I. Solomon, *J. Am. Chem. Soc.*, 2000, **122**, 8495.

[339] M. P. Mehn, K. Fujisawa, E. L. Hegg and L. Que Jr., *J. Am. Chem. Soc.*, 2003, 125, 7828.

[340] A. Treffry, Z. Zhao, M. A. Quail, J. R. Guest and P. M. Harrison, *Biochemistry*, 1997, **36**, 432.

[341] I. Borovok, O. Landman, R. Kreisberg-Zakarin, Y. Aharanowitz and G. Cohen, *Biochemistry*, 1996, **35**, 1981.

[342] M. T. Gardner, G. Deinum, Y. Kim, G. T. Babcock, M. J. Scott and R. H. Holm, *Inorganic Chemistry*, 1996, **35**, 6878.

[343] M. E. Andersson, M. Hogbom, A. Rinaldo-Matthis, K. K. Anderson, B. M. Sjoberg and P. Nordlund, *J. Am. Chem. Soc.* 1999, **121**, 2346.

[344] J. P. Collman, L. Fu, A. Zingg and F. Diederich, *Chem. Commun*. 1997, 193.

[345] T. Komatsu, S. Hayakawa, E. Tsuchida and H. Nishide, *Chem. Commun*. 2003, 50.

[346] J. Seibin and J. H. Junkin, *J. Am. Chem. Soc.* 1960, **82**, 1057.

[347] N. Farrell, D. H. Dolphin and B. R. James, *J. Am. Chem. Soc.*, 1978, **100**, 324.

[348] S. K. Cheung, C. J. Grims, J. Wong and C. A. Reed, *J. Am. Chem. Soc.*, 1976, **98**, 5028.

[349] R. H. Holmn, *Coordination Chemistry Reviews*, 1990, **110**, 183.

[350] J. W. Bucher, *The Porphyrins* ed. by D. Dolphin Academic New York, 1978, Vol. 1, p389.

[351] J. Tachibana and T. Imamura, *Chem. Lett.* 1990, 2085.

[352] M. Hoshino and Y. Iimura, *J. Phys. Chem.* 1992, **96**, 179.

[353] J. Tachibana, T. Imamura and Y. Sasaki, *Bull. Chem. Soc. Jpn.,* 1998, **71**, 363.

[354] T. Fujihara, N. H. Rees, K. Umakoshi, J. Tachibana, Y. Sasaki, W. McFarlane and T. Imamura, *Chem. Lett.,* 2000, 102.

Chapter-2

Sorption of Nitrogen, Oxygen and Argon on Silver Exchanged Zeolite A

2.1. INTRODUCTION

Zeolites are of immense interest in gas and chemical industries for purification and separation due to their unique adsorption properties. The extra framework cations invariably present in zeolites play significant role in determining their adsorptive properties [1]. In particular, if co-ordinately unsaturated metal ions can be incorporated inside the zeolite cavities, novel adsorption behaviour may be fashioned on the basis of coordination of guest molecules. Exchangeable transition metal ions in activated zeolites are generally co-ordinately unsaturated and are known to readily form complexes with a variety of guest molecules [2]. Synthetic zeolites of type A, X and mordenite having alkali and alkaline earth metals as the extra framework cations have been extensively studied and are mainly used as the nitrogen selective adsorbents for the adsorptive separation of oxygen from air [3-9]. However, the maximum attainable purity by adsorption processes using these adsorbents is still around 95% with separation of 0.934 mole percent argon present in the air being a limiting factor to achieve 100% oxygen purity. To over come this oxygen purity limit, adsorbents having nitrogen as well as argon selectivity over oxygen need to be developed.

Zeolite A is the synthetic low silica zeolite having Si/Al ratio 1. Zeolite A may be viewed as an assemblage of truncated octahedra, each composed of 24 tetrahedra. These are variously referred to as cuboctahedra, sodalite cavities or β-cages (Figure-2.1). These cuboctahedra are octahedrally joined at 4-rings by four bridging oxygen atoms. There are 12 negative charges in the framework and that are balanced by cations in each unit cell. Most of these cations in zeolite A are accessible to the adsorbate molecules either directly or through the 6-member rings.

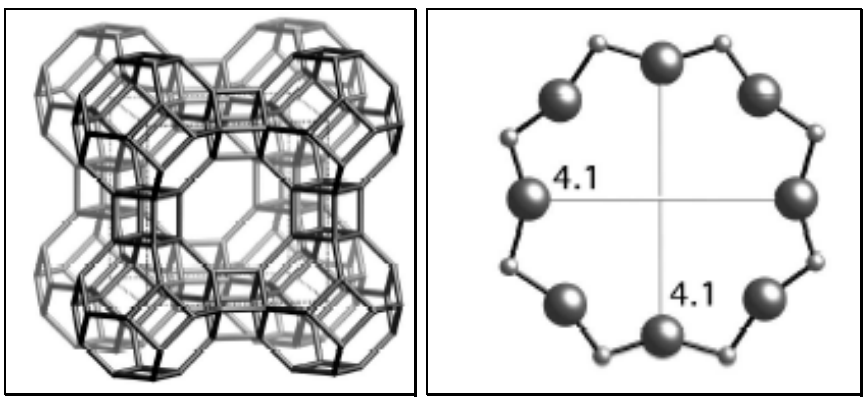

Figure-2.1. Framework Structure of Zeolite A

Ag^+ is the only noble monopositive cation that forms mononuclear species with appreciable stability in aqueous solution. No hydrolysis occurs. Of the all noble metals, only Ag^+ can be exchanged easily and completely into zeolites from aqueous solution. Stoichimetric ion exchange, impossible to achieve for most cations, is frequently observed for Ag^+. Silver is also known to have strong influence on the adsorption properties of some zeolites. Ralek et al. [11] were the first to use dehydrated, brick red AgA as a water sensor to detect small amount of moisture, on the basis of their observations of colour changes from brick-red to orange, to yellow and finally to white, but no explanation of this phenomenon was given at that time. Later it was believed that the colour change was due to formation of silver clusters (Ag_n^0) in the cavities of silver zeolite A. These neutral silver species were assumed to form at elevated temperatures via an auto reduction process in which O_2 from the zeolite framework was released. Recently, it was showed that activation at room temperature under high vacuum is already sufficient to produce the yellow form of $Ag^+_xNa^+_{12-x}A$. The fully reversible colour change which depends on the hydration state of the silver zeolite was attributed to electronic charge transfer transitions from the oxygen lone pairs of the zeolite framework to the empty 5s orbital of the Ag^+ ions, denoted as $Ag^+(5s)\leftarrow O(n)$. More recently, Ozin [12-14] developed a series of silver or silver halide sodalites, which he speculates may act as chemical, electronic and optical sensors and may be useful as information storage materials. Silver containing zeolites are found useful as catalysts in a variety of chemical reactions such as ethylene epoxidation, photochemical dimerisation, synthesis of 2-6 glycosil linkage, photochemical water splitting, photochemical chlorine production and several other reactions [15].

In this chapter, the adsorption of nitrogen, oxygen and argon on silver exchanged zeolite A having various amount of silver ions are studied at ambient temperatures to develop a superior adsorbent, which has potential for the selective adsorption of nitrogen and argon from air in order to overcome the present oxygen purity limit of 95% by adsorption processes. The adsorption data obtained at ambient temperatures are fitted in various models such as Langmuir, Virial and Dubinin-Astakhov. Adsorption capacity, adsorption selectivity and isosteric heat of adsorption were determined form these adsorption data. The forces contributing to the interaction of nitrogen and argon with silver exchanged zeolite A is also discussed in detail.

2.2. EXPERIMENTAL

2.2.1. Materials

Zeolites A from *Zeolites and Allied Product, Bombay, India* and Silver Nitrate (99.9%) from *Ranbaxy Fine Chemicals Ltd., New Delhi, India* were used as the starting materials for the adsorbent preparation. Oxygen (99.99%), Nitrogen (99.99%), Argon (99.99%) and Helium (99.99%) from *Hydrogas India Pvt. Ltd., Bombay, India* were used for the adsorption isotherm measurements.

2.2.2. Silver ion Exchange

Silver ions form mononuclear species with appreciable stability in aqueous solution. These cations were introduced into the highly crystalline sodium form of zeolite by the conventional cation exchange from aqueous $AgNO_3$ solution. Typically, the zeolite was refluxed with aqueous $AgNO_3$ solution, in the solid / liquid ratio 1:80 at 353K for 4 hours. The residue was filtered, washed with hot distilled water, until the washings were free from Ag^+ ions. Zeolite samples having different silver exchange were prepared by altering the silver ion concentration of the ion exchange solution. The samples were dried at a temperature below 353K in air or vacuum. All the activities were carried out in absence of direct contact with light. Ion exchange of Ag^+ into zeolite A is highly facile and completes in a single stage and can occur even at ambient conditions due to the high exchange selectivity of Ag^+ over Na^+ [10]. The extent of silver exchange in zeolites was determined by using *Shimadzu AA-680* atomic absorption spectrometer.

2.2.3. X-ray Powder Diffraction

X-ray powder diffraction studies at ambient temperature were carried out using *Philips X'pert MPD system* in the 2θ ranges of 5-65 degrees using CuKα1 (λ = 1.54056Å). The diffraction patterns of the starting material show that it is highly crystalline showing the reflections in the range 5-35 degrees typically of zeolites. *In situ* X-ray diffraction for AgA having 100% silver exchange was measured at various temperatures ranging from ambient to 723K in air using *Anton Paar* high temperature reaction chamber *XRK 900* attached on *Philips X'pert MPD system*. The temperature was increased from room temperature to 723K at a heating rate of 10K min^{-1}.

2.2.4. SEM and EDX

Microscopic analysis of zeolite NaA, AgNaA and AgA samples were collected using *LEO 1430 VP* variable pressure scanning electron microscope equipped with *INCA Oxford* EDX facility.

2.2.5. DRIFT Spectroscopy

Diffuse reflectance infrared Fourier transform spectroscopic study of the adsorbed N_2 molecules were carried out at various temperatures ranging from 303K to 673K using *Perkin Elmer Spectrum GX* equipped with the *Selector DRIFT* accessory (*Graseby Specac, P/N 199900 series*) incorporating an environmental chamber assembly. The samples were activated *in situ* at 673K (heating rate 10K min^{-1}) under constant N_2 flow (30cc min^{-1}). The spectra were recorded for self-supporting zeolite wafer sample in the range of 400-4000cm^{-1} while decreasing the temperature from 673K to 303K. Typically, 30 scans were co-added at a resolution of 4cm^{-1}. The constant nitrogen flow was maintained through out the process.

2.2.6. Activation and Isotherm Measurements

The presence of water in the zeolite significantly affects the validity of the adsorption isotherms. Therefore, prior to adsorption measurements, the samples were initially dried at 353K for 24hours. The samples were further activated *in situ* by increasing the temperature (at a heating rate <1K min^{-1}) to 673K under vacuum ($5x10^{-3}$mmHg) and maintained at 673K for 8hours before the sorption measurements. Nitrogen, oxygen and argon adsorption was measured at 288.2K and 303.0K using a static volumetric system (*Micromeritics Instrument Corporation, USA, Model ASAP 2010).* Adsorption temperature was maintained (±0.1K) by circulating water from a constant temperature bath *(Julabo F25, Germany).* Requisite amount of the adsorbate gas was injected into the volumetric set up at volumes required to achieve a targeted set of pressures ranging from 0.1 to 850mmHg. Three pressure transducers of capacities 1mmHg (Accuracy within 0.12% of the reading); 10mmHg (Accuracy within 0.15% of the reading) and 1000mmHg (Accuracy within 0.073% of full scale) were used for the pressure measurements. A minimum equilibrium interval of 5 seconds with a relative target tolerance of 5.0% of the targeted pressure and an absolute target tolerance of 5.000 mmHg were used to determine equilibrium for each measurement point. The adsorption and desorption was completely reversible and it is possible to

remove the adsorbed gases by simple evacuation. The schematic representation of the static volumetric set-up (*Micromeritics ASAP 2010*) used for the adsorption measurements is given in Figure-2.2.

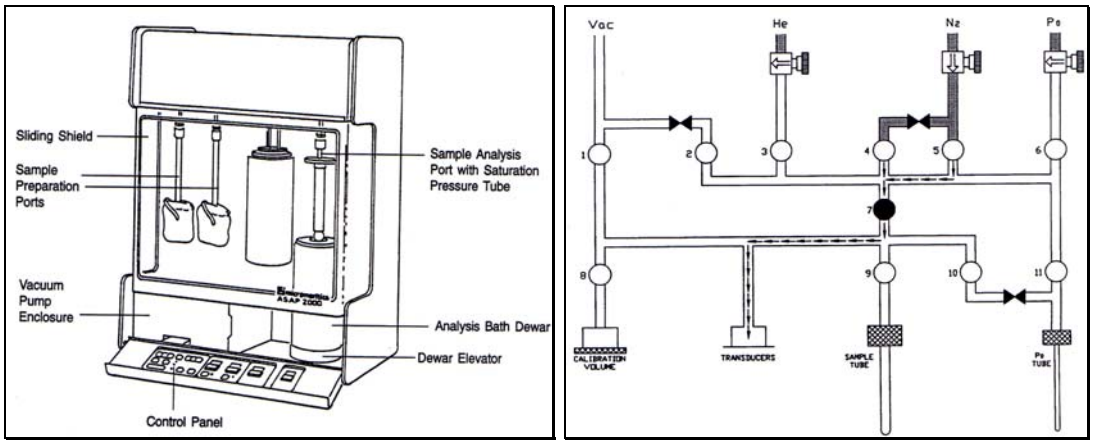

Figure-2.2. Schematic diagram of analyser components of Micromeritics ASAP 2010

The isotherms were fitted in various equations like Langmuir equation, Virial equation, and Dubinin-Astakhov equation.

Langmuir equation

$$q = \frac{bP}{1+bP}$$

Virial equation

$$\ln (p/q) = A + Bq + Cq^2 + \ldots\ldots..$$

Henry's Constant, K, were determined from the Virial coefficient using the equation

$$K = \exp (-A)$$

Dubinin-Astakhov equation

$$\log (V) = \log (V_0) - [RT/ \beta E_0]^N \times [\log P_0/P]^N$$

where q is the amount of gas adsorbed per unit weight of the adsorbent, b is k_a/k_d, the ratio of the adsorption and desorption constants, P is the equilibrium pressure, P_0 is the saturation vapour pressure, A, B and C are the first, second and third Virial coefficients respectively, V is the volume adsorbed at equilibrium pressure, V_0 is the micropore capacity, T is the analysis bath temperature, R is universal gas constant, E_0

is the characteristic energy, N is the Astakhov exponent and β is the affinity coefficient of the analysis gas.

Adsorption capacity, selectivity and isosteric heat of adsorption were determined from the adsorption isotherms measured at 288.2K and 303.0K.

The pure component selectivity of two gases A and B was calculated by using the equation,

$\alpha_{A/B}=[V_A/V_B]_{P,T}$

where V_A and V_B are the volumes of gas A and B respectively adsorbed at any given pressure P and temperature T.

Isosteric heats of adsorption were from the adsorption data collected at 288.2K and 303.0K using Clausius-Clapeyron equation.

$\Delta_{ad}H^o = R\ \{[\partial \ln p]/[\partial(1/T)]\}_\theta$

where R is the universal gas constant, θ is the fraction of the adsorbed sites at a pressure *p* and temperature T.

The error in the calculated values of Henry's constant, adsorption selectivity and heat of adsorption estimated from propagation of error method were 0.5%, 0.4%, and 0.4% respectively.

2.3. RESULTS AND DISCUSSION

The X-ray diffraction patterns of the starting material show that it is highly crystalline showing the reflections in the range 5 to 35 typically of zeolites. The structures of the zeolites were retained after the cation exchange. No loss of crystallinity was observed during silver exchange. However, intensities of the peaks corresponding to 2θ values 10.16, 12.46,14.37, 16.10, 20.4 and 32.55 have changed. The *in situ* XRD measurements at high temperatures up to 723K show that the silver exchanged also possess high thermal stability. The X-ray diffraction patterns of various amounts of silver exchanged zeolite A and that of AgA at various temperatures are given in Annexure I. SEM pictures of AgA and NaA are given in Figure-2.3. EDX measurement also confirms the absence of Na^+ ions in completely silver exchanged zeolite A. Comparison of AgA morphology with starting NaA shows that cubic morphology and crystallite size is retained on silver exchange in these zeolites.

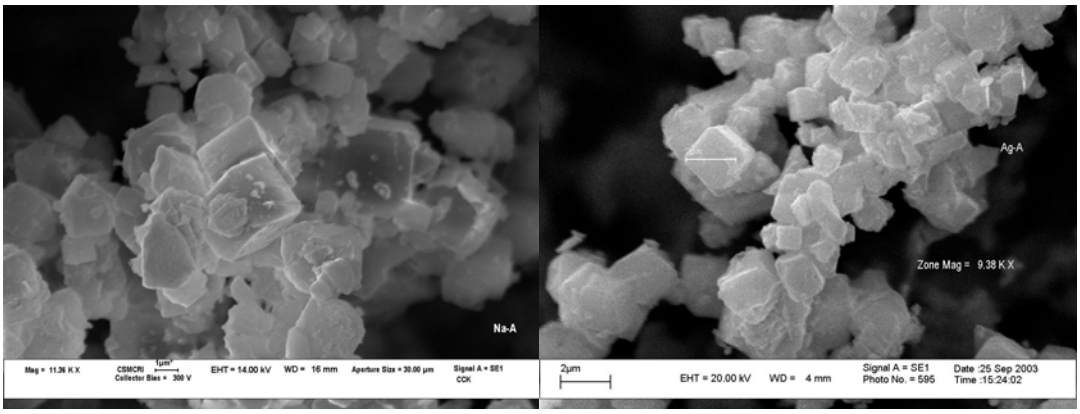

Figure-2.3. SEM images of zeolite NaA and AgA

2.3.1. Activation and Colour changes

Silver exchanged zeolite A reversibly changed its colour from white to brick red upon vacuum dehydration at 623 K. Ralek et al. first reported [11] that the white hydrated silver form of zeolite A exhibits a red colour after dehydration at 623 K, which has been later confirmed by many authors. The dehydrated silver exchanged zeolite A has been reported to adsorb visible light at 500 nm. The colour changes observed for AgA on heating under vacuum have been attributed to the formation of $(Ag_n)^{x+}$ clusters inside the sodalite cavity of zeolite A. It is reported that on vacuum dehydration silver ions migrates and undergoes auto reduction to form Ag^0, which interacts with silver ions to form clusters. Various types of clusters varying from linear Ag^+-Ag^0-Ag^+ to $(Ag_5)^{4+}$, $(Ag_8)^{6+}$ and $(Ag_{12})^{8+}$ have been reported depending on the zeolite type and the extent of silver exchange [12-23].

In case of zeolite AgA, yellow colour observed at lower temperatures (<373 K) is explained to be due to weakly interacting $(Ag_3)^+$ clusters. At higher temperatures (<600 K), the red brick colour observed is attributed to the presence of four interacting $(Ag_3)^+$ clusters inside the sodalite cages of zeolite AgA. However, there is an alternative explanation for the formation and interaction of $(Ag_3)^{2+}$ clusters often presented as responsible for the colour changes observed in silver exchanged zeolite A [24-26]. From UV-VIS diffuse reflectance and quantum chemical extended Huckel molecular orbital electronic dipole induced transitions calculations on Na_6Ag_6A, colour changes are attributed to electronic transitions from the lone pairs of oxygen atoms of the zeolite framework to the empty 5s orbital of Ag^+ ions, i.e., ligand to metal transfer (LMCT).

2.3.2. Equilibrium Adsorption Isotherms

N_2, O_2 and Ar adsorption isotherms on fully silver exchanged zeolite A (AgA) at 303.0 K are given in Figure-2.4. AgA shows an equilibrium adsorption capacity of 22.3cc g^{-1}, 4.36cc g^{-1} and 6.25cc g^{-1} respectively for nitrogen, oxygen and argon at 303K and 101.3kPa. It is observed that on silver exchange, nitrogen and argon adsorption values show more than four fold increase at all equilibrium pressures compared to NaA. However, the increase in the oxygen adsorption is only around 1.5 times. The argon adsorption capacity is higher than that of oxygen at all equilibrium pressures in the pressure range studied. In the low-pressure region, the nitrogen adsorption capacity increases sharply with increase in pressure and the adsorption isotherm posses a very high slope. At equilibrium pressures above 50kPa, the slope of the adsorption isotherm decreases.

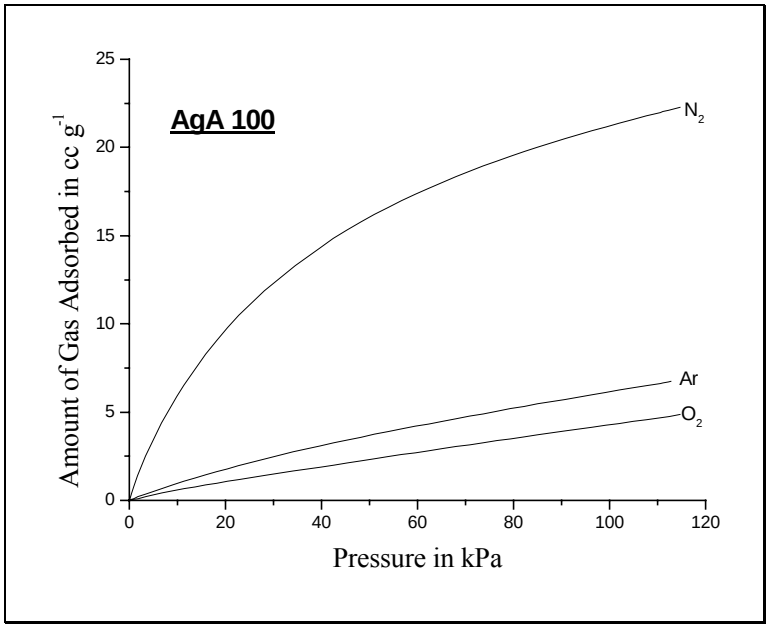

Figure-2.4. Adsorption Isotherms for N_2, O_2 and Ar on AgA at 303.0K

Nitrogen, oxygen and argon adsorption isotherms on various amounts of silver exchanged zeolite A and NaA at 303.0K are given in Figure-2.5. The number after AgA denotes the percentage of silver ion exchanged in the zeolite A, i.e. 100%, 80%, 70%, 60%, 40% and 20% silver exchanged zeolite A is denoted as AgA 100, AgA 80, AgA 70, AgA 60, AgA 40 and AgA 20 respectively. In the case of AgA 80, the nature of the adsorption isotherms remains similar to that of AgA 100. The nitrogen adsorption increases sharply with pressure in the low-pressure region and the nitrogen adsorption isotherm posses a non-linear shape. The nitrogen and argon adsorption

capacities are higher than that of oxygen at all equilibrium pressures. The increases in nitrogen and argon adsorption capacities are higher than that for oxygen.

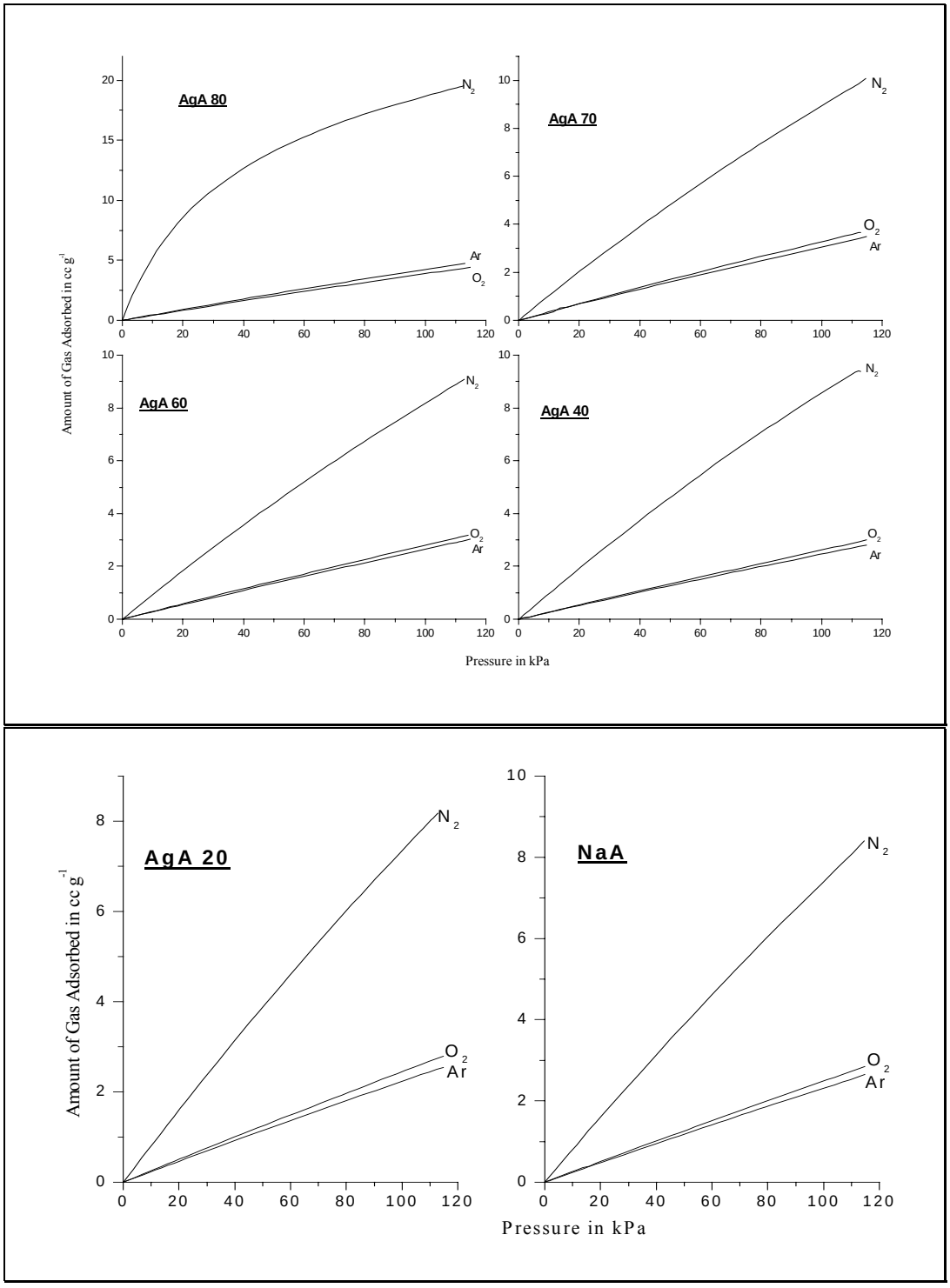

Figure-2.5. Adsorption Isotherms for N_2, O_2 and Ar in AgNaA and NaA at 303.0K

In the case of zeolites having 70% or less than 70% silver exchange, i.e., for AgA 70, AgA 60 AgA 40 and AgA 20 the adsorption isotherms obtained are similar to that of NaA. The adsorption capacities for nitrogen, oxygen and argon increase with increase

in the amount of silver for these samples, the increase in the adsorption capacities for nitrogen, oxygen and argon with pressure are linear and hence the shape of the adsorption isotherms remains linear.

The equilibrium adsorption capacities for the adsorption of nitrogen, oxygen and argon on zeolite A containing different amounts of silver ions are determined from the adsorption isotherms and the values at 101.3kPa are given in Table-2.1. The nitrogen, oxygen and argon adsorption capacities increase on silver ion exchange. However, after exchanging more than 70% of the extra framework cations of zeolite A with silver ions, the adsorption capacity increase is sharp. The magnitude of the increase in the adsorption capacity for nitrogen is much higher than that of argon and oxygen. The observed increase in the adsorption capacity follows the order nitrogen>> argon> oxygen.

Table-2.1. Equilibrium Adsorption Capacity for N_2, O_2 and Ar on AgNaA

Adsorbent	Equilibrium Adsorption Capacity in molecules / unit cell at 101.3kPa					
	288.2K			303.0K		
	Nitrogen	Oxygen	Argon	Nitrogen	Oxygen	Argon
NaA	6.55	2.12	1.84	4.58	1.53	1.42
AgA 20	7.22	2.21	2.08	5.09	1.68	1.54
AgA 40	8.51	2.40	2.38	6.55	1.99	1.89
AgA 60	9.75	3.09	2.88	6.86	2.35	2.22
AgA 70	11.17	3.65	3.46	7.83	2.88	2.66
AgA 80	19.96	4.68	5.21	16.86	3.55	3.87
AgA 100	25.17	4.69	6.74	20.77	4.23	6.07

The adsorption data obtained at 288.2K and 303.0K were fitted in Langmuir equation and the slope, intercept and Langmuir constant were determined. The values for the slope and Langmuir constant, b increases for nitrogen, oxygen and argon on silver exchange and showed a sharp increase at silver exchange levels higher than 70% with increase in the percentage of silver in zeolite A, while that of intercept decreases with increase in silver content of zeolite A. The Langmuir fitting data on different amount of silver exchanged zeolite A at 303.0K are given in Table-2.2.

Table-2.2. Langmuir Fittings data at 303.0K for N_2, O_2 and Ar in AgNaA

System	Slope	Intercept	Vm = 1/slope	Langmuir Constant, b	Correlation coefficient
NaA N_2	0.01202	0.1085	83.17	0.1109	0.9970
NaA O_2	0.01260	0.3433	79.39	0.0367	0.9965
NaA Ar	0.01732	0.3659	57.74	0.0473	0.9805
AgA 20 N_2	0.01334	0.1082	74.94	0.1233	0.9971
AgA 20 O_2	0.01591	0.3468	0.6286	0.0459	0.9822
AgA 20 Ar	0.02089	0.3765	47.86	0.0555	0.9963
AgA 40 N_2	0.01535	0.08936	65.16	0.1718	0.9940
AgA 40 O_2	0.01024	0.3278	97.62	0.0312	0.9954
AgA 40 Ar	0.02418	0.3370	41.36	0.0717	0.9961
AgA 60 N_2	0.01633	0.09337	61.23	0.1748	0.9993
AgA 60 O_2	0.01860	0.2994	53.78	0.0621	0.9953
AgA 60 Ar	0.01568	0.3193	63.76	0.0491	0.9934
AgA 70 N_2	0.01586	0.08472	63.04	0.1873	0.9995
AgA 70 O_2	0.02236	0.2497	44.73	0.0895	0.9978
AgA 70 Ar	0.03024	0.2620	33.07	0.1155	0.9854
AgA 80 N_2	0.03823	0.01378	26.16	2.7739	0.9989
AgA 80 O_2	0.01876	0.2104	53.31	0.0891	0.9854
AgA 80 Ar	0.01891	0.1914	52.88	0.0988	0.9930
AgA 100 N_2	0.03288	0.01155	30.41	2.8466	0.9978
AgA 100 O_2	0.01606	0.1928	62.25	0.0833	0.9916
AgA 100 Ar	0.02113	0.1601	47.33	0.1319	0.9920

The nitrogen, oxygen and argon adsorption data obtained at 288.2K and 303.0K were also fitted in Virial equation. The Virial coefficients A_0, A_1 and A_2 were determined from the Virial plots. The Henry's constants were calculated from the Virial coefficient. The Values for the Virial coefficients A_0, A_1, A_2 and Henry's constant K at 303.0K are given in Table-2.3.

Table-2.3. Virial coefficients and Henry's Constant at 303.0K for N_2, O_2 and Ar in AgNaA

System	A_0	A_1	A_2	Correlation Coefficient, R^2	Henry Constant, K $\times 10^{-5}$ ccg^{-1}Pa^{-1}
NaA N_2	4.5501	-0.0361	0.0244	0.9822	7.93
NaA O_2	5.7148	-0.6782	1.1721	1.0000	2.47
NaA Ar	5.7765	-0.1943	0.3108	1.0000	2.32
AgA 20 N_2	4.5491	-0.0162	0.0100	0.9098	7.93
AgA 20 O_2	5.6889	0.0134	-0.0116	0.6656	2.54
AgA 20 Ar	5.7999	-0.1175	0.1980	0.9813	2.27
AgA 40 N_2	4.3596	-0.0212	0.0141	0.9891	9.59
AgA 40 O_2	5.6540	-0.0815	0.1129	0.9570	2.63
AgA 40 Ar	5.7029	-0.1768	0.2741	0.8574	2.50
AgA 60 N_2	4.4036	-0.0276	0.0189	0.9979	9.18
AgA 60 O_2	5.5627	-0.0677	0.1007	0.8416	2.88
AgA 60 Ar	5.6335	-0.1309	0.2069	0.7909	2.68
AgA 70 N_2	4.2914	-0.0059	0.0089	0.9979	10.27
AgA 70 O_2	5.3177	0.1473	-0.1184	0.9732	3.68
AgA 70 Ar	5.5359	-0.2563	0.1742	0.9808	2.96
AgA 80 N_2	2.3367	0.0735	-0.0035	0.9997	72.49
AgA 80 O_2	5.2213	-0.1092	0.1238	0.9786	4.05
AgA 80 Ar	5.1242	-0.0703	0.0695	0.9477	4.46
AgA 100 N_2	2.0907	0.1174	-0.3009	0.9996	92.71
AgA 100 O_2	5.1587	-0.0394	0.0519	0.9855	4.31
AgA 100 Ar	5.0750	-0.1231	0.1092	0.9055	4.69

The Henry's constants for nitrogen, oxygen and argon adsorption at 288.2K and 303.0 K on various adsorbent samples are given in Table-2.3. As observed from the data, the values of the Henry's constants for all the three gases increase on silver exchange. The order of increase in the Henry constants is nitrogen>>argon>oxygen which is different from the order nitrogen>oxygen>argon observed for sodium form of the zeolite A. These data show (a) very stronger interaction of nitrogen molecules with

the silver exchanged zeolite A surface (b) argon molecules also have strong interaction in silver exchanged zeolite A compared to oxygen molecules.

The nitrogen, oxygen and argon adsorption data obtained at 288.2K and 303.0K were also fitted in Dubinin-Astakhov equation. Slope of the Dubinin-Astakhov transformed isotherm decreases with increase in silver exchange. The values for intercept, energy and volume increases for all the three gases. The magnitude of the increase follows the order nitrogen>>argon>oxygen. The values of the slope, intercept, energy and volume at 303.0K are given in Table-2.4.

Table-2.4. Dubinin-Astakhov Fittings data at 303.0K for N_2, O_2 and Ar in AgNaA

System	Slope	Intercept	Energy kJ mol^{-1}	Volume cc g^{-1}	Correlation coefficient	Affinity Coefficient	Exponent
NaA N_2	-0.9569	0.9165	11.91	8.25	0.9999	0.227	1.0366
NaA O_2	-0.9814	0.4493	10.29	2.81	0.9999	0.250	1.0021
NaA Ar	-0.9813	0.4142	10.71	2.60	0.9999	0.244	1.0214
AgA 20 N_2	-0.9534	0.9127	12.00	8.18	0.9999	0.227	1.0412
AgA 20 O_2	-0.9822	0.4383	10.43	2.74	0.9999	0.250	1.0201
AgA 20 Ar	-0.9790	0.4004	10.68	2.51	0.9999	0.244	1.0151
AgA 40 N_2	-0.9356	0.9760	12.37	9.46	0.9999	0.227	1.0594
AgA 40 O_2	-0.9910	0.4672	10.39	2.93	0.9999	0.250	1.0265
AgA 40 Ar	-0.9748	0.4393	10.86	2.75	0.9999	0.244	1.0319
AgA 60 N_2	-0.9358	0.9569	12.33	9.06	0.9999	0.227	1.0544
AgA 60 O_2	-0.9758	0.4963	10.49	3.14	0.9999	0.250	1.0199
AgA 60 Ar	-0.9808	0.4734	10.69	2.97	0.9999	0.244	1.0191
AgA 70 N_2	-0.9306	0.9948	12.39	9.88	0.9999	0.227	1.0544
AgA 70 O_2	-0.9678	0.5620	10.74	3.65	0.9999	0.250	1.0405
AgA 70 Ar	-0.9525	0.5233	11.48	3.34	0.9999	0.244	1.0780
AgA 80 N_2	-0.5229	1.2778	22.36	18.96	0.9998	0.227	1.4010
AgA 80 O_2	-0.9639	0.6365	10.73	4.33	0.9999	0.250	1.0336
AgA 80 Ar	-0.9609	0.6742	10.52	4.72	0.9999	0.244	1.0352
AgA 100 N_2	-0.5307	1.3511	22.01	22.45	0.9999	0.227	1.3525
AgA 100 O_2	-0.9663	0.6780	10.66	4.76	0.9999	0.250	1.0279
AgA 100 Ar	-0.9496	0.7399	11.20	5.49	0.9999	0.244	1.0389

2.3.3. Adsorption Selectivity

Nitrogen/oxygen selectivity ($\alpha_{N2/O2}$) increases after the silver exchange on zeolite A. Even though sodium and silver forms of the zeolite contain same number of cations, i.e. 12, the $\alpha_{N2/O2}$ is very high (around 4 times) AgA in the low-pressure region (Table-2.5).

Table-2.5. Adsorption Selectivity for N_2, O_2 and Ar on AgNaA at 303K

Adsorbent	Adsorption Selectivity					
	$\alpha N_2/O_2$		$\alpha N_2/Ar$		$\alpha Ar/O_2$	
	3.33kPa	101.99kPa	3.33kPa	101.99kPa	3.33kPa	101.99kPa
NaA	3.1	3.0	3.4	3.2	0.90	0.93
AgA 20	3.2	3.1	3.3	3.2	0.98	0.99
AgA 40	3.6	3.5	3.6	3.5	1.00	1.01
AgA 60	4.0	3.8	3.4	3.2	1.18	1.20
AgA 70	4.7	4.2	3.5	3.1	1.34	1.35
AgA 80	14.8	4.8	10.0	3.2	1.48	1.51
AgA 100	15.4	5.1	10.1	3.9	1.51	1.63

AgA also shows an increase in the nitrogen/argon selectivity ($\alpha_{N2/Ar}$). The increase in $\alpha_{N2/Ar}$ is also very high in the low-pressure region. Like the nitrogen-oxygen selectivity, nitrogen/argon selectivity also decreases with increase in pressure (Table-2.5). In alkali and alkaline earth cation-exchanged zeolites oxygen and argon adsorption are nearly same or are marginally oxygen selective. AgA shows argon-oxygen selectivity value 1.63 at 101.3kPa. Furthermore, argon/oxygen selectivity, $\alpha_{Ar/O2}$ increases with increase in equilibrium pressure.

2.3.4. Heat of Adsorption

The isosteric heat of adsorption for nitrogen, oxygen and argon were calculated from the adsorption data at 288.2K and 303.0K and are given in Table-2.6. Heat of adsorption values calculated for the parent NaA is in close agreement with those

reported in the literature [1]. As observed form the data, the heat of adsorption value for nitrogen show substantial increase on zeolite A after exchanging more than 70% of the extra framework cations of the zeolite with silver ions. The nitrogen heat of adsorption on zeolite A having less than 70% silver exchanged zeolites remains almost same as that of the parent sodium form. N_2 heat of adsorption value at low coverage is very high (38-43kJ mol^{-1}) in the silver exchanged zeolites having higher than 80% silver exchange compared to that of the corresponding alkali metal ion exchanged zeolites (20-26kJ mol^{-1}) reported in the literature [1, 6]. The heats of adsorption for in silver exchanged zeolites are even higher than those for bivalent alkaline earth metal exchange zeolites (CaX = 26.5 kJ mol^{-1} and CaA = 22.2 kJ mol^{-1}). The heat of adsorption value for argon and oxygen also increases (Table-2.6) after silver exchange, but the magnitude of the increase is low compared to that for nitrogen. The high values for the nitrogen heat of adsorption on silver exchanged zeolites indicate strong interaction of the nitrogen molecules with the extra framework silver cations.

Table-2.6. Isosteric Heat of Adsorption for N_2, O_2 and Ar in AgNaA

Adsorbent	Isosteric Heat of Adsorption in kJ mol^{-1}		
	Nitrogen	Oxygen	Argon
NaA	20.4	15.3	13.0
AgA 20	20.3	15.1	14.6
AgA 40	20.4	15.2	15.2
AgA 60	21.3	15.2	15.1
AgA 70	21.6	15.3	15.4
AgA 80	38.9	15.5	15.9
AgA 100	42.8	15.4	16.4

The dependence of heat of adsorption for N_2, O_2 and Ar on AgA with percentage silver exchange is shown in Figure-2.6. Heat of adsorption of N_2 shows non-linear dependence on silver content of the zeolite with minor variation up to 70% of silver exchange beyond which an exponential increase is observed with the increase in silver exchange of zeolite A. Heat of adsorption of Ar increases marginally on silver

exchange and over takes that of oxygen at higher silver exchange levels, while that of oxygen remains unchanged. In the case of other cation exchanged zeolites, the heat of adsorption for oxygen is slightly higher than that of argon. This indicates that the argon molecules are capable of interacting strongly with the silver exchanged zeolites in comparison with oxygen molecules.

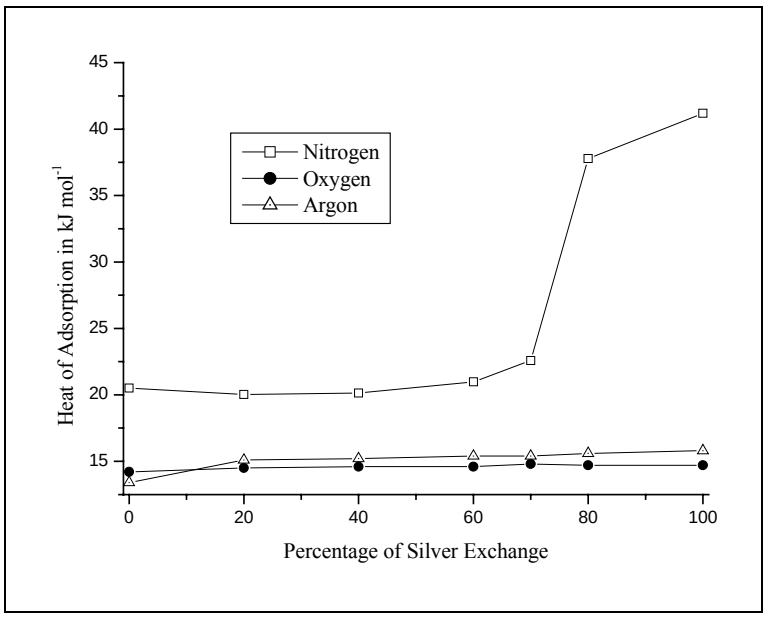

Figure-2.6. Variation of Heat of Adsorption of N_2, O_2 and Ar with percentage of Silver exchange in zeolite A

The non-linear nature of nitrogen adsorption isotherm increases on exchanging the extra framework sodium cations of the zeolite with silver ions. The sharp increase in the adsorption capacity in the low-pressure region (<30kPa), abnormally high value of the Henry constants and high heats of adsorption for N_2 at low adsorption coverage show the presence of co-ordinately unsaturated sites in the zeolite cavities / channels, that interacts strongly with nitrogen molecules in silver exchanged zeolites. Further, dependence of N_2 heat of adsorption shows a sharp decrease with increase in the adsorption coverage reflecting the limited number of such sites.

The various interactions contributing towards the total energy of physical adsorption include dispersion, ϕ_D, polarization, ϕ_P, field-dipole interactions, $\phi_{F\mu}$, field-quadrupole ϕ_{FQ}, close range repulsion interactions, ϕ_R and sorbate-sorbate interactions, ϕ_{SP} [1, 6].

$$\phi = -(\phi_D - \phi_R) - \phi_P - \phi_{F\mu} - \phi_{FQ} - \phi_{SP}$$

At low sorbate coverage, contributions from field-dipole and sorbate-sorbate interactions are negligible in the present systems as nitrogen, oxygen and argon are

non polar, therefore, total energy of physical sorption at low adsorption coverage is given by,

$\phi = -(\phi_D - \phi_R) - \phi_P - \phi_{FQ}$

Substituting the terms for various interactions, the equation becomes

$\phi = -\frac{1}{4} Q (\partial F/\partial R) - \frac{1}{2} (\alpha_s /k) F_2 - \Sigma A/r^6 + \Sigma B/r^{12}$

where Q is quadrupole moment, k is a constant (in S.I. units, $k = 9 \times 10^9$), F is the field, and α_s is the polarizability of the sorbate molecule.

Sorbate molecules can interact with the zeolite surface through lattice oxygen atoms and accessible extra framework cations and Al and Si atoms. The Al and Si atoms present at the centre of tetrahedra are also not directly exposed to the sorbate molecules and also possess small polarizability values. Consequently, their interactions with the sorbate molecules are negligible. Therefore, the principal interactions of these sorbate molecules with the zeolite surface are with lattice oxygen atoms and extra framework cations. As seen above, electrostatic interactions between the sorbate molecules and extra framework cations of the zeolite depend on the quadrupole moments of the sorbate molecule and are expected to follow the order, $N_2>O_2>Ar$ in agreement with quadrupole moment values of 0.31, 0.11 and zero for N_2, O_2, Ar respectively. Alkali and alkaline earth metal ion exchanged zeolites A and X display the similar trend as observed from heats of adsorption data for N_2, O_2 and Ar in these zeolites [1, 27-30]. In fact, heats of adsorption at zero coverage for nitrogen and oxygen has been reported to show correlation with the charge density of the extra framework cations. Nitrogen interacts most strongly with the Li^+ ions in the zeolite due to its higher charge density. Despite the same charge and larger size (1.26Å) or lower charge density of the silver ions compared to sodium cations (0.97Å), silver exchanged zeolites show stronger interactions with the nitrogen molecules as observed from sorption selectivity and heats of sorption data given in Tables-2.5 and 2.6. For example, nitrogen selectivity and heat of adsorption in all silver exchange zeolites is high compared to Na^+ or Ca^{2+} exchanged zeolites. This is an anomalous observation because on comparing the calculated electrostatic interactions between isolated Na^+, Ag^+ and Ca^{2+} cations and induced dipole of nitrogen molecule follow the order Ca^{2+}(118.0kJ mol^{-1}) > Na^+(31.5kJ mol^{-1}) > Ag^+(19.7kJ mol^{-1}).

As discussed in the earlier section, silver exchanged zeolites A on vacuum dehydration at higher temperature form clusters that possess charge higher than +1. The electrostatic interactions of these clusters with adsorbed N_2 molecules will be higher than that with isolated Ag^+ ions, which might be responsible for higher heats of adsorption for N_2 in silver exchanged zeolites. Further, it is reported that under prolonged evacuation at higher temperatures (>523K) some of the Ag^+ ions present inside the supercage undergoes reversible intrazeolite auto reduction to Ag^0 by extracting with lattice oxygen with desorption of oxygen is reported [21] from thermal studies. Ag^0 migrates inside beta cage and interacts with Ag^+ present there to form silver clusters. If this occurs during the activation process, positively charged structural defects would result on zeolite surface inside the zeolite cavities that also might have electrostatic interaction with N_2 molecules. However, this explanation for stronger interactions of N_2 molecules with silver exchanged zeolites is not tenable due to following reasons. The silver clusters in zeolites A has been reported [12-19] to be present in the sodalite cage and, thereby, ruling out the possibility of direct interaction of the N_2 molecules with silver clusters as N_2 molecules due to their higher kinetic diameter (2.67Å) cannot enter the sodalite cage which have smaller pore openings (2.2Å). Though, N_2 is observed to have stronger interactions with silver exchanged zeolite, the same cannot be said for oxygen molecules despite the fact that oxygen also has quadrupole moment albeit smaller in value. The heats of adsorption observed for oxygen molecules in the zeolites as well as Ar selectivity over oxygen in silver exchanged zeolites discard the formation of positively charged holes on evacuation in the samples studied by us. Their presence should have resulted into higher heats of adsorption due to chemisorption of oxygen atoms in the lower pressures to repair the oxygen deficient structural defects. This observation show that factors other than electrostatic interactions are responsible for stronger N_2 interactions in silver exchanged zeolite.

The higher heats of adsorption for N_2 observed in all silver exchanged zeolites can be explained in terms of π-complexation of nitrogen molecules with silver ions present inside the zeolites super cage [5, 31-32]. From the electronic configuration on N_2 [KK $(\sigma_{2s})^2 (\sigma_{2s}^*)^2 (\sigma_{2px})^2 (\pi^2_{2py})^2 (\pi^2_{2pz})^2 (\pi^2_{2py}{}^*)^0 (\pi^2_{2pz}{}^*)^0$] and Ag^+ [Kr] $4d^{10}$ $5s^0$ show the highest occupied and lowest unoccupied molecular orbitals in N_2 molecule are the bonding π_{2p} orbitals and antibonding π_{2p}^* orbitals respectively. Ag^+ ions has

completely occupied highest energy 4d orbitals along with unoccupied 5s orbitals. The energy difference between the lowest unoccupied molecular orbitals Ag^+ ions present in zeolite and highest occupied molecular orbital of nitrogen molecule is reported to be around 8eV. This facilitates electron transfer by both σ-donation (electron transfer from bonding π_{2p} orbitals of N_2 molecules to 5s orbital of Ag^+ ions) and d-π_{2p}^* back donation (electron transfer from completely occupied 4d orbital of Ag^+ ions to unoccupied π_{2p}^* of N_2 molecule). This π-complexation of nitrogen molecules with silver ions of the zeolites results into stronger interaction between silver exchanged zeolite and nitrogen molecules. However, in O_2 molecule electronic configuration [KK $(\sigma_{2s})^2(\sigma_{2s}^*)^2$ $(\sigma_{2px})^2$ $(\pi^2_{2py})^2$ $(\pi^2_{2pz})^2$ $(\pi^2_{2py}{}^*)^1$ $(\pi^2_{2pz}{}^*)^1$], two anti bonding π_{2p} orbitals are occupied by one electron each thus making it difficult for π-complexation. This is also reflected in the higher energy difference (11eV) between the lowest unoccupied molecular orbitals of Ag^+ ions present in zeolite X and highest occupied molecular orbital of oxygen molecule. Therefore, an anomalous increase observed for N_2 adsorption in silver exchanged zeolites is not seen for O_2.

Diffuse Reflectance Infrared Fourier Transform (DRIFT) spectroscopic study of the adsorbed N_2 molecules also supports stronger interaction of nitrogen molecules with extra framework silver ions present in the zeolite. N_2 molecules being totally symmetric do not absorb IR radiation. However, N_2 molecules adsorbed in zeolites experience induced dipole moment, which varies during vibration, and induced band is observed. The magnitude of the induced dipole moment depends on the strength of the interaction of the nitrogen molecules with the extra framework cations. At 303K, N_2 molecules adsorbed on AgA give the adsorption band at 2085cm^{-1}. Transition metal complexes are reported to interact with N_2 through end-on coordination (M-N≡N). This M-N_2 bonding is interpreted in terms of the σ-donation and π–back donation. It is further reported that ν(N≡N) shifts in the range 2220-1850cm^{-1} on π-complexation with transition metals from 2331cm^{-1} expected for free N_2 molecule. For example, N≡N stretching frequency in dinitrogen complexes with $[Ru(N_2)(NH_3)_5]Br_2$, $Co(N_2)(PPh_3)_3$, $[Os(N_2)(NH_3)_5]Cl_2$ and $Ir(N_2)Cl(PPh_3)_2$ are observed at 2105, 2093, 2022 and 2105cm^{-1} respectively [33]. N≡N stretching frequency at 2085cm^{-1} observed for N_2 molecule adsorbed in zeolite AgA is closer to these values confirming the π-complexation between nitrogen molecule and Ag^+ cations of the zeolites.

Argon molecules show higher interaction with Ag^+ ion exchanged zeolites and oxygen molecules don't show marked increase in adsorption values. Consequently, small argon sorption selectivity is observed over oxygen in silver exchanged zeolites. Munakata et al. [34] studied the adsorption of noble gases such as Kr and Xe on silver exchanged mordenite at 273K. Their experimental results also indicate that the silver mordenite has higher adsorption capacity of the adsorption of noble gases.

From the pure rotational spectra of the complexes of Ar with NaCl, AgCl, and Ar-Ag bond length had been found to be considerably shorter than that in Ar-Na bond length [35]. In addition, Ar-Ag bond energy was estimated using *ab initio* calculations to be ~23kJ mol^{-1} in Ar-AgF which is significantly larger than the corresponding value of 10kJ mol^{-1} for Ar-NaCl. These higher bond energies between Ar-AgF has also been supported by the electron density contour plots of some valence molecular orbitals which show significant overlap between Ar and Ag metal, particularly for the Ar(pσ)-Ag(dσ) bonding orbital. Significant electron donation up to (~ 0.11) electrons from Ar to metal halide is observed from Mulliken orbital populations. Similar explanation is put forth by Grosse et al. [36] form their studies on adsorption of Xenon using ^{129}Xe NMR spectroscopy in zeolites X and Y. Unlike other cations, silver exchanged zeolites have been reported to display the displacement of ^{129}Xe chemical shifts to lower values, i.e., upfield with respect to corresponding sodium form of these zeolites. This unusual upfield shifts and the distinctly higher isosteric heats of adsorption (26.5 and 31.2kJ mol^{-1}) for Xe in Ag^+ sites compared to sodium form (18.5kJ mol^{-1}) of zeolite Y [37] at low Xenon concentration is attributed to specific interactions (d_π-d_π) presumably between 4d orbitals of Ag^+ cations and 5d orbitals of xenon molecules.

These studies on Xe and Ar clearly show the existence of special interactions Ar (pσ) -Ag (dσ) bonding orbital for the Ar and Ag^+ and (d_π-d_π) between 5d orbitals of Xenon and 4d orbitals of Ag^+ cations. The argon selectivity observed for silver exchanged zeolites in our case can be explained from the special interactions, Ar (pσ)-Ag (dσ), between bonding molecular orbitals.

The variations observed for N_2 adsorption in terms of the adsorption capacity, Langmuir constant, Henry constants, adsorption selectivity and heats of adsorption for different amount of silver exchanged zeolite A (Tables-2.1, 2.2, 2.3, 2.5 and 2.6) can be explained in terms of difference in number of accessible/co-ordinately unsaturated

Ag^+ cations present in the zeolite. The adsorption N_2 capacity as well $\alpha_{N2/O2}$ adsorption selectivity is much higher (Table-2.5) in fully exchanged AgA compared to NaA in the pressure range studied. For example, AgA shows equilibrium N_2 adsorption capacity of 20.8 molecules per unit cell at 303K and 101.3kPa compared 4.6 molecules per unit cell in NaA. Similarly, $\alpha_{N2/O2}$ selectivity values at 3.33kPa are 3.1 and 15.4 for NaA and AgA respectively.

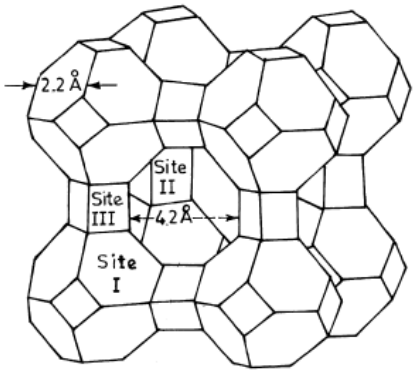

Figure-2.7. Framework structure of zeolite A. Near the centre of each line segment is an oxygen atom. Silicon and aluminium atoms alternate the tetrahedral intersections. Extra framework cation positions are labelled with Roman numerals.

Dependence of N_2 heats of adsorption on percentage silver exchange in zeolite A (Figure-2.6) shows an exponential rise at around 70% silver exchanges. These sharps increase in heat value show that N_2 selective in zeolite A arises only after 70% sodium cations are exchanged with silver cations. It is reported that [38], in $Ag_{12}A$ three Ag^+ ions present within the sodalite unit of the hydrated form move closer to the planes of the nearest 6-rings upon dehydration. Simultaneously, the Ag^+ ions present at the 4-ring site, and at the 8-ring sites undergo reduction and these Ag^+ ions become nearly zero coordinate, 2.9Å from the nearest framework oxide ions. The sum of the ionic radii of Ag^+ and O^{2-} is 2.6Å and the other Ag-O bond distance in the zeolite structure range from 2.2 to 2.5Å. Therefore, the Ag^+ ions present at the 4-ring site, and at the 8-ring sites with Ag-O bond distance of 2.9Å are least adequately coordinated Ag^+ ions are the energetically potential adsorption sites in the supercage. In terms of the accessibility of Ag^+ ions, cations located at 6-ring, 4-ring and 8-ring are expected to interact with N_2 molecules as normally observed for sodium or calcium cations present at these locations. However, the factor, which makes N_2 molecules interaction with silver cations stronger and higher, is the presence of co-ordinately unsaturated Ag^+ ions at 4-ring and 8-ring locations, which can have

stronger π-complexation with nitrogen molecules as explained in earlier section. Nearly similar heats of adsorption observed that of NaA for AgNaA samples (Figure-2.6) having Ag^+ exchange less than 70% silver exchange can be explained in terms of locations of Ag^+ in partially silver exchanged zeolite A. It has been reported that [39] in partially silver exchanged zeolite $Na_{4.4}Ag_{7.6}A$, dehydrated under vacuum at 643K, three sodium ions occupy 8-ring sites and the remaining 1.4 sodium and 6.6 silver ions located at 6-ring sites and one reduced silver per unit cell is located in sodalite cage. Thus, there are no Ag^+ ions present at 4-ring and 8-ring sites, which due to their unsaturated coordination react strongly with N_2 molecules.

2.4. REFERENCES

[1] R. M. Barrer, *Zeolites and Clay Minerals as Sorbents and Molecular Sieves*, Academic Press, London, 1978.

[2] E. Y. Choi, Y. Kim and K. Seff, *Microporous and Mesoporous Materials*, 2000, **41**, 61-68.

[3] S. Sircar, *Ind. Eng. Chem. Res*., 2002, **41**, 1389-1392

[4] R. V. Jasra, N. V. Choudary and S. G. T. Bhat, *Separation Science and Technology*, 1991, **26**, 885-930.

[5] R. T. Yang, Y. D. Chen, J. D. Peck and N. Chen, *Ind. Eng. Chem. Res.,* 1996, **35**, 3093-3099.

[6] R. T. Yang, *Adsorbents: Fundamentals and Applications*, Wiley Interscience, New York, 2003.

[7] C. C. Chao, *U. S. Pat. No. 4,859,217*, 1989.

[8] C. C. Chao, J. D. Sherman, J. T. Mullhaupt and C. M. Bolinger, *U. S. Pat. No. 5,174,979*, 1992.

[9] C. G. Coe, J. F. Kirner, R. Pierantozzi and T. R. White, *U. S. Pat. No. 5,152,813*, 1992.

[10] D. W. Breck, W. G. Eversole, R. M. Milton, T. B. Reed and T. L. Thomas, *J. Am. Chem. Soc.*, 1956, **78,** 5963-5971.

[11] M. Ralek, P. Jiru, O. Grubner and H. Bayer, *Collect. Czech. Chem. Commun.* 1962, **27**, 142-146.

[12] M. D. Baker, J. Godber and G. A. Ozin, *J. Phys. Chem.*, 1985, **89**, 2299-2304.

[13] M. D. Baker, G. A. Ozin and J. Godber, *J. Phys. Chem.*, 1985, **89**, 305-311.

[14] M. D. Baker, G. A. Ozin and J. Godber, *Catal. Rev. - Sci. Eng.*, 1985, **27**, 591-651.

[15] T. Sun and K. Seff, *Chemical Reviews,* 1994, **94**, 857-870.

[16] V. S. Gurin, N. E. Bogdanchikova and V. P. Petranovskii, *J. Phys. Chem. B* 2000, **104**, 12105-12110.

[17] Y. Kim and K. Seff, *J. American Chem. Soc.*, 1977, **99**, 7055-7057.

[18] Y. Kim and K. Seff, *J. American Chem. Soc.*, 1978, **100**, 175-180

[19] Y. Kim and K. Seff, *J. American Chem. Soc.*, 1978, **100**, 6989-6996.

[20] H. G. Karge, *Metal Microstructures in Zeolites*, 1982, 10-109.

[21] P. A. Jacobs and J. B. Uytterhoeven, *JCS Faraday Trans. I*, 1979, **75**, 56-64.

[22] L. R. Gellens, W. J. Mortier, R. A. Schoonheydt and J. B. Uytterhoeven, *J. Phys. Chem.*, 1981, **85**, 2783-2788.

[23] R. A. Schoonheydt and H. Leeman, *J. Phys. Chem.*, 1989, **93**, 2048 -2053.

[24] R. Seifert, A. Kunzmann and G. Calzaferri, *Angew. Chem. Int. Ed*., 1998, **37**, 1521-1524.

[25] R. Seifert, R. Rytz and G. Calzaferri, *J. Phys. Chem. A*, 2000, **104**, 7473-7483.

[26] G. Calzaferri, C. Leiggner, S. Glaus, D. Schurch and K. Kuge, *Chem. Soc. Rev.*, 2003, **32**, 29-37.

[27] N. V. Choudary, R. V. Jasra and S. G. T. Bhatt, *Ind. Eng. Chem. Res.*, 1993, **32**, 548-552.

[28] R. V. Jasra, N. V. Choudary and S. G. T. Bhatt, *Ind. Eng. Chem. Res.*, 1996, **35**, 4221-4229.

[29] N. V. Choudary, R. V. Jasra and S. G. T. Bhatt, *Indian Journal of Chemistry*, 1999, **39A**, 34-39.

[30] B. Tyagi, C. D. Chudasama and R. V. Jasra, *Indian chemical society*, 2001, **78**, 551-563.

[31] N. D. Hutson, S. U. Rege and R. T. Yang, *AIChE Journal*, 1999, **45**, 724-734.

[32] N. D. Hutson, D. A. Reisner, R. T. Yang and B.H. Toby, *Chem. Matter.*, 2000, **12**, 3020-3031.

[33] K. Nakamoto, *Infrared and Raman Spectra of Inorganic and Coordination Compounds – Part B: Applications in Coordination, Organometallic and Bioinorganic Chemistry*, Fifth Edition, Wiley Interscience, New York, 1997, 173-177.

[34] K. Munakata, S. Kaanjo, S. Yamatsuki, A. Koga, and D. Ianovski, *J. Nuclear Science and Technology*, 2003, **40**, 695-697.

[35] C. J. Evans, D. S. Rubino and M. C. L. Gerry, *Phys. Chem. Chem. Phys.*, 2000, **2**, 3943-3948.

[36] R. Grosse, R. Burmeister, B. Boddinberg, A. Gedeon and J. Fraissard, *J. Phys. Chem.*, 1991, **95**, 2443-2447.

[37] J. Watermann and B. Boddinberg, *Zeolites*, 1993, 427-429.

[38] Y. Kim and K. Seff, *J. Phys. Chem.*, 1987, **91**, 671-674.

[39] Y. Kim and K. Seff, *J. Phys. Chem.*, 1978, **82**, 1071-1077.

Chapter-3

Sorption of Nitrogen, Oxygen and Argon on Other Silver Exchanged Zeolites

3.1. INTRODUCTION

Since their introduction in the 1950's, synthetic zeolites have been used in numerous applications such as catalysis, ion exchange, drying, and separation by selective adsorption [1]. The most commonly used zeolite for these applications especially, for the selective adsorption of gases, are zeolite A and the faujasite analogy (types X and Y). Faujasite zeolites are composed of silica and alumina tetrahedra which are joined together to form the truncated octahedral or sodalite structure. These sodalite units are connected with tertiary units, hexagonal prisms in faujasite, to form the structured zeolite unit cell. In these structures, the SiO_2 groups are electro neutral, but the $(AlO_2)^-$ groups are not, and thus introducing a negative charge to the structure which is offset by the presence of a charge compensating, non-framework cation (e.g., Na^+, Li^+, Ca^{2+}). The aluminosilicate framework of faujasite type zeolite consists of a diamond-like array of linked octahedra, which are joined tetrahedrally through the 6-rings. The linkage between adjoining truncated octahedra is a double 6-ring, leading to a highly porous structure.

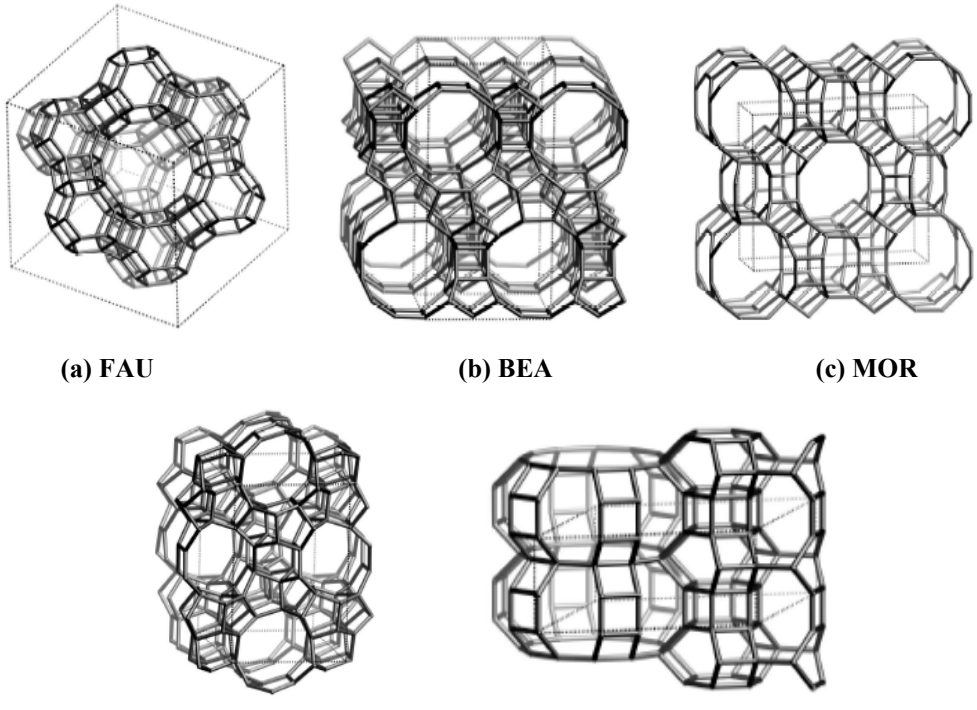

(a) FAU **(b) BEA** **(c) MOR**

(d) ZSM-5 **(e) LTL**

Figure-3.1. Framework Structure Zeolites of type FAU, BEA, MOR, MFI and LTL

Zeolites of types BEA, MOR, ZSM-5 and LTL have channels in the 3D structures. BEA (Figure-3.1b) has two different channels of sizes 6.6 × 6.7Å and 5.6 × 5.6Å.

Zeolite mordenite has elliptical straight cylindrical one-dimensional channels, running parallel to the c axis (Figure-3.1c) with minor and major axes as 5.8 and 7.0Å respectively. The main channels are circumscribed by 12-ring oxygen atoms of the framework has dimensions of 6.5 × 7.0Å and open in the b direction into smaller side channels circumscribed by 8-rings having a dimensions of 2.6 × 5.7Å and leading towards the next main channel. The structure of ZSM-5 (Figure-3.1d) consists of pentasile units linked together into chains, which together form layers. Two different types of channels of sizes 5.1 × 5.5Å and 5.3 × 5.6Å are found in ZSM-5 structure. The crystal structure of zeolite L is based on the 18 tetrahedra unit (ε-cage) found in the feldspathoid and erionite. It consists of columns of symmetrical ε-D6R-ε (18 tetrahedra) units cross-linked to others by single oxygen bridges resulting in a planar 12-membered ring wide channel of 7.1Å diameter.

It is known that the extra framework cations in the zeolite are largely responsible for the adsorptive capacity of these materials [1, 2]. This is primarily due to the van der Waals and Columbic interactions between the charge compensating cations of the zeolite and the adsorbing gas. Because of the extra framework cations are so significantly influencing the adsorption properties of the zeolites, numerous attempts have been made to optimise these properties by (i) increasing the number of cation sites (the cation exchange capacity, CEC) by creating zeolites with high aluminium content, and (ii) by synthesizing zeolites containing various combinations of alkaline and alkaline earth cations [2, 3].

Kuhl reported [4] a procedure for the synthesis of low silica X-type zeolite (LSX). This material is an aluminium saturated X-type zeolite with a SiO_2/Al_2O_3 ratio of 2.0 (or Si/Al = 1.0). Commercial X-zeolite, which is typically available as the Na^+ form (known commercially as 13X), is not aluminium saturated and contains 86 aluminium atoms per unit cell, while the LSX zeolite contains 96 aluminium atoms per unit cell. Silver is known to strongly influence the adsorption characteristics of some alumino silicate zeolites. Habgood measured [5] isotherms for N_2, O_2, C_2H_6 and C_2H_4 adsorbed on Ag-X zeolite and compared to those same gas isotherms measured on alkali and alkaline earth cation exchanged X zeolite. The alkali and alkaline earth cations are all of a stable noble gas electronic configuration, where as the d-orbitals of the silver ion give it much more intense directional properties. It was concluded that the silver ion has a much stronger polarizing power than the sodium ion which is of

the same total charge and very similar in size. Huang measured [6] adsorption of CO, N_2, O_2, CO_2 and C_2H_4 on Ag-X and Ag-Y zeolites.

The use of silver exchanged zeolites of the type mordenite and X as argon selective adsorbents are reported in the literature. Knaebel et al. [7] reported silver exchanged mordenite for the selective adsorption of argon from oxygen-argon mixture. Kandybin et al [8] and Chiang et al. [9] reported the use of silver exchanged zeolite X as argon selective adsorbent for the production of high purity oxygen by PSA methods. Yang et al. reported [10] the synthesis of a mixed Li/Ag ion-exchanged X-type zeolite (Si/Al = 1.25 with approximately 17 Ag^+ per unit cell), and discussed its possible superior properties for air separation. Hutson et al. [11] have recently reported the synthesis of mixed Li/Ag X-type zeolite in which the addition of very small amounts of Ag^+ and the proper dehydration conditions resulted in enhanced adsorptive characteristics and increased energetic heterogeneity as compared to those of the near fully exchanged Li^+-zeolites.

The effect of silver ion exchange on the adsorption properties of zeolite A is described detail in Chapter-2. Silver exchanged zeolite A (AgA) interacts strongly with N_2 molecules and possess nitrogen as well as argon adsorption selectivity over oxygen. AgA shows equilibrium adsorption capacity of 22.3cc g^{-1}, 4.36cc g^{-1} and 6.25cc g^{-1} respectively for nitrogen, oxygen and argon at 303.0K and 101.3kPa, and N_2/O_2 selectivity 5-15.4 and Ar/O_2 selectivity 1.5 to 1.6 at 303.0K in the pressure range studied. In this Chapter, the adsorption studies of nitrogen, oxygen and argon were extended to other zeolites, with an objective to explore the structure on the adsorption properties. Adsorption of nitrogen, oxygen and argon silver ion exchanged zeolites of type X, Y, L, BEA, MOR and ZSM-5 were studied at different temperatures. The resulting nitrogen adsorptive characteristics of these materials and related adsorptive capacity are correlated with the cation/cluster locations within the zeolite.

3.2. EXPERIMENTAL

3.2.1. Materials

Zeolites X from Zeolites and Allied Products, Bombay, India, Zeolite Y (SiO_2/Al_2O_3 = 5.5) from Süd-Chemie AG, Germany, Zeolite L, ZSM-5, Mordenite and BEA from Zeocat, Uetikon, Switzerland and silver nitrate (99.9%) from Ranbaxy Fine Chemicals Ltd., New Delhi, India were used as the starting materials for the adsorbent

preparation. Oxygen (99.99%), Nitrogen (99.99%), Argon (99.99%) and Helium (99.99%) from Hydrogas India Pvt. Ltd., Bombay, India were used for the adsorption isotherm measurements. The chemical composition, BET surface area and channel/ cavity size of the various zeolites used for the adsorption studies are given in Table-3.1.

Table-3.1. Properties and Chemical Composition of the Zeolites

Zeolite Type	Channel size in Å	Channel/ cavity diameter in Å	BET Surface Area in m^2g^{-1}	Chemical Composition on anhydrous basis wt%		
				Na_2O	Al_2O_3	SiO_2
NaX	7.4 × 7.4	12.0	542	24.6	19.0	56.4
NaY 5.5	7.4 × 7.4	12.0	810	3.0	22.0	71.0
Zeolite L [a]	7.1 × 7.1	7.1	312	0.1	18.3	64.2
BEA	6.6 × 6.7; 5.6 × 5.6	6.7	612	1.2	7.8	91.0
Na Mordenite 060	6.5 × 7.0; 2.6 × 5.7	7.0	50	7.5	12.4	80.1
Na Mordenite 510	6.5 × 7.0; 2.6 × 5.7	7.0	450	0.04	7.8	92.1
Na ZSM-5 (25)	5.1 × 5.5; 5.3 × 5.6	5.6	371	3.0	6.4	90.8
N a ZSM-5 (40)	5.1 × 5.5; 5.3 × 5.6	5.6	379	1.5	3.8	94.7
Na ZSM-5 (100)	5.1 × 5.5; 5.3 × 5.6	5.6	348	1.8	1.8	90.1
Na ZSM-5 (400)	5.1 × 5.5; 5.3 × 5.6	5.6	334	1.5	0.4	98.0
Na ZSM-5 (900)	5.1 × 5.5; 5.3 × 5.6	5.6	315	1.5	0.2	98.1

[a] K_2O=17.5%.

3.2.2. Silver ion Exchange

The silver cations were introduced into the highly crystalline sodium form of zeolite by the conventional cation exchange from aqueous $AgNO_3$ solution following procedure described in section 2.2.2. Typically, the zeolite was refluxed with aqueous $AgNO_3$ solutions, containing 1.5 times excess of Ag^+ ions over the quantity of base Na^+, in the solid / liquid ratio 1:80 at 353K for 4 hours. The residue was filtered, washed with hot distilled water, until the washings were free from Ag^+ ions and dried at a temperature below 353K in vacuum / air. All the activities were carried out in absence of direct contact with light. The extent of silver exchange in zeolites was determined by using Shimadzu AA-680 atomic absorption spectrometer.

3.2.3. X-ray Powder Diffraction

X-ray powder diffraction studies at ambient temperature were carried out using PHILIPS X'pert MPD system in the 2θ ranges of 5-65 degrees using CuKα1 (λ = 1.54056Å). The diffraction patterns of the starting materials show that these are highly crystalline showing the reflections in the range 5 to 35 degrees typically of zeolites. The structures of the zeolites were retained after the cation exchange. No loss of crystallinity was observed during silver exchange.

3.2.4. SEM and EDX

Microscopic analysis of sodium and silver forms of the zeolites were carried out using LEO 1430 VP variable pressure scanning electron microscope equipped with INCA Oxford EDX facility. EDX measurement confirms the absence of sodium ions in the silver ion exchanged zeolites.

3.2.5. Activation and Isotherm Measurements

The samples were initially dried at 353K for 24h and further activated in situ by increasing the temperature (at a heating rate <1K $min.^{-1}$) to 673K under vacuum ($5x10^{-3}$mmHg) for 8hours before the sorption measurements. Nitrogen, oxygen and argon adsorption was measured at 288.2K and 303.0K using a static volumetric system (Micromeritics Instrument Corporation, USA, Model ASAP 2010) as explained in section 2.2.6. The isotherms were fitted in various equations like Langmuir equation, Virial equation and Dubinin-Astakhov equation. Henry's constant, adsorption capacity, adsorption selectivity and isosteric heat of adsorption were determined from the adsorption data obtained at different temperatures as described in section 2.2.6.

3.3. RESULTS AND DISCUSSION

3.3.1. Activation and Colour changes

Silver exchanged zeolite X became yellow and zeolite Y (SiO_2/Al_2O_3 5.5) became dark yellow when heated at 623K under vacuum, apparently due to water desorption. These colour changes were reversible with respect to the adsorption and desorption of water molecules. However, silver exchanged ZSM-5 with silica/alumina ratio 400 and 900 irreversibly changes their colour to dark brown during the vacuum dehydration at 623K. Other zeolites studied turn grey during the vacuum dehydration process.

Colours changes observed for the hydrated and vacuum dehydrated forms of the silver exchanged zeolites are given in Table-3.2.

Table-3.2. Change in the colours of the Adsorbents on vacuum dehydration

Adsorbent	Colour of the hydrated form	Colour after vacuum dehydration at 673K	Possible silver species
AgX	Slightly grey	Yellow	Ag_3^{2+}
AgY 5.5	Slightly grey	Dark Yellow	Ag_3^{2+}
AgL	White	Grey	Ag^0
Ag BEA	White	Grey tan	Ag^0
Ag MOR 060	Slightly grey	Grey	Ag^0
Ag MOR 510	White	Grey	Ag^0
Ag ZSM-5 (25)	White	Grey	Ag^0
Ag ZSM-5 (40)	White	Grey	Ag^0
Ag ZSM-5 (100)	White	Grey	Ag^0
Ag ZSM-5 (400)	Pale yellow	Dark brown	-
Ag ZSM-5 (900)	Pale yellow	Dark brown	-

Ralek et al. [12] first reported that the white hydrated silver form of zeolite A exhibits a red colour after dehydration at 623K, which has been later confirmed by many authors. The dehydrated silver exchanged zeolite A has been reported to adsorb visible light at 500 nm. It is reported that on vacuum dehydration silver ions migrates and undergoes auto reduction to form Ag^0, which interacts with silver ions to form clusters. Various types of clusters varying from linear Ag^+-Ag^0-Ag^+ to Ag_5^{4+}, Ag_8^{6+} and Ag_{12}^{8+} have been reported depending on the zeolite type and the extent of silver exchange [13-27]. However, in AgX and AgY, only yellow colour is observed even at higher temperatures (723K) under vacuum showing the presence of isolated Ag_3^{2+} clusters in these zeolites. As explained in Chapter-2, the colour changes are attributed to electronic transitions from the lone pairs of oxygen atoms of the zeolite framework to the empty 5s orbital of Ag^+ ions, i.e., ligand to metal transfer (LMCT). X-ray powder diffraction data of the vacuum dehydrated grey coloured silver exchanged zeolites show peaks at d = 2.36, 1.44, 1.23 and 1.18 (2θ = 38.1, 64.4, 77.6 and 81.6) corresponding to Ag^0. The grey colour is due to the formation of Ag^0 resulting from the partial reduction of Ag^+ ions during the vacuum dehydration process.

Jacobs et al. [22] have showed that the reduction of silver zeolites A and Y by thermal vacuum dehydration involves auto reduction of silver ions by intrazeolite water and lattice oxygen in two clearly defined temperature ranges.

(i) Low temperature region

$$2(Ag^{+}\text{-}Z\text{-}O^{-}) + H_2O \xrightarrow{25\text{-}250^{o}C} \tfrac{1}{2}O_2 + 2Ag^{0} + \underset{\text{Framework Hydroxyl}}{2Z\text{-}OH}$$

(ii) High temperature region

$$2(Ag^{+}\text{-}Z\text{-}O^{-}) \xrightarrow{127\text{-}380^{o}C} \tfrac{1}{2}O_2 + 2Ag^{0} + \underset{\text{Zeolite lattice}}{Z\text{-}O^{-}} + \underset{\text{Lewis Acid site}}{Z^{+}}$$

Depending on the silver exchange level, the Ag^0 atoms so produced are either immobilised at precursor Ag^+ ion sites or migrate to subsequently interact with other Ag^0 atoms or Ag^+ ions forming Ag_n^{q+} clusters. In the case of Ag ZSM-5 (400) and Ag ZSM-5 (900), the numbers of cations are very small. The brown colours observed during the vacuum dehydration of AgZSM-5 (400) and AgZSM-5 (900) might be due to the formation of small amount of silver oxide during the ion exchange/activation process. Also the colour changes on AgZSM-5 (400) and AgZSM-5 (900) are irreversible with the adsorption and desorption of water molecules.

3.3.2. Equilibrium Adsorption Isotherms

The nitrogen, oxygen and argon adsorption isotherms on fully silver exchanged zeolite X (AgX) and NaX at 303.0K are given in Figure-3.2. The nitrogen, oxygen and argon equilibrium adsorption capacities increase on silver exchange. Nitrogen shows the maximum increase in the adsorption capacity. The over all increase in the nitrogen adsorption capacity is about 75% to that of the parent sodium form. In the low-pressure region the equilibrium nitrogen adsorption capacity increases sharply with pressure and the nitrogen adsorption isotherm becomes non-linear. Yang et al. [10] reported similar sharp increase in the nitrogen adsorption capacity in the low-pressure region for AgX and LSAgX. The shape of the oxygen and argon adsorption isotherms remains linear after the silver ion exchange. The increase in the argon adsorption capacity is higher than that of oxygen. Like silver exchanged zeolite A, AgX also shows argon selectivity over oxygen.

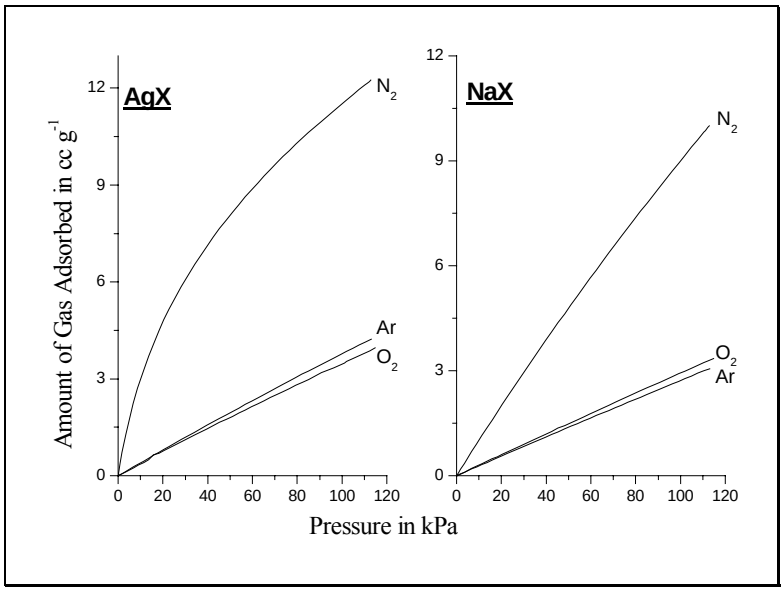

Figure-3.2. Adsorption Isotherms in AgX and NaX at 303.0K

The nitrogen, oxygen and argon adsorption isotherms on silver exchanged zeolite Y (5.5) and the parent sodium form of zeolite Y (5.5) at 303.0K are given in Figure-3.3. In zeolite Y (5.5) the observed increase in equilibrium nitrogen adsorption values on silver exchange is more than 100%. In the low-pressure region the equilibrium nitrogen adsorption capacity increases sharply with pressure and the nitrogen adsorption isotherm becomes non-linear. The oxygen and argon adsorption capacities also increase on silver exchange, but the shape of the adsorption isotherm remains linear. The magnitude of increase in the argon adsorption is higher than that of oxygen adsorption and AgY (5.5) also shows argon selectivity over oxygen.

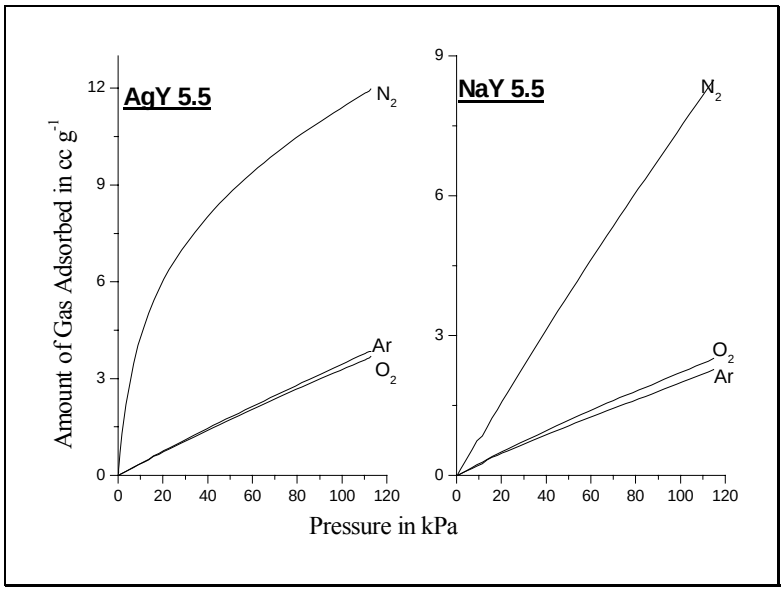

Figure-3.3. Adsorption Isotherms in AgY 5.5 and NaY 5.5 at 303.0K

Silver exchanged mordenite type zeolite also shows nitrogen as well as argon selectivity over oxygen. Like AgX and AgY (5.5), silver mordenite also shows sharp increase in the equilibrium nitrogen adsorption capacity in the low-pressure region (<30kPa) and the nitrogen adsorption isotherm becomes non-linear. The adsorption isotherms on silver and sodium form of mordenite 060 are given in Figure-3.4.

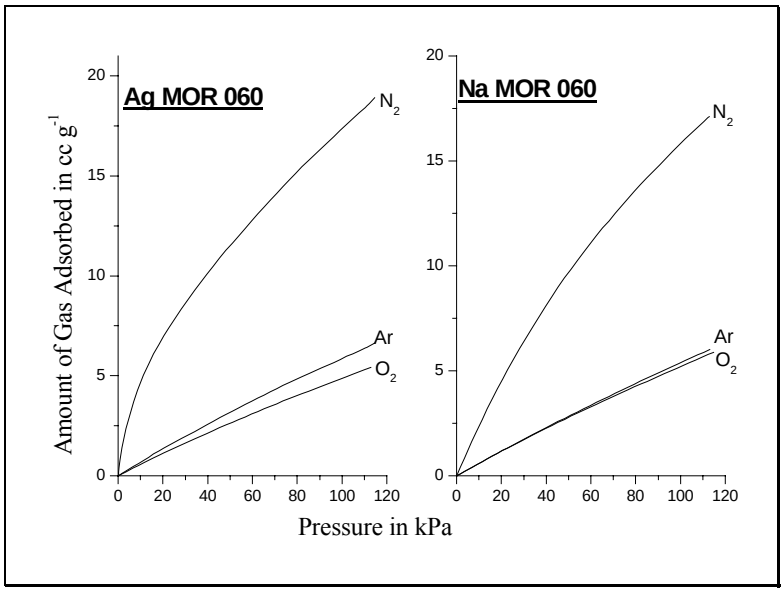

Figure-3.4. Adsorption Isotherms in Ag MOR 060 and NaMOR 060 at 303.0K

The adsorption isotherms on silver and sodium form of zeolite beta at 303.0K are given in Figure-3.5. The adsorption capacities for nitrogen, oxygen and argon increase on silver exchange. Like other silver exchanged zeolites, Ag BEA also shows non-linear nitrogen adsorption isotherm and argon selectivity over oxygen.

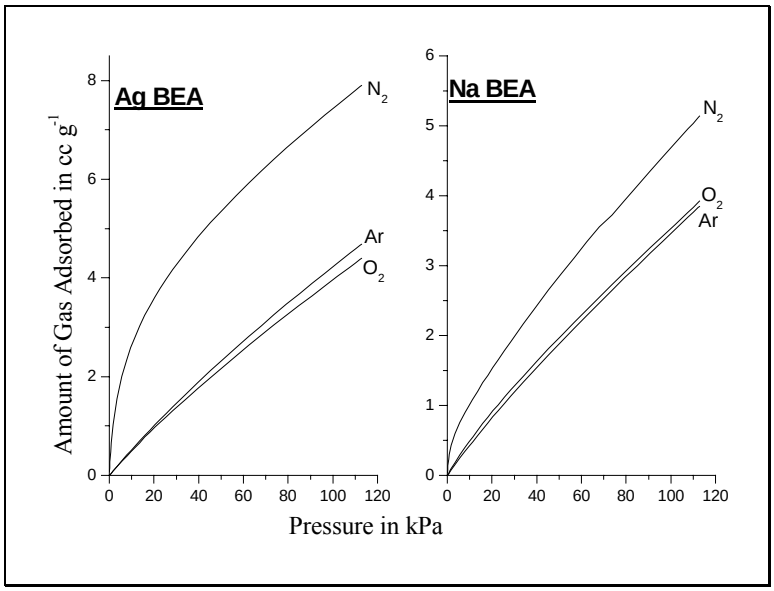

Figure-3.5. Adsorption Isotherms in Ag BEA and Na BEA at 303.0K

The nitrogen, oxygen and argon adsorption isotherms on silver and sodium form of zeolite L at 303.0K were shown in Figure-3.6. The adsorption capacities for nitrogen, oxygen and argon increase on silver exchange, but the shape of nitrogen adsorption isotherm remains linear. AgL also shows nitrogen and argon selectivity over oxygen.

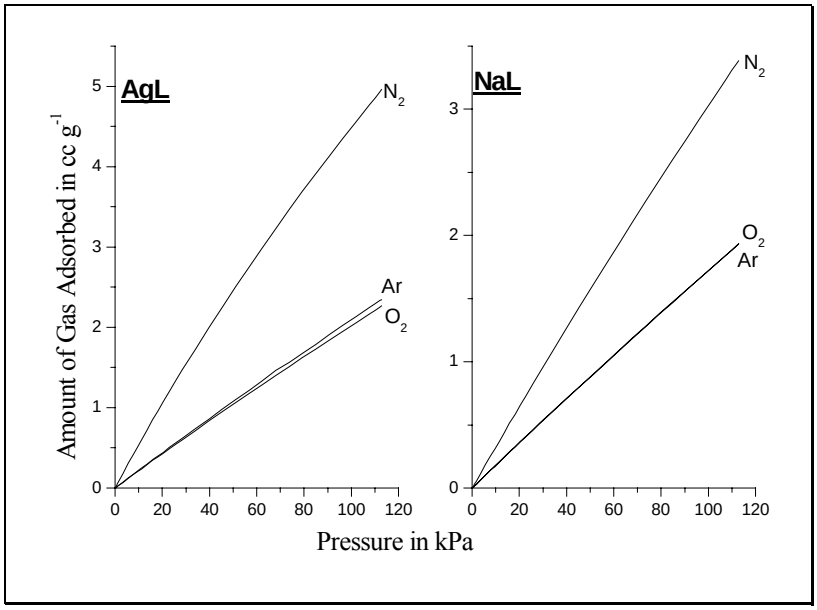

Figure-3.6. Adsorption Isotherms on Zeolite L at 303.0K

The nitrogen, oxygen and argon adsorption isotherms on silver and sodium form of ZSM-5 (25) at 303.0K were shown in Figure-3.7. In the case of ZSM-5 (25) also, the non-linear nitrogen adsorption isotherm and argon-oxygen selectivity were observed.

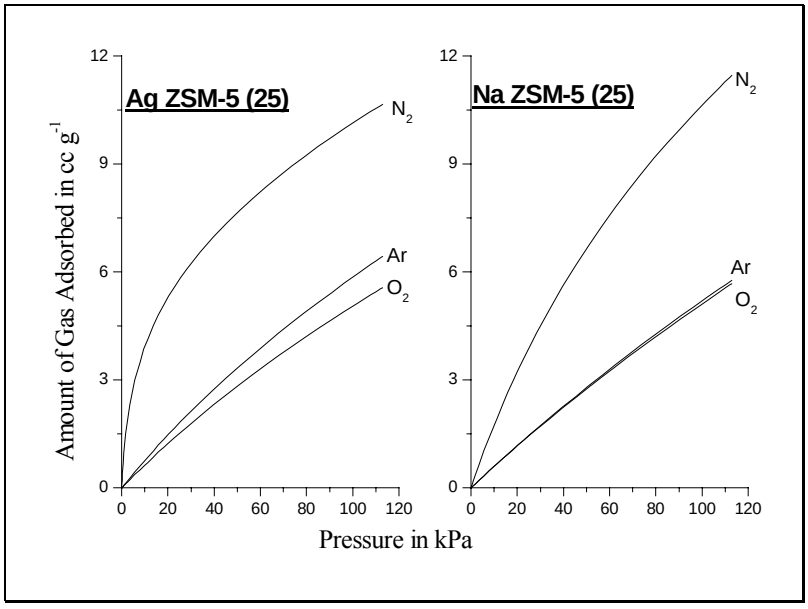

Figure-3.7. Adsorption Isotherms in Ag ZSM-5 (25) and Na ZSM-5 (25) at 303.0K

The adsorption isotherms on silver exchanged ZSM-5 (40) and Na ZSM-5 (40) at 303.0K are given in Figure-3.8. The nitrogen adsorption sharply increases with pressure in the low-pressure region and the nitrogen adsorption isotherm becomes non-linear after silver ion exchange. The adsorption isotherms for oxygen and argon remained unchanged on silver ion exchange.

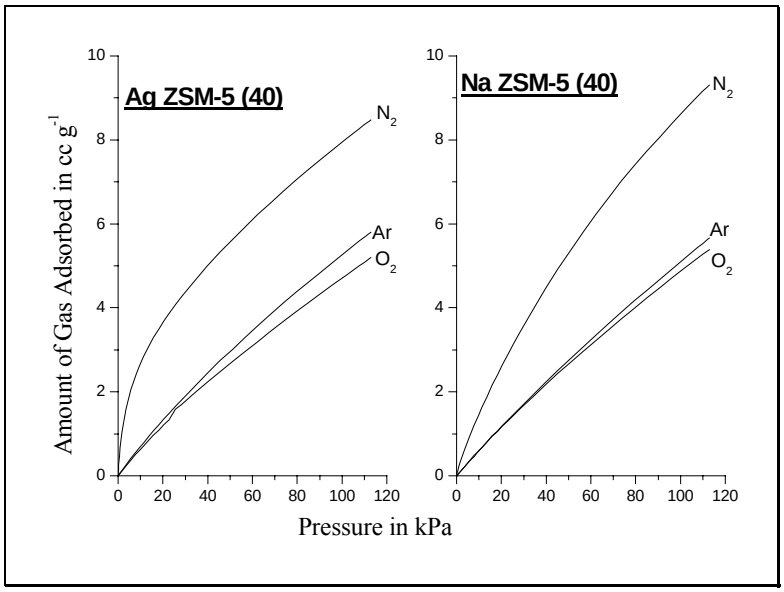

Figure-3.8. Adsorption Isotherms in Ag ZSM-5 (40) and Na ZSM-5 (40) at 303.0K

Figure-3.9 represents the nitrogen, oxygen and argon adsorption isotherms on silver and sodium forms of ZSM-5 (100) at 303.0K. The sharp increase in the nitrogen adsorption with pressure in the low-pressure region is observed in this case too.

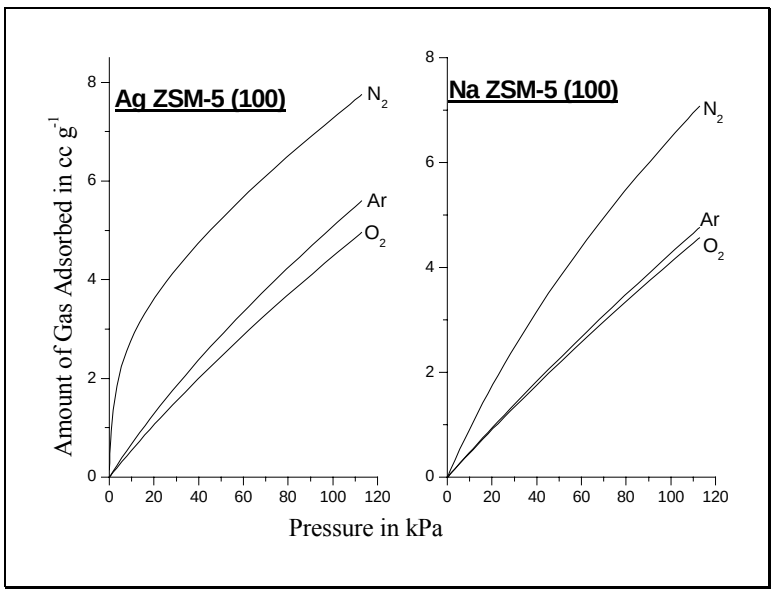

Figure-3.9. Adsorption Isotherms in Ag ZSM-5 (100) and Na ZSM-5 (100) at 303.0K

The adsorption isotherms for nitrogen, oxygen and argon on silver and sodium forms of ZSM-5 (400) are shown in Figure-3.10. The sharp increase in the nitrogen adsorption with pressure is limited to a very small pressure range.

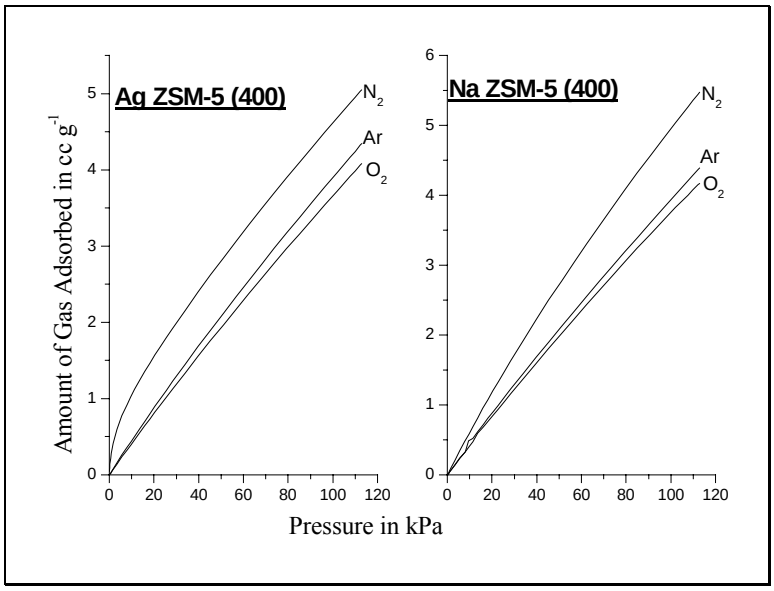

Figure-3.10. Adsorption Isotherms in Ag ZSM-5 (400) and Na ZSM-5 (400) at 303.0K

Figure-3.11 compares the nitrogen, oxygen and argon adsorption isotherms on silver and sodium forms of ZSM-5 (900) at 303.0K. In this case, sharp increase in the nitrogen adsorption with pressure is limited to a few Pascal pressure.

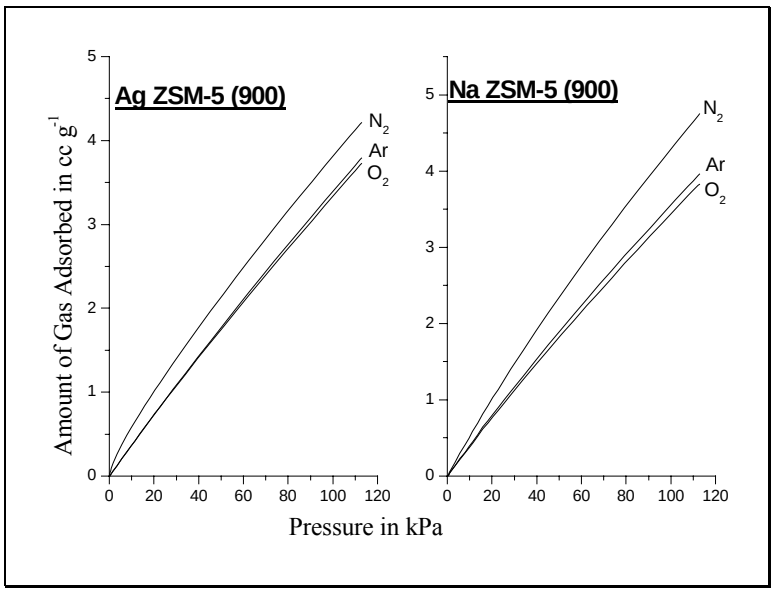

Figure-3.11. Adsorption Isotherms in Ag ZSM-5 (900) and Na ZSM-5 (900) at 303.0K

In all the silver exchanged ZSM-5 zeolites, similar trend in the adsorption properties were observed. The nitrogen adsorption shows sharp increase with equilibrium

pressures in the low-pressure region. The pressure range of the sharp increase is up to 30kPa in AgZSM-5 (25). In the case of AgZSM-5 (40), the pressure range decreases slightly on increasing the SiO_2/Al_2O_3 ratio from 25 to 40. On further increasing the SiO_2/Al_2O_3 ratio to 100 the pressure range of the sharp increase in the nitrogen adsorption further decreases. The sharp increase in the nitrogen adsorption is limited to a very small pressure range in AgZSM-5 (400) and AgZSM-5 (900), in which the number of extra framework cations are very low. This can be attributed to the decrease in the number of extra framework silver cations, which interact very strongly with the nitrogen molecules.

The equilibrium adsorption capacities for the adsorption of nitrogen, oxygen and argon on various silver exchanged zeolites are determined from the adsorption isotherms and the values at 101.3kPa and 303.0K are given in Table-3.3. The nitrogen, oxygen and argon adsorption capacities increased on silver ion exchange. The magnitude of the increase in the adsorption capacity for nitrogen is much higher than that of argon and oxygen. The increase in the adsorption capacity follows the order nitrogen>>argon>oxygen.

Table-3.3. Equilibrium Adsorption Capacity for N_2, O_2 and Ar at 303.0K

Adsorbent	Equilibrium Adsorption Capacity in molecules / unit cell at 101.3kPa					
	Sodium form			Silver form		
	Nitrogen	Oxygen	Argon	Nitrogen	Oxygen	Argon
Zeolite X	5.50	1.80	1.67	10.87	3.29	3.59
Zeolite Y 5.5	2.89	1.21	1.06	7.53	2.19	2.29
Zeolite L	0.34	0.20	0.20	1.20	0.54	0.56
BEA	0.83	0.63	0.61	1.38	0.74	0.79
MOR 060	2.19	0.75	0.75	2.93	0.83	0.99
MOR 510	0.57	0.53	0.60	0.93	0.61	0.72
ZSM-5 (25)	2.85	1.38	1.40	2.99	1.50	1.74
ZSM-5 (40)	2.26	1.29	1.35	2.15	1.28	1.43
ZSM-5 (100)	1.70	1.08	1.12	1.92	1.19	1.35
ZSM-5 (400)	1.30	0.99	1.03	1.21	0.96	1.03
ZSM-5 (900)	1.12	0.90	0.93	1.00	0.88	0.89

The adsorption data obtained for various sodium and silver form of the adsorbents at 288.2K and 303.0K were fitted in Langmuir equation and the slope, intercept and Langmuir constant were determined. The values for the slope and Langmuir constant, b increases for nitrogen, oxygen and argon on silver exchange, while that of intercept decreases. The Langmuir constants for the adsorption of N_2, O_2 and Ar on various silver exchanged zeolites at 303.0K are given in Table-3.4.

Table-3.4. Langmuir Constant on Various Silver Exchanged Zeolites at 303.0K

Adsorbent	Langmuir Constant b at 303.0K					
	Sodium form			Silver form		
	Nitrogen	Oxygen	Argon	Nitrogen	Oxygen	Argon
Zeolite X	0.1597	0.0338	0.0435	2.2873	0.1267	0.0769
Zeolite Y 5.5	0.0700	0.1942	0.1869	3.9793	0.1238	0.1120
Zeolite L	0.0841	0.0684	0.0507	0.2551	0.0770	0.0714
BEA	1.4010	0.4739	0.2857	3.5651	0.3115	0.2762
MOR 060	0.6623	0.1733	0.1217	2.0367	0.2016	0.2101
MOR 510	0.3175	0.0960	0.1475	1.0247	0.1197	0.1578
ZSM-5 (25)	0.8547	0.2016	0.1873	4.3253	0.3236	0.3759
ZSM-5 (40)	0.9174	0.2915	0.2128	3.2000	0.4464	0.4184
ZSM-5 (100)	0.5348	0.1416	0.1404	3.9588	0.2695	0.4149
ZSM-5 (400)	0.2770	0.1477	0.1629	1.5106	0.1397	0.1866
ZSM-5 (900)	0.2577	0.1484	0.1656	0.6410	0.1302	0.1103

The nitrogen, oxygen and argon adsorption data obtained at 288.2K and 303.0K were also fitted in Virial equation. The Virial coefficients A_0, A_1 and A_2 were determined from the Virial plots. The Henry's constants were calculated from the Virial coefficient. The values for the Henry's constant K at 303.0K are given in Table-3.5. As observed from the data, the values of the Henry's constants for all the three gases increase on silver exchange. The order of increase in the Henry constants is nitrogen>>argon>oxygen which is different from the order nitrogen>oxygen>argon observed for sodium form of the zeolites. These data show (a) very strong interaction of nitrogen molecules with the silver exchanged zeolite surface (b) argon molecules

also have strong interaction with silver exchanged zeolites as compared to oxygen molecules.

Table-3.5. Henry's Constant on Various Silver Exchanged Zeolites at 303.0K

Adsorbent	Henry's Constant K (10^{-5}ccg^{-1}Pa^{-1}) at 303.0K					
	Sodium form			Silver form		
	Nitrogen	Oxygen	Argon	Nitrogen	Oxygen	Argon
Zeolite X	10.2	3.0	2.9	45.9	3.5	3.9
Zeolite Y 5.5	5.5	2.2	1.8	84.6	3.5	3.9
Zeolite L	3.2	1.8	1.8	5.5	2.1	2.2
BEA	58.2	5.6	4.4	104.0	5.2	5.2
MOR 060	25.0	5.7	5.9	103.8	5.6	6.7
MOR 510	4.3	3.9	4.1	47.7	6.9	8.1
ZSM-5 (25)	20.7	5.9	5.7	138.8	6.5	7.5
ZSM-5 (40)	26.8	6.7	5.9	101.8	6.9	7.7
ZSM-5 (100)	9.6	4.5	4.6	89.5	5.5	7.1
ZSM-5 (400)	5.8	4.0	4.0	78.9	4.1	4.6
ZSM-5 (900)	5.3	3.8	3.9	13.5	3.5	3.3

The nitrogen, oxygen and argon adsorption data obtained at 288.2K and 303.0K were also fitted in Dubinin-Astakhov equation. Slope of the D-A plot decreases on increase in silver exchange. The values for intercept, energy and volume increases for all the three gases. The magnitude of the increase follows the order nitrogen>> argon> oxygen. The value of the Dubinin-Astakhov energy at 303.0K is given in Table-3.6.

Table-3.6. Dubinin-Astakhov Energy on Various Silver Exchanged Zeolites at 303.0K

Adsorbent	Dubinin-Astakhov Energy kJ mol^{-1}					
	Sodium form			Silver form		
	Nitrogen	Oxygen	Argon	Nitrogen	Oxygen	Argon
Zeolite X	12.19	10.38	10.63	20.56	10.94	10.89
Zeolite Y 5.5	11.61	11.31	11.81	26.63	10.86	11.05
Zeolite L	11.72	10.51	10.69	12.76	10.85	10.84
BEA	17.15	12.09	11.85	24.44	11.70	12.00
MOR060	15.05	11.21	11.18	19.52	11.33	11.68
ZSM-5 (25)	15.69	11.26	11.52	26.97	11.92	12.53
ZSM-5 (40)	15.39	11.60	11.65	23.42	12.38	12.42
ZSM-5 (100)	14.22	10.99	11.21	27.02	11.61	12.54
ZSM-5 (400)	12.88	11.11	11.60	16.70	10.96	11.42
ZSM-5 (900)	12.71	11.01	11.41	13.72	10.92	11.12

3.3.3. Adsorption Selectivity

Nitrogen/oxygen selectivity ($\alpha_{N2/O2}$) increases after the silver exchange in all types of the zeolites studied. Even though sodium and silver forms of the zeolite contain same number of cations, the $\alpha_{N2/O2}$ is very high (up to 7 times) for the silver form of the zeolite in the low-pressure region (Table-3.7). The value of $\alpha_{N2/O2}$ in silver exchanged zeolites decreases as pressure increases and finally reduces to that of the sodium form. $\alpha_{N2/O2}$ is as high as 23 at 3.33kPa in AgY 5.5. The silver form of the zeolite also shows an increase in the nitrogen/argon selectivity ($\alpha_{N2/Ar}$). The increase in $\alpha_{N2/Ar}$ is also very high in the low-pressure region. Like the nitrogen-oxygen selectivity, nitrogen/argon selectivity also decreases with increase in pressure (Table-3.7).

All the silver exchanged zeolites shows marginal argon selectivity over oxygen. The argon/oxygen selectivity is a unique property of silver exchanged zeolites. Earlier studies were also reported this argon/oxygen selectivity in silver exchanged mordenite and X type zeolites [7-9]. In alkali and alkaline earth cation-exchanged zeolites, oxygen and argon adsorption remains nearly same or marginally oxygen selective [28-30]. Argon/oxygen selectivity, $\alpha_{Ar/O2}$ marginally increases with increase in

pressure. All the silver exchanged zeolites shows argon selectivity over oxygen at 101.99 kPa and 303.0 K. AgZSM-5 (25) shows highest value (1.65) for argon/oxygen selectivity, followed by AgA (1.63).

Table-3.7. Adsorption Selectivity in sodium and silver exchanged zeolites at 303K

Adsorbent	Adsorption Selectivity					
	$\alpha N_2/O_2$		$\alpha N_2/Ar$		$\alpha Ar/O_2$	
	3.33kPa	101.99kPa	3.33kPa	101.99kPa	3.33kPa	101.99kPa
NaX	3.4	3.1	3.7	3.3	0.92	0.93
AgX	10.6	3.2	9.5	2.9	1.11	1.11
NaY 5.5	3.5	3.4	3.8	3.7	0.90	0.91
AgY 5.5	23.1	3.0	20.7	2.7	1.11	1.12
Zeolite L	1.8	1.7	1.8	1.7	1.0	1.00
AgL	2.5	2.2	2.5	2.1	1.02	1.04
NaBEA	3.3	1.3	4.0	1.3	0.82	0.98
AgBEA	8.8	1.8	8.7	1.7	1.00	1.07
NaMOR 060	4.1	2.9	4.2	2.8	0.97	1.02
AgMOR 060	12.1	3.5	10.1	2.8	1.20	1.22
NaMOR 510	1.1	1.1	1.0	1.0	1.08	1.07
AgMOR 510	4.8	1.6	4.1	1.4	1.17	1.13
NaZSM-5 (25)	3.3	1.9	3.5	1.8	0.98	1.02
AgZSM-5 (25)	10.3	1.9	8.8	1.6	1.49	1.65
NaZSM-5 (40)	2.9	1.7	2.9	1.6	0.97	1.05
AgZSM-5 (40)	6.9	1.6	6.3	1.5	1.21	1.25
NaZSM-5 (100)	2.1	1.6	2.0	1.5	1.03	1.04
AgZSM-5 (100)	9.8	1.6	7.7	1.4	1.17	1.23
NaZSM-5 (400)	1.5	1.3	1.5	1.3	1.02	1.05
AgZSM-5 (400)	4.3	1.2	3.8	1.2	1.12	1.15
NaZSM-5 (900)	1.4	1.2	1.3	1.2	1.03	1.03
AgZSM-5 (900)	2.1	1.1	2.1	1.1	1.02	1.05

3.3.4. Heat of Adsorption

The isosteric heat of adsorption for nitrogen, oxygen and argon were calculated from the adsorption data at 288.2K and 303.0K and are given in Table-3.8. As observed from the table, the heat of adsorption values for nitrogen show substantial increase on silver exchange in zeolites. Heat of adsorption values for sodium form of the zeolite and AgX are in close agreement with those reported in the literature [10, 28-30].

Table-3.8. Isosteric Heats of Adsorption in sodium and silver form of the zeolites

	Heat of adsorption in kJ mol^{-1}					
	Sodium from			Silver form		
	Nitrogen	Oxygen	Argon	Nitrogen	Oxygen	Argon
Zeolite X	19.4	15.1	12.4	31.5	15.5	15.8
Zeolite Y 5.5	19.8	15.8	15.0	42.8	15.9	17.7
Zeolite L	19.0	14.4	14.3	21.9	15.3	17.0
BEA	23.4	17.6	16.9	35.1	17.5	17.2
MOR 060	27.0	17.4	17.5	33.9	17.0	17.0
MOR 510	20.1	15.6	18.8	31.6	15.8	16.0
ZSM-5 (25)	26.8	16.3	17.3	42.8	16.1	16.8
ZSM-5 (40)	25.3	16.4	16.4	41.5	16.4	16.9
ZSM-5 (100)	23.2	16.1	15.6	38.3	15.8	16.8
ZSM-5 (400)	19.0	16.2	16.6	25.0	16.0	16.6
ZSM-5 (900)	19.5	16.3	16.4	19.9	16.1	17.1

N_2 heat of adsorption value at low coverage is very high (19 to 43kJ mol^{-1}) in the silver exchanged zeolites compared to that of the corresponding alkali metal ion exchanged zeolites (19 to 26kJ mol^{-1}) reported in the literature [28-30]. The heat of adsorption for nitrogen in silver exchanged zeolites is even higher than that for bivalent alkaline earth metal exchange zeolites (CaX = 26.5kJ mol^{-1} and CaA = 22.2kJ mol^{-1}). The heat of adsorption value for argon and oxygen also increases (Table-3.8) after silver exchange, but the magnitude of the increase is low compared to that for nitrogen. The values of N_2 heat of adsorption in silver exchanged zeolites decreases with increase in coverage.

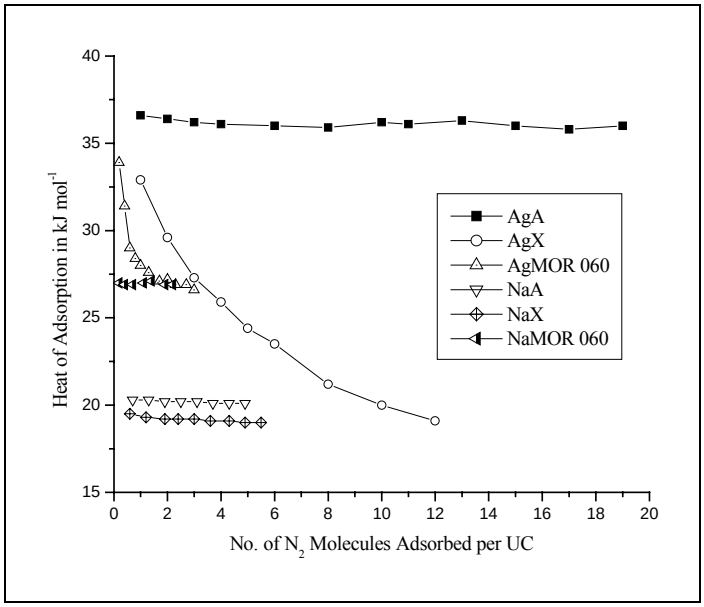

Figure-3.12. Variation of Heat of Adsorption with Coverage

The dependence of the heat of adsorption on adsorption coverage for different zeolites is shown in Figure-3.12. In AgA, N_2 heats of adsorption decrease from 36.5kJ mol^{-1} at one molecule per unit cell to 35.8kJ mol^{-1} at 19 molecules per unit cell coverage. On the other hand in AgX, it decrease form 32.9kJ mol^{-1} at one molecule per unit cell to 19.1kJ mol^{-1} at 12 molecules per unit cell adsorption coverage. In the case of silver mordenite, the N_2 heat of adsorption decreases from 32.9kJ mol^{-1} at 0.2 molecules per unit cell to 28kJ mol^{-1} at one molecule per unit cell. In the case of silver exchanged zeolite Y, BEA and ZSM-5, similar decrease in the nitrogen heat of adsorption was observed with coverage. In the case of oxygen and argon, the heat of adsorption remained almost unaffected with adsorption coverage.

As explained in Chapter –2, the non-linear shape of the nitrogen adsorption isotherm, High values for Langmuir constant, Henry's constant, nitrogen selectivity, nitrogen heat of adsorption and the strong interaction of the nitrogen molecules with other silver exchanged zeolites can be explained in terms of the π -complexation of the nitrogen molecules with the co-ordinately unsaturated silver ions present in the zeolite cavities and channels. The N≡N stretching frequency at around 2090cm^{-1} observed for N_2 molecules adsorbed in zeolite AgX, AgY, Ag ZSM-5, Ag Mordenite and Ag BEA also confirming the π-complexation between nitrogen molecule and Ag^+ cations of the zeolites. The variations observed for nitrogen adsorption in terms of the nitrogen adsorption capacity, Langmuir constant, Henry's constant, heats of adsorption and

nitrogen selectivity for different silver exchanged zeolites (Tables 3.3, 3.4, 3.5, 3.6 and 3.8) can be explained in terms of difference in the number of accessible co-ordinately unsaturated Ag^+ cations present in these zeolites. The argon-oxygen selectivity observed for silver exchanged zeolites can also be explained in terms of the interactions between the argon ($p\sigma$) and silver ($d\sigma$) bonding molecular orbitals as explained in Chapter-2.

3.3.5. Faujasite type zeolites

Framework structure of faujasite type zeolite along with the extra framework cation locations is given in Figure-3.13. The cations are located in six crystallographically different sites. The cation locations of Ag^+ ions in zeolite AgX and AgY has been reported by Lee et al. [31] and Eulenberger et al. [32] respectively from X-ray diffraction studies. In AgX, 32 cations are located either at site I (centre of the hexagonal prism connecting the sodalite ages) or site I′ (near the 6-ring window of the prism on the inside of sodalite cage). The other 32 Ag^+ ions are located at site II (on the either side of the single 6-ring window between the sodalite and supercage). The distance between these Ag^+ cations and framework oxygen is reported to be 2.273Å, similar to that between Ag^+ cation at 6-ring and framework oxygen in $Ag_{12}A$ [33]. 23 Ag^+ ions are located at three different III′ sites (opposite 4-ring near the wall of the supercage or the edge of 12-ring). These Ag^+ ions are located at three different III′ sites with Ag-O distances 2.702, 2.31, and 2.45Å.

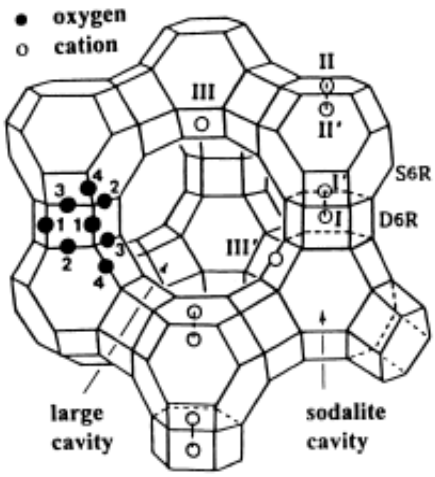

Figure-3.13. Framework structure of zeolite X. Near the centre of each line segment is an oxygen atom. The numbers 1 to 4 indicates the different oxygen atoms. Silicon and aluminium atoms alternate the tetrahedral intersections, except that Si substitutes for about4% of the Al atoms. Extra framework cation positions are labelled with Roman numerals.

Cations present at site I or I′ are inside the hexagonal prisms and are not accessible to N_2 molecules. So they do not contribute towards N_2 adsorption. Of the accessible cations at site II and III′, the cations located at site III′ with a Ag-O distance 2.702Å will be co-ordinately unsaturated and cations located at other sites (II or remaining III′) are strongly interacting with framework oxygen of the zeolite as observed from the Ag-O distances 2.27-2.45Å. Therefore, in AgX, the Ag^+ cations located at site III′ with Ag-O distance 2.702Å being co-ordinately unsaturated will strongly interact with N_2 molecules through π-complexation. Hutson et al. [34] also explained the stronger N_2 adsorption in AgX in terms of more accessible Ag^+ cations located at site II^*, as termed by them, from Neutron diffractions studies.

In AgY, 10.7 Ag^+ cations at the centre of hexagonal prism (site I), 10.7 Ag^+ cations inside the sodalite cage at the 6- ring forming the base of hexagonal prism (site I′) and 28.3±0.6 Ag^+ cations at the 6- ring facing towards supercage (site II) are reported with a Ag-O distance of 2.32Å. Similar Ag^+ ion locations have been reported from neutron diffraction studies. Silver cations located at site I and I′ are not accessible to N_2 molecules for interaction and therefore would not contribute towards N_2 adsorption. Ag^+ cations present at site II having Ag-O distance 2.32Å does not show unsaturated coordination as observed for AgA and AgX. In view of this, no increase of N_2 adsorption is expected on exchanging Ag^+ in NaY as reported by Hutson et al [34]. However, as seen from Tables 3.3, 3.4 and 3.5, we have observed 2 times increase in N_2 adsorption capacity as well as 15 and 2 times increase in Henry constant and initial heat of adsorption respectively for nitrogen on exchanging silver in NaY. The Si/Al ratio of the sample studied by Hutson et al. [34] and Eulenberger et al. [32] was 2.4 and it is much lower than the Si/Al ratio 5.5 of our sample. Furthermore, in our case, yellow colour of the sample was observed on vacuum dehydration at 623K reflecting the formation of weakly interacting silver cluster inside sodalite cages as reported for AgX [15-16]. Gellens et al. was reported the formation of yellow colour in AgY, on vacuum dehydration at higher temperatures [35]. The number of extra framework silver cations in our sample is 30 compared to 56 in the samples studied by Hutson et al. [34]. Though, data on Ag^+ cation locations is not available for AgY with number of cations equal to 30 or near to this value in the literature, it seems that some of the Ag^+ cations in such samples present in the supercage sites are co-ordinately unsaturated and are interacting strongly with N_2 molecules.

3.3.6. Mordenite and ZSM-5 type Zeolites

Zeolite mordenite has elliptical straight cylindrical one-dimensional channels, running parallel to the c axis [36] (Figure-3.1) with minor and major axes as 5.8 and 7.0Å respectively. The main channels are circumscribed by 12-ring oxygen atoms of the framework and open in the b direction into smaller side channels circumscribed by 8-rings having a minimum free diameter of 3.9Å and leading towards the next main channel. However, halfway to the neighbouring large channel each side channel branches through two distorted 8-ring of 2.8Å minimum free diameters into two similar side channels opening into the next main one. Of the total eight sodium ions per unit cell, four are located at the centre of each distorted 8-ring. This effectively isolates the main channel from one another and leaves each main channel lined with two rows of side pockets. It is reported [37] that molecules as large as argon can access to these pockets. The remaining four sodium ions are reported [38] to occupy at random sites of the 8-ring and 12-ring positions in the main channel of the zeolite.

Nitrogen heat of adsorption in sodium mordenite (Figure-3.4) does not show variation with adsorption coverage reflecting the energetically uniform surface. In silver exchanged mordenite, high heat of adsorption for N_2 is observed at lower coverage (1 molecule per unit cell). However, at adsorption coverage higher than one molecule per unit cell, heats of adsorption values do not vary with coverage and is closer to the value observed for sodium mordenite. This is also seen in N_2 adsorption isotherms for silver and sodium mordenite (Figure-3.4) wherein the nitrogen adsorption sharply increases with pressure in the low equilibrium pressures (<20kPa) region. These observations show the presence of some limited number of sites in silver mordenite, which have higher interactions with nitrogen molecules. Nitrogen adsorption data indicate the presence of limited number of co-ordinately unsaturated Ag^+ ions in silver exchanged mordenite as observed for zeolite A, and X. However, there is no crystallographic data available for the Ag^+ ion in mordenite as it is available for zeolite A and X to confirm this.

From the observed dependence of heat of adsorption with the number of sodium and silver cations inside ZSM-5, the heat of adsorption of oxygen and argon show a little variation with the change in number of sodium/silver cations in ZSM-5. On the contrary, N_2 heat of adsorption shows significant dependence on the number of extra framework cations. These data show that nitrogen adsorption selectivity in zeolites is

mainly due to its interaction with the zeolite extra framework cations, Furthermore, we can observe that ZSM-5 (900) having nearly no sodium cations has nitrogen heat of adsorption of around 19kJ mol^{-1} which is little higher than that of oxygen (16.3kJ mol^{-1}) and argon (16.4kJ mol^{-1}) in the same sample. Therefore, the contribution of dispersion type interactions between these adsorbate molecules and ZSM-5 surface is in the range of 16 to 19kJ mol^{-1}. Similar values for zeolite mordenite without extra framework cations were reported to be 18.9, 16.8 and 17.7kJ mol^{-1} respectively [30]. The contribution of dispersion, repulsion and polarization forces towards heats of adsorption of nitrogen in mordenite reported by Barrer [1] based on theoretical calculations is 18.8kJ mol^{-1}.

Dependence of N_2 heat of adsorption with adsorption coverage shows trend similar to that observed in mordenite. Majority of the studies [39-41] of the silver structure and coordination in ZSM-5 have concluded that Ag^+ ions are present as dispersed isolated ions in the zeolite. Using the EXAFS, Bordiga et al. [41, 42] have shown that at least 97% of the Ag^+ ions are present as isolated ions with average Ag-O distance 2.3Å. From their study using combined quantum mechanics and interatomic potential function method, Silhan et al. [43] have concluded that the Ag^+ ions preferentially occupy the sites on the intersection of the main and sinusoidal channels of ZSM-5 with Ag-O distance between 2.32 –2.36Å. Compared to this, sodium cations in ZSM-5 are reported to be present either in the straight or sinusoidal channel. This study does not show co-ordinately unsaturated silver ions in ZSM-5. However, higher heat of N_2 adsorption observed for silver ZSM-5 does show the presence of such sites in Ag-ZSM-5.

The heats of adsorption data and the Henry constants given for the three adsorbates in Na and Ag exchanged zeolites given in Table-3.4 show that these value have some correlation with cavity size of the zeolites and this effect is more prominent for nitrogen adsorption. For example, the Henry constants for Na form of zeolites having cage structure with almost spherical cavities like zeolite A (diameter = 11.4Å) and X (diameter = 12Å) are of lower values in the range 5.5 to 10.2. On the other hand, the Henry constants for Na- forms of zeolites with channel type structure like mordenite (6.5 × 7.0Å), ZSM-5 (5.1 × 5.5Å and 5.3 × 5.6Å) is in the range 20 to 58. Similar trend is observed for the nitrogen heat of adsorption. From the Henry constant values for silver exchanged zeolites, similar conclusions are drawn as the Henry constants

for channel type zeolites vary from 104 to 138 where those for cage structured zeolites are in the range of 46 to 93 only. However, these differences are not as distinct in heat of adsorption data. These observations show that sorbate molecules have higher interactions with extra framework cations as well as lattice oxygen atoms of the zeolites like mordenite and ZSM-5 having smaller channel type structures. In sodium mordenite, rotational restriction of the adsorbed N_2 molecules inside zeolite channel has been proposed. Such a restriction results into higher quadrupole-cation field gradient interaction leading to higher adsorption of nitrogen molecule in mordenite. One can expect similar rotational restriction for oxygen and argon molecules but the effect is more prominent due to be higher quadrupole moment of nitrogen. On the other hand, sorbed molecules will not have such rotational restriction in large cavity sized zeolites A, X and Y. The non-specific interaction of the lattice oxygen atoms of the zeolite mordenite, ZSM-5 with sorbate molecules is expected to higher as the channel of these zeolites are smaller (Table-3.1) compared to zeolite A and X cavities. As a result, molecules sorbed in smaller sized zeolites will have higher electrostatic as well as non-specific interactions with the zeolite cations and /or lattice oxygen atoms.

The adsorption of nitrogen, oxygen and argon on ZSM-5 zeolite having various SiO_2/Al_2O_3 ratios are carried out at ambient temperatures. The variation in the nitrogen heat of adsorption in sodium and silver form of ZSM-5 zeolites with various numbers of cations is given in Figure-3.14.

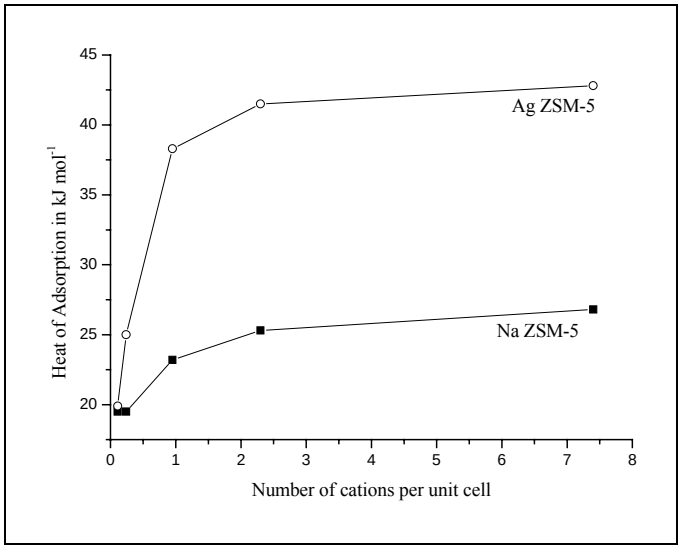

Figure-3.14. Variation of N_2 heat of adsorption in ZSM-5 with number of cations per unit cell

As the number of cations per unit cell increases, the nitrogen heat of adsorption increases in both sodium and silver form. However, if the number of cations per unit cell exceeds 3, the nitrogen heat of adsorption remains almost unaffected by the number of cations per unit cell. The magnitude of the increase in nitrogen heat of adsorption in silver form is much higher than that in sodium form. In ZSM-5 zeolite having around 8 cations per unit cell, the sodium form of the zeolite shows nitrogen heat of adsorption value 26.8kJ mol^{-1}, while the silver form shows nitrogen heat of adsorption value 42.8kJ mol^{-1}. In the case of ZSM-5 zeolite having less than one cation per unit cell, the sodium and silver forms of the zeolite shows nitrogen heat of adsorption values 19.5kJ mol^{-1} and 19.9kJ mol^{-1} respectively.

3.4. REFERENCES

[40] R. M. Barrer, *Zeolites and Clay Minerals as Sorbents and Molecular Sieves*, Academic Press, London, 1978.

[41] R. T. Yang, *Adsorbents: Fundamentals and Applications*, Wiley Interscience, New York, 2003.

[42] R. V. Jasra, N. V. Choudary and S. G. T. Bhat, *Separation Science and Technology*, 1991, **26**, 885-930.

[43] G. H. Kuhl, *Zeolites*, 1987, **7**, 451.

[44] H. W. Habgood, *Can. J. Chem.*, 1964, **42**, 2340.

[45] Y. J. Huang, *Catalysis*, 1974, **32**, 482, 31

[46] K. S. Knaebel and A. I. Kandybin, *U. S. Pat. No. 5,226,933*, 1993

[47] A. I. Kandybin, R. A. Anderson and D. L. Reichley, *U. S. Pat. No. 5,470,378*, 1995.

[48] R. L Chiang, R.D. Whitley, J. E. Ostroski and D. P. Dee, *U. S. Pat. No. 6,432,170*, 2002.

[49] R. T. Yang, Y. D. Chen, J. D. Peck and N. Chen, *Ind. Eng. Chem. Res.,* 1996, **35**, 3093-3099.

[50] N. D. Hutson, S. U. Rege and R. T. Yang, *AIChE Journal*, 1999, **45**, 724-734.

[51] M. Ralek, P. Jiru, O. Grubner and H. Bayer, *Collect. Czech. Chem. Commun.,* 1962, **27**, 142-146.

[52] M. D. Baker, J. Godber and G. A. Ozin, *J. Phys. Chem.*, 1985, **89**, 2299-2304.

[53] M. D. Baker, G. A. Ozin and J. Godber, *J. Phys. Chem.*, 1985, **89**, 305-311.

[54] M. D. Baker, G. A. Ozin and J. Godber, *Catal. Rev. - Sci. Eng.*, 1985, **27**, 591-651.

[55] T. Sun and K. Seff, *Chemical Reviews,* 1994, **94**, 857-870.

[56] V. S. Gurin, N. E. Bogdanchikova and V. P. Petranovskii, *J. Phys. Chem. B,* 2000, **104**, 12105-12110.

[57] Y. Kim and K. Seff, *J. American Chem. Soc.*, 1977, **99**, 7055-7057.

[58] Y. Kim and K. Seff, *J. American Chem. Soc.*, 1978, **100**, 175 -180

[59] Y. Kim and K. Seff, *J. American Chem. Soc.*, 1978, **100**, 6989-6996.

[60] H. G. Karge, *Metal Microstructures in Zeolites*, 1982, 10-109.

[61] P. A. Jacobs and J. B. Uytterhoeven, *JCS Faraday Trans. I*, 1979, **75**, 56-64.

[62] L. R. Gellens, W. J. Mortier, R. A. Schoonheydt and J. B. Uytterhoeven, *J. Phys. Chem.*, 1981, **85**, 2783 –2788.

[63] R. A. Schoonheydt and H. Leeman, *J. Phys. Chem.*, 1989, **93**, 2048 -2053.

[64] R. Seifert, A. Kunzmann and G. Calzaferri, *Angew. Chem. Int. Ed*., 1998, **37**, 1521-1524.

[65] R. Seifert, R. Rytz and G. Calzaferri, *J. Phys. Chem. A*, 2000, **104**, 7473-7483.

[66] G. Calzaferri, C. Leiggner, S. Glaus, D. Schurch and K. Kuge, *Chem. Soc. Rev.*, 2003, **32**, 29-37.

[67] N. V. Choudary, R. V. Jasra and S. G. T. Bhatt, *Ind. Eng. Chem. Res.*, 1993, **32**, 548-552.

[68] R. V. Jasra, N. V. Choudary and S. G. T. Bhatt, *Ind. Eng. Chem. Res.*, 1996, **35**, 4221-4229.

[69] N. V. Choudary, R. V. Jasra and S. G. T. Bhatt, *Indian Journal of Chemistry*, 1999, **39A**, 34-39.

[70] S. H. Lee, Y. Kim, K. Seff, *Microporous and Mesoporous Materials*, 2000, **41**, 49-59.

[71] G. R. Eulenberger, D. P. Shoemaker and J. G. Keil, *J. Phys. Chem.*, 1967, **71**, 1812-1819.

[72] Y. Kim and K. Seff, *J. Phys. Chem.*, 1987, **91**, 671 – 674.

[73] N. D. Hutson, D. A. Reisner, R. T. Yang and B.H. Toby, *Chem. Matter*, 2000, **12**, 3020-3031.

[74] L. R. Gellens, W. J. Mortier and J. B. Uytterhoeven, *Zeolites*, 1981, **1**, 11-18.

[75] D. W. Breck, *Zeolites Molecular Sieves: structure, chemistry and use*, Wiley Interscience, New York, 1974.

[76] D. T. Hayhurst and M. D. Sefcik, *Intrazeolite Chemistry, ACS Symposium Series*, No.218, American Chemical Society, Wahington DC, 1983, 333-334.

[77] W. M. Meier, *Z. Kristallogr*, 1961, **115**, 439-450.

[78] M. Matsuoka, E. Matsuda, K. Tsuji, H. Yamashita and M. Anpo, *J. Mol. Catal. A: Chemical*, 1996, **107**, 399-403.

[79] M. Anpo, S. G. Zhang, H. Mishima, M. Matsuoka and H. Yamashita, *Catal. Today*, 1997, **39**, 159-168.

[80] S. Bordiga, G. T. Palomino, D. Arduino, C. Lamberti, A. Zecchina and C. O. Arean, *J. Mol. Catal. A: Chemical,* 1999, **146**, 97-106.

[81] S. Bordiga, C. Lamberti, G. T. Palomino, F. Geobaldo, D. Arduino and A. Zecchina, *Microporous Mesoporous Materials*, 1999, **30**, 129-135.

[82] M. Silhan, D. Nachtigallova and P. Nachtigall, *Phys. Chem. Chem. Phys.*, 2001, **3**, 4791-4795.

Chapter-4

Sorption of Nitrogen, Oxygen and Argon on Transition Metal Ion Exchanged Zeolites

4.1. INTRODUCTION

Zeolites are inorganic, crystalline, microporous solids; their window diameters are in the range of 1 to 20Å. Zeolites are of immense interest in gas and chemical industries for purification and separation due to their unique adsorption properties. The extra framework cations invariably present in zeolites play significant role in determining their adsorptive properties [1]. Nitrogen and oxygen adsorption studies in zeolites are largely confined to alkali and alkaline earth cation exchanged zeolites, that too for zeolites A and X. There are limited studies reported on the adsorption of these gases in transition metal ion exchanged zeolites. This is despite the fact that transition metal ions due to presence of d-shell can coordinate to adsorbate molecules and show different adsorption behaviour compared to filled shell cations. Though, transition metal ion exchanged zeolites have been studied for catalytic applications, their adsorption behaviour has not been sincerely looked into.

The main reason for this appears to be due to the difficulty in exchanging the transition metal ions into zeolites and retaining zeolite structure after the cation exchange. Transition-metal-containing zeolites can be prepared in many ways: by ion exchange, either from aqueous solution [2-3] or by solid-state reaction [4-5], by hydrothermal synthesis [6] and by adsorption and decomposition of volatile organometallic compounds [7]. Ion exchange from aqueous solution has been mainly used to introduce transition-metal cations into zeolites A and X [2-3]. The results are not always simple. Often, only a fraction of the original cations, usually sodium ions, can be replaced, and attempts to overcome this may reveal a relatively sharp upper limit to exchange. If the exchanging cation can be hydrolysed, the H^+ concentration in solution may increase by several orders of magnitude, encouraging H^+ exchange. This can lead to zeolite framework modification, damage, destruction, or dissolution, especially of low-silica aluminosilicate zeolites. For example, hydrolysis of the zeolite framework to give five-coordinate Al^{3+} was observed in partially Co^{2+} and Ni^{2+}exchanged forms of zeolite A [2]. Finally, hydrolysed metal cations of the general formula $[M_mO_n(OH)_p]^{q+}$ may exchange into, or form within the zeolite [8]. For partially Co^{2+}exchanged zeolite Y, both X-ray diffraction and electronic reflectance spectroscopy have been used to determine the positions of the Co^{2+} ions, their movement upon dehydration and the structures of their complexes. While the Co^{2+}

ions in partially dehydrated zeolite Y are tetrahedrally coordinated to three framework oxygen atoms and one water molecule or its fragment (OH^- or O^{2-}), the Co^{2+} ions in fully hydrated zeolite Y are octahedrally coordinated to six water molecules. Those studies also showed that the Co^{2+} ions prefer sites I and I′ over site II in partially dehydrated zeolite Y, whereas they move to site I upon full dehydration to avoid three coordination and to achieve six-coordination. Far-IR spectroscopy has been used to locate and characterise the principal transition-metal ion sites in faujasite zeolites [9]. Co^{2+} ions were found at sites I, I′, and III′ in the fully dehydrated zeolites (Si/Al=1.25 and 2.5). However, in an X-ray diffraction study, Co^{2+} was found only at sites I and I′ in both partially and fully dehydrated zeolite Y (Si/Al=2.4). Among the transition-metal elements - manganese, cadmium, zinc- all of which have d^5 or d^{10} electron configurations, have been fully exchanged into zeolites A and X. The adsorption properties of zeolites containing more complex transition-metal ions are established with the positions and occupancies of those ions within the zeolite cavities.

The present Chapter investigated the adsorption of nitrogen, oxygen and argon in cobalt, manganese, cadmium, copper, nickel and zinc exchanged zeolites. The adsorption data has been correlated with the cation locations and the nature of the cationic species formed inside zeolite cavities.

4.2. EXPERIMENTAL

4.2.1. Materials

Zeolites A and X from Zeolites and Allied Products, Bombay, India, ZSM-5 and Mordenite from Zeocat, Uetikon, Switzerland and cobalt nitrate, copper nitrate, manganese nitrate, nickel nitrate, cadmium nitrate and zinc nitrate from E Merck India Ltd., Bombay, India, were used as the starting materials for the adsorbent preparation. Oxygen (99.99%), nitrogen (99.99%), argon (99.99%) and helium (99.99%) from Hydrogas India Pvt. Ltd., Bombay, India, were used for the adsorption isotherm measurements.

4.2.2. Cation ion Exchange

The transition metal cations were introduced into the highly crystalline sodium form of zeolite by the conventional cation exchange from aqueous solution. Typically, the zeolite was refluxed with 0.05M aqueous solution of the corresponding metal ion in

the solid / liquid ratio 1:80 at 353K for 4 hours. The residue was filtered, washed with hot distilled water, until the washings were free from ions and dried in air at room temperature. Zeolite samples having different degree of cation exchange were prepared by subjecting repeated ion exchange into the zeolites. The extent of ion exchange into the zeolites was determined by the complexometric titration with EDTA.

4.2.3. X-ray Powder Diffraction

X-ray powder diffraction studies at ambient temperature were carried out using PHILIPS X'pert MPD system in the 2θ ranges of 5-65 degrees using CuKα1 (λ = 1.54056Å). The diffraction patterns of the starting materials show that they are highly crystalline showing the reflections in the range 5 to 35 degrees typically of zeolites. The structures of the zeolites were retained after the cation exchange. In the case of some cations like copper, nickel, zinc etc., loss of crystallinity was observed during the ion exchange process. Percentage crystallinity of the transition metal ion exchanged zeolites was determined form the X-ray diffraction pattern by considering the intensity of five major peaks. The sodium form of the zeolite was considered as an arbitrary standard for the calculations.

4.2.4. Activation and Isotherm Measurements

Prior to adsorption measurements, the samples were initially dried at 353K for 24h. The samples were further activated in situ by increasing the temperature (at a heating rate <1K $min.^{-1}$) to 673K under vacuum (5×10^{-3}mmHg) and the temperature and vacuum was maintained for 8h before the sorption measurements. Nitrogen, oxygen and argon adsorption was measured at 288.2K and 303.0K using a static volumetric system (Micromeritics ASAP 2010) as described in Chapter-2. The adsorption data obtained is fitted in various equations such as Langmuir equation, Virial equitation and Dubinin- Astakhov equation. The values for Langmuir constant, Henry's constant etc. was determined from these data. Isosteric heat of adsorption and adsorption selectivity were determined from the adsorption data at 288.2K and 303.0K as described in Chapter-2. Surface area and pore size distribution of the various cation-exchanged zeolites were determined from the N_2 adsorption data at 77.35K. The

nitrogen adsorption at 77.35K was also measured using Micromeritics ASAP 2010 after activating the sample at 673K under vacuum.

4.3. RESULTS AND DISCUSSION

4.3.1. Cobalt (II) Exchanged Zeolite X

Complete Co^{2+}exchange of NaX was attempted from aqueous solution at 353K, but the complete Co^{2+}exchange was not achieved and the results are sufficiently complex. For example, hydronium ions may have attacked the zeolite framework to a minor degree, leading to a loss of Al^{3+} ions and crystallinity; this increases with the temperature of exchange. Co^{2+} in fully dehydrated zeolites A and X causes strong six-ring deformations as seen from the UV-VIS-NIR spectra [10]. The theoretical study, which used cluster models for Co (II) in an isolated six- ring without coordinating H_2O or OH^-, showed that the effective coordination number of Co (II) depends on the local Si and Al arrangement, and the aluminium deficient six-rings behave differently from $Si_3Al_3O_6$ six-rings [10].

The extent of the cobalt ion exchange on different zeolite X samples was determined by complexometric titration with EDTA using murexide indicator. The number in the sample name indicates the percentage of ion exchange. The structure of the zeolite X retained during the cations exchange process. The percentage crystallinity and unit cell dimension were determined from the X-ray powder pattern. The values of the percentage crystallinity and unit cell dimension are also given in Table-4.1.

Table-4.1. Unit cell dimensions and Surface area of Cobalt Exchanged Zeolites

Adsorbent	% Crystallinity	Unit Cell Dimension	BET Surface Area m^2g^{-1}	t-plot	
				Micropore Area m^2g^{-1}	External Surface Area m^2g^{-1}
Na X	100	24.94	542.2	518.4	23.7
CoX 46	84.1	24.91	675.7	623.1	52.6
CoX 71	79.6	24.91	695.8	616.4	79.4
CoX 88	78.7	24.91	662.1	541.1	121.0
CoX 93	71.9	24.90	668.7	508.0	160.6

The surface area and pore size distributions of the various cobalt exchanged zeolite X samples were determined from the N_2 gas adsorption data at 77.35K. The surface area of the zeolite X increases on cobalt ion exchange. This is due to the decrease in the number of extra framework cations while replacing monovalent sodium ions with divalent cobalt ions. The external surface area determined from the t-plot also increases with percentage of cobalt exchange. This can be explained in terms of the structural deformation leading into the formation of amorphous phase during the vacuum dehydration of the cobalt ion exchanged zeolite X at higher temperatures.

Nitrogen, oxygen and argon adsorption isotherms measured on various cobalt (II) exchanged zeolite X were measured at 288.2K and 303.0K and the adsorption isotherms on CoX 71 at 303.0K are given in Figure-4.1. All the cobalt ion exchanged zeolite X gives similar adsorption isotherms at ambient temperatures. The nitrogen adsorption sharply increases with pressure and percentage of cation exchange in the low-pressure region and the nitrogen adsorption isotherm becomes non-linear. Oxygen adsorption capacity also increases and argon adsorption capacity remains almost unaffected. The oxygen adsorption increases linearly with pressure. The magnitude of the increase in the adsorption capacity of oxygen is much lower than that of nitrogen in the low-pressure region. The sharp increase in the nitrogen adsorption in the low-pressure region shows strong interaction of the nitrogen molecules with some of the extra framework cobalt ions.

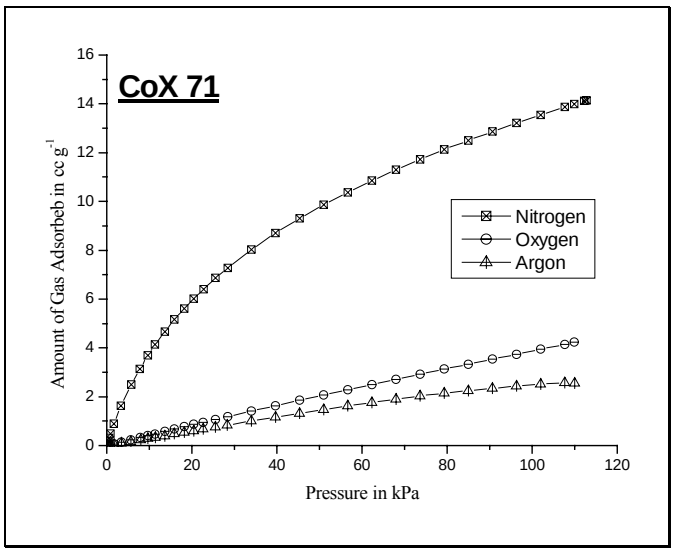

Figure-4.1. Adsorption isotherms on CoX 71 at 303.0K

The equilibrium adsorption capacities for nitrogen, oxygen and argon on zeolite X containing different amounts of cobalt ions are determined from the adsorption isotherms and the number of molecules adsorbed per unit cell at 101.3kPa are given in Table-4.2. The nitrogen and oxygen adsorption capacities increase on cobalt ion exchange up to 71%, beyond which it shows decreasing trend. Adsorption capacities of oxygen increases marginally, while that of argon do not show significant change on cobalt exchanging. The magnitude of the increase in the adsorption capacities for nitrogen is much higher than that of oxygen.

Table-4.2. Equilibrium Adsorption Capacity for N_2, O_2 and Ar on NaCoX

Adsorbent	Equilibrium Adsorption Capacity in molecules / unit cell at 101.3kPa					
	288.2K			303.0K		
	Nitrogen	Oxygen	Argon	Nitrogen	Oxygen	Argon
NaX	7.7	2.4	2.2	5.5	1.8	1.7
CoX 46	8.5	2.5	2.1	7.0	2.0	1.7
CoX 71	10.0	2.6	2.1	8.4	2.1	1.6
CoX 88	9.2	2.7	2.1	7.9	2.1	1.6
CoX 93	7.8	2.7	2.0	6.7	2.1	1.5

The adsorption data obtained at 288.2K and 303.0K were fitted in Langmuir equation and the slope, intercept and Langmuir constant were determined. The values for the Langmuir constant b increases for nitrogen, oxygen and argon on cobalt exchange and increases linearly with increase in the percentage of cobalt exchange on zeolite X. The Langmuir fitting data on different amount of cobalt ion exchanged zeolites X at 303.0K are given in Table-4.3.

Table-4.3. Langmuir Fittings Data at 303.0K on Co (II) Exchanged Zeolites

Adsorbent	Slope			Langmuir constant b		
	Nitrogen	Oxygen	Argon	Nitrogen	Oxygen	Argon
NaX	0.014	0.0099	0.014	0.160	0.034	0.044
CoX 46	0.055	0.022	0.019	0.746	0.104	0.048
CoX 71	0.057	0.033	0.022	2.465	0.111	0.057
CoX 88	0.080	0.057	0.100	2.703	0.148	0.245
CoX 93	0.082	0.063	0.127	4.103	0.187	0.271

The nitrogen, oxygen and argon adsorption data obtained at 288.2K and 303.0K were also fitted in Virial equation. The Virial coefficients A_0, A_1 and A_2 were determined from the Virial plots. The values for the Henry's constant K were calculated from the Virial coefficient. The Values of the Virial coefficients A_0 and Henry's constant K at 303.0K are given in Table-4.4. Henry's constant value for nitrogen increases with increase in the cobalt content in the zeolite. Henry's constant for oxygen and argon remains almost unaffected.

Table-4.4. Virial Coefficients and Henry's Constant at 303.0K on Co (II) Exchanged Zeolites

Adsorbent	A_0			Henry's Constant K (10^{-5}ccg^{-1}Pa^{-1})		
	Nitrogen	Oxygen	Argon	Nitrogen	Oxygen	Argon
NaX	4.296	5.528	5.568	10.22	2.98	2.86
CoX 46	3.971	6.230	5.927	14.15	1.48	2.00
CoX 71	2.571	5.608	5.908	57.37	2.75	2.04
CoX 88	2.784	5.862	6.260	46.33	2.14	1.43
CoX 93	2.652	5.830	6.104	52.90	2.20	1.68

The nitrogen, oxygen and argon adsorption at 288.2K and 303.0K were also fitted in Dubinin-Astakhov equation. The values of the slope, intercept, energy and volume determined and valued of slope and energy at 303.0K are given in Table-4.5.

Table-4.5. Dubinin-Astakhov Fittings at 303.0K on Co (II) Exchanged Zeolites

Adsorbent	Slope			Energy kJ mol^{-1}		
	Nitrogen	Oxygen	Argon	Nitrogen	Oxygen	Argon
NaX	-0.940	-0.988	-0.985	12.19	10.38	10.63
CoX 46	-0.788	-1.091	-0.985	14.59	10.46	10.74
CoX 71	-0.545	-0.961	-0.986	21.19	10.82	10.80
CoX 88	-0.523	-0.950	-0.917	21.89	11.08	12.56
CoX 93	-0.484	-0.936	-0.907	23.39	11.36	12.04

The adsorption selectivity for the pure components were calculated at different pressures and the values is given in Table-4.6. The nitrogen-oxygen selectivity in the

low-pressure region increases from 3.4 to 21.8 during cobalt exchange. Nitrogen-argon selectivity also increases from 6 to 30 on cobalt exchange.

Table-4.6. Adsorption Selectivity on Co (II) Exchanged Zeolites

Adsorbent	Adsorption Selectivity					
	$\alpha N_2/O_2$		$\alpha N_2/Ar$		$\alpha O_2/Ar$	
	3.33kPa	101.99kPa	3.33kPa	101.99kPa	3.33kPa	101.99kPa
NaX	3.4	3.1	3.7	3.3	1.08	1.07
CoX 46	7.7	3.3	8.3	3.7	1.08	1.12
CoX 71	20.7	4.1	30.3	6.4	1.46	1.57
CoX 88	20.6	3.7	28.7	5.3	1.39	1.45
CoX 93	21.8	3.6	28.6	4.9	1.31	1.42

The isosteric heat of adsorption for nitrogen, oxygen and argon adsorption on cobalt exchanged zeolite X calculated using Clausius-Clapeyron equation and are given in Table-4.7. The heats of adsorption values for nitrogen and oxygen increases and that for argon remain unaffected on cobalt exchange in zeolite X.

Table-4.7. Isosteric heat of Adsorption on Co (II) Exchanged Zeolites

Adsorbent	Heat of Adsorption in kJ mol^{-1}		
	Nitrogen	Oxygen	Argon
NaX	19.4	15.1	13.4
CoX 46	32.4	17.2	13.3
CoX 71	33.8	17.9	13.9
CoX 88	34.7	17.4	14.1
CoX 93	35.7	18.1	14.1

Adsorbate molecules can interact with the zeolite surface through lattice oxygen atoms and accessible extra framework cations and Al and Si atoms. The Al and Si atoms present at the centre of tetrahedra are not directly exposed to the sorbate molecules. Consequently, their interactions with the sorbate molecules are negligible. Therefore, the principal interactions of these sorbate molecules with the zeolite surface are with lattice oxygen atoms and extra framework cations. The electrostatic

interactions between the sorbate molecules and the extra framework cations of the zeolite depend on the quadrupole moments of the sorbate molecules and are expected to follow the order, N_2>O_2>Ar in agreement with quadrupole moment values of 0.31, 0.11 and zero for N_2, O_2, Ar respectively.

Zeolite X is a synthetic aluminium rich analogue of the naturally occurring mineral faujasite (Figure-4.2). The 14-hedron with 24 vertices known as the sodalite cavity or β-cage may be viewed as its principal building block. These β-cages are connected tetrahedrally at six-rings by bridging oxygen to give double six-rings (D6Rs, hexagonal prisms) and concomitantly, an interconnected set of even larger cavities (supercage) accessible in three dimensions through 12-ring (24-membered) windows.

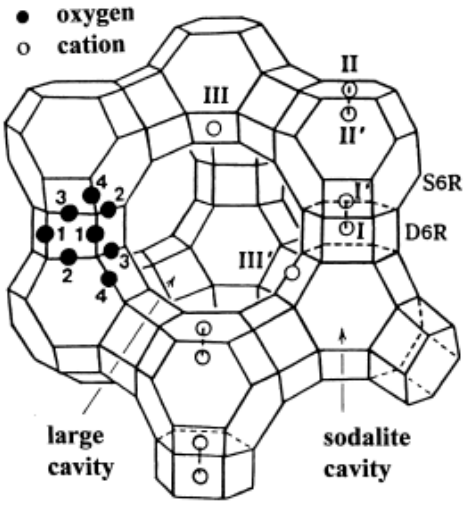

Figure-4.2. The framework structure of zeolite X, near the centre of the each line segment is an oxygen atom. The numbers 1–4 indicates the different oxygen atoms. Silicon and aluminium atoms alternate at the tetrahedral intersections, except that Si substitutes f or Al at about 4% of the Al positions. Extra framework cation positions are labelled with Roman numerals

The Si and Al atoms occupy the vertices of these polyhedra. The oxygen atoms lie approximately midway between each pair of Si and Al atoms but are displaced from those points to give near-tetrahedral angles about Si and Al. Single six-rings (S6Rs) are shared by sodalite and supercage, and may be viewed as the entrances to the sodalite units. Each unit cell has eight sodalite units, eight supercage, 16 D6Rs, 16 12-rings, and 32 S6Rs. Exchangeable cations that balance the negative charge of the aluminosilicate framework are found within the zeolite cavities [11]. They are usually found at the following sites shown in Figure-4.2: site I at the centre of the D6R, I′ in the sodalite cavity on the opposite side of one of the D6Rs six-rings from site I, II′ inside the sodalite cavity near a S6R, II at the centre of the S6R or displaced from this

point into a supercage, III in the supercage on a twofold axis opposite a four-ring between two 12-rings, and III′ somewhat or substantially off III (off the twofold axis) on the inner surface of the supercage.

The crystal structure of cobalt exchanged zeolite X having 38 and 46 cobalt ions per unit cell are reported in the literature [12]. Co^{2+} ions prefer site II and Co^{2+} ions occupy sites I′, II and III′ in zeolite X. In the sample with maximum cobalt exchange, cobalt ions are found at five different crystallographic sites and sodium ions at one. Eight Na^{+} ions per unit cell half-fill site I. Sixteen Co^{2+} ions per unit cell are found at two different I′ positions. Site-II positions are occupied by 19 Co^{2+} ions per unit cell. A site-II′ position is occupied by only one Co^{2+} ion per unit cell. The remaining 10 Co^{2+} ions are found at site III′. The octahedral Na-O distance, 2.623Å, is somewhat longer than the sum of the ionic radii of Na^{+} and O^{2-}, (0.97+1.32= 2.29Å). Co^{2+} ions are occupied in two different site-I′ positions, where the Co-O distances are 2.149Å and 2.32Å. Nineteen Co^{2+} ions are found at site II. Each Co (II) ion binds to three O atoms at 2.129Å. Each Co (II) ion extends 0.57Å into the supercage from its three-O plane. Only one Co^{2+} ion is found at site II′. The Co-O distances are 2.33Å. The Co (II′) ion extends 1.09Å into the sodalite cage from its three-oxygen plane. The remaining 10 Co^{2+} ions are found at site III′. Each of these binds to two framework oxygen atoms with Co-O distance 2.30Å and 2.27Å. The spectroscopic studies of the cobalt exchanged zeolites [13] shows that the cobalt ion migrates towards the smaller cavities and occupy well-defined cation sites. In zeolite X, the extra framework cations in sites I and I′ are not accessible to the oxygen, nitrogen and argon molecules. The cation sitting in site II and II′ can interact with the adsorbate molecules through the six member ring windows and the cations in site III and III′ can interact directly with these adsorbate molecules. The distance between Co^{2+} ions in site III′ and the framework oxygen atoms are long (2.30Å and 2.27Å) and these Co^{2+} ions are co-ordinately unsaturated compared to other cobalt ions. These co-ordinately unsaturated Co^{2+} ions interact strongly with the nitrogen molecules resulting in high value for heat of adsorption, Henry's constant, adsorption selectivity and adsorption capacity for nitrogen in the low-pressure region.

The electrostatic interaction of nitrogen, oxygen and argon will be high in cobalt-exchanged zeolite compared to the sodium form. The size of cobalt (0.74Å) is smaller

than that of sodium (0.94Å) resulting in high charge density on the cobalt ions favours the strong interaction of nitrogen and oxygen possessing quadrupole moments of 0.31 and 0.11 respectively.

4.3.2. Manganese (II) Exchanged Zeolites

The X-ray powder diffraction of the various manganese-exchanged zeolites were measured and the patterns show the retention of the zeolite structure after the manganese ion exchange. Complete exchange of the sodium ions with manganese ions was observed. The surface area and pore size distributions of the various manganese-exchanged zeolites were determined from the N_2 gas adsorption data at 77.35K and the values are given in Table-4.8.

Table-4.8. Unit cell dimensions and Surface area of Mn (II) exchanged Zeolites

SAMPLE	% Crystallinity	Unit Cell Dimension	BET Surface Area m^2g^{-1}	t-plot	
				Micropore Area m^2g^{-1}	External Surface Area m^2g^{-1}
NaA	100	24.62	-	-	-
MnA 41	97	24.59	315.9	304.2	11.7
MnA 59	95	24.59	426.1	396.5	29.7
MnA 74	95	24.60	489.2	454.5	34.7
MnA 89	92	24.59	526.0	484.9	41.1
MnA 99	89	24.58	501.9	462.3	39.6
Na X	100	24.94	542.2	518.4	23.7
MnX 47	98	24.93	575.0	540.5	34.5
MnX 60	96	24.94	563.8	527.2	36.6
MnX 71	93	24.93	562.3	516.3	46.0
MnX 79	92	24.92	509.6	466.4	43.2
MnX 90	91	24.92	519.6	471.5	48.0
MnX 100	88	24.91	523.6	475.8	47.8

The surface area of the zeolites increases on manganese exchange. This is due to the decrease in the number of extra framework cations while replacing monovalent

sodium ions with divalent manganese ions. Like cobalt-exchanged zeolite X, the external surface area of the manganese-exchanged zeolites also increases with the increase in the percentage of manganese exchange. This is due to the strong interaction of the manganese ions to zeolite structure resulting in the formation of amorphous phase, probably due to dealumination during the vacuum dehydration process.

Adsorption isotherms on Mn (II) exchanged zeolite A and X are given in Figure-4.3. In manganese-exchanged zeolite A, the values for nitrogen, oxygen and argon adsorption capacities increase at all equilibrium pressures studied. The adsorption of these gases increases linearly with pressure. In the case of manganese (II) exchanged zeolite X also, the adsorption capacities for nitrogen, oxygen and argon increases with manganese exchange levels. But the increase in the nitrogen adsorption is sharp in the low-pressure region and the nitrogen adsorption isotherm becomes non-linear. The oxygen and argon adsorption capacities increase linearly with pressure.

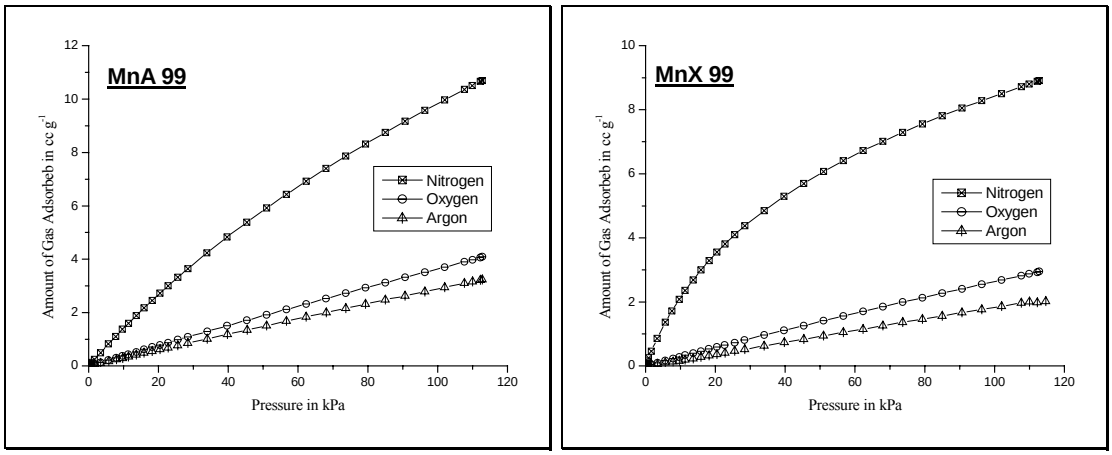

Figure-4.3. Adsorption isotherms on MnA 99 and MnX 99 at 303.0K

The equilibrium adsorption capacities for the adsorption of nitrogen, oxygen and argon on zeolite A and zeolite X containing different amounts of manganese ions are determined from the adsorption isotherms and the number of molecules of nitrogen, oxygen and argon adsorbed per unit cell of various manganese exchanged zeolites A and X at 101.3kPa and 288.2K and 303.0K are given in Table-4.9. In manganese-exchanged zeolite A, the nitrogen, oxygen and argon adsorption capacity increases with increase in manganese exchange, while in the case of manganese exchanged

zeolite X, the adsorption capacities of nitrogen and oxygen increases marginally with manganese percentage, and that of argon remains almost unaffected.

Table-4.9. Equilibrium Adsorption Capacity for N_2, O_2 and Ar on Mn (II) Exchanged Zeolites

Adsorbent	Equilibrium Adsorption Capacity in molecules / unit cell at 101.3kPa					
	288.2K			303.0K		
	Nitrogen	Oxygen	Argon	Nitrogen	Oxygen	Argon
NaA	6.55	2.12	1.84	4.58	1.53	1.42
MnA 41	8.02	2.62	2.19	5.65	1.97	1.69
MnA 59	8.70	2.98	2.38	6.23	2.17	-
MnA 74	9.06	3.10	2.58	6.48	2.30	1.81
MnA 89	9.14	3.14	2. 64	6.53	2.32	1.84
MnA 99	9.29	3.22	2.69	6.66	2.38	1.86
NaX	7.7	2.4	2.2	5.5	1.8	1.7
MnX 47	6.13	2.02	1.58	4.63	1.64	1.19
MnX 60	6.18	2.14	1.51	4.75	1.65	1.18
MnX 71	6.26	2.23	1.50	4.74	1.67	1.21
MnX 79	6.32	2.33	1.52	5.82	1.65	1.19
MnX 90	6.37	2.37	1.53	4.88	1.63	1.18
MnX 100	6.42	2.40	1.56	4.93	1.66	1.20

The adsorption data obtained at 288.2K and 303.0K were fitted in Langmuir equation and the slope, intercept and Langmuir constant were determined. The values of the slope and the Langmuir constant for the adsorption of nitrogen, oxygen and argon on different amount of manganese ion exchanged zeolite A and zeolite X at 303.0K are given in Table-4.10. In manganese exchanged zeolite A, the values of slope and Langmuir constant b increases linearly for nitrogen with increase in manganese percentage, while those for oxygen and argon decreases. In manganese exchanged zeolite X, the values of slope and Langmuir constant b increases linearly for nitrogen and oxygen with increase in manganese percentage, while those for argon decreases with increase in manganese exchange.

Table-4.10. Langmuir Fittings at 303.0K on Mn (II) Exchanged Zeolites

Adsorbent	Slope			Langmuir constant b		
	Nitrogen	Oxygen	Argon	Nitrogen	Oxygen	Argon
NaA	0.012	0.013	0.017	0.111	0.037	0.047
MnA 41	0.024	0.023	0.024	0.308	0.087	0.080
MnA 59	0.028	0.022	-	0.448	0.091	-
MnA 74	0.030	0.020	0.020	0.441	0.086	0.079
MnA 89	0.034	0.019	0.022	0.565	0.082	0.076
MnA 99	0.035	0.018	0.021	0.562	0.075	0.075
NaX	0.014	0.0099	0.014	0.160	0.034	0.044
MnX 47	0.065	0.030	0.026	1.064	0.086	0.060
MnX 60	0.078	0.035	0.026	1.695	0.118	0.056
MnX 71	0.088	0.039	0.024	2.000	0.137	0.055
MnX 79	0.089	0.043	0.023	2.022	0.144	0.053
MnX 90	0.093	0.044	0.022	2.241	0.146	0.047
MnX 100	0.097	0.081	0.021	2.500	0.309	0.045

The nitrogen, oxygen and argon adsorption data obtained at 288.2K and 303.0K were also fitted in Virial equation. The Virial coefficients A_0, A_1 and A_2 were determined from the Virial plots. The Henry's constants were calculated from the Virial coefficient. The values for the Virial coefficient A_0 and Henry's constant K at 303.0K are given in Table-4.11. The Henry's constant values for the adsorption of nitrogen and oxygen increases in manganese exchanged zeolites. The magnitude of increase in the value of Henry's constant is higher for zeolite X compared to zeolite A. the Henry's constant for nitrogen adsorption increases from 7.9 to 14.7 in zeolite A on increasing the amount of manganese from 0-99%, while that in zeolite X increases from 10.0 to 29.5 at the same manganese exchange level. Henry's constant for oxygen adsorption also increases from2.5-4 in zeolite A and 3 to 4 in zeolite X. The Henry's constant for argon adsorption also increases on the manganese exchange in zeolite A from 2.3 to 3, while it decreases from 2.9 to 1.7 in zeolite X.

Table-4.11. Virial coefficient and Henry's Constant at 303.0K on Mn (II) Exchanged Zeolites

Adsorbent	A_0			Henry's Constant K (10^{-5}ccg^{-1}Pa^{-1})		
	Nitrogen	Oxygen	Argon	Nitrogen	Oxygen	Argon
NaA	4.55	5.72	5.78	7.93	2.47	2.32
MnA 41	4.20	5.46	5.69	11.21	3.18	2.53
MnA 59	3.99	5.36	-	13.85	3.52	-
MnA 74	3.94	5.31	5.56	14.65	3.72	2.88
MnA 89	3.93	5.27	5.52	14.72	3.86	2.91
MnA 99	3.91	5.25	5.50	14.90	3.92	2.98
NaX	4.30	5.53	5.57	10.22	2.98	2.86
MnX 47	3.88	5.31	5.97	15.49	3.94	1.91
MnX 60	3.55	5.23	6.06	21.53	4.00	1.74
MnX 71	3.47	5.22	6.04	23.27	4.04	1.78
MnX 79	3.25	5.52	6.05	29.05	4.00	1.76
MnX 90	3.52	5.62	6.07	29.27	3.98	1.73
MnX 100	3.25	5.34	6.04	29.53	4.01	1.78

The nitrogen, oxygen and argon adsorption data obtained at 288.2K and 303.0K were also fitted in Dubinin-Astakhov equation. The values of the slope and energy at 303.0K are given in Table-4.12. The slope of the Dubinin-Astakhov transformed isotherm for nitrogen adsorption decreases with manganese percentage, while that of oxygen and argon remains almost unaffected. The Dubinin- Astakhov energy for the adsorption of nitrogen and oxygen also increases with manganese exchange in zeolite X, while that for argon remains unaffected. In manganese-exchanged zeolite A, the value of Dubinin-Astakhov energy for the adsorption of nitrogen increased from 12 to 14.5 in zeolite A and 12 to 21 in zeolite X. The energy value for oxygen and argon remained without much variation on manganese exchange in both the zeolites.

Table-4.12. Dubinin-Astakhov Fittings data at 303.0K on Mn (II) Exchanged Zeolites

Adsorbent	Slope			Energy kJ mol^{-1}		
	Nitrogen	Oxygen	Argon	Nitrogen	Oxygen	Argon
NaA	-0.957	-0.981	-0.981	11.91	10.29	10.71
MnA 41	-0.894	-0.967	-0.972	13.07	10.62	11.00
MnA 59	-0.856	-0.967	-	13.71	10.67	-
MnA 74	-0.847	-0.972	-0.974	13.75	10.60	10.84
MnA 89	-0.825	-0.968	-0.971	14.44	10.61	10.81
MnA 99	-0.816	-0.972	-0.968	14.45	10.60	10.88
NaX	-0.940	-0.988	-0.985	12.19	10.38	10.63
MnX 47	-0.727	-0.967	-0.979	16.44	10.59	10.77
MnX 60	-0.635	-0.956	-0.981	18.78	10.76	10.82
MnX 71	-0.597	-0.775	-0.965	19.82	10.86	10.76
MnX 79	-0.573	-0.948	-1.017	20.06	10.87	10.16
MnX 90	-0.561	-0.948	-0.984	20.64	11.17	10.76
MnX 100	-0.550	-0.884	-0.972	21.32	11.78	10.98

Pure component adsorption selectivity for nitrogen and oxygen at different equilibrium pressures was calculated and the values at 303.0K are given in Table-4.13. The values of nitrogen/oxygen, nitrogen/argon and oxygen/argon selectivity increases on manganese exchange. The increase in these nitrogen selectivity values is high in the low-pressure region and the selectivity value decreases with increase in the equilibrium adsorption pressure. The nitrogen/oxygen selectivity increases from 3.1 to 4.6 in the low-pressure region, on exchanging the sodium ions of zeolite A with manganese ions. In zeolite X, the nitrogen/oxygen selectivity increases from 3.4 to 10.6 in the low-pressure region. But in the high-pressure region the nitrogen/oxygen selectivity decreases below that of the sodium form. Nitrogen/argon selectivity also increases on manganese exchange on both the zeolites in the low-pressure region. The sodium forms of the zeolites shows similar adsorption properties towards oxygen and argon. On exchanging the extra framework sodium ions with manganese ions, the zeolites became oxygen selective over argon and the values of the oxygen/argon

selectivity increase with increase in the manganese exchange and equilibrium adsorption pressure.

Table-4.13. Adsorption Selectivity on Mn (II) Exchanged Zeolites

Adsorbent	Adsorption Selectivity					
	$\alpha N_2/O_2$		$\alpha N_2/Ar$		$\alpha O_2/Ar$	
	3.33kPa	101.99kPa	3.33kPa	101.99kPa	3.33kPa	101.99kPa
NaA	3.1	3.0	3.4	3.2	0.90	0.93
MnA 41	4.14	3.06	4.79	3.66	1.16	1.20
MnA 59	4.30	2.93	5.63	3.66	1.31	1.25
MnA 74	4.50	2.92	5.38	3.51	1.20	1.20
MnA 89	4.65	2.72	5.90	3.48	1.27	1.28
MnA 99	4.63	2.84	6.28	3.60	1.36	1.27
NaX	3.4	3.1	3.7	3.3	1.08	1.07
MnX 47	7.16	3.03	9.76	3.88	1.36	1.28
MnX 60	8.98	2.86	14.05	4.08	1.56	1.43
MnX 71	9.16	2.71	15.85	3.83	1.51	1.41
MnX 79	10.0	2.42	16.35	3.59	1.69	1.48
MnX 90	10.3	2.70	17.57	4.00	1.62	1.48
MnX 100	10.6	2.67	18.92	4.08	1.78	1.53

The heat of adsorption for nitrogen, oxygen and argon on manganese exchanged zeolite A and X were calculated and the values are given in Table-4.14. The nitrogen heat of adsorption increases on manganese exchange in zeolite A and X. The magnitude of the increase in nitrogen heat of adsorption in zeolite X is much higher than that in zeolite A. In zeolite A, the N_2 heat of adsorption value increases from 20.0kJ mol^{-1} to 26.5kJ mol^{-1}, while that in zeolite X increases from 19.5kJ mol^{-1} to 40.0kJ mol^{-1}. The heat of adsorption values for oxygen and argon remains same as that of the parent sodium form of the zeolite. In both the type of zeolites similar behaviour was observed. The N_2 heat of adsorption shows a high value in the low-pressure region and its value decreases with increase in coverage.

Table-4.14. Isosteric heat of Adsorption on Mn (II) Exchanged Zeolites

Adsorbent	Heat of Adsorption in kJ mol^{-1}		
	Nitrogen	Oxygen	Argon
NaA	20.4	15.3	13.0
MnA 41	22.2	14.6	13.3
MnA 59	24.1	14.8	-
MnA 74	25.6	15.1	13.6
MnA 89	25.3	15.5	14.5
MnA 99	26.5	15.2	14.1
NaX	19.4	15.1	13.4
MnX 47	28.7	15.2	13.9
MnX 60	33.4	15.4	14.0
MnX 71	35.2	15.1	14.2
MnX 79	37.3	15.3	14.8
MnX 90	40.0	15.4	14.4
MnX 100	39.5	15.4	14.1

The framework structure of zeolite A is given in Figure-4.4. There are 12 negative charges that are balanced by cations in each unit cell. For $Na_{12}A$, 8 Na^+ ions are located at Site I at the centre of the six-member ring, 3 at site II at the eight-member aperture directly obstructing the entrance and 1 at site III near the four-member ring inside the cavity. The sodium ions can be easily replaced by other cations.

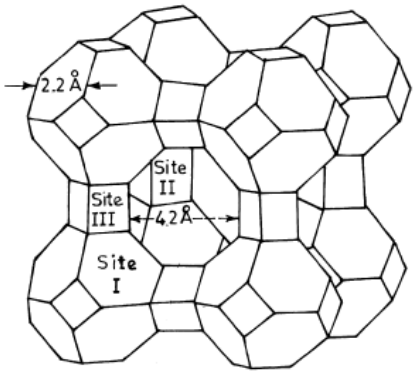

Figure-4.4. Framework structure of zeolite A. Near the centre of each line segment is an oxygen atom. Silicon and aluminium atoms alternate the tetrahedral intersections. Extra framework cation positions are labelled with Roman numerals.

In the dehydrated structure of MnA [16], the framework bond angles of dehydrated MnA are also very similar to those in NaA. Thus the adsorption properties of both the sodium and manganese form of zeolite A is expected to have same adsorption properties. The small variations in the adsorption properties are due to the difference in the interaction of sodium and manganese ions with the adsorbate molecules. The manganese ions are located on the threefold axis close to the planes of the six ring windows. The manganese ions are recessed 0.108Å into the sodalite unit from the [111] plane. The manganese ions are triagonally co-ordinated to three framework oxygen atoms at a distance 2.11Å. These Mn^{2+} ions sitting on the six ring windows are not directly available to interact with the guest molecules such as N_2, O_2 and Ar. The increase in the nitrogen heat of adsorption in manganese (II) exchanged zeolites compared to NaA is due to the difference in the coordination environment. EPR fine structure of manganese ions in zeolite A [17] detects the strong variation in the coordination environment. In fully dehydrated Mn_{46}-X [18], 16 Mn^{2+} ions fill site I at the centre of D6R and the remaining 30 Mn^{2+} ions are located at the 32-fold site II in the supercage. Mn^{2+} ions at site I at the centres of D6Rs and are each coordinated octahedrally by six framework oxygen atoms. Of the 32 site II positions, 30 are occupied. Each Mn^{2+} ion coordinates at 2.130Å to three framework oxygen atoms. No manganese ions are present in site III or site III′, which can interact directly with the adsorbate molecules. The sorption of small molecules such as CO, ethylene and cyclopropane has not been shown to effect this arrangement [19, 20]. In manganese exchanged zeolites, the Mn (II) d-orbitals are severely contracted as compared to those of Mn^0 so that the synergic bonding normally attributed to metal–nitrogen complexes is severely inhibited.

Zeolites exchanged with divalent cations are known to enhance the adsorption of nitrogen, mainly due to the electrostatic interactions. Even though, the number of cations decreases on manganese exchange, the interactions of the adsorbate molecules with the manganese cations will increase because of the smaller size and higher charge on the Mn^{2+} (0.80Å) ions compared to Na^+ (0.95Å) ions resulting in higher charge density. The manganese ions are mainly occupying at cation sites in the sodalite cages, which are directly not accessible to the adsorbate molecules such as nitrogen and argon. But these cations can interact with these adsorbate molecules through the six membered ring. The increase in the adsorption capacity, selectivity,

heat of adsorption, Langmuir constant and Henry's constant for nitrogen and oxygen on exchanging the Na^+ with Mn^{2+} is due to the increased electrostatic interaction of these adsorbate molecules with divalent Mn^{2+} cation.

4.3.3 Cadmium (II) Exchanged Zeolites

The X-ray powder diffraction of the various cadmium-exchanged zeolites were measured and the pattern shows that the structure of the zeolite retained after the cadmium ion exchange. No loss of crystallinity was observed during cadmium exchange. The surface area and pore size distributions of the various cadmium-exchanged zeolites were determined from the N_2 gas adsorption data at 77.35K and the values are given in Table-4.15. The surface area of the zeolites increases on cadmium exchange. This is due to the decrease in the number of extra framework cations while replacing monovalent sodium ions with divalent cadmium ions. Like cobalt and manganese exchanged zeolite X, the external surface area of the cadmium-exchanged zeolites also increases with percentage of cadmium exchange.

Table-4.15. Unit cell dimensions and Surface area of Cadmium Exchanged Zeolites

SAMPLE	% Crystallinity	Unit Cell Dimension	BET Surface Area m^2g^{-1}	t-plot	
				Micropore Area m^2g^{-1}	External Surface Area m^2g^{-1}
NaA	100	24.62	-	-	-
CdA38	96	24.60	523.0	507.8	15.2
CdA 55	95	24.59	485.7	447.3	38.4
CdA 67	93	24.59	469.3	431.6	37.6
CdA 85	93	24.58	455.2	415.9	39.3
CdA 99	92	24.58	449.6	412.0	37.6
Na X	100	24.94	542.2	518.4	23.7
CdX 41	95	24.92	576.0	530.9	45.1
CdX 57	95	24.92	555.6	510.8	44.8
CdX 70	94	24.91	559.8	512.8	47.1
CdX 88	93	24.91	560.6	515.6	45.1
CdX 98	92	24.90	559.6	510.4	49.1

Adsorption isotherms for nitrogen, oxygen and argon on different extent of cadmium-exchanged zeolites A and X were measured at 288.2K and 303.0K. Adsorption isotherms on cadmium exchanged zeolite A and X are given in Figure-4.5. In both the type of zeolites, the adsorption of all the three gases increases marginally. The adsorption of these gases increases linearly with pressure and the shape of the adsorption isotherm remained almost linear in zeolite A. in the case of the nitrogen adsorption isotherm on cadmium exchanged zeolite X, the slope of the isotherm is higher in the low pressure region compared to that in the high pressure region. The oxygen and argon adsorption increases linearly with equilibrium pressure through out the pressure range studied.

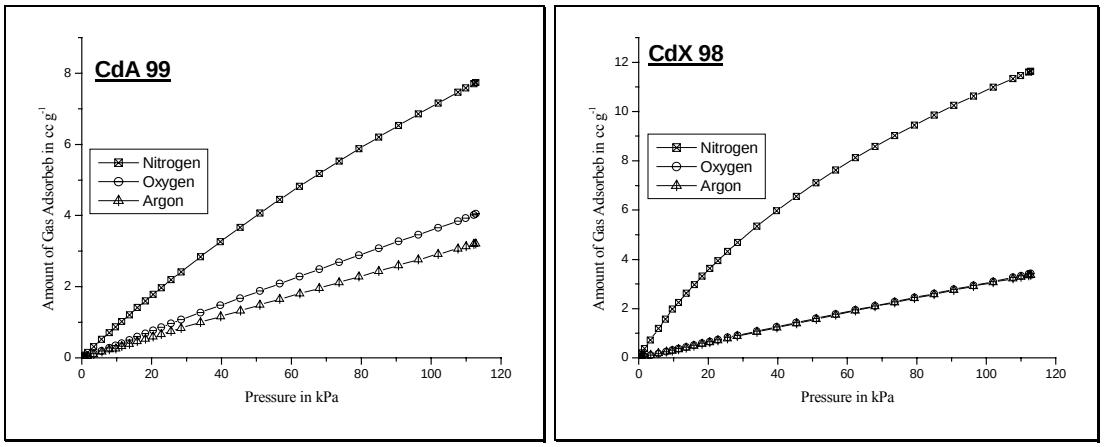

Figure 4.5. Adsorption isotherms on CdA and CdX at 303.0K

The equilibrium adsorption capacities for the adsorption of nitrogen, oxygen and argon on zeolite A and zeolite X containing different amounts of cadmium ions are determined from the adsorption isotherms and the number of molecules of nitrogen, oxygen and argon adsorbed per unit cell of zeolite A and X containing various amount of cadmium at 101.3kPa are given in Table-4.16. The nitrogen, oxygen and argon adsorption capacities increase on cadmium ion exchange. The nitrogen adsorption capacity increases from 6.5-molecules/unitcell in sodium form of zeolite A to 7.6 molecules/unit cell in the cadmium form. Oxygen and argon adsorption capacities also increase nearly by 1molecule/unit cell in zeolite A, on cadmium exchange. In zeolite X, the nitrogen adsorption capacity in creases from 7.7molecules/unit cell in sodium form to 10.3molecules/unit cell in the 98% cadmium exchanged zeolite. But the increase in the oxygen and argon adsorption is much less compared to zeolite A.

Table-4.16. Equilibrium Adsorption Capacity for N_2, O_2 and Ar on Cadmium Exchanged Zeolites

Adsorbent	Equilibrium Adsorption Capacity in molecules / unit cell at 101.3kPa					
	288.2K			303.0K		
	Nitrogen	Oxygen	Argon	Nitrogen	Oxygen	Argon
NaA	6.55	2.12	1.84	4.58	1.53	1.42
CdA38	7.29	2.82	2.79	5.32	2.10	2.09
CdA 55	7.43	3.05	2.81	5.35	2.29	2.09
CdA 67	7.49	3.10	2.84	5.37	2.36	2.12
CdA 85	7.57	3.14	2.87	5.40	2.47	2.13
CdA 99	7.63	3.18	3.03	5.44	2.52	2.18
NaX	7.7	2.4	2.2	5.5	1.8	1.7
CdX 41	8.10	2.20	2.16	5.66	1.55	1.55
CdX 57	8.14	2.35	2.29	6.05	1.77	1.75
CdX 70	8.18	2.42	2.39	6.09	1.77	1.77
CdX 88	10.31	3.02	3.00	7.85	2.22	2.19
CdX 98	10.33	3.02	3.01	7.86	2.23	2.20

The adsorption data obtained at 288.2K and 303.0K were fitted in Langmuir equation and the slope, intercept and Langmuir constant were determined. The values for the slope and Langmuir constant b increases for nitrogen, oxygen and argon on cadmium exchange and increases linearly with increase in cadmium percentage. In zeolite A, the value of Langmuir constant increases from 0.111 in the sodium form of the zeolite to 0.361 in the 99% cadmium exchanged zeolite. The Langmuir constant for oxygen adsorption also increases from 0.037 to 0.086 on cadmium exchange. In the case of argon adsorption on zeolite A, the Langmuir constant value increases from 0.047 to 0.060 on increasing the cadmium exchange level fro 0-99%. In the case of zeolite X, the Langmuir constant value for nitrogen adsorption increases from 0.16 to 1.14 on replacing the extra framework sodium ions with cadmium ions. The Langmuir constant values for oxygen and argon also increase on cadmium exchange. The

Langmuir fitting data on different amount of cadmium ion exchanged zeolites A and X at 303.0K are given in Table-4.17.

Table-4.17. Langmuir Fittings data at 303.0K on Cadmium Exchanged Zeolites

Adsorbent	Slope			Langmuir constant b		
	Nitrogen	Oxygen	Argon	Nitrogen	Oxygen	Argon
NaA	0.012	0.013	0.017	0.111	0.037	0.047
CdA38	0.028	0.022	0.020	0.300	0.082	0.075
CdA 55	0.031	0.022	0.019	0.355	0.095	0.068
CdA 67	0.035	0.018	0.019	0.337	0.090	0.065
CdA 85	0.035	0.017	0.013	0.352	0.084	0.063
CdA 99	0.036	0.017	0.175	0.361	0.086	0.060
NaX	0.014	0.010	0.014	0.160	0.034	0.044
CdX 41	0.042	0.006	0.021	0.610	0.095	0.056
CdX 57	0.053	0.038	0.032	0.980	0.093	0.055
CdX 70	0.055	0.026	0.027	1.000	0.089	0.054
CdX 88	0.058	0.024	0.015	1.118	0.090	0.052
CdX 98	0.060	0.026	0.038	1.142	0.091	0.050

The nitrogen, oxygen and argon adsorption data obtained at 288.2K and 303.0K were also fitted in Virial equation. The Virial coefficients A_0, A_1 and A_2 were determined from the Virial plots. The Henry's constants were calculated from the Virial coefficient. Henry's constant for nitrogen adsorption increases on cadmium exchange on both the zeolites. The Henry's constant for nitrogen adsorption increases from 8 to 13 on increasing the cadmium exchange level 0 to 99 percentage on zeolite A. While in zeolite X, Henry's constant for nitrogen adsorption increases from 10 to 19 on completely replacing the extra framework sodium cations of the zeolite with cadmium ions. Henry's constant for oxygen and argon adsorption on cadmium-exchanged zeolite A increases marginally and that in zeolite X remained almost unaffected on cadmium exchange. The values for the first Virial coefficient A_0 and Henry's constant K at 303.0K are given in Table-4.18.

Table-4.18. Virial Coefficient and Henry's Constant at 303.0K on Cadmium Exchanged Zeolites

Adsorbent	A_0			Henry's Constant K ($10^{-5}ccg^{-1}Pa^{-1}$)		
	Nitrogen	Oxygen	Argon	Nitrogen	Oxygen	Argon
NaA	4.55	5.71	5.78	7.93	2.47	2.32
CdA38	4.43	5.51	5.43	8.87	3.04	3.28
CdA 55	4.31	5.33	5.49	10.01	3.63	3.21
CdA 67	4.47	5.52	5.62	11.58	3.71	3.31
CdA 85	4.42	5.43	5.74	12.01	3.80	3.41
CdA 99	4.56	5.53	5.57	12.88	3.99	3.56
NaX	4.30	5.53	5.57	10.22	2.98	2.86
CdX 41	4.07	6.08	5.79	12.80	2.71	2.30
CdX 57	3.78	5.60	5.67	17.15	2.77	2.58
CdX 70	3.79	5.68	5.65	16.94	2.56	2.64
CdX 88	3.49	5.51	5.62	22.78	3.02	2.73
CdX 98	3.70	5.71	5.71	19.49	2.98	2.68

The nitrogen, oxygen and argon adsorption data obtained at 288.2K and 303.0K were also fitted in Dubinin-Astakhov equation. The values of the slope, intercept, energy and volume are determined from the Dubinin-Astakhov fitting data and the values for slope and Dubinin-Astakhov energy at 303.0K are given in Table-4.19. The value of Dubinin-Astakhov energy for nitrogen adsorption increases on cadmium exchange in both the zeolites. In zeolite A the Dubinin-Astakhov energy for nitrogen adsorption increases from 11.9 to 13.4 on increasing the cadmium exchange level from 0 to 99%. The value of Dubinin-Astakhov energy for nitrogen adsorption increases from 12 to 17 in zeolite X on replacing the extra framework sodium ions with cadmium ions.

Table-4.19. Dubinin-Astakhov Fittings at 303.0K on Cadmium Exchanged Zeolites

Adsorbent	Slope			Energy kJ mol^{-1}		
	Nitrogen	Oxygen	Argon	Nitrogen	Oxygen	Argon
NaA	-0.957	-0.981	-0.981	11.91	10.29	10.71
CdA38	-0.902	-0.965	-0.973	12.15	10.72	10.90
CdA 55	-0.879	-0.970	-0.973	13.35	10.74	10.76
CdA 67	-0.885	-0.987	-0.977	13.22	10.63	10.78
CdA 85	-0.880	-0.983	-0.989	13.37	10.70	10.62
CdA 99	-0.896	-0.985	-0.979	13.14	10.65	10.84
NaX	-0.940	-0.988	-0.985	12.19	10.38	10.63
CdX 41	-0.814	-1.052	-0.954	14.66	10.94	11.09
CdX 57	-0.745	-0.953	-0.963	16.08	10.80	10.94
CdX 70	-0.735	-0.957	-0.967	16.26	10.70	10.91
CdX 88	-0.713	-0.968	-0.984	16.78	10.67	10.59
CdX 98	-0.710	-0.973	-0.952	16.97	10.61	11.03

Adsorption selectivity for the pure component adsorption of nitrogen oxygen and argon are also calculated and the values at 303.0K are given in Table-4.20.

Table-4.20. Adsorption Selectivity on Cadmium Exchanged Zeolites

Adsorbent	Adsorption Selectivity					
	$\alpha N_2/O_2$		$\alpha N_2/Ar$		$\alpha O_2/Ar$	
	3.33kPa	101.99kPa	3.33kPa	101.99kPa	3.33kPa	101.99kPa
NaA	3.1	3.0	3.4	3.2	0.90	0.93
CdA38	3.13	2.58	2.94	2.61	0.98	1.00
CdA 55	3.26	2.32	3.68	2.69	1.13	1.16
CdA 67	3.08	2.15	3.27	2.35	1.06	1.09
CdA 85	3.66	2.39	3.84	2.64	1.05	1.10
CdA 99	3.25	2.18	3.38	2.28	1.04	1.05
NaX	3.4	3.1	3.7	3.3	1.08	1.07
CdX 41	6.71	3.69	6.75	3.74	1.02	1.02
CdX 57	7.46	3.44	7.48	3.52	1.01	1.02
CdX 70	7.17	3.29	8.01	3.48	1.10	1.07
CdX 88	8.11	3.42	8.22	3.44	1.01	1.01
CdX 98	8.81	3.53	8.94	3.55	1.02	1.07

The values of nitrogen-oxygen, nitrogen-argon and oxygen-argon selectivity increases on cadmium exchange. The increase in these nitrogen selectivity values is high in the low-pressure region and the selectivity value decreases with increase in the equilibrium adsorption pressure.

The isosteric heat of adsorption from the adsorption data at various temperatures using Clausius-Clapeyron equation and the values are given in Table-4.21. The heat of adsorption values for nitrogen, oxygen and argon increases with increase in the amount of cadmium exchanged. In zeolite A, the nitrogen heat of adsorption increases from 20.0kJ mol^{-1} to 26.0kJ mol^{-1}, but the increase in oxygen and argon heat of adsorption values are marginal. In zeolite X, the N_2 heat of adsorption increases from 19.0kJ mol^{-1} to 29.1kJ mol^{-1}. In the case of zeolite X also the magnitude of increase in oxygen and argon heat of adsorption is very small.

Table-4.21. Isosteric heat of Adsorption on Cadmium Exchanged Zeolites

Adsorbent	Heat of Adsorption in kJ mol^{-1}		
	Nitrogen	Oxygen	Argon
NaA	20.4	15.3	13.0
CdA38	22.8	14.4	14.3
CdA 55	23.7	14.5	14.6
CdA 67	24.2	14.5	14.3
CdA 85	26.4	14.8	15.0
CdA 99	27.0	15.1	15.1
NaX	19.4	15.1	13.4
CdX 41	26.7	14.4	13.9
CdX 57	27.1	14.1	14.2
CdX 70	28.2	14.4	14.2
CdX 88	27.8	14.7	14.3
CdX 98	29.1	14.7	14.3

In fully dehydrated cadmium exchanged zeolite A [21, 22], all the six Cd^{2+} ions per unit cell lie on three fold axes near the six ring centres, four in large cavity and two in

sodalite cavity. The four Cd^{2+} ions extend 0.480Å into the large cavity from the plane of the oxygen ring are coordinated with three framework oxygen atoms at a distance of 2.215Å. These four Cd^{2+} ions can coordinate with N_2 molecules entering in the large cavity. The remaining two Cd^{2+} ions extended 0.642Å to the sodalite cavity from the plane of the oxygen ring are coordinated with three framework oxygen atoms at distance of 2.256Å.

In dehydrated $Cd_{46}X$, Cd^{2+} ions occupy two different crystallographic sites of high occupancy [23]. Sixteen Cd^{2+} fill site I at the centres of the D6Rs. Each Cd^{2+} ions is octahedrally coordinated with framework oxygen atoms at a distance of 2.35Å. The remaining 30 Cd^{2+} ions nearly fill the 32-fold site II in the single six rings each is three coordinate to planar framework oxygen atoms at 2.16Å, is shorter than the sum of covalent radii [24]. These Cd^{2+} ions are three coordinated and slightly recessed, 0.19Å into the supercage from the plane of the three oxygen atoms. The Cd^{2+} cations sitting in the site I and site II are not accessible to the adsorbate molecules directly, but they can interact through the six ring. The interactions between the nitrogen molecules and Cd^{2+} are much weaker, since the Cd^{2+} ions are strongly coordinated with three framework oxygen atoms. Thus the formation of the metal–nitrogen complexes is inhibited.

The bonding between the Cd^{2+} ions and the N_2 is usually described in terms of the Chatt-Dewar model. [25] A σ-component arises from the overlapping of the filled N_2 orbital and vacant 5s orbital of Cd^{2+}, and a π-component occurs by the overlap of the filled 4d orbital of Cd^{2+} and vacant π* antibonding orbital of N_2. The Cd^{2+} (0.98 Å) ions are poor back donors compared to Ag^{+} (1.26 Å) ions due to their difference in the ionic radii. The filled 4d orbitals of Cd^{2+} therefore do not reach as far out in space as those of Ag^{+} and Cd^{2+} cannot back bond effectively. Therefore the metal ligand bond lengths in π-complexes of Cd^{2+} [26] are longer than to those for Ag^{+}[27].

4.3.4. Copper (II) Exchanged Zeolites

In the case of copper (II) exchanged zeolites, the zeolite structures gets damaged during the ion exchange and high temperature vacuum dehydration process. This is due to the highly corrosive nature of the Cu(II) ions to the zeolite framework. The X-

ray powder diffraction studies of the zeolite of type A and X exchanged with Cu(II) ions shows large decrease in the crystallinity. The external surface area calculated from the t-plot increases in ZSM-5 type zeolite exchanged with Cu^{2+}. In the case of Cu^{2+} ion exchanged mordenite type zeolite, the effect on the zeolite structure was much lower compared to that in other zeolites. The BET surface area, micropore area and external surface area are calculated from the nitrogen adsorption data at 77.35K and the values are given in Table-4.22.

Table-4.22. Crystallinity and Surface Area of Copper Exchanged Zeolites

Adsorbent	% Crystallinity	BET Surface Area m^2g^{-1}	t-plot	
			Micropore Area m^2g^{-1}	External Surface Area m^2g^{-1}
NaA	100	-	-	-
CuA 37	24	147.8	68.1	79.7
Na X	100	542.2	518.4	23.7
CuX 35	81	524.7	441.0	83.7
CuX 52	43	351.4	254.1	97.3
Na MOR	100	334.8	280.6	54.2
Cu MOR 47	95	390.1	371.5	18.6
Cu MOR 98	90	388.1	371.8	16.4
Na ZSM-5	100	347.7	232.8	114.9
Cu ZSM-5 51	96	394.5	252.6	141.9
Cu ZSM-5 99	87	365.3	219.5	145.8

Adsorption isotherms of nitrogen, oxygen and argon on copper exchanged zeolites of type A, X, mordenite and ZSM-5 are measured at 288.2K and 303.0K. The adsorption of nitrogen, oxygen and argon decreases on Cu^{2+} ion exchange in all the zeolites studied. The decreases in the adsorption of these gases are very high in zeolite A and X. This large decrease in the adsorption of nitrogen, oxygen and argon on these zeolites are due to the loss in crystallinity of the zeolite samples during the cation exchange and high temperature vacuum dehydration processes. The adsorption isotherms on copper exchanged zeolite of type mordenite and ZSM-5 at 303.0K are given in Figure-4.6.

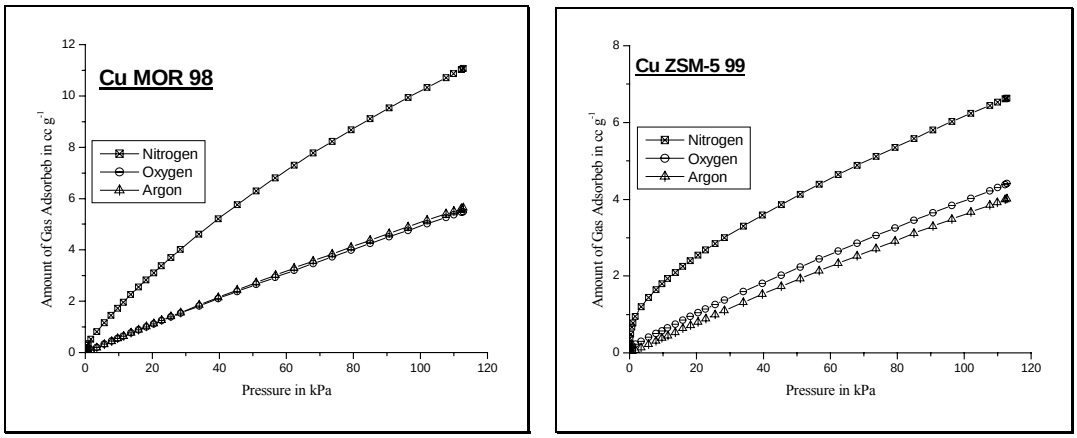

Figure 4.6. Adsorption isotherms on Cu MOR at 303.0K

The adsorption of nitrogen, oxygen and argon decreases on ZSM-5 type zeolite also. The nitrogen adsorption isotherm shows a sharp increase in the low-pressure region. The equilibrium adsorption capacities of nitrogen, oxygen and argon on zeolites containing different amounts of copper ions are determined from the adsorption isotherms and the values at 101.3kPa are given in Table-4.23.

Table 4.23. Equilibrium Adsorption Capacity for N_2, O_2 and Ar on Copper Exchanged Zeolites

Adsorbent	Equilibrium Adsorption Capacity in molecules / unit cell at 101.3kPa					
	288.2K			303.0K		
	Nitrogen	Oxygen	Argon	Nitrogen	Oxygen	Argon
NaA	6.55	2.12	1.84	4.58	1.53	1.42
CuA 37	3.12	1.42	1.41	2.31	0.97	0.96
NaX	7.71	2.4	2.2	5.5	1.8	1.7
CuX 35	2.93	1.59	1.53	3.31	1.96	1.89
CuX 52	2.54	1.45	1.40	2.91	1.81	1.76
Na MOR	2.54	0.92	0.93	2.19	0.75	0.75
Cu MOR 47	1.92	0.91	0.94	2.20	0.96	0.99
Cu MOR 98	1.76	0.92	0.96	2.06	0.99	1.05
Na ZSM-5	3.26	1.42	1.44	2.85	1.38	1.40
Cu ZSM-5 51	1.89	1.35	1.36	2.21	1.41	1.42
Cu ZSM-5 99	1.91	1.34	1.36	2.22	1.40	1.42

The nitrogen, oxygen and argon adsorption capacities are decreased on copper ion exchange. The adsorption data obtained at 288.2K and 303.0K were fitted in Langmuir equation and the slope, intercept and Langmuir constant were determined. The values for the slope and Langmuir constant b increases for nitrogen, oxygen and argon on copper exchange and increases linearly with increase in copper percentage. The Langmuir fitting data on different amount of copper ion exchanged zeolite X, mordenite and ZSM-5 at 303.0K are given in Table-4.24.

Table-4.24. Langmuir Fitting data at 303.0K on Copper Exchanged Zeolites

Adsorbent	Slope			Langmuir constant b		
	Nitrogen	Oxygen	Argon	Nitrogen	Oxygen	Argon
NaA	0.012	0.013	0.017	0.111	0.037	0.047
CuA 37	0.028	0.040	0.053	0.176	0.098	0.116
NaX	0.014	0.010	0.014	0.160	0.034	0.044
CuX 35	0.029	0.031	0.047	0.111	0.098	0.099
CuX 52	0.063	0.043	0.052	0.180	0.089	0.091
Na MOR	0.023	0.026	0.018	0.662	0.173	0.122
Cu MOR 47	0.046	0.029	0.020	0.962	0.187	0.131
Cu MOR 98	0.041	0.026	0.023	0.633	0.161	0.148
Na ZSM-5	0.041	0.030	0.027	0.855	0.202	0.187
Cu ZSM-5 51	0.082	0.057	0.032	1.023	0.330	0.163
Cu ZSM-5 99	0.115	0.091	0.028	2.495	0.617	0.126

The nitrogen, oxygen and argon adsorption data obtained at 288.2K and 303.0K were also fitted in virial equation. The virial coefficients A_0, A_1 and A_2 were determined from the virial plots. The Henry's constants were calculated from the virial coefficient. The Henry's constant values for nitrogen, oxygen and argon decreased on copper exchanged zeolites of type A and X. This can be attributed to the degradation of the zeolite structure during the ion exchange and vacuum dehydration process. In the case of mordenite and ZSM-5 type zeolites, the values for Henry's constant of N_2 and O_2 adsorption increased on copper exchange and the value for N_2 adsorption is as high as 1000 in Cu ZSM-5. The values of A_0 and Henry's constant at 303.0K are given in Table-4.25.

Table-4.25. Virial Coefficients and Henry Constant at 303.0K on Copper Exchanged Zeolites

Adsorbent	A_0			Henry's Constant K (10^{-5}ccg^{-1}Pa^{-1})		
	Nitrogen	Oxygen	Argon	Nitrogen	Oxygen	Argon
NaA	4.55	5.72	5.78	7.93	2.47	2.32
CuA 37	5.82	6.23	6.37	2.14	1.47	1.33
NaX	4.30	5.53	5.57	10.22	2.98	2.86
CuX 35	5.41	5.69	6.15	3.35	2.52	1.60
CuX 52	5.79	6.15	6.26	2.29	1.60	1.44
Na MOR	3.40	4.88	4.85	25.0	5.7	5.9
Cu MOR 47	1.39	4.84	4.92	186.4	5.95	5.48
Cu MOR 98	2.75	4.83	4.88	247.9	6.01	5.68
Na ZSM-5	3.59	4.84	4.88	20.7	5.9	5.7
Cu ZSM-5 51	-0.34	4.79	5.10	1049.6	6.22	4.56
Cu ZSM-5 99	-0.53	4.58	5.27	1272.0	7.71	3.88

The nitrogen, oxygen and argon adsorption data obtained at 288.2K and 303.0K were also fitted in Dubinin-Astakhov equation. The values of the slope and energy at 303.0K are given in Table-4.26. Dubinin-Astakhov energy for the N_2 adsorption in mordenite and ZSM-5 type zeolites are high compared to other zeolites.

Table-4.26. Dubinin-Astakhov Fitting data at 303.0K on Copper Exchanged Zeolites

Adsorbent	Slope			Energy kJ mol^{-1}		
	Nitrogen	Oxygen	Argon	Nitrogen	Oxygen	Argon
NaA	-0.957	-0.981	-0.981	11.91	10.29	10.71
CuA 37	-0.924	-0.973	-0.978	12.51	10.36	10.86
NaX	-0.940	-0.988	-0.985	12.19	10.38	10.63
CuX 35	-0.956	-0.970	-0.961	11.98	10.80	11.37
CuX 52	-0.931	-0.974	-0.969	12.56	10.72	10.95
Na MOR	-0.801	-0.935	-0.955	15.05	11.21	11.18
Cu MOR 47	-0.713	-0.934	-0.949	15.54	10.99	11.27
Cu MOR 98	-0.814	-0.937	-0.945	14.30	10.92	11.22
Na ZSM-5	-0.762	-0.929	-0.933	15.69	11.26	11.52
Cu ZSM-5 51	-0.681	-0.888	-0.939	16.29	11.35	11.36
Cu ZSM-5 99	-0.527	-0.822	-0.952	21.04	12.26	11.20

Adsorption selectivity for the pure gases on various copper exchanged zeolites was calculated from the adsorption data. The adsorption selectivity values at 288.2K are given in Table-4.27.

Table-4.27. Adsorption Selectivity on Copper Exchanged Zeolites

Adsorbent	Adsorption Selectivity					
	$\alpha N_2/O_2$		$\alpha N_2/Ar$		$\alpha O_2/Ar$	
	3.33kPa	101.99kPa	3.33kPa	101.99kPa	3.33kPa	101.99kPa
NaA	3.1	3.0	3.4	3.2	0.90	0.93
CuA 37	2.7	2.2	2.8	2.1	0.99	0.98
NaX	3.4	3.1	3.7	3.3	1.08	1.07
CuX 35	1.53	1.37	2.16	1.91	1.41	1.40
CuX 52	1.61	1.39	1.73	1.50	1.08	1.09
Na MOR	4.1	2.9	4.2	2.8	0.97	1.02
Cu MOR 47	4.64	2.03	4.55	1.93	0.98	0.97
Cu MOR 98	3.40	1.84	3.50	1.82	1.03	0.99
Na ZSM-5	3.3	1.9	3.5	1.8	0.98	1.02
Cu ZSM-5 51	3.30	1.50	3.66	1.49	1.11	0.99
Cu ZSM-5 99	3.28	1.43	3.59	1.52	1.05	1.03

The isosteric heat of adsorption for the adsorption of nitrogen, oxygen and argon were calculated from the adsorption data at 288.2K and 303.0K using Clausius-Clapeyron equation. The heat of adsorption for all the three gases decreases on copper exchange in zeolite A and X. This is attributed to the structural degradation that occurred during the cation exchange and vacuum dehydration processes. In the case of mordenite and ZSM-5 type zeolites, the isosteric heat of adsorption for nitrogen increases on copper exchange. The isosteric heat of adsorption values for oxygen and argon remained almost similar to that of the parent sodium form. Heats of adsorption values for the adsorption of nitrogen, oxygen and argon on various copper exchanged zeolites are given in Table-4.28.

Table-4.28. Isosteric heat of Adsorption on Copper Exchanged Zeolites

Adsorbent	Heat of Adsorption in kJ mol^{-1}		
	Nitrogen	Oxygen	Argon
NaA	20.4	15.3	13.0
CuA 37	18.6	14.3	12.8
NaX	19.4	15.1	13.4
CuX 35	19.4	14.6	14.3
CuX 52	18.9	14.1	13.9
Na MOR	27.0	17.4	17.5
Cu MOR 47	46.8	18.7	18.6
Cu MOR 98	59.6	18.3	17.9
Na ZSM-5	26.8	16.3	17.3
Cu ZSM-5 51	48.8	17.3	18.4
Cu ZSM-5 99	62.7	17.4	18.6

Decrease in the values for adsorption capacity, selectivity, heat of adsorption and Henry's constant were observed in Cu (II) exchanged zeolite of type A and X. But in the case of Cu (II) exchanged mordenite and ZSM-5 types of zeolites, there is a large increase in the adsorption properties in the very low-pressure region. The values for adsorption capacity, selectivity, heat of adsorption, Langmuir constant and Henry's constant is very high in the low-pressure region.

On heating at higher temperatures in vacuum or inert gas flow, a part of the Cu^{2+} ion in Cu (II) ZSM-5 undergoes auto reduction to Cu^{+} [29, 30]. An infrared spectroscopic study shows that on out gassing the Cu (II) ZSM-5 at 773 K the IR band at 970 cm^{-1} increased at the expense of the band at 918cm^{-1}, which is assigned to Cu^{2+} ions [29]. The X-ray absorption near-edge structure (XANES) spectra confirm the monovalent state of copper in CuZSM-5 [31, 32]. Dinitrogen molecules interact very strongly with the Cu^{+} ions in the zeolite cavities at room temperature [31-34]. The strong IR band obtained at 2295 cm^{-1} indicating the existence of strong interaction between the monovalent copper ions and N_2 molecules [32]. The strong interaction of the Cu^{+} with N_2 was further confirmed from the high heat of adsorption of N_2 on the Cu^{+} species [33, 34]. Similar to ZSM-5, mordenite type zeolite also shows the reduction of Cu^{2+} to Cu^{+} on vacuum dehydration. The N_2 heat of adsorption, Henry's constant, etc. shows the very strong interaction of the N_2 molecules with the copper species.

4.3.5 Nickel (II) and Zinc (II) Exchanged Zeolites

The stability of the zeolite structure having first-raw transition metals are well studied as a function of metal ion content per unit cell [35]. It was reported that the stability of the nickel exchanged zeolite decreases with the increase in nickel ion exchange and ion exchange temperature and the structure of zeolite collapses at higher nickel loading [36]. The hydrated Ni^{2+} ions hydrolyse with in the zeolite, with dealumination of the zeolite framework [35]. The crystal structure of fully and partially hydrated single crystals of partially Ni^{2+} ions exchanged zeolite A was determined [37]. Upon dehydration crystal damage was observed. In fully hydrated crystal structure, extensive hydrolysis of the framework give five-coordinate Al^{3+} was observed. In addition, hydronium ions were found in the secondary coordination spheres of hydrolysed Ni^{2+} ions. This acidity is likely to be responsible for the loss of crystallinity upon further dehydration.

Table-4.29. Surface Area of Nickel and Zinc Exchanged Zeolites

Adsorbent	**% Crystallinity**	BET Surface Area m^2g^{-1}	t-plot	
			Micropore Area m^2g^{-1}	External Surface Area m^2g^{-1}
NaX	100	542.2	518.4	23.7
NiX 51	68	647.7	593.5	54.3
ZnX 55	83	682.4	635.0	47.3
ZnX 98	61	662.2	610.1	52.1
NaA	100	24.62	-	-
NiA 45	57	455.3	317.8	137.5
NiA 73	41	291.4	41.9	249.5
ZnA 51	73	502.7	450.9	51.8
ZnA 99	58	487.4	423.4	54.9

The X-ray powder diffraction of the various nickel and zinc exchanged zeolites were measured and the pattern shows the retention of the zeolite structure after the ion exchange. Loss of crystallinity was observed during the ion exchange and the dehydration process and the loss of crystallinity increases with increase in metal loading. The surface area and pore size distributions of the various cation-exchanged

zeolites were determined from the N_2 gas adsorption data at 77.35K and the values are given in Table-4.29. The surface area of the zeolites increases on the exchange of divalent cations, but at higher nickel loading, the structure of zeolite collapses. The increase in the value of external surface area determined from the t-plot and the shape of the isotherm at 77.35K also indicates the partial degradation of the zeolite structure with the nickel ion exchange.

Adsorption isotherms for nitrogen, oxygen and argon on different zinc and nickel-exchanged zeolites were measured at 288.2K and 303.0K. Figure-4.7 represents the nitrogen, oxygen and argon adsorption isotherm at 303.0K on ZnA and ZnX. Adsorption of all the three gases decreased on zinc exchange. But the magnitude of decrease is high for nitrogen.

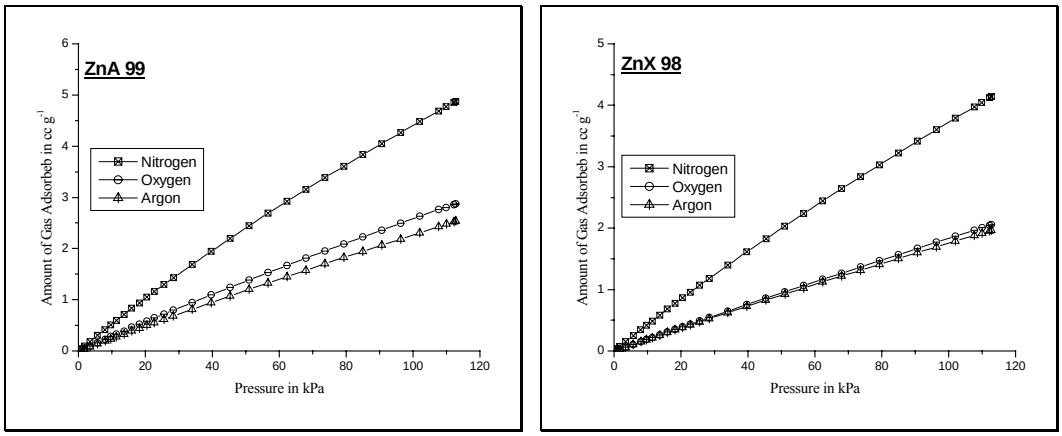

Figure 4.7. Adsorption isotherms on ZnA and ZnX at 303.0K

The adsorption isotherms for nitrogen, oxygen and argon on NiA and NiX at 303.0K are given in Figure-4.8. The adsorption capacities for nitrogen, oxygen and argon decrease on nickel exchange.

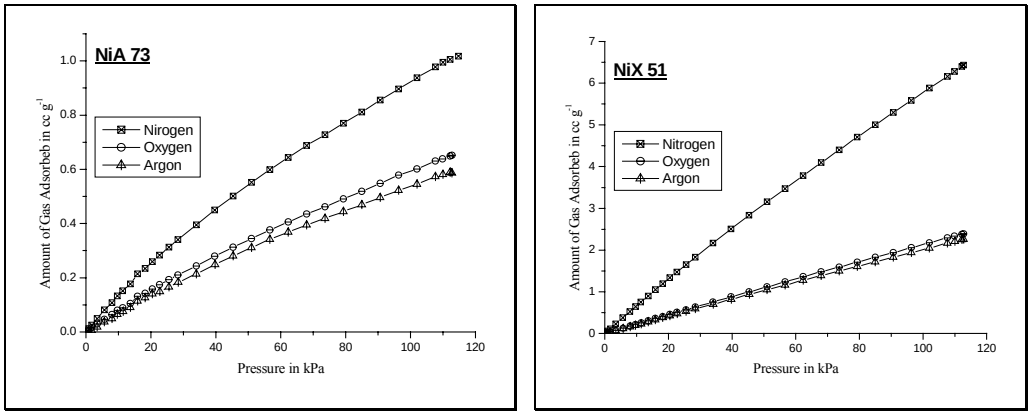

Figure 4.8. Adsorption isotherms on NiA and NiX at 303.0K

The equilibrium adsorption capacities for the adsorption of nitrogen, oxygen and argon on zeolite A and zeolite X containing different amounts of zinc and nickel ions are determined from the adsorption isotherms and the values at 101.3kPa are given in Table-4.30. The nitrogen, oxygen and argon adsorption capacities also decrease on zinc and nickel ion exchange in both the zeolites.

Table-4.30. Equilibrium Adsorption Capacity for N_2, O_2 and Ar on Nickel and Zinc Exchanged Zeolites

Adsorbent	Equilibrium Adsorption Capacity in molecules / unit cell at 101.3kPa					
	288.2K			303.0K		
	Nitrogen	Oxygen	Argon	Nitrogen	Oxygen	Argon
NaX	7.7	2.4	2.2	5.5	1.8	1.7
NiX 51	3.98	1.71	1.65	4.27	1.91	1.85
ZnX 55	3.31	1.45	1.39	3.58	1.78	1.58
ZnX 98	3.25	1.38	1.27	3.37	1.64	1.47
NaA	6.55	2.12	1.84	4.58	1.53	1.42
NiA 45	3.68	1.56	1.50	4.01	1.87	1.79
NiA 83	3.31	1.47	1.39	3.64	1.76	1.59
ZnA 51	3.49	1.44	1.31	3.97	1.79	1.75
ZnA 99	3.39	1.39	1.29	3.89	1.82	1.77

The adsorption data obtained at 288.2K and 303.0K were fitted in Langmuir equation and the slope, intercept and Langmuir constant were determined. The values for the slope and Langmuir constant b decreases for nitrogen, oxygen and argon on zinc and nickel ion exchange. The Langmuir fitting data on different amount of zinc and nickel ions exchanged zeolites A and X at 303.0K are given in Table-4.31.

Table-4.31. Langmuir Fitting data at 303.0K on Nickel and Zinc Exchanged Zeolites

Adsorbent	Slope			Langmuir constant b		
	Nitrogen	Oxygen	Argon	Nitrogen	Oxygen	Argon
NaX	0.014	0.0099	0.014	0.160	0.034	0.044
NiX 51	0.024	0.029	0.030	0.184	0.073	0.070
ZnX 55	0.030	0.042	0.020	0.149	0.098	0.044
ZnX 98	0.040	0.032	0.044	0.196	0.070	0.095
NaA	0.012	0.013	0.017	0.111	0.037	0.047
NiA 45	0.026	0.039	0.052	0.167	0.098	0.126
NiA 83	0.242	0.297	0.272	0.611	0.435	0.341
ZnA 51	0.016	0.027	0.020	0.116	0.098	0.065
ZnA 99	0.040	0.045	0.037	0.244	0.149	0.104

The nitrogen, oxygen and argon adsorption data obtained at 288.2K and 303.0K were also fitted in Virial equation. The Virial coefficients A_0, A_1 and A_2 were determined from the Virial plots. The Henry's constants were calculated from the Virial coefficient. The values for the Virial coefficients A_0, A_1, A_2 and Henry's constant K at 303.0K are given in Table-4.32

Table-4.32. Virial Coefficient and Henry's Constant at 303.0K on Nickel and Zinc Exchanged Zeolites

Adsorbent	A_0			Henry's Constant K ($10^{-5}ccg^{-1}Pa^{-1}$)		
	Nitrogen	Oxygen	Argon	Nitrogen	Oxygen	Argon
NaX	4.23	5.528	5.568	10.22	2.98	2.86
NiX 51	4.73	5.87	5.96	6.63	2.11	1.93
ZnX 55	4.77	5.48	5.63	6.39	3.12	2.69
ZnX 98	4.95	5.64	5.78	5.32	2.67	2.31
NaA	4.55	5.71	5.78	7.93	2.47	2.32
NiA 45	4.91	5.94	6.05	5.57	1.98	1.77
NiA 83	6.23	6.82	7.23	1.49	0.82	0.54
ZnA 51	5.15	5.83	6.08	4.37	2.20	1.72
ZnA 99	5.15	6.00	5.99	4.36	1.85	1.87

The nitrogen, oxygen and argon adsorption data obtained at 288.2K and 303.0K were also fitted in Dubinin- Astakhov equation. The values of the slope, intercept, energy and volume at 303.0K are given in Table-4.33.

Table-4.33. Dubinin-Astakhov Fitting data at 303.0K on Nickel and Zinc Exchanged Zeolites

Adsorbent	Slope			Energy kJ mol^{-1}		
	Nitrogen	Oxygen	Argon	Nitrogen	Oxygen	Argon
NaX	-0.940	-0.988	-0.985	12.19	10.38	10.63
ZnX 55	-0.944	-0.959	-0.990	12.10	11.08	10.69
ZnX 98	-0.929	-0.977	-0.967	12.33	10.61	11.01
NiX 51	-0.932	-0.947	-0.988	12.32	10.53	10.73
NaA	-0.957	-0.981	-0.981	11.91	10.29	10.71
NiA 45	-0.936	-0.958	-0.963	12.31	10.94	11.33
NiA 83	-0.816	-0.850	-0.867	14.37	12.50	12.44
ZnA 51	-0.959	-0.963	-0.975	11.86	10.68	10.86
ZnA 99	-0.913	-0.947	-0.965	12.67	11.01	11.02

Adsorption selectivity for the pure gases on various zinc and nickel exchanged zeolites was calculated from the adsorption data. The adsorption selectivity values at 303.0K are given in Table-4.34.

Table-4.34. Adsorption Selectivity on Nickel and Zinc Exchanged Zeolites at 303.0K

Adsorbent	Adsorption Selectivity					
	$\alpha N_2/O_2$		$\alpha N_2/Ar$		$\alpha O_2/Ar$	
	3.33kPa	101.99kPa	3.33kPa	101.99kPa	3.33kPa	101.99kPa
NaX	3.4	3.1	3.7	3.3	1.08	1.07
NiX 51	3.56	2.71	3.92	3.00	1.10	1.11
ZnX 55	2.64	2.22	2.69	2.33	1.02	1.05
ZnX 98	3.12	2.23	3.28	2.29	1.08	1.04
NaA	3.1	3.0	3.4	3.2	0.90	0.93
NiA 45	3.07	2.74	3.46	3.02	1.10	1.11
NiA 83	2.05	1.68	2.43	2.14	1.18	1.27
ZnA 51	2.23	2.10	2.55	2.33	1.14	1.11
ZnA 99	2.0	1.71	2.28	1.83	1.14	1.07

The heat of adsorption for nitrogen, oxygen and argon on various nickel and zinc exchanged zeolites of type A and X were determined form the adsorption data at 288.2K and 303.0K and the values are given in Table-4.35. The nitrogen heat of adsorption on NaNiA and NaZnX increases on cation exchange, while that in NaNiX and NaZnA remains almost unaffected during the cation exchange. The heat of adsorption for oxygen and argon remains unaffected on all these zeolites.

Table-4.35. Isosteric heat of Adsorption on Nickel and Zinc Exchanged Zeolites

Adsorbent	Heat of Adsorption in kJ mol^{-1}		
	Nitrogen	Oxygen	Argon
NaX	19.4	15.1	13.4
NiX 51	21.78	16.16	15.43
ZnX 55	21.31	14.44	13.20
ZnX 98	25.61	14.38	13.45
NaA	20.4	15.3	13.0
NiA 45	26.81	15.39	14.32
NiA 83	27.92	15.41	14.30
ZnA 51	19.92	14.20	13.32
ZnA 99	19.13	14.26	13.89

Decrease in the values for adsorption capacity, selectivity, heat of adsorption, Langmuir constant and Henry's constant were observed in Zn (II) and Ni (II) exchanged zeolites. This can be explained in terms of the loss of crystallinity and structural dealumination of the zeolites during the cation exchange and dehydration process.

In the case of nickel exchanged zeolites, extensive hydrolysis of the framework give five-coordinate Al^{3+} was observed [35]. In addition, hydronium ions were found in the secondary coordination spheres of hydrolysed Ni^{2+} ions [36]. This acidity is likely to be responsible for the loss of crystallinity upon further dehydration [37]. In Zn^{2+} ion exchanged zeolites, over exchange, framework dealumination and intra zeolitic hydrolysis of Zn^{2+} ions were observed [38]. Aqueous Zn^{2+} ion exchange at $80^{o}C$ resulted in over exchange due the uptake of $Zn(OH)_2$. High temperature vacuum dehydration resulted in the loss of framework aluminium atoms as aluminate ions and the zeolite became silicon rich. The aluminate lost by the framework retained in the

sodalite cavities. Monomeric tetrahedral aluminate ions AlO_4^{5-} were identified on Zn^{2+} ion exchanged zeolite X [39]. The dealumination of the zeolite framework that occurred during the high temperature vacuum dehydration process was confirmed by solid-state NMR studies [40].

4.4. REFERENCES

[1] D. W. Breck, *Zeolite Molecular Sieves,* Wiley, New York, 1974.

[2] P. E. Riley and K. Seff, *J. Phys. Chem.,* 1975, **79**, 1594-1601.

[3] R. L. Firor and K. Seff, *J. Phys. Chem.,* 1978, **82**, 1650-1655

[4] R. M. Haniffa and K. Seff, *J. Phys. Chem. B*, 1998, **102**, 2688-2695.

[5] R. M. Haniffa and K. Seff, *Microporous and Mesoporous Materials,* 1998, **25**, 137-149.

[6] P. Feng, X. Bu and G.D. Stucky, *Nature,* 1997, **388**, 735-741.

[7] G. C. Shen, T. Shido and M. Ichikawa, *J. Phys. Chem.,* 1996, **100**, 16947-16956.

[8] C. Ronay and K. Seff, *Zeolites,* 1993, **13**, 97-101.

[9] M. D. Baker, J. Godber and G. A. Ozin, *Catal. Rev. Sci.- Eng.,* 1985, **27**, 591–651.

[10] K. Pierloot, A. Delabie, C. Ribbing, A. A. Verberckmoes and R. A. Schoonheydt, *J. Phys. Chem. B,* 1998, **102**, 10789-10798.

[11] D. H. Olson, *Zeolites*, 1995, **15**, 439-443.

[12] D. Base and K. Seff, *Microporous and Mesoporous Materials*, 1999, **33**, 265-280.

[13] A. A. Verberckmoes, B. M. Weckhuysen and R. A. Schoonheydt, *Microporous and Mesoporous Materials*, 1998, **22**, 165-178.

[14] P. E. Riley and K. Seff, *Inorganic Chemistry*, 1974, **13**, 1355-1360.

[15] Y. H. Yeom, Y. Kim and K. Seff, *J. Phys. Chem.,* 1996, **100**, 8373-8377.

[16] R. Y. Yanagida. T. B. Vance Jr. and K. Seff, *Inorganic Chemistry*, 1974, **13**, 723-727.

[17] D. E. De Vos, B. M. Weckhuysen and T. Bein, *J. Am. Chem. Soc.,* 1996, **118**, 9615-9622.

[18] S. B. Jang, M. S. Jeong, Y. Kim, K. Seff, *J. Phys. Chem. B*, 1997, **101**, 9041-9045.

[19] M. N. Bae, Y. Kim and K. Seff, *Microporous and Mesoporous Materials*, 1998, **26**, 101-107.

[20] E. Y. Choi, Y. Kim, Y. W. Han and K. Seff, *Microporous and Mesoporous Materials*, 2000, **40**, 247-255.

[21] S. B. Jang, Y. Kim and K. Seff, *Bull. Korean Chem. Soc.,* 1994, **15**, 236.

[22] E. Y. Choi, Y. Kim, Y. W. Han and K. Seff, *Microporous and Mesoporous Materials*, 2000, **41**, 61-68.

[23] J. H. Kwon, S.B. Jang, Y. Kim and K. Seff, *J. Phys. Chem.,* 1996, **100**, 13720-13724.

[24] *Handbook of Chemistry and Physics*, The Chemical Rubber Co. Cleveland, 1990.

[25] J. Chatt and L. A. Duncanson, *J. Chem. Soc.,* 1953, 2939-2947.

[26] Y. H. Yeom, Y. Kim, S. H. Song and K. Seff, *J. Phys. Chem. B,* 1997, **101**, 2138-2142.

[27] Y. Kim and K. Seff, *J. Am. Chem. Soc.,* 1978, **100**, 175-183.

[28] M. F. Ciraolo, P. Norby, J. C. Hanson, D. R. Corbin and C. P. Grey, *J. Phys. Chem. B*, 1999, **103**, 346.

[29] J. Siirkony, *Journal of Molecular Structure*, 1997, **410-411**, 137-140.

[30] Y. Kuroda, R. Kumashiro and M. Nagao, *Applied Surface Science,* 2002, **196**, 408-422.

[31] Y. Kuroda, R. Kumashiro, A. Itadani, M. Nagao and H. Kobayashi, *Phys. Chem. Chem. Phys.,* 2001, **3**, 1383-1390.

[32] Y. Kuroda, T. Okamoto, R. Kumashiro, Y. Yoshikawa and M. Nagao, *Chemical Communications,* 2002, 1758–1759.

[33] Y. Kuroda, A. Itadani, R. Kumashiro, T. Fujimoto and M. Nagao, *Phys. Chem. Chem. Phys.,* 2004, **6**, 2534-2541.

[34] A. Itadani, R. Kumashiro, Y. Kuroda and M. Nagao, *Thermochimica Acta*, 2004, **416**, 99-104.

[35] D. Base and K. Seff, *Microporous and Mesoporous Materials*, 2000, **40**, 219-232.

[36] D. H. Olson, *J. Phys. Chem.*, 1968, **72**, 4366-4373.

[37] T. Bhat. G. P. Babu and A. N. Bhat, *JCS Faraday Trans*., 1995, **91**, 3983-3986.

[38] L. B. McCusker and K. Seff, J. *Phys. Chem.*, 1981, **85**, 405-410.

[39] D. Base, S. Zhen and K. Seff, *J. Phys. Chem. B*, 1999, **103**, 5631-5636.

[40] D. Base and K. Seff, *Microporous and Mesoporous Materials*, 2000, **40**, 233-245.

Chapter-5

Catalysis and Photocatalysis Using Transition Metal Ion Exchanged Zeolites

Part-1

Catalytic Epoxidation of Styrene with Molecular Oxygen Using Cobalt Exchanged Zeolite X

5.1.1. INTRODUCTION

Zeolites are crystalline inorganic, microporous solids with well-defined channels and cavities having window diameters of the order of 1nm. The framework is sufficiently open to accommodate neutral molecules and cations. They have been widely used and studied as ion exchangers, sorbents and catalysts in industrial processes [1]. The extra framework cations present in zeolites play significant role in determining their adsorption and catalytic properties [2]. In particular, if co-ordinately unsaturated metal ions can be incorporated inside the zeolite cavities, novel adsorption and catalytic behaviour may be fashioned on the basis of coordination of guest molecules. Exchangeable transition metal ions in activated zeolites are generally co-ordinately unsaturated and readily form complexes with a variety of guest molecules [3]. For applications, transition-metal ions are often introduced by ion-exchange; these can coordinate more selectively to guest molecules than filled-shell cations and often have easy access to other oxidation states, so their introduction into the zeolite allows new mechanisms for their function as sorbents and catalysts. As a result, transition metal containing zeolites have been shown to catalyse a wide range of organic reactions such as hydroformylation of olefins, hydrosulfurization of alcohols, oxidation of alkanes, conversion of olefins to thiols, composition of nitro methane and Fischer–Tropsch catalysis [4].

Epoxidation of styrene-to-styrene oxide is practically very important reaction, since styrene oxide is an intermediate in the synthesis of fine chemicals and pharmaceuticals. Epoxidation of terminal olefin is difficult to accomplish, requiring very long reaction time. Conventional production of styrene oxide is based on the dehydrochlorination of styrene chlorohydrin with a base or by using organic peracids. However, peracids are very expensive, hazardous to handle, non-selective for the epoxide formation and also lead to formation of undesirable products, creating a lot of waste. Homogeneous catalysis using transition metal complexes for the epoxidation also lead to a large volume of waste because of their separation problem.

In order to overcome these limitations, the conventional route for epoxidation of alkenes is being attempted to be replaced by environmental friendly re-usable

heterogeneous catalysts such as Ti/SiO_2 [5-7], TS-1 [7-10, 15], Ti-MCM-41 [10], Fe or V/SiO_2 [7], TBS-2, TS-2 [11] γ-Al_2O_3 [12], gold supported on Al_2O_3, Ga_2O_3, In_2O_3 and Tl_2O_3 [13] MgO and other alkaline earth oxides [14] catalysts, using TBHP [5, 13-15], H_2O_2 [6–8, 10-12] or urea–H_2O_2 adduct [13], as an oxidizing agent. With H_2O_2 as an oxidizing agent, although the styrene conversion was very high, the selectivity for styrene oxide was very poor. On the other hand, with TBHP [5] and urea–H_2O_2 adduct [9] as oxidizing agents, high styrene oxide selectivity (>80%) was observed, but only at a low styrene conversion (9.8 and 17.7%, respectively). However, this procedure demands the use of anhydrous H_2O_2 and also the catalyst loading is as high as 20-wt % of the styrene. The isomerisation of styrene oxide was suppressed by the addition of NaOH solution into the reaction medium and a highest epoxide selectivity of 96.5% without affecting styrene conversion was reported [15].

On the other hand, molecular oxygen is the most desirable oxidant for the epoxidation of alkenes with respect to environmental and economic considerations. Cobalt ions and complexes are well-known catalysts for the selective oxidation of alkanes and alkylbenzenes with O_2 [16]. Cobalt complexes have also been used for the epoxidation of alkenes with tert-butyl hydroperoxide and iodosylbenzene [17]. The catalytic oxidation of terminal olefins including styrene by O_2 to the corresponding 2-ketones and 2-alcohols using a cobalt (II) complex was reported [18-19], but no styrene oxide was observed. Cobalt salen complexes were reported to show catalytic activity for epoxidation of styrene with O_2, but a sacrificial co-reductant, isobutyraldehyde, was necessary [20]. $CoCl_2$ was investigated for the oxidation of monoterpenes with O_2, and it was found that the allylic oxidation proceeded dominantly [21]. Several heterogeneous cobalt catalysts have been applied for the selective oxidation of alkanes, especially cyclohexane, [22-26] but very few contribute to the development of heterogeneous catalysts for epoxidation of alkenes with O_2 [27-28]. Some transition metal salts and complexes and even scarce heterogeneous catalysts such as CoAlPO-36 were reported to show activity for the epoxidation reactions with O_2 [29-31], but in most cases, a co-reductant was indispensable. Several homogeneous catalysts such as ruthenium complexes, ruthenium- and iron-substituted polyoxometalates can utilise O_2 as the oxidant for the

epoxidation of alkenes without need of the co-reductant [32-33], but very few heterogeneous catalysts are known. It is, therefore, important to develop a novel reusable solid catalyst, to achieve high styrene conversion particularly at high styrene oxide selectivity in the epoxidation of styrene with molecular oxygen.

Recently, Co^{2+} [34] and Fe^{2+}[35] exchanged faujasite type zeolites are reported to catalyse the epoxidation of styrene with O_2 in the absence of a co-reductant. Almost similar results are obtained in both the cases. A highest styrene conversion of 46% with maximum epoxide selectivity 63% was reported in both the cases.

The present work was undertaken with the objective of investigating the catalytic epoxidation reaction of styrene with molecular oxygen using cobalt-exchanged zeolite X as the catalyst and testing the effect of water molecules in the reaction system on the conversion of styrene-to-styrene oxide. Cobalt (II) exchanged zeolite X having various alkali and alkaline earth metal promoters have been used as the catalyst for the epoxidation reaction to improve the styrene conversion and the styrene oxide selectivity.

5.1.2. EXPERIMENTAL

5.1.2.1. Materials

Zeolites X from Zeolites and Allied Products, Bombay, India and cobalt nitrate hexahydrate, potassium chloride, cesium chloride, magnesium chloride hexahydrate, calcium chloride dihydrate, strontium chloride hexahydrate and barium chloride dihydrate from S. D. Fine Chemicals Ltd., Bombay, India were used as the starting materials for the catalyst preparation. Styrene (99%) from Sigma-Aldrich Corporation Bombay, India, N, N-dimethylformamide (99.7%) from Qualigens Fine Chemicals Ltd., Bombay, India and oxygen (99.9%) from Inox Air Products Ltd., Bombay, India were used for the epoxidation studies.

5.1.2.2. Cation Exchange

The commercially obtained zeolite X was in sodium form. The sodium cations of the zeolite X were replaced with various alkali and alkaline earth metal cations by ion

exchanging with potassium, rubidium, cesium, magnesium, calcium, strontium and barium salt solution at 353K separately or in combination. The ion exchange process was repeated several times to achieve the complete replacement of sodium ions with other alkali and alkaline earth metals. Cobalt cations were introduced into this highly crystalline zeolite X by the cobalt ion exchange from aqueous solution. Typically, the zeolite was refluxed with 0.05M aqueous solution of the cobalt nitrate in the solid / liquid ratio 1:80 at 353K for 4hours. The residue was filtered, washed with hot distilled water, until the washings were free from nitrate ions and dried in air at room temperature. Zeolite X samples having different amount of cobalt exchange were prepared by subjecting repeated ion exchange into the zeolite. The extent of cobalt exchange in zeolite X was determined by the complexometric titration of the original solution and filtrate obtained after the ion exchange with EDTA using murexide indicator.

5.1.2.3. X-ray Powder Diffraction

X-ray powder diffraction studies of various cobalt-exchanged zeolite X at ambient temperature were carried out using PHILIPS X'pert MPD system in the 2θ range of 5-65 degrees using CuKα1 (λ = 1.54056Å). The diffraction patterns of the starting materials show that these are highly crystalline showing the reflections in the range 5 to 35 degrees typically of zeolites. The structures of the zeolites were retained after the cation exchange.

5.1.2.4. Surface Area and Pore Size Distribution

Surface area and pore size distribution of the various cobalt-exchanged zeolites were determined from the N_2 adsorption data at 77.35K. The equilibrium nitrogen adsorption at 77.35K was measured using Micromeritics ASAP 2010. The samples were activated at 373K under vacuum (5×10^{-3}mmHg) for 12hours before the N_2 sorption measurements. The surface areas of different catalyst samples were determined by applying BET and Langmuir equations in the N_2 adsorption data at 77.35K and the micropore area, micropore volume and external pore area by applying t-plot.

5.1.2.4. Diffuse Reflectance Spectroscopy

Diffuse Reflectance Spectroscopic (DRS) studies were carried out using Shimadzu UV-3101PC equipped with an integrating sphere. $BaSO_4$ was used as the reference material. The spectra were recorded at room temperature in the wavelength range of 200-750nm.

5.1.2.5. Catalytic Epoxidation Reactions

The cobalt ion exchanged zeolites dried at room temperature were used for the catalytic studies with out any further activation. The catalytic epoxidation reactions were carried out in liquid phase as a batch reaction at 373K. Typically, a 50ml round bottom flask equipped with an efficient water condenser is kept in a constant temperature oil bath whose temperature was maintained at 373±2K. 10 mmol styrene along with 20 ml N, N-dimethylformamide (DMF) and 200mg catalyst were added to the flask. The reaction was started by bubbling O_2 at atmospheric pressure into the reaction mixture at the rate of 6-8ml min^{-1}. Tridecane was used as internal standard. The reaction mixture was magnetically stirred at 600 rpm. After 4 hours of reaction, the catalyst was separated by centrifuging the reaction mixture and the liquid organic products were analysed with a gas chromatograph (Hewlett-Packard Model 6890, USA) having a flame ionisation detector and HP-5 capillary column (30m length and 0.32mm diameter, packed with silica-based supel cosil), programmed oven (temperature range 348-493K), and N_2 as carrier gas. Reaction kinetics was monitored by withdrawing small amount of the sample from the reaction flask at a time intervals of 30 minutes and analysing its composition by GC. Calibrations of GC peak areas of styrene and styrene oxide were carried out using solutions having known amounts of styrene and styrene oxide. The conversion was calculated on the basis of mole percent of styrene, the initial mole percent of styrene was divided by initial area percent (styrene peak area from GC) to get the response factor. The unreacted moles of styrene remained in the reaction mixture were calculated by multiplying response factor with the area percentage of the GC peak for styrene obtained after the reaction. The conversion, selectivity and turnover frequency (TOF) were calculated as follows:

$$\text{Conversion (mol\%)} = \frac{\text{(initial mol\%) - (final mol\%)}}{\text{initial mol\%}} \times 100$$

$$\text{Styrene Oxide Selectivity} = \frac{\text{GC peak area of Styrene Oxide}}{\text{GC peak area of all products}} \times 100$$

$$\text{TOF} = \frac{\text{No. of moles of Styrene oxide formed}}{\text{No. of moles of cobalt in the catalyst x Reaction time}}$$

5.1.2.6. Catalyst Regeneration

The spent catalyst was recovered from the reaction mixture by filtration and thoroughly washed with DMF, distilled water and then dried in air at room temperature.

5.1.3. RESULTS AND DISCUSSION

Complete Co^{2+}exchange of NaX was attempted from aqueous solution at 353K, but the complete Co^{2+}exchange was not achieved. The structure of the zeolite X retained during the cations exchange process. The X-ray powder pattern of various cobalt ion exchanged zeolite X shows the loss of crystallinity during the cobalt ion exchange process. The X-ray powder diffraction patterns of various catalysts are given in Annexure I. Hydronium ions generated in the aqueous solution may have attacked the zeolite framework to a minor degree, leading to a loss of Al^{3+} ions and crystallinity. The theoretical study, which used cluster models for Co (II) in an isolated six- ring without coordinating H_2O or OH^-, showed that the effective coordination number of Co (II) depends on the local Si and Al arrangement, and the aluminium deficient six-rings behave differently from $Si_3Al_3O_6$ six-rings [36].

The surface area and pore size distributions of the various cobalt exchanged zeolite X samples were determined from the N_2 gas adsorption data at 77.35K. The values of BET surface area; Langmuir surface area, micropore volume, micropore area and external surface area were calculated by fitting the adsorption data in the corresponding theories and the values are given in Table-5.1.1. The number in the name of the catalyst denotes the percentage of cobalt ion exchange in the zeolite.

Table-5.1.1. Surface Area and Pore Volume of Various Catalyst Samples

Catalyst	BET Surface Area m^2g^{-1}	Langmuir Surface Area m^2g^{-1}	Dataset by applying t-plot		
			Micropore Volume cm^3g^{-1}	Micropore Area m^2g^{-1}	External Surface Area m^2g^{-1}
NaX	508.1	672.1	0.2168	464.2	43.8
NaCoX 10	548.7	724.7	0.2353	504.4	44.3
NaCoX 19	556.0	730.4	0.2363	509.4	46.6
NaCoX 34	619.2	819.6	0.2657	568.3	50.9
NaCoX 69	639.7	847.0	0.2691	575.8	63.9
NaCoX 81	652.3	863.1	0.2735	600.6	51.7
NaCoX 92	676.0	888.1	0.2859	623.9	52.1
NaCoX 96	676.3	888.7	0.2885	621.7	54.5
KCoX 19	558.3	732.3	0.2447	527.1	31.2
RbCoX 22	553.7	728.1	0.2387	514.8	38.9
CsCoX 20	518.4	681.1	0.2165	466.9	51.5
MgCoX 22	667.7	876.8	0.2819	608.0	59.7
CaCoX 19	567.4	749.2	0.2436	522.3	45.1
SrCoX 18	325.6	427.6	0.1391	299.7	25.9
BaCoX 15	406.7	534.7	0.1706	367.8	38.9
CsBaCoX 20	432.3	571.2	0.1822	390.2	41.4
KBaCoX 21	414.7	543.7	0.1786	385.5	29.1
KSrCoX 20	255.9	338.0	0.1102	236.3	19.7

The surface area of the zeolite X increases on cobalt ion exchange. This is due to the decrease in the number of extra framework cations while replacing monovalent sodium ions with divalent cobalt ions. On replacing sodium ions with divalent cations such as cobalt, one Co^{2+} replaces two Na^{+} ions; therefore half the cations are present in the zeolite. The external surface area determined from the t-plot also increases with percentage of cobalt exchange. This can be explained in terms of the structural

deformation occurred during the cation exchange process and/or vacuum dehydration at higher temperatures.

Diffuse reflectance spectroscopy (DRS) detects the d-d transitions of Co^{2+} in the near infrared region and the $O \rightarrow Co^{2+}$ charge transfer transition in the ultraviolet region [36]. Diffuse reflectance spectra of NaCoX having various amount of cobalt ion exchange was given in Figure-5.1.1.

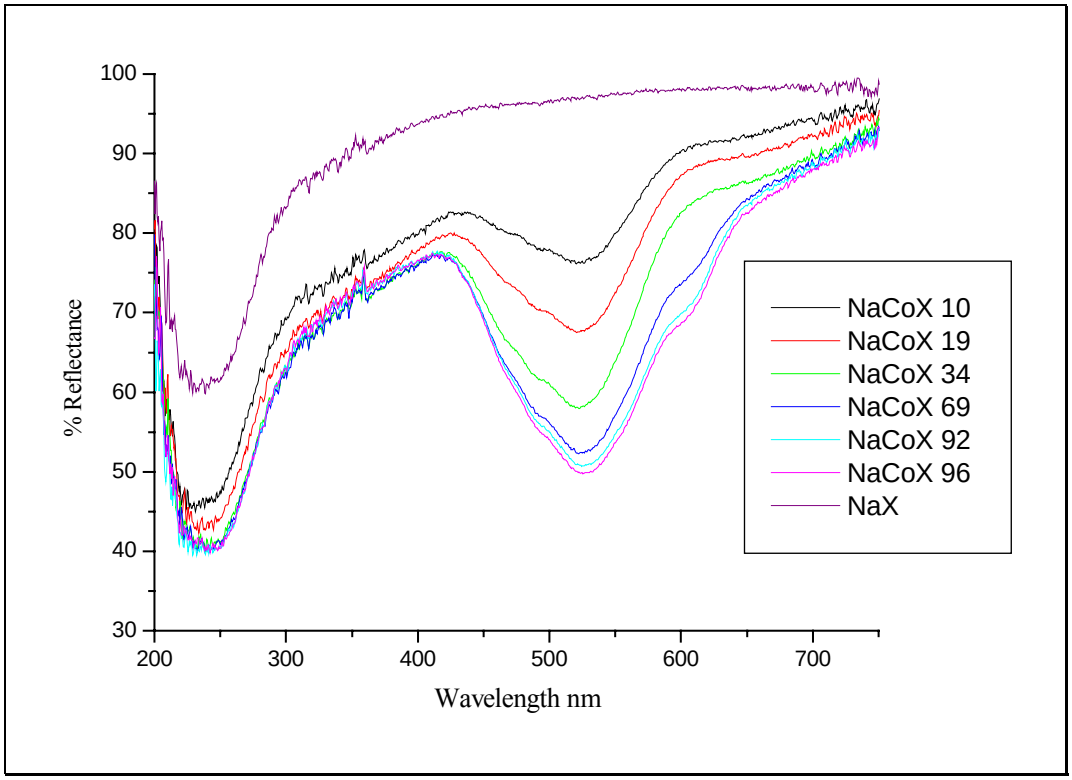

Figure-5.1.1. Diffuse reflectance spectra of various amounts of cobalt ion exchanged zeolite X

In the hydrated pink sample, spectral minima appear around 530nm in the visible region and 240nm in the UV region. These absorptions are assigned to the transitions of the octahedral $[Co(H_2O)_6]^{2+}$ complex located in the super cages of the zeolite X [36]. The intensity of both the peaks at 530nm and 240nm increases correspondingly with the amount of cobalt exchange.

5.1.3.1. Epoxidation of Styrene-to-Styrene Oxide Using Molecular Oxygen

Styrene was converted into styrene oxide at 373K with molecular oxygen in DMF using cobalt-exchanged zeolite X as catalyst. Styrene oxide and benzaldehyde were

formed as the main products. The schematic reaction of the styrene epoxidation reaction is as shown below:

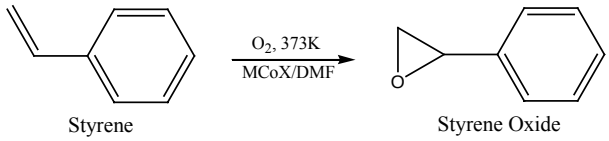

The catalytic activity of various amount of cobalt ion exchanged zeolite X towards the epoxidation reaction of styrene was determined by the reaction between molecular oxygen and styrene at 373K in presence of these catalysts. 0.2g of the catalyst was used in all the reactions independent of the extent of cobalt exchange. Catalysts air-dried at room temperature after the cation exchange processes were used for the epoxidation reactions with out any thermal treatment or activation. The conversion and selectivity obtained for different cobalt exchanged zeolites are shown in Figure-5.1.2.

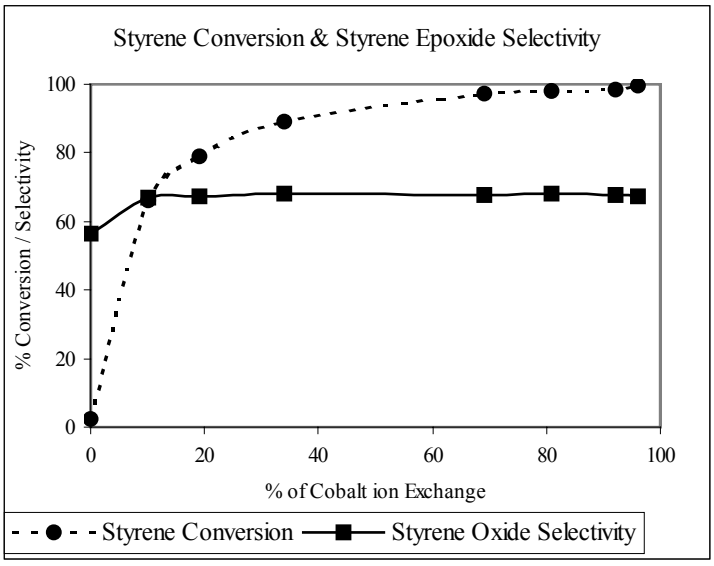

Figure-5.1.2. Styrene Epoxidation reactions as a function of percentage cobalt ion exchange

The styrene conversion increases sharply on exchanging the zeolite X the extra framework cations with cobalt ions and further increases with increase in cobalt percentage. 66% conversion of styrene takes place during the 4hours of reaction time using NaCoX containing 10% cobalt ions. The styrene conversion exceeds 97%, when the cobalt percentage increases to 69%. The styrene oxide selectivity also increases from on cobalt exchange. The styrene oxide selectivity increases from 56%

in NaX to 66% in NaCoX 10, but the selectivity remained almost unaffected with the further increase in the amount of cobalt ions in the zeolite. This increase in the styrene conversion at higher cobalt exchange levels may be due to the occupation of the cobalt ions in the more accessible locations in the zeolite structure. The conversion and selectivity obtained for various amounts of cobalt-exchanged zeolite X for the oxidation of styrene with molecular oxygen are compared in Table-5.1.2.

Table-5.1.2. Performance of NaCoX Catalysts in Styrene Epoxidation

Catalyst	% Conversion of Styrene	%Selectivity of Styrene Oxide	TOF ($hour^{-1}$)
NaX	2.5	56.5	-
NaCoX 10	66.0	66.9	25.3
NaCoX 19	77.9	67.5	15.9
NaCoX 34	87.6	65.1	9.7
NaCoX 69	97.2	67.7	5.6
NaCoX 81	97.9	68.0	4.8
NaCoX 92	98.4	66.4	4.2
NaCoX 96	99.8	66.9	4.1

Styrene = 10mmol; DMF = 20ml; catalyst = 200mg; O_2 = 6-8 ml min^{-1}; duration = 4 hours

The value of turn over factor (TOF) decreases with increase in the amount of cobalt in the zeolite. This decrease in the value of the TOF may be because of the following two reasons; at higher cobalt exchange levels, some of the cobalt ions may go into the cation locations inside the sodalite cavities and makes themselves inaccessible to the oxygen molecules or due to the occupancy of the cobalt ions in the neighbouring sites, which make some of the cobalt sites inactive to the styrene epoxidation reaction.

5.1.3.2. Kinetics of Styrene Oxidation

Kinetics of the styrene conversion and styrene oxide formation was determined by analysing the samples withdrawn at regular intervals from the reaction mixture by GC. The changes in the concentrations of styrene and styrene oxide relative to the concentration of the internal standard, as a function of time is show in Figure-5.1.3.

The styrene conversion and styrene oxide formation increases with time and reaches near the maximum value at 210min. Further increase in reaction time up to 270min doesn't effect the concentrations of both styrene and styrene oxide. On further increase in the reaction time leads to the decrease in the styrene oxide concentration, the styrene oxide formed underwent ring-opening reactions and products like styrene glycol were formed.

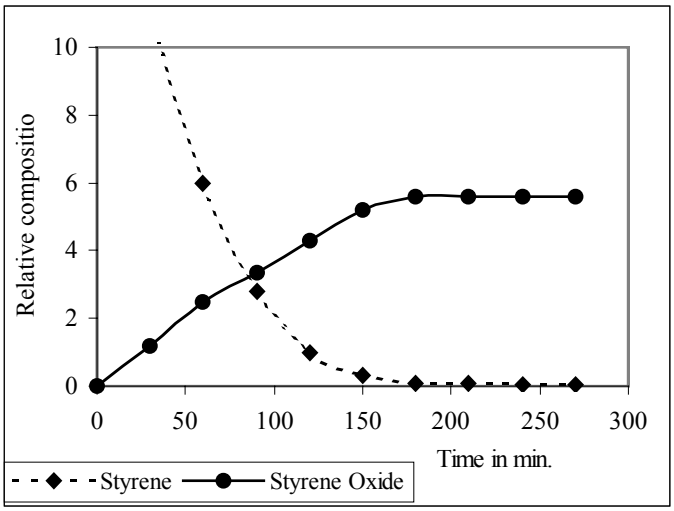

Figure-5.1.3. Kinetics of Styrene Conversion and Styrene Oxide formation Using NaCoX 96

Zeolite X is a synthetic Aluminium rich analogue of the naturally occurring mineral faujasite (Figure-5.1.4). The 14-hedron with 24 vertices known as the sodalite cavity or β-cage may be viewed as its principal building block. These β-cages are connected tetrahedrally at six-rings by bridging oxygen to give double six-rings (D6Rs, hexagonal prisms) and concomitantly, an interconnected set of even larger cavities (supercage) accessible in three dimensions through 12-ring (24-membered) windows. The Si and Al atoms occupy the vertices of these polyhedra. The oxygen atoms lie approximately midway between each pair of Si and Al atoms but are displaced from those points to give near-tetrahedral angles about Si and Al. Single six-rings (S6Rs) are shared by sodalite and supercage, and may be viewed as the entrances to the sodalite units. Each unit cell has eight sodalite units, eight supercage, 16 D6Rs, 16 12-rings, and 32 S6Rs. Exchangeable cations that balance the negative charge of the aluminosilicate framework are found within the zeolite cavities. They are usually found at the six different sites: site I at the centre of the D6R, I′ in the sodalite cavity

on the opposite side of one of the D6Rs six-rings from site I, II′ inside the sodalite cavity near a S6R, II at the centre of the S6R or displaced from this point into a supercage, III in the supercage on a twofold axis opposite a four-ring between two 12-rings, and III′ somewhat or substantially off III (off the twofold axis) on the inner surface of the supercage.

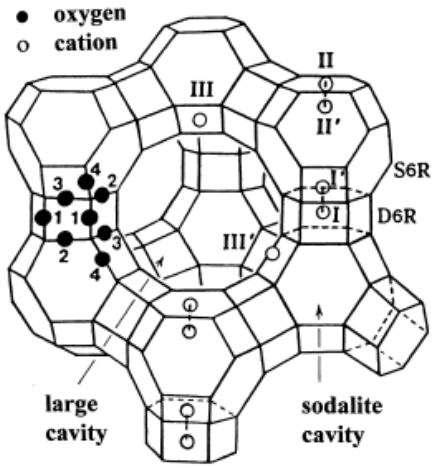

Figure-5.1.4. The framework structure of zeolite X, near the centre of the each line segment is an oxygen atom. The numbers 1–4 indicates the different oxygen atoms. Silicon and aluminium atoms alternate at the tetrahedral intersections, except that Si substitutes f or Al at about 4% of the Al positions. Extra framework cation positions are labelled with Roman numerals

The crystal structures various amounts of cobalt-exchanged zeolite X are reported in the literature [4]. Co^{2+} ions prefer site II and Co^{2+} ions occupy sites I′, II and III′. The cations sitting in the site I′ are inaccessible to the oxygen molecules. The cation sitting in site II can interact with the oxygen molecules through the six member ring windows and the cations in site III′ can interact directly with oxygen. The distance between Co^{2+} ions in site III′ and the framework oxygen atoms are long (Co-O distance 2.30Å and 2.27Å) and these Co^{2+} ions are responsible in the activation of the oxygen molecules for the styrene epoxidation reaction.

5.1.3.3. Catalytic Oxidation with Air

The catalytic oxidation was carried out using air as the source for the molecular oxygen. Instead of oxygen, air was bubbled into the reaction at the rate of 10cc min^{-1}. Atmospheric air was bubbled into the reaction system with out any purification or

drying by using an air pump. The values of styrene conversion, styrene oxide selectivity and TOF were similar to that of the reactions carried out using chemically pure (99.9%) oxygen as the oxidant. The conversion, selectivity and TOF values obtained are given in Table-5.1.3.

Table-5.1.3. Performance of NaCoX Catalyst in Styrene Epoxidation Using Air

Catalyst	% Conversion of Styrene	%Selectivity of Styrene Oxide	TOF ($hour^{-1}$)
NaCoX 92	99.2	66.4	4.2
NaCoX 96	99.4	65.5	4.0

Styrene = 10mmol; DMF = 20ml; catalyst = 200mg; Air ≅10ml min^{-1}; duration = 4hours

5.1.3.4. Effect of Water on the Catalytic Properties of Cobalt Exchanged Zeolite X

The effect of water in the reaction medium was explored by carrying out four reactions, in which the reaction system contain different amount of water molecules. In the first reaction the solvent was dried and catalyst was also dehydrated at 353K under vacuum (10^{-3}Torr) for 24 hours. The styrene conversion was only 41.8% with a styrene oxide selectivity of 67.8%. In the second reaction the solvent was used with out drying and catalyst was dehydrated at 353K under vacuum (10^{-3}Torr) for 24 hours. The styrene conversion increased to 64.5% with styrene oxide selectivity of 66.9%. The third reaction was carried out using the catalyst and solvent in the original condition with out any activation or drying. The styrene conversion increased to 98.4% with styrene oxide selectivity of 66.4%. In the fourth reaction, 1.0ml water was added to the reaction system and the styrene conversion further increased to 99.9% with styrene oxide selectivity of 65.3%. The turn over factor also increases form 1.8 to 4.2 on increasing the amount of water in the reaction system. In all reactions the same catalyst, NaCoX 92 was used for the catalytic studies. It was found that the presence of water in the catalyst/reaction medium has very strong influence on the styrene conversion. The catalytic activities of NaCoX 92 with various amount of

water in the reaction system are studied. The styrene conversion, styrene oxide selectivity and turn over frequency of these reactions are given in Table-5.1.4.

Table-5.1.4. Effect of Water on the Catalytic Activity

Reaction system	% Conversion of Styrene	%Selectivity of Styrene Oxide	TOF ($hour^{-1}$)
DMF (dried) and catalyst dried at 353K / vacuum (10^{-3}Torr)	41.8	67.8	1.8
DMF without drying and catalyst dried at 353K / vacuum (10^{-3}Torr)	64.9	66.9	2.8
DMF and catalyst both without drying	98.4	66.4	4.2
DMF, catalyst (both without drying) and 1.0 ml H_2O	99.9	65.3	4.2

Styrene = 10mmol; DMF = 20ml; Catalyst = NaCoX 92; amount = 200mg;

$O_2 \cong$ 6-8ml min^{-1}; duration = 4hours

5.1.3.4. Effect of Alkali Metal Cationic Promoters on Catalytic Epoxidation of Styrene with Molecular Oxygen Using Cobalt Exchanged Zeolite X

The effects of alkali metal cationic promoters on the catalytic epoxidation of styrene-to-styrene oxide with molecular oxygen using cobalt-exchanged zeolites were studied. The sodium ions of the zeolite were exchanged with alkali metals cations such as K^+, Rb^+ and Cs^+. In these alkali metal ion exchanged zeolites, around 20% of the extra framework cations were replaced with cobalt ions by ion exchange from aqueous solution. The catalytic properties of Na^+, K^+, Rb^+ and Cs^+ containing CoX was determined by the same reaction conditions and the comparison of the catalytic properties of these alkali metal promoted CoX samples are given in Table-5.1.5. The catalytic epoxidation of styrene-to-styrene oxide with molecular oxygen using cobalt-exchanged zeolite X having alkali metal promoters shows increased selectivity of styrene oxide with decrease in the position in the periodic table. Styrene conversion increases from 77.9% in NaCoX to 98.5+% in KCoX, RbCoX and CsCoX. The styrene oxide selectivity also increases form 67.5% in NaCoX to 71.3, 71.8 and 76.6% in KCoX, RbCoX and CsCoX respectively. The turn over factor also increases on replacing the co-cations other alkali metal cations such as potassium, rubidium and

cesium. TOF increases from 15.9 to 22.7, 24.0 and 26.4 on replacing the sodium ions of CoX with potassium, rubidium and cesium respectively.

Table-5.1.5. Styrene Epoxidation using CoX having various alkali metal promoters

Catalyst	% Conversion of Styrene	%Selectivity of Styrene Oxide	TOF ($hour^{-1}$)
NaCoX 19	77.9	67.5	15.9
KCoX 19	98.7	71.3	22.7
RbCoX 21	98.6	71.8	24.0
CsCoX 20	99.8	76.6	26.4

Styrene = 10mmol; DMF = 20ml; catalyst = 200mg; O_2 = 6-8ml min^{-1}; duration = 4hours

5.1.3.5. Effect of Alkaline Earth Metal Cationic Promoters on Catalytic Epoxidation of Styrene with Molecular Oxygen Using Cobalt Exchanged Zeolite X

The effects of alkaline earth metal co-cations on the catalytic epoxidation of styrene-to-styrene oxide with molecular oxygen using cobalt-exchanged zeolites were studied. The sodium ions of the zeolite were exchanged with alkaline earth metals cations such as Mg^{2+}, Ca^{2+}, Sr^{2+} and Ba^{2+}. In these alkaline earth metal ion exchanged zeolites, around 20% of the extra framework cations were replaced with cobalt ions by ion exchange from aqueous solution. The catalytic activities of Mg^{2+}, Ca^{2+}, Sr^{2+} and Ba^{2+} containing CoX were measured by the same reaction conditions. The catalytic epoxidation of styrene-to-styrene oxide with molecular oxygen using cobalt-exchanged zeolite X having alkaline earth metal promoters shows increase in styrene conversion and styrene oxide selectivity. Styrene conversion is 99+% for all the catalysts. The styrene oxide selectivity also increases form 67.5% in NaCoX to 74.6, 82.9, 85.1 and 82.6% respectively in MgCoX, CaCoX, SrCoX and BaCoX. The comparison of the catalytic properties of the alkaline earth metal ion promoted CoX samples are given in Table-5.1.6. TOF increases from 15.9 to 21.1, 24.9, 27.4, and 32.5 on replacing the sodium ions of CoX with magnesium, calcium, strontium and barium respectively. The increases in the TOF for CoX having alkaline earth metal

promoters are higher than that having alkali metal cationic promoters. The styrene oxide selectivity increases with increase in the atomic number of the promoter.

Table-5.1.6. Styrene Epoxidation using CoX having alkaline earth metal promoters

Catalyst	% Conversion of Styrene	%Selectivity of Styrene Oxide	TOF ($hour^{-1}$)
NaCoX 19	77.9	67.5	15.9
MgCoX 22	99.5	74.6	21.1
CaCoX 19	99.8	82.9	24.9
SrCoX 18	99.9	85.1	27.4
BaCoX 15	99.9	82.6	32.5

Styrene = 10mmol; DMF = 20ml; catalyst = 200mg; O_2 = 6-8ml min^{-1}; duration = 4hours

The conversion, selectivity and TOF shows that the cobalt-exchanged zeolite X having alkali and alkaline earth metal ions shows that these catalysts are potential in the catalytic epoxidation of styrene-to-styrene oxide using molecular oxygen. It was confirmed in this study that alkaline earth metal cations are more effective promoters than alkali metal cations, when loaded into zeolite X with cobalt ions. This observation is contrary to the ranking of zeolite basicity. Similar effects of alkali and alkaline earth metal cationic promoters were observed for the kinetics of ammonia synthesis catalysed by ruthenium supported on zeolite X [37].

However, the mechanism of cobalt promotion by these alkaline earth metals ions is also an open question at this time. The following are the probable ways by which the cationic promoters enhance the catalytic epoxidation reaction of styrene to styrene oxide using molecular oxygen: these alkali and alkaline earth metal promoters might help (i) to disperse the cobalt ions well inside the zeolite pores to act as an efficient catalyst, (ii) increase the adsorption of oxygen in the zeolites, (iii) enhance the rate of styrene oxide formation by lowering the barrier for dioxygen dissociation in the rate-determining step (iv) stabilise the reaction intermediate formed during the reaction or (v) to act as a bifunctional catalyst for the styrene epoxidation reaction.

5.1.3.6. Effect of Alkali -Alkaline Earth Metal Mixed Cationic Promoters on Catalytic Epoxidation of Styrene with Molecular Oxygen Using Cobalt Exchanged Zeolite X

The effects of mixture of alkali-alkaline earth metal co-cations on the catalytic epoxidation of styrene-to-styrene oxide with molecular oxygen using cobalt-exchanged zeolites were studied. The sodium ions of the zeolite were exchanged with a mixture of alkali-alkaline earth metals cations such as K^+, Cs^+, Sr^{2+} and Ba^{2+}. Around 20% of the extra framework cations of these zeolites were replaced with cobalt ions by ion exchange from aqueous solution. The three alkali-alkaline earth metal cationic combinations studied are CsBaCoX, KBaCoX and KSrCoX. The styrene conversion and styrene oxide selectivity are very high compared to the corresponding NaCoX. The styrene conversion was 99+% and styrene oxide selectivity was 80+% in all the cases. The catalytic activities of the three catalysts are compared in Table-5.1.7. TOF is also high in these CoX containing mixed cationic promoters.

Table-5.1.7. Styrene Epoxidation using CoX having alkali and alkaline earth metal promoters

Catalyst	% Conversion of Styrene	%Selectivity of Styrene Oxide	TOF ($hour^{-1}$)
NaCoX 19	77.9	67.5	15.9
CsBaCoX 20	99.4	80.4	27.8
KBaCoX 21	99.8	83.1	26.9
KSrCoX 20	99.6	81.0	26.5

Styrene = 10mmol; DMF = 20ml; catalyst = 200mg; O_2 = 6-8 $mlmin^{-1}$; duration = 4hours

5.1.3.7. Reactions Using Spend Catalysts

The catalytic activity of the catalysts remained unaffected after several reaction cycles. Catalysts were recovered from the reaction mixture by centrifuging and the recovered catalyst was washed with DMF and then with distilled water to remove all the organic phases adsorbed on the catalyst. The conversion and selectivity obtained

at second and third cycle are given in Table-5.1.8. The number in roman letters denotes the reaction cycle number using the same catalyst.

Table-5.1.8. Performance of Spend MCoX Catalysts in Styrene Epoxidation

Catalyst	% Conversion of Styrene	%Selectivity of Styrene Oxide	TOF ($hour^{-1}$)
NaCoX 92 I	98.4	66.4	4.2
NaCoX 92 II	99.3	67.2	4.3
NaCoX 92 III	99.2	66.9	4.2
NaCoX 96 I	99.8	66.9	4.1
NaCoX 96 II	99.6	66.1	4.0
NaCoX 96 III	99.5	65.5	4.0
KCoX 19 I	98.7	71.3	22.7
KCoX 19 II	99.1	72.1	23.0
CsCoX 20 I	99.8	76.6	26.4
CsCoX 20 II	99.8	76.6	26.4
SrCoX 18 I	99.9	85.1	27.4
SrCoX 18 II	99.9	85.3	27.5
BaCoX 15 I	99.9	82.6	32.5
BaCoX 15 II	99.9	82.6	32.5

Styrene = 10mmol; DMF = 20ml; catalyst = 200mg; O_2 = 6-8 ml min^{-1}; duration = 4 hours

The analysis of the liquid phase separated from the reaction mixture does not show the presence of cobalt cations in solution, indicating the absence of any leaching of the cobalt metal ions during the catalytic reaction. The possibility of the decrease in the catalytic activity is minimum in the present catalytic system, because the reaction is carrying out only at 373K and activation/thermal treatment is also not required for the catalyst before the catalytic reaction.

5.1.4. REFERENCES

[83] R. M. Barrer, Zeolites and Clay Minerals as Sorbents and Molecular Sieves, Academic Press, London, 1978.

[84] D. W. Breck, Zeolite Molecular Sieves, Wiley-Inter Science, New York, 1974.

[85] E. Y. Choi, Y. Kim, Y. W. Han and K. Seff, Microporous and Mesoporous Materials, 2000, **41**, 61-68.

[86] D. Base and K. Seff, Microporous and Mesoporous Materials, 1999, **33**, 265-280.

[87] R. V. Grieken, J. L. Sotelo, C. Martos, J. L. G. Fierro, M. L. Granados and R. Mariscal, Catalysis Today, 2000, **61**, 49–54.

[88] Q. Yang, S. Wang, J. Lu, G. Xiong, Z. Feng, Q. Xin and C. Li, Applied Catalysis A: General, 2000, **194 –195**, 507–514.

[89] Q. Yang, C. Li, J. L. Wang, P. Ying, X. Xin and W. Shi, Stud. Surf. Sci. Catal., 2000, **130**, 221.

[90] S. B. Kumar, S. P. Mirajkar, G. C. G. Pais, P. Kumar and R. Kumar, Journal of Catalysis, 1995, **156**, 163-166.

[91] S. C. Laha and R. Kumar, Journal of Catalysis, 2001, **204**, 64–70.

[92] W. Zhang, M. Froba, J. Wang, P. Tanev, J. Wong and T. J. Pinnavaia, J. Am. Chem. Soc., 1996, **118**, 9164.

[93] Z. Fu, D. Yin, D. Yin, Q. Li, L. Zhang and Y. Zhang, Microporous and Mesoporous Materials, 1999, **29**, 351–359.

[94] V. R. Choudhary, N. S. Patil and S. K. Bhargava, Catalysis Letters, 2003, **89**, 55.

[95] N. S. Patil, R. Jha, B. S. Uphade, S. K. Bhargava and V. R. Choudhary, Applied Catalysis A: General, 2004, **275**, 87–93.

[96] N. S. Patil, B. S. Uphade, P. Jana, S. K. Bharagava, and V. R. Choudhary, Journal of Catalysis, 2004, **223**, 236–239.

[97] C. V. Rode, U. N. Nehete and M. K. Dongare, Catalysis Communications, 2003, **4**, 365–369.

[98] R. A. Sheldon and J. K. Kochi, Metal-Catalysed Oxidation of Organic Compounds, Academic, New York, 1981.

[99] J. D. Koola and J. K. Kochi, J. Org. Chem., 1987, **52**, 4545.

[100] A. Zombeck, D. E. Hamilton and R. S. Drago, J. Am. Chem. Soc., 1982, **104**, 6782.

[101] D. E. Hamilton, R. S. Drago and A. Zombeck, J. Am. Chem. Soc., 1987, **109**, 374.

[102] B. Rhodes, S. Rowling, P. Tidswell, S. Woodward and S. M. Brown, J. Molecular Catalysis A: Chemical, 1997, **116**, 375.

[103] M. J. da Silva, P. Robles-Dutenhefner, L. Menini and E. V. Gusevskaya, J. Molecular Catalysis A: Chemical, 2003, **201**, 71.

[104] G. Sankar, R. Raja and J. M. Thomas, Catalysis Letters, 1998, **55**, 15.

[105] J. M. Thomas, R. Raja, G. Sankar and R. G. Bell, Nature, 1999, **398**, 227.

[106] I. Belkhir, A. Germain, F. Fajula and E. Fache, J. Chem. Soc., Faraday Trans., 1998, **94**, 1761.

[107] A. F. Masters, J. K. Beattie and A. L. Roa, Catal. Lett, 2001, **75**, 159.

[108] J. M. Thomas and R. Raja, Chem. Commun., 2001, 675.

[109] J. M. Thomas, Angew. Chem., Int. Ed., 1999, **38**, 3588.

[110] D. Dhar, Y. Koltypin, A. Gedanken and S. Chandrasekaran, Catalysis Letters, 2003, **86**, 197.

[111] C.L. Hill and C.M. Prosser-McCartha, Coord. Chem. Rev., 1995, **143**, 407.

[112] R. I. Kureshy, N. H. Khan, S. H. R. Abdi, A. K. Bhatt and P. Iyer, J. Molecular Catalysis A: Chemical, 1997, **121**, 25.

[113] R. Raja, G. Sankar and J.M. Thomas, Chem. Commun., 1999, 829.

[114] R. Neumann and M. Dahan, Nature, 1997, **388**, 353.

[115] Y. Nishiyama, Y. Nakagawa and N. Mizuno, Angew. Chem. Int. Ed., 2001, **40**, 3639

[116] Q. Tang, Y. Wang, J. Liang, P. Wang, Q. Zhang and H. Wan, Chem. Commun., 2004, 440-441.

[117] J. Liang, Q. Zhang, H. Wu, G. Meng, Q. Tang and Y. Wang, Catalysis Communications, 2004, **5**, 665–669.

[118] A. A. Verberckmoes, B. M. Weckhuysen and R. A. Schoonheydt, Microporous and Mesoporous Materials, 1998, **22**, 165-178.

[119] T. Becue, R. J. Davis and J. M. Garces, J. Catalysis, 1998, **179**, 129-137.

Chapter-5

Catalysis and Photocatalysis Using Transition Metal Ion Exchanged Zeolites

Part-2

Photochemical Oxidation of Bromide to Bromine in Aqueous Dispersion of Silver Exchanged Zeolites

5.2.1. INTRODUCTION

Zeolites are crystalline aluminosilicates with anionic frameworks having well defined channels and cages of strictly regular dimensions [1-2]. These empty intracrystalline spaces are in the nanometer or subnanometer length scale and are termed micropores. Zeolite microcrystals are investigated as hosts for supramolecular organisation of clusters, complexes and molecules. They offer possibilities to design precise and reversible functionalities, which have the potential to become useful in a solar energy conversion system because in favourable cases very stable materials have been obtained [3-4]. The possibility to arrange zeolite microcrystals of good quality and narrow size distribution as dense monograin layers on different types of substrates allows the discovery of specific properties. The photoactive guests can be an organic photo sensitiser, an inorganic semiconductor or a combination of both. The combination of a zeolite host and photoactive sites renders solid photocatalysts in which the high surface area and the adsorbent capacity provided by zeolites co-operate to increase the efficiency of the photocatalytic process. In addition, the zeolite pores define a compartmentalised space in which multi-component systems can be easily assembled by a stepwise procedure. Other positive effects derived from the encapsulation of a guest inside zeolites are a higher photo stability of the sensitiser, the observation of quantum size effects for semiconductor clusters and a favourable polar environment for photoinduced electron transfer. Zeolite based photocatalysts are promising for the abatement of air and water pollution using solar light, as well as for de-NOx and de-SOx processes, photo reduction of CO_2 by H_2O, photo oxygenation of saturated hydrocarbons, photo splitting of water into hydrogen and oxygen, photogeneration of hydrogen peroxide and other photo-processes of much current interest, particularly in environmental sciences and for the development of renewable energy resources alternative to fossil fuels [5].

The use of transition metal ion-exchanged zeolites is promising for the development of photocatalysts that decompose environmental pollutants. Some of these zeolites such as CuZSM-5 are also useful as non-photochemical catalysts for car exhaust gas treatment and other thermal de-NOx, de-SOx processes. Thus, not surprisingly Cu- and Ag-ion exchanged zeolites have been also studied as photocatalysts [5]. Using a combination of XAFS, photoluminescence and diffuse reflectance optical measurements the coordination and aggregation state of these ions have been

addressed [6]. These noble metal ions have been proposed to be monomers, dimers and clusters, their relative concentration strongly dependent on the zeolite host. Within ZSM-5, mordenite and Beta, these ions exist predominantly as isolated species with low coordination number [6] and they can act as photocatalysts for the decomposition of NOx [7]. Simple ion exchange of ZSM-5 with Cu^{2+} followed by evacuation at temperatures higher than 100°C is sufficient to transform Cu(II)ZSM-5 into Cu(I)ZSM-5, according to EPR spectroscopy [8-9]. Interestingly, while Cu(II)ZSM-5 does not emit, Cu(I)ZSM-5 exhibits an emission between 420–550nm. Cu(I)ZSM-5 photocatalytically decomposes NO into N_2 and O_2 at temperatures as low as 2°C. [8-9]. Ag-containing zeolites have been tested for the removal of NO_x from air [10-12]. Ag(I)-ZSM-5 has been prepared and characterised spectroscopically in relation to its efficient photocatalytic activity for the decomposition of NO to N_2 and O_2. By combining measurements of photoluminescence and EXAFS with theoretical models the occurrence of several local environments for Ag^+ ions and even the presence of $(Ag^+)_n$ sites has been proposed. Calculations indicate that for NO coordinated to silver clusters, the N–O bond is stronger in the ground state, while for certain excited states the N–N and O–O bonds are stronger [13]. Ag (I) ions exchanged within a zeolite tend to get reduced either spontaneously or chemically forming clusters of silver metal encapsulated within the zeolite internal micropores. Calzaferri and co-workers have made significant contributions in the use of AgA zeolite as a photocatalyst. Depending on the aggregation state of these clusters and their size, the colour of the zeolite varies from white, yellow to red [14]. These zeolite-encapsulated silver clusters exhibit intense photoluminescence, with variable λ_{em} depending on the nuclearity of the silver clusters. Moreover, it has been found that intrazeolite energy transfer from monomer Ag sites (higher excited state energy) to oligomeric clusters (lower energy) is very efficient.

In an early report, Jacobs and co-workers studied the efficiency of zeolite-encapsulated Ag clusters for the photocatalytic splitting of water [15]. Similarly, Calzaferri reported that when silver zeolite A is illuminated in the presence of water, molecular oxygen is evolved and Ag^+ reduces to Ag^0 [14]. In the photochemical splitting of water, oxygen generation is always much more difficult than the photogeneration of H_2 since the process for oxygen formation requires four electrons and the mechanism goes through the intermediary of a series of activated oxygen

intermediates. The quantum yield of AgA for oxygen formation is high, reaching the maximum at neutral pH. An investigation of the spectral response shows an interesting effect known as self-sensitisation [14]. This term refers to the fact that while the initial photoresponse is only for UV wavelengths; the response extends gradually to the red reaching 600 nm as the reaction proceeds. The reason for this is that during the photochemical reaction, partially reduced Ag clusters are formed and these new chromophores shift the absorption band towards the red. The zeolite structure acts in controlling the size of the clusters and, as a consequence of the operation of a quantum size regime, also controls the energy levels of the orbitals of the Ag clusters [14]. The major problem to solve to convert oxygen evolution in a truly photocatalytic process is the reoxidation of reduced Ag back to the original Ag(I) state. It has also been reported that silver clusters entrapped on zeolite A can effect the photocatalytic decomposition of carbaryl, carbofuran and malathion with an efficiency that is 164, 120, and 35 times faster than the corresponding direct irradiation of the pesticides in the absence of any photocatalyst [16]. The efficiency of the photocatalytic degradation depends on the size of the Ag clusters, yellow and red AgA solids being less efficient [16].

Recent studies shows that the aqueous dispersions of very pure Ag^+ exchanged zeolites were not photoactive, but that zeolites containing silver chloride were strongly photoactive provided that an excess of Ag^+ was present. In fact the zeolite was found not to be necessary for the photochemical oxygen evolution from silver chloride. The reduced silver species are reoxidised which makes the system catalytic [17, 18]. The self-sensitisation of the photochemical activity of AgCl is due to silver clusters adsorbed on its surface. A comparison of the energetic positions of the AgCl band gap [19] and the silver clusters shows that the silver clusters have empty energy levels below the conduction band of AgCl [20]. In the absence of silver clusters, AgCl does not absorb light below the indirect band gap transition, which is in the near UV at 3.3eV (380nm). Their presence enables a new electronic transition from the AgCl valence band to empty silver cluster energy levels. The energy for this transition is lower than the energy needed for an optical transition from the AgCl valence band to the AgCl conduction band. Nevertheless, this new optical transition in the visible spectral range still initiates the oxidation of water, because the conduction band is not directly involved in water oxidation [21]. Thus, the photocatalytic oxidation on AgCl

is extended from the near UV into the visible range of the spectrum. AgCl layers on SnO_2 coated glass plates [22], AgCl photo-anodes sensitized with AgBr [23] and gold colloid modified AgCl [24] are used for more effective photocatalytic splitting of water.

The objective of the present work was to explore the redox property of the silver exchanged zeolites for the photochemical oxidation of bromide to bromine using sunlight and to develop excellent catalysts for the production of bromine from seawater and solar light conversion. The self-sensitisation of the reaction due to formation of silver clusters is also investigated in the present study.

5.2.2. EXPERIMENTAL

5.2.2.1. Materials

Zeolites A and X from Zeolites and Allied Products, Bombay, India, Zeolite Y (SiO_2/Al_2O_3 = 5.5) from Süd-Chemie AG, Germany, Zeolite L, ZSM-5, Mordenite and BEA from Zeocat, Uetikon, Switzerland, silver nitrate (99.9%), potassium bromide and sodium bromide from Ranbaxy Fine Chemicals Ltd., New Delhi, India were used as the starting materials for the photochemical studies.

5.2.2.2. Silver ion Exchange

Silver cations were introduced into the highly crystalline sodium form of zeolite by the conventional cation exchange from aqueous $AgNO_3$ solution. Typically, the zeolite was refluxed with aqueous $AgNO_3$ solutions, containing 1.5 times excess of Ag^+ ions over the quantity of base Na^+, in the solid / liquid ratio 1:80 at 353K. The residue was filtered, washed with hot distilled water, until the washings were free from Ag^+ ions as tested with sodium chloride solution and dried at 353K. All the activities were carried out in absence of direct contact with light. The extent of silver exchange in zeolites was determined by using Shimadzu AA-680 atomic absorption spectrometer.

5.2.2.3. X-ray Powder Diffraction

X-ray powder diffraction studies at ambient temperature were carried out using Philips X'pert MPD system in the 2θ ranges of 5-65 degrees using CuKα1 (λ = 1.54056Å). The diffraction patterns of the starting materials show that these are highly crystalline samples showing the reflections in the range 5 to 35 degrees

typically observed for zeolites. The structures of the zeolites were retained after the cation exchange as no loss of crystallinity was observed during silver exchange.

5.2.2.4. SEM and EDX

SEM and EDX measurements were carried out using Leo 1430 VP variable pressure scanning electron microscope equipped with Oxford INCA EDX facility.

5.2.2.5. Surface Area and Pore Size Distribution

The nitrogen adsorption at 77.35K was measured using Micromeritics ASAP 2010 after activating the sample at 673K under vacuum. Surface area and pore size distribution of the various silver exchanged zeolites were determined from the N_2 adsorption data at 77.35K.

5.2.2.6. Photochemical studies

Photochemical oxidation of bromide to bromine is studied in presence of silver exchanged zeolites. A known amount of aqueous bromide solution was acidified with dilute HCl to pH below 4. The solution was mixed with a known amount of silver exchanged zeolite and the mixture was irradiated with a light source for 4-6 hours. The light sources used were 100W tungsten lamp, 125W medium pressure mercury vapour lamp and sunlight, separately or in combination. The concentration of bromide was varied from 0.05 to 5M and the amount of silver zeolite varied from 0.1g to 5.0g in the reaction mixture. The bromine formed during the photochemical reaction was collected by distillation and amount was determined by idiometric titration using starch indicator.

5.2.3. RESULTS AND DISCUSSION

5.2.3.1. X-ray powder diffraction

X-ray powder diffraction pattern of the various silver exchanged zeolites were compared with that of the parent sodium form. No loss of crystallinity was observed during the silver ion exchange. The X-ray diffraction pattern of various silver exchanged zeolites and the parent sodium forms are given in Annexure I.

5.2.3.2. Surface Area and Pore size Distribution

The surface area and pore size distributions of the various silver exchanged zeolites were determined from the N_2 gas adsorption data at 77.35K. The values for the BET

surface area, Langmuir surface area were calculated by applying BET and Langmuir equations respectively in the adsorption data and micropore area, external surface area and micropore volume were calculated by applying t-plot. The values for the BET surface area, Langmuir surface area, micropore area, external surface area and micropore volume are given in Table-5.2.1. The nitrogen adsorption data at 77.35K shows the retention of the porous nature of the zeolite structure during the silver ion exchange process. The surface area and pore volume of the zeolite samples marginally changes on silver ion exchange. This may be due to replacement of smaller sodium ions (0.97Å) with bigger silver ions (1.26Å) and the difference in the cation locations of sodium and silver ions in the zeolites. Silver ions are occupying crystallographically different sites, which will also affect the effective surface area and pore volume measured by nitrogen adsorption.

Table-5.2.1. Surface Area and Pore Volume

Catalyst	**BET Surface Area m^2g^{-1}**	Langmuir Surface Area m^2g^{-1}	t-plot		
			Micropore Volume cm^3g^{-1}	Micropore Area m^2g^{-1}	External Surface Area m^2g^{-1}
AgA	16.0	22.0	0.0102	14.0	2.0
AgX	593.1	851.1	0.2412	544.2	48.9
AgY 5.5	510.4	673.1	0.2255	483.4	27.0
Agβ	576.7	771.5	0.1909	409.6	167.1
Ag L	311.6	412.4	0.1353	289.3	22.4
Ag MOR	348.2	461.7	0.1517	287.9	60.3
Ag ZSM-5	355.2	473.8	0.1063	229.5	125.7

5.2.3.3. SEM and EDX

The scanning electron microscopic images of various silver exchanged zeolites are given in Figure-5.2.1. The images show no changes in the surface morphology of the zeolites during the silver ion exchange. The EDX analysis data shows the absence of sodium and confirms its complete replacement during the ion exchange process. The atomic concentration of oxygen, silicon, aluminium and silver obtained from the EDX analysis is given in Table-5.2.2.

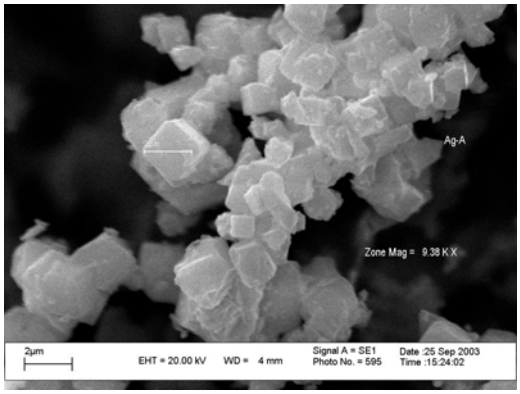

AgA

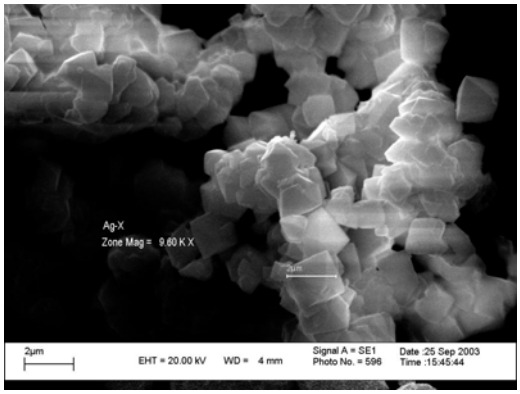

AgX

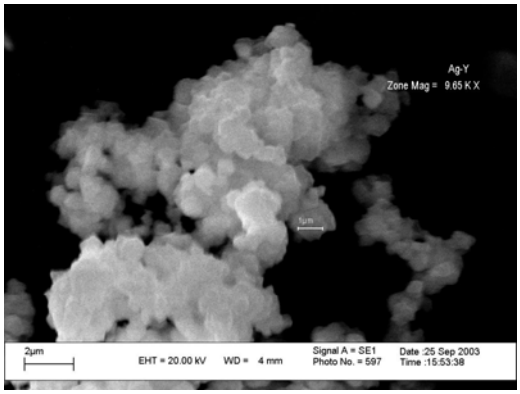

Ag Y

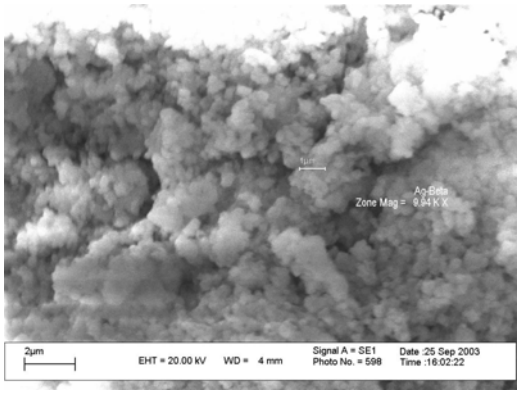

Agβ

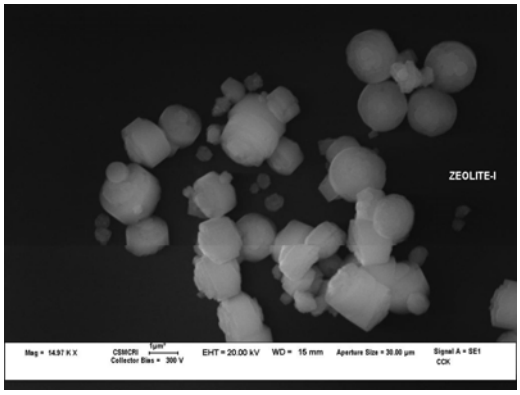

Zeolite L

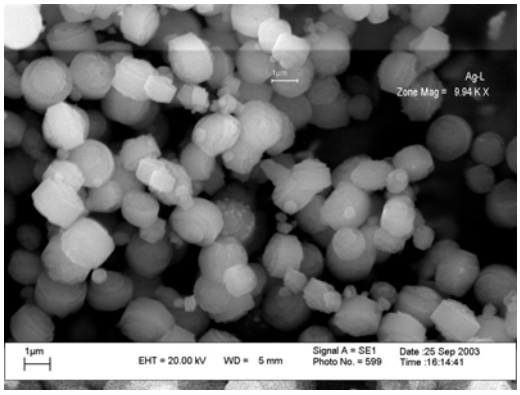

AgL

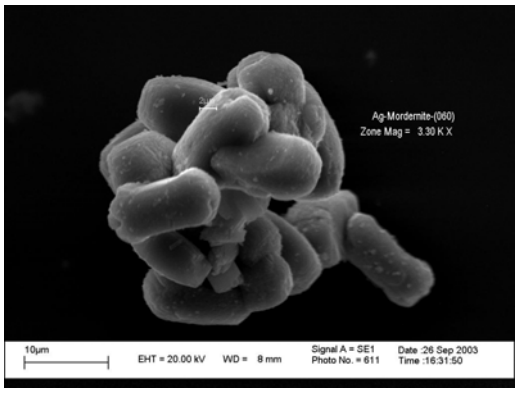

Ag Mordenite

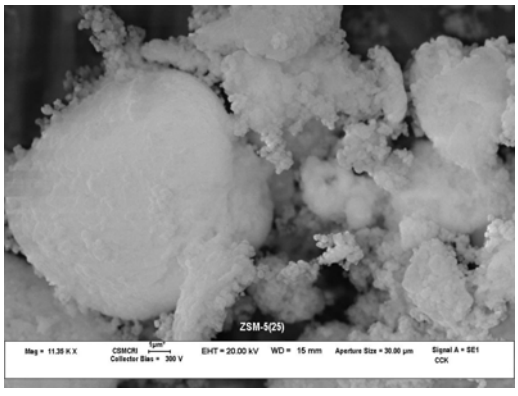

Ag ZSM-5

Figure-5.2.1. SEM Images of Various Silver Exchanged Zeolites

Table-5.2.2. Atomic percentage from EDX analysis

Zeolite	Atomic Percentage			
	Oxygen	Silicon	Aluminium	Silver
AgA	67.7	9.8	6.4	16.1
AgX	66.6	12.1	5.9	14.8
AgY 5.5	73.6	15.5	3.9	7.0
Agβ	72.3	25.1	1.5	1.2
Ag L	77.6	17.8	3.8	0.85
Ag MOR	63.5	25.0	2.4	8.6
Ag ZSM-5	73.7	16.0	1.0	8.1

5.2.3.4. Photo Chemical Oxidation of Br^-

The photochemical oxidations of bromide to bromine in aqueous dispersion of silver exchanged zeolites were studied in the presence of sunlight. At pH below 4 bromide ions in an aqueous medium converts into bromine in the presence of silver exchanged zeolite and sunlight. The typical reaction is represented as follows;

$$Br^- \xrightarrow{AgZ+h\nu} \tfrac{1}{2}Br_2 \uparrow$$

The photochemical oxidation reaction of bromide to bromine in the presence of various types of silver exchanged zeolites is studied in sunlight. Silver exchanged zeolites of type A, X, Y, beta, L, mordenite and ZSM-5 were used for the photochemical oxidation studies. The intensity of the sunlight during the reaction period was determined using a LUX meter. The photochemical activities of various silver exchanged zeolites are summarised in Table-5.2.3. All the silver exchanged zeolites, independent of the structural type, amount, number of cations, cation locations and bromide solution concentration, shows similar results for the photo oxidation of bromide to bromine in the presence of sunlight. The liberation of bromine was observed only from acidic solution at a pH below 4. The results in Table-5.2.3 show that only a very small amount the bromide ions were converted to bromine. The pH of the solution remained unaffected (i.e., pH < 4.0) during the reaction. The reaction does not complete after five hours, the reaction becomes very slow and continues for several days before the catalyst becomes deactivated to the photochemical oxidation reaction. The deactivated catalyst was reactivated by

reoxidising the reduced silver metal particles to silver ions by heating at 673K in O_2 / airflow for 4 hours.

Table-5.2.3. Photochemical Oxidation Data

Exp. No.	Catalyst	Conc. of acidic KBr soln.	Light Source	Duration in Hrs.	Light intensity LUX	Amount of Br_2 librated in mg
1	0.5g AgA	0.1M	Sunlight	5.0	54900 - 95600	5.11
2	0.5g AgX	0.1M	Sunlight	5.0	53400 - 94300	5.83
3	0.5g AgY	0.1M	Sunlight	5.0	57300 - 96100	5.41
4	0.5g Agβ	0.1M	Sunlight	5.0	89700 - 94900	3.92
5	0.5g AgL	0.1M	Sunlight	5.0	37900 - 75400	4.08
6	0.5g Ag MOR	0.1M	Sunlight	5.0	37900 - 72100	5.35
7	0.5g Ag ZSM-5	0.1M	Sunlight	5.0	49500 - 67500	4.47
8	0.5g AgA	0.05	Sunlight	5.0	51200 - 92600	5.13
9	0.5g AgA	0.5	Sunlight	5.0	53200 - 94900	5.12
10	0.5g AgA	1.0	Sunlight	5.0	52900 - 94100	5.04
11	0.5g AgA	5.0	Sunlight	5.0	56500 - 96500	5.09
12	1.0 g AgA	0.1	Sunlight	5.0	59700 - 89900	5.23
13	2.0 g AgA	0.1	Sunlight	5.0	62500 - 87800	5.15
14	5.0 g AgA	0.1	Sunlight	5.0	49700 - 92600	5.16
15	0.5g AgA recovered	0.1	Sunlight	5.0	55600 - 97500	2.93

The activity of the silver exchanged zeolites decreases on the reactivation process. The decease in the photocatalytic activity may due the following three reasons. (i) The reduction and reoxidation of silver ions in zeolites are not completely reversible. (ii) During the photochemical oxidation reaction, the reduced silver in the zeolite cavities may come out of the zeolite structure and these silver metal particles may not go back into its previous position during the reoxidation process. (iii) Some of the silver ions may also be leached out into the solution from the zeolite matrix during the reaction.

5.2.3.5. Self-sensitisation Studies

Self-sensitisation means that systems, which are first insensitive to light of a certain wavelength, become photoactive after they have been illuminated with light of higher energy. In the photochemical oxidation of bromide to bromine using aqueous

dispersion of silver exchanged zeolites, the system is not sensitive to visible light, but after the irradiation of UV light the reaction starts, further the reaction proceeds, the more its spectral sensitivity shifts from the initial UV to the visible, then to the red spectral range In order to prove that self-sensitisation occurred during the reaction, four experiments were carried out with different light sources. In one experiment 0.5g of silver zeolite A [$Ag_{12}A$] was dispersed in 100 ml of 0.5M KBr solutions in a round bottom flask. A pH of 3.5 was obtained by adding hydrochloric acid and the reaction mixture was irradiated with 100W tungsten lamp for 6 hours. In another experiment a similar reaction mixture was irradiated with 125W medium pressure mercury vapour lamp in a quartz reactor for 6 hours. In the third experiment a similar reaction mixture was irradiated with a combination of 100W tungsten lamp and 125W medium pressure mercury vapour lamp for 6 hours and in the fourth experiment sunlight was used as the light source instead of 100W tungsten lamp or 125W medium pressure mercury vapour lamp. The formation of bromine was detected only in experiments 18 and 19, where a combination of visible and VU light was irradiated on the reaction mixture.

Table-5.2.4. Photochemical reactions using different light sources

Exp. No.	Catalyst	Conc. of KBr Soln	Light source	Duration in hrs.	Observation
16	0.5g AgA	0.5M	Tungsten lamp	6.0	Br_2 not detected
17	0.5g AgA	0.5M	UV lamp	6.0	Br_2 not detected
18	0.5g AgA	0.5M	Tungsten + UV lamp	6.0	Br_2 detected
19	0.5g AgA	0.5M	Sunlight	6.0	Br_2 detected

The results of experiments 16-19 given in Table-5.2.4 show that the photochemical oxidation of bromide to bromine takes place only in the presence of sunlight or UV-VIS - light combination. This means that the reaction starts only with the irradiation of UV light and the reaction proceeds further with visible light. Solar spectrum contains both UV and visible components in the required amounts and hence solar light is a better source for the photochemical oxidation of bromide to bromine using aqueous dispersion of silver exchanged zeolites.

Upon illumination of silver exchanged zeolites in aqueous dispersions, the silver ions reduced to Ag^0 and oxygen was evolved. This photochemical reaction provides an opportunity for exploring the photochemical conversion of solar energy because water splitting, nitrogen fixation and CO_2 reduction, all involved the oxidation of oxide in water to molecular oxygen. It was observed that the photochemical oxygen production from water with silver zeolites was a self-sensitisation reaction, i.e., further the reaction proceeds, the more its spectral sensitivity shifts from the initial UV to the visible, then to the red spectral range. This phenomenon was attributed to the aggregation of reduced silver atoms, which became new chromophores at longer wavelengths. The greatest difficulty in the use of silver zeolites for water splitting is the generation of protons. These cations are very difficult to remove from the zeolite cation locations and hindered the catalytic reaction.

Below pH = 4, Br_2 was produced when a silver zeolite dispersion in Br^- containing solution was irradiated with sunlight. Cl_2 evolution was reported in a similar way by irradiating with light of wavelength 360nm [25]. Self-sensitisation was observed in both the cases. This photochemical reaction has potential for solar energy conversion and bromine / chlorine production by directly using seawater a natural source. In this reaction, no protons were generated upon silver ion reduction to silver atoms. If the silver atoms can be reversibly oxidised to silver ions completely and which returns to the zeolite cages, silver zeolites may be excellent catalysts for the production of chlorine and bromine from seawater and solar light conversion.

5.2.4. REFERENCES

[1] D. W. Breck, Zeolite Molecular Sieves, Wiley-Inter Science, New York, 1974.

[2] R. M. Barrer, Zeolites and Clay Minerals as Sorbents and Molecular Sieves, Academic Press, London, 1978.

[3] T. Sun and K. Seff, Chemical Reviews, 1994, **94**, 857 – 870.

[4] R. Beer, G. Calzaferri, J. Li and W. Waldck, Coordination Chemistry Reviews, 1991, **111**, 193-200.

[5] A. Corma and H. Garcia, Chem. Commun. 2004, 1443-1459.

[6] H. Yamashita, M. Matsuoka, M. Anpo and M. Che, J. Phys. IV, 1997, **7**, 941–942.

[7] M. Matsuoka, H. Yamashita and M. Anpo, Hyomen, 1995, **33**, 773–81cf. CA 1996:132057.

[8] M. Anpo, Y. Shioya, H. Yamashita, E. Giamello, C. Morterra, M. Che, H. H. Patterson, S. Webber and S. Ouellette, J. Phys. Chem., 1994, **98**, 5744–50.

[9] M. Anpo, T. Nomura, Y. Shioya, M. Che, D. Murphy and E. Giamello, Stud. Surf. Sci. Catal., 1993, **75**, 2155–8.

[10] K. Yoshida and Y. Yamashita, Japanese Pat. No. JP 11028365, 1999.

[11] M. Anpo, S. G. Zhang, M. Matsuoka and H. Yamashita, Catalysis Today, 1997, **39**, 159–168.

[12] K. Mishima, S. Anho and H. Yamashita, Japanese Pat. No. JP 08099020, 1996

[13] S. M. Kanan, M. A. Omary, H. H. Patterson, M. Matsuoka and M. Anpo, J. Phys. Chem. B, 2000, **104**, 3507–3517.

[14] G. Calzaferri, Photochem. Photoelectrochem. Convers. Storage Sol. Energy, Proc. Int. Conf., 9th, 1993, 141–57.

[15] P. A. Jacobs, J. B. Uytterhoeven and H. Bayer, JCS Chem. Comm. 1977, 128-129.

[16] G. Calzaferri, C. Leiggner, S. Glaus, D. Schurch and K. Kuge, Chem. Soc. Rev. 2003, **32**, 29-37.

[17] M. Lanz, D. Schürch and G. Calzaferri, J. Photochem. Photobiol. A: Chem., 1999, **120**, 105–117.

[18] G. Calzaferri, D. Brühwiler, S. Glaus, D. Schürch, A. Currao and C. Leiggener, J. Imaging Sci. Technol., 2001, **45**, 331–339.

[19] S. Sumi, T. Watanabe, A. Fujishima and K. Honda, Bull. Chem. Soc. Jpn., 1980, **53**, 2742–2747.

[20] S. Glaus, G. Calzaferri and R. Hoffmann, Chem. Eur. J., 2002, **8**, 1786–1794.

[21] S. Glaus and G. Calzaferri, J. Phys. Chem. B, 1999, **103**, 5622–5630

[22] D. Schurch, A. Currao, S. Sarkar, G. Hodes and G. Calzaferri, J. Phys. Chem. B., 2002, **106**, 12764-12775.

[23] K. Pfanner, N. Gfeller and G. Calzaferri, J. Photochemistry and Photobioogy A: Chemistry, 1996, **95**, 175-180.

[24] A. Currao, V. R. Reddy and G. Calzaferri, ChemPhysChem, 2004, **5**, 720-724.

[25] G. Calzaferri and W. Spani, J. Photochemistry, 1986, **32**, 151-155.

Chapter-6

Summary, Conclusion and Future Prospects

Zeolites are crystalline aluminosilicates having crystallographically well-defined channels and cavities. The framework structure of zeolites are composed of a three dimensional network of basic structural units consisting SiO_4 and AlO_4 tetrahedrons linked to each other by sharing apical oxygen atoms. The resulting aluminosilicate structure, which is generally highly porous, possesses three-dimensional pores the access to which is through molecular sized windows. Most zeolites contain exchangeable extra framework cations in their channels and cavities, as needed to balance the anionic charge of their frameworks. They may also contain easily replaceable guest molecules such as water or organic molecules.

Separation of oxygen, nitrogen and argon from air is one of the commercially important separation processes. Adsorption processes for the separation of oxygen and nitrogen from air are being increasingly used for commercial purposes for the last three decades. At present, 20% of the world's oxygen demand is met by adsorption based air separation process. However, the maximum attainable purity by adsorption processes is around 95% with separation of 0.934-mole percent argon present in the air being a limiting factor to achieve 100% oxygen purity. Furthermore, the adsorption-based air separation processes are economically not competitive to cryogenic fractionation of air for production levels more than 200-ton oxygen and 50-ton nitrogen per day. Development of adsorbent is central to overcome the limitations of the existing processes. Therefore, focus on the studies of novel adsorbents is given in this thesis.

The first chapter describes the various types of adsorbents used/studied for the adsorptive separation of air components. The adsorbents used for the air separation can be classified into nitrogen selective, nitrogen-argon selective and oxygen selective depending on the gases, which are getting adsorbed. Nitrogen molecule possesses a quadrupole moment (0.31) higher than oxygen molecule (<0.11) and is expected to interact strongly with polar surfaces. This difference in adsorption affinities with polar surface forms the basis for separation of these gases from air wherein nitrogen is retained on the adsorbent surface and oxygen enriched air is recovered as a product. The different zeolites studied for O_2 enrichment by adsorption methods include, NaCaA, NaMgA, NaX, CaX, SrX, CaSrX, LiX, LSLiX, natural and synthetic forms of chabazite, mordenite and clinoptilolite. The potential break through in the adsorbent development was achieved by the investigation of Chao on LSLiX. Chao

found that the nitrogen adsorption capacity significantly increases when the Si/Al ratio decreases to one and a threshold of ~80% lithium exchange for zeolite X and ~70% lithium exchange for LSX must be reached for increase nitrogen adsorption capacity, beyond which the amount of nitrogen increased linearly with lithium content. Later on several studies were reported by incorporating various co-cations on LSLiX. The forces contributing to the total energy of physical adsorption between nitrogen/oxygen/argon molecules on zeolite surface and the factors like zeolite type, Si/Al ratio, number, location and nature of the extra frame work cations, extent of cation exchange, residual water content, extent of dehydration and dehydration conditions, which are strongly influencing the adsorption properties of the zeolites are also discussed. The nitrogen/oxygen ratio in air is approximately 4, much less work needed to separate air by using oxygen selective adsorbent. Oxygen selective adsorbents such as carbon molecular sieves, zeolites, pore size engineered zeolites, titanosilicate molecular sieves, transition metal complexes etc. are reported for nitrogen production from air by pressure swing adsorption. The oxygen adsorption selectivity can be due to the combination of kinetic and steric factors or equilibrium effects. The kinetic diameters of O_2, N_2 and Ar (3.46Å 3.64Å and 3.4Å) are often used to explain the kinetic selectivity of the molecular sieves. Different methods used for the modification of carbon molecular sieves, zeolites and other molecular sieves to increase the oxygen selectivity are also discussed in this chapter. In the case of cerium-exchanged zeolite X, the oxygen selectivity is due to the stronger interaction of the oxygen molecules with the non-stoichimetric cerium oxide formed during the vacuum dehydration process. The metal complexes of d-block elements such as cobalt, manganese, iron, copper, nickel, ruthenium, chromium, molybdenum, etc. are known to reversibly bind with oxygen. These metal complexes bind dioxygen molecules in solution or solid form at or above room temperature. The syntheses of such adsorbents are also done by ship-in-a-bottle concept wherein oxygen selective metal complexes are synthesised inside the cavities/pores of microporous solids like zeolites. Among the oxygen binding metal complexes, lithium cyanocobaltate ($Li_3Co(CN)_5.2DMF$) shows the highest oxygen capacity (55cc g^{-1}) for any solid adsorbent at ambient temperature.

The second chapter deals with the study of adsorption of oxygen, nitrogen and argon in silver exchanged zeolite A. It has been reported for the first time that completely

silver exchanged zeolite A (AgA) interacts strongly with N_2 molecules and possess nitrogen as well as argon adsorption selectivity over oxygen. AgA shows equilibrium adsorption capacity of 22.3cc g^{-1}, 4.36cc g^{-1} and 6.25cc g^{-1} respectively for nitrogen, oxygen and argon at 303.0K and 101.3kPa. In addition to the high nitrogen selectivity, AgA also possesses Ar selectivity over oxygen and is useful to overcome the present oxygen purity limit of 95% by adsorption methods. Zeolite A having varying amount of silver ions were prepared and the adsorption of nitrogen oxygen and argon were studied at ambient temperatures. The N_2 adsorption on these zeolites shows non-linear dependence of adsorption capacity and heat of adsorption on silver content. The nitrogen adsorption capacity and heat of adsorption remains almost unaffected until silver exchange level reaches 70%. On further increasing the silver exchange level from 70% to 80%, both N_2 heat of adsorption and nitrogen adsorption capacity increased sharply from 20.1 to 38.9kJ mol^{-1} and from 8.7 to 18.8cc g^{-1} respectively and then increases linearly with amount of silver. At this stage, the silver ions start to occupy the 4-ring site and 8-ring site in the zeolite A. During the vacuum dehydration at higher temperatures these Ag^+ ions present at the 4-ring site, and at the 8-ring sites undergo reduction and these Ag^+ ions become nearly zero coordinate. These nearly zero co-ordinate non-framework silver ions present in the zeolites interact with the nitrogen molecules through π-complexation using the empty pπ orbital of N_2 molecules and the completely filled dπ orbitals of the silver ions, resulting in very high values for adsorption capacity, heat of adsorption, adsorption selectivity, Langmuir constant and Henry's constant. Heat of adsorption for argon also increases on silver exchange, while that of oxygen remains almost unaffected. The comparatively increased interactions of the argon molecules with the silver exchanged zeolites are due to the electron transfer by overlapping of the Ar (pσ)-Ag (dσ), bonding molecular orbitals.

In the third chapter, the effect of silver ion exchange on the adsorption of nitrogen, oxygen and argon on zeolite X, zeolite Y, zeolite L, mordenite, BEA and ZSM-5 are studied. The adsorption capacity, adsorption selectivity and heat of adsorption were determined from the adsorption data at 288.2K and 303.0K. The N_2 heat of adsorption (32.9 to 42.2kJ mol^{-1}) and N_2/O_2 selectivity (9-24) is very high in the Henry's region. These observations indicate strong interaction of the nitrogen molecules with silver ions present in the zeolite cavities and channels. The higher N_2 heats of adsorption and

N_2/O_2 selectivity observed in all silver exchanged zeolites can be explained in terms of the π-complexation of nitrogen molecules with the co-ordinately unsaturated silver ions present in the zeolite cavities and channels. In the case of the Ag^+-N_2 system, electron transfer can occur by both σ-donation (electron transfer form bonding π_{2p} orbitals of N_2 molecules to 5s orbital of Ag^+ ions) and d-π_{2p}^* back donation (electron transfer from completely occupied 4d orbital of Ag^+ ions to unoccupied π_{2p}^* of N_2 molecule). This π-complexation of nitrogen molecules with silver ions of the zeolites results into stronger interaction between silver exchanged zeolite and nitrogen molecules. The variations observed for N_2 adsorption in terms of the Henry constants, heats of adsorption and N_2 adsorption capacity and selectivity for different silver exchanged zeolites can be explained in terms of difference in number of accessible Ag^+ cations present in these zeolites. Like zeolite A, all other silver exchanged zeolites also show argon selectivity over oxygen.

The fourth chapter describes the post synthesis modification of the zeolites by ion exchanging with various transition metal cations such as cobalt, manganese, nickel, copper, zinc, cadmium etc. and the effect of these cation in the selective adsorption of nitrogen, oxygen and argon on the zeolites. The adsorption isotherms measured are fitted into various equations like Virial, Langmuir and Dubinin-Astakhov. The Henry's constant, Langmuir constant, adsorption capacity, selectivity and heat of adsorption were determined from the adsorption data. Cobalt exchanged zeolite X shows N_2 heat of adsorption in the range 35-40kJ mol^{-1}, O_2 heat of adsorption also increases from 15-23kJ mol^{-1} and the Ar heat of adsorption remains unchanged. Similar trends are observed on manganese and cadmium exchanged zeolites, but the increase in the N_2 heat of adsorption values is comparatively less. Copper exchanged ZSM-5 and mordenite type zeolites shows very high values for Henry's constant, heat of adsorption etc. for N_2 adsorption in the very low-pressure region. This may be due to the reduction of Cu^{2+} to Cu^+ during the vacuum dehydration process. It is evident from the rectilinear shape of the adsorption isotherm, adsorption selectivity, Henry's constant, Langmuir constant and isosteric heat of adsorption values that the nitrogen molecules interact very strongly with cations like cobalt, manganese and copper in some zeolites. In the case of Zn^{2+} exchanged zeolites, the Zn^{2+} ions undergo partial hydrolysis in the zeolite cavities resulting in decrease in the adsorption capacities of these adsorbates. But in the case of copper and nickel-exchanged zeolites of type A

and X, structural degradation was observed during the ion exchange and vacuum dehydration processes resulting in a large decrease in the adsorption capacity.

The fifth chapter described the use of the transition metal ion exchanged zeolites as the catalysts and photocatalysts. The first part deals with the catalytic epoxidation of styrene-to-styrene epoxide using molecular oxygen in presence of Co^{2+} exchanged zeolite X. Styrene epoxidation using molecular oxygen is one of the commercially and scientifically important reactions. Styrene conversion around 99.5% with styrene oxide selectivity of 65% was obtained using NaCoX. The effect of water on the styrene conversion and selectivity was studied using the reaction system using varying concentration of water. Various alkali and alkaline earth cationic promoters were used in the catalyst to increase the styrene conversion and styrene oxide selectivity. A maximum styrene oxide selectivity of 85.2% was obtained with SrCoX and near close results was also obtained with other catalysts like CaCoX and BaCoX. These studies explore the presence of water and alkaline earth metal promoters in the styrene oxidation reactions using molecular oxygen in the presence of cobalt exchanged zeolite X. The second part of the chapter deals with the photocatalytic oxidation of bromide to bromine using aqueous dispersion of silver exchanged zeolites. At a pH below 4, on irradiating an aqueous dispersion of silver exchanged zeolites oxidises the bromide ions in the solution liberates to bromine with sunlight. It was observed that the photochemical oxidation of bromide to bromine with silver zeolites is a self-sensitisation reaction. Self-sensitisation means that systems, which are first insensitive to light of a certain wavelength, become photoactive after they have been illuminated with light of higher energy. This phenomenon was attributed to the aggregation of reduced silver atoms, which will act as new chromophores for absorbing visible light of longer wavelengths.

Future Prospects

- **Novel Approach for Adsorbent Development**

  Present study has established that zeolite encapsulated with co-ordinately unsaturated transition metal ions show very strong adsorption properties due to confinement effects observed in molecular sized cavities. Abnormally high adsorption capacity and selectivity observed for nitrogen and argon observed with silver encapsulated zeolites show that co-ordinately unsaturated metal ion might

have strong interaction with adsorbate molecules, which might be gainfully used for the separation of air components. Through this work a novel adsorbent system with high nitrogen adsorption capacity and selectivity as well a novel potential methodology for modification of microporous solids for developing new adsorbents were developed.

- **High Purity O_2 by Adsorption Process**

  The maximum attainable oxygen purity by adsorption processes is only around 95%, with separation of 0.934-mole percent argon present in the air being a limiting factor to achieve 100% oxygen purity. In the case of alkali and alkaline earth metal ion exchanged zeolites, oxygen shows small selectivity over argon. The silver exchanged zeolites gives a new class of adsorbents having nitrogen as well as argon selectivity over oxygen. Adsorption processes (PSA/VSA/PVSA) using these adsorbents can definitely over come the present oxygen purity limit of 95% by adsorption processes.

- **Argon Adsorption on Silver Exchanged Zeolites**

  The study of argon adsorption on silver exchanged zeolites are scientifically interesting and challenging from the point of understanding the forces responsible for strong interactions of the argon molecules with silver exchanged zeolites. Nitrogen has quadrupole moment whereas argon is an inert molecule. Silver exchanged zeolites show enhanced interactions with both the gases unlike conventional cation exchanged zeolites. Obviously, the forces responsible for interactions of nitrogen and inert gas molecules with silver ions apparently of different nature will offer interesting scientific study.

- **Bacteria Free Oxygen for Medical Applications**

  The adsorption based portable oxygen generator units are largely used for medical applications. The antibacterial properties of Ag zeolites are well explored in the literature. This anti bacterial property of the silver exchanged can be used for the production of bacteria free O_2 for medical purposes.

- **Synthetic N_2 Fixation**

  Synthetic nitrogen fixation is another very interesting topic actively proposes for last several years. The activation of nitrogen is the difficulty in the process.

Transition metal dinitrogen complexes are widely used for this purpose. Similar to these dinitrogen complexes, N_2 π-complexes of transition metal ion exchanged zeolites also gives IR band around 2100cm^{-1}. The high N_2 heat of adsorption also confirms the strong interaction of the N_2 molecules with transition metal ion exchanged zeolites. This N_2 π-complexes in zeolite cavities can also be used for N_2 for fixation more easily, economically and successfully.

- **Oxidation and Epoxidation with Molecular Oxygen**

Oxidation and epoxidation with molecular O_2 are commercially and scientifically very important reactions. The use of Co^{2+} exchanged zeolite X as a catalyst for the styrene epoxidation using molecular oxygen was explored in the present study. Similar catalyst system can be used for a wide verity of commercially important oxidation and epoxidation reactions. The effect of water and co-cations in the conversion and selectivity was also investigated and their strong influence in the conversion and selectivity was established. However, the role of water and co-cations in the reaction is not completely clear. Future investigation in this direction will definitively help in the development of novel catalyst systems having complete selectivity for the desired product.

- **Photochemical Oxidation for Solar Energy Conversion**

Solar energy conversion is an extensively explored active area of research. Water splitting, carbon dioxide reduction and nitrogen are the most desirable processes. Hydrated silver zeolites are light sensitive materials. On irradiating with UV light in the presence of water, silver ions in the zeolite cavities undergo redox reaction and forms charged silver clusters. These silver clusters acts as chronophers and absorbs visible light. This absorbed energy can be used for a wide verity of photochemical reactions. Silver zeolites can be used as a photocatalyst for the bromine/chlorine/H_2 production from seawater by utilising sunlight and will be a promising tool for solar energy conversion in future.

Annexure-I

X-Ray Powder Diffraction Patterns of Various Adsorbents and Catalysts

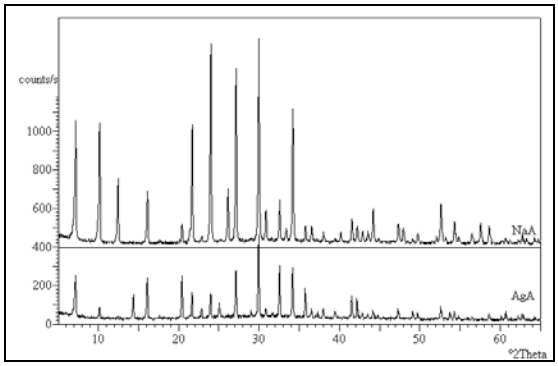

NaA-AgA

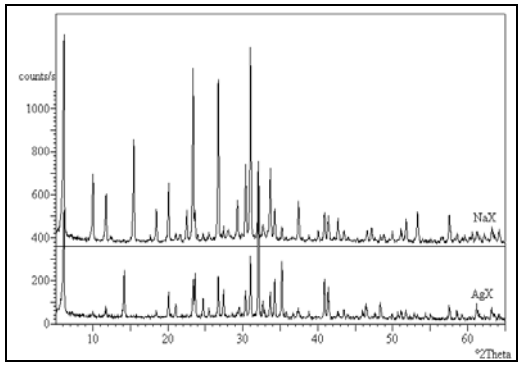

NaX-AgX

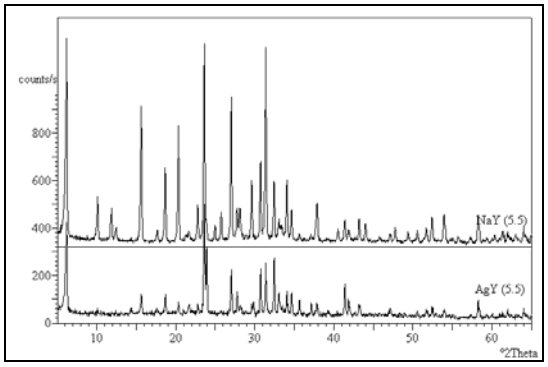

NaY (5.5)-AgY (5.5)

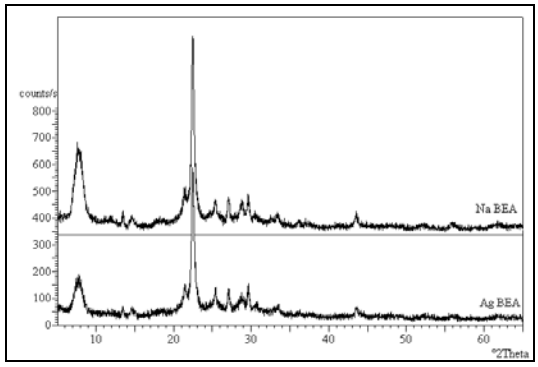

Na BEA-Ag BEA

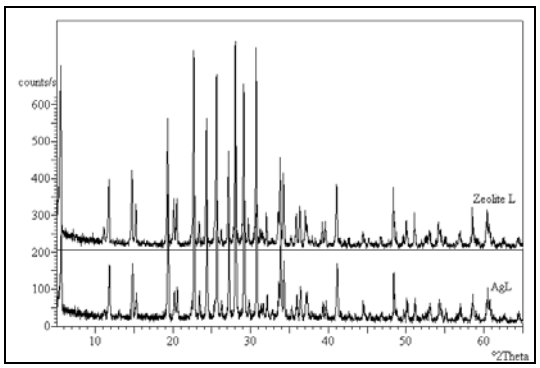

NaL-AgL

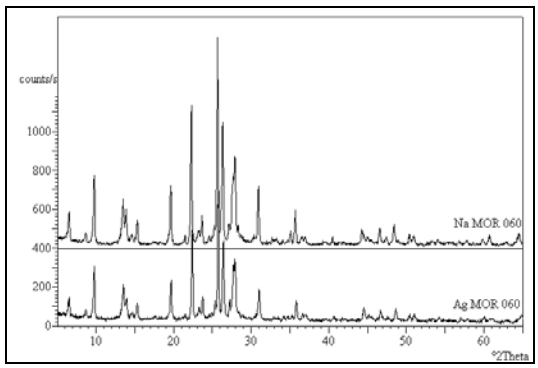

NaMOR060-AgMOR060

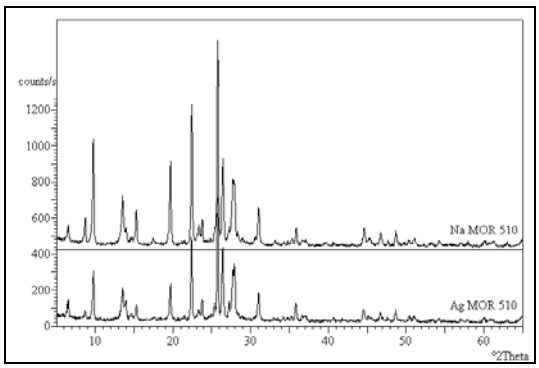

NaMOR510-AgMOR510

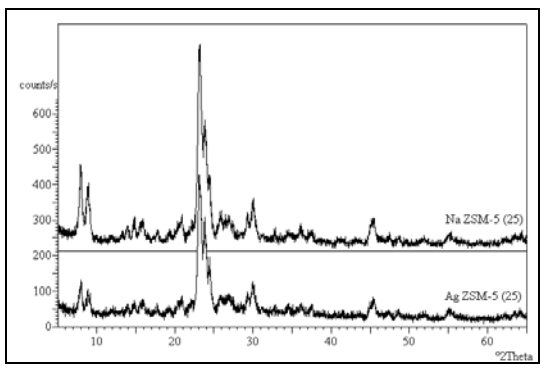

NaZSM-5 (25)-AgZSM-5 (25)

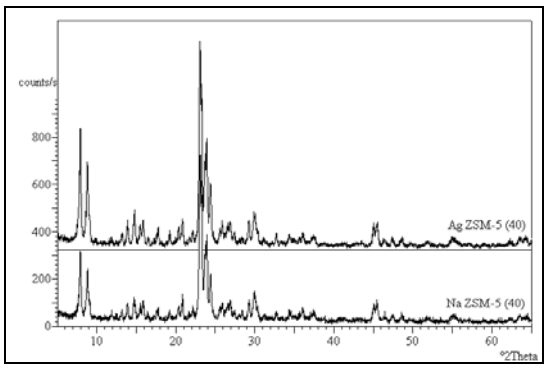

NaZSM-5 (40)-AgZSM-5 (40)

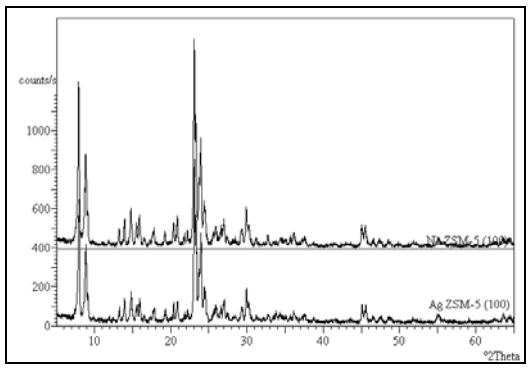

NaZSM-5 (100)-AgZSM-5 (100)

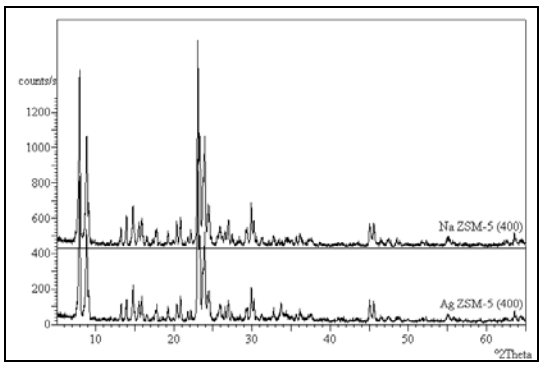

Na ZSM-5 (400)-Ag ZSM-5 (400)

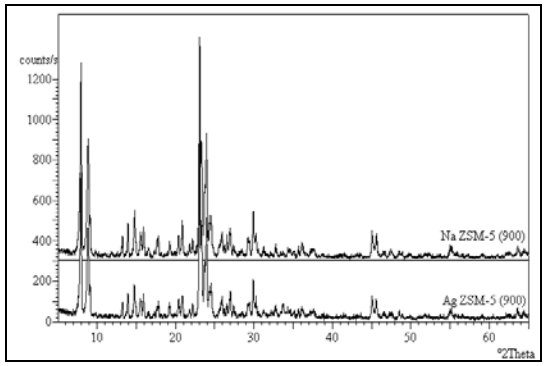

Na ZSM-5 (900)-Ag ZSM-5 (900)

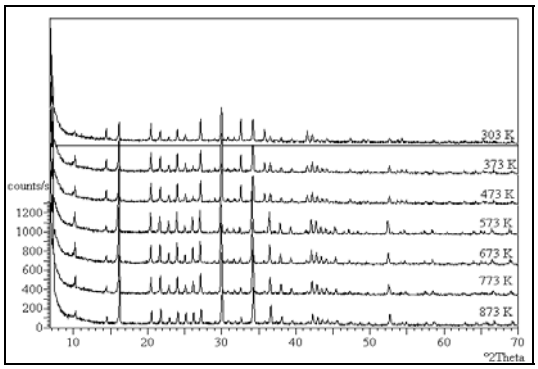

AgA at Various Temperatures

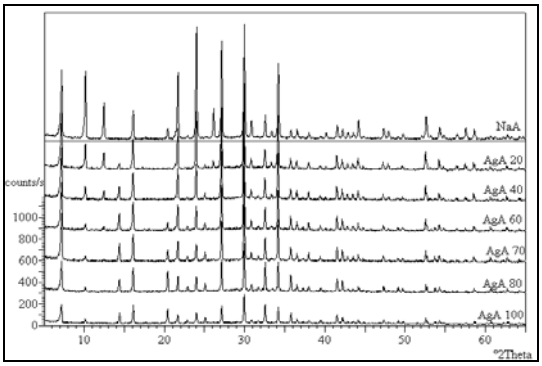

NaAgA with different amounts of silver

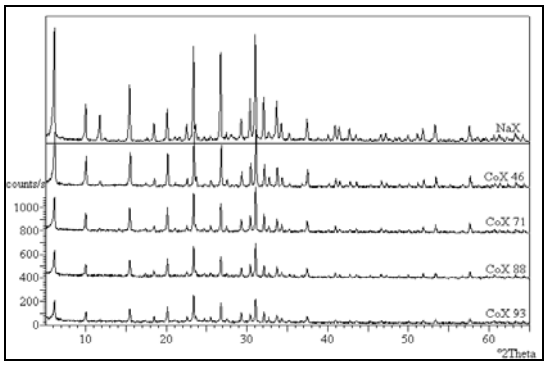

NaCoX

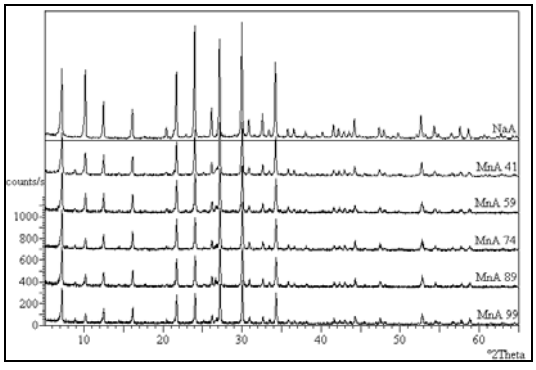

NaMnA

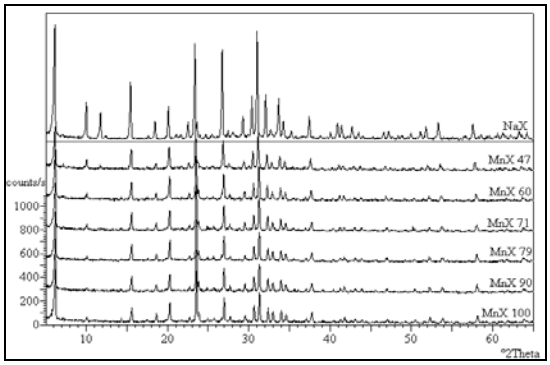

NaMnX

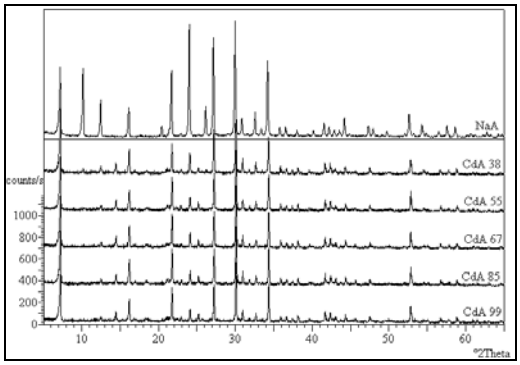

NaCdA

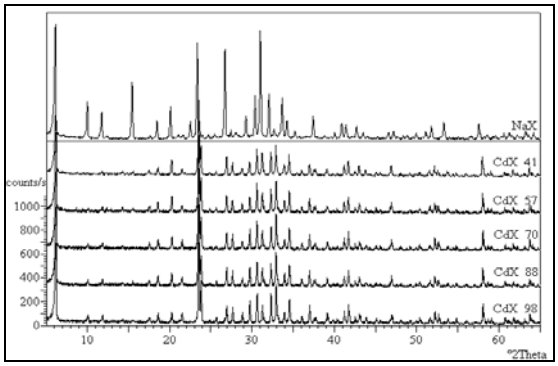

NaCdX

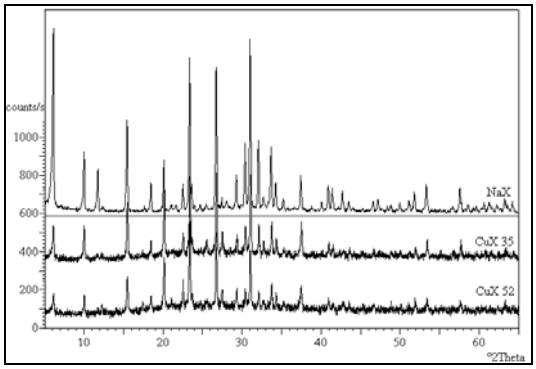

NaCuX

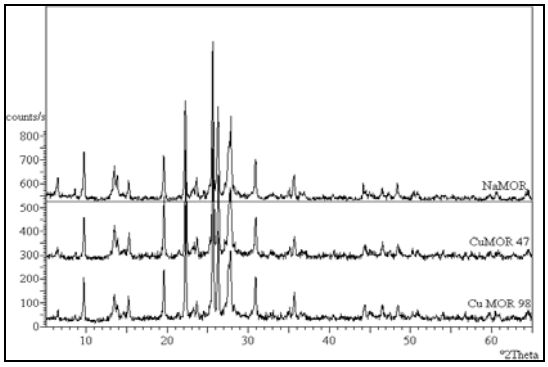

NaCuMOR

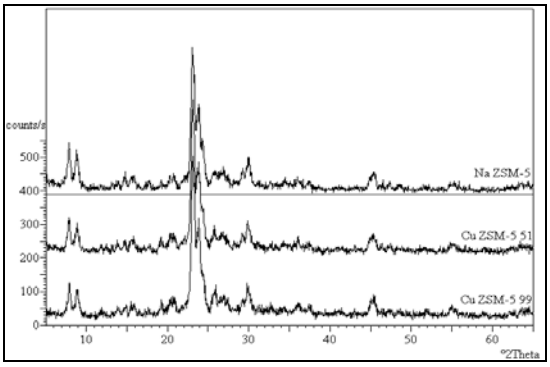

NaCuZSM-5

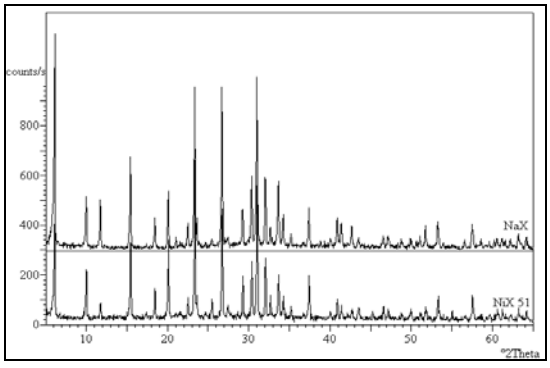

NaNiX

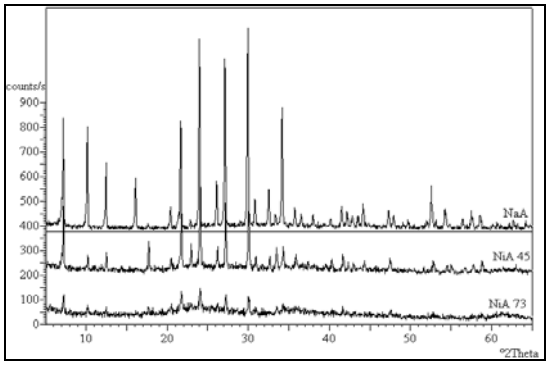

NaNiA

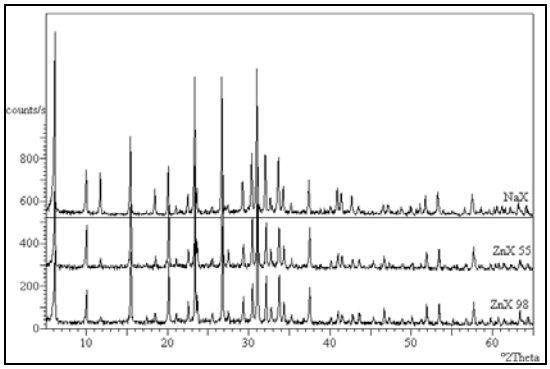

NaZnA

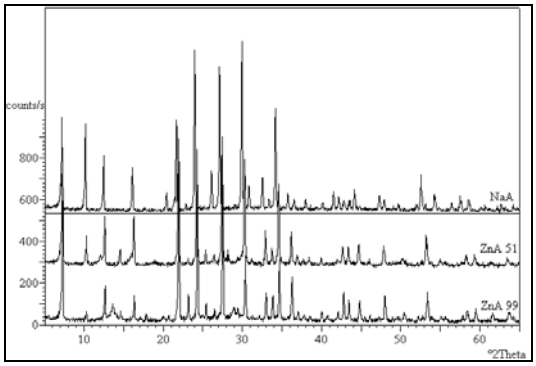

NaZnX

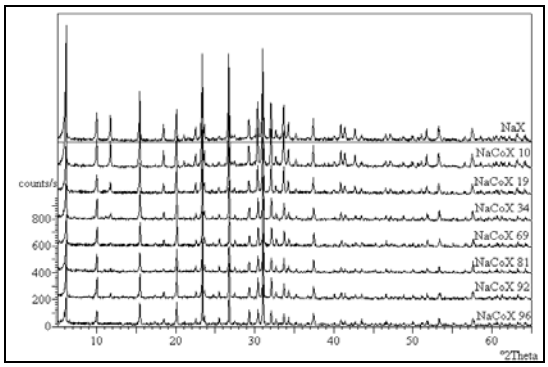

NaCoX

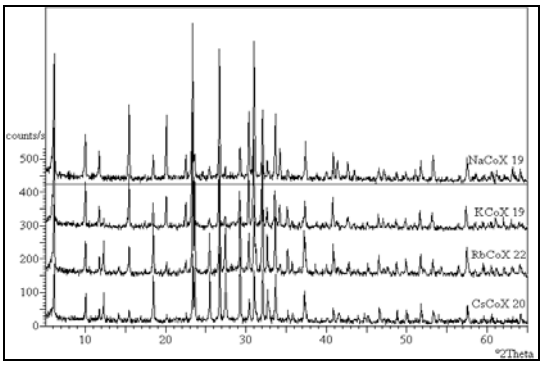

CoX having alkali metal promoters

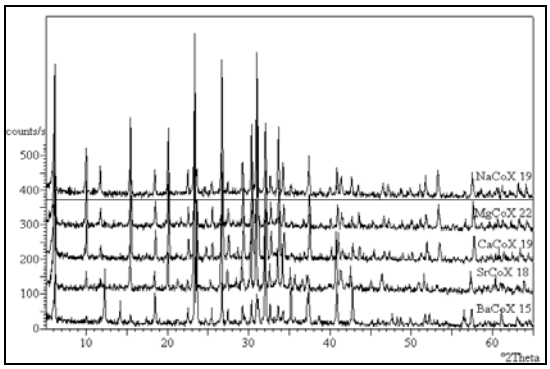

CoX with alkaline earth metal promoters

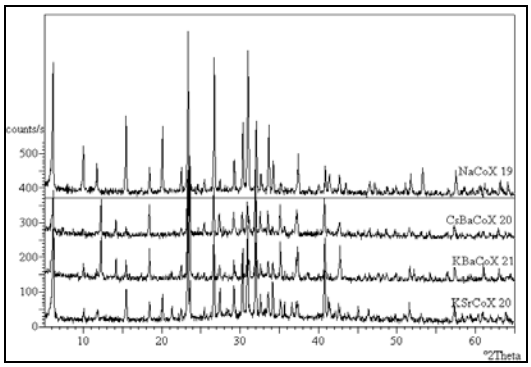

CoX with mixed promoters

Annexure-II

RESUME

JINCE SEBASTIAN

Contact Information

Senior Research Fellow, Silicates and Catalysis Discipline
Central Salt and Marine Chemicals Research Institute
Gijubhai Badheka Marg, Bhavnagar - 364 002, India.
E-mail: jincesebastian@hotmail.com
Tel: +91 93 77 10 4443 (Mobile); +91 278 25 55 808 (R)
Fax: +91 278 25 67 562 / 25 66 970 (O)

EDUCATIONAL QUALIFICATIONS

Degree / Diploma	*Year (s) of Study*	*Class/Division*	***Institute / College / Board / University***
Ph. D. Chemistry	2000 -	Submitting in December 2004	Central Salt and Marine Chemicals research Institute / Bhavnagar University, Bhavnagar-364002, India
M. Sc. Chemistry	1997 - 1999	First (68.6%)	St. Berchmanns' College, Changanacherry / Mahatma Gandhi University, Kottayam, Kerala, (State) India.
B. Sc. Chem. (Main), Phys. and Maths (Sub.)	1994 - 1997	First (82.1%)	Sacred Heart College, Thevara, Kochi / Mahatma Gandhi University, Kottayam, Kerala (State), India.
Pre Degree	1992 - 1994	First (60.0%)	Pavanatma College Murickassery / Mahatma Gandhi University, Kottayam, Kerala (State), India.
S.S.L.C.	1992	First (67.3%)	St. George's High School, Vazhathope North / Board of Public Examinations Government of Kerala, Kerala (State), India

PERSONAL

Name of Father	(Late) P. M. Sebastian
Age and Date of Birth	27 Years, 03 May 1977
Marital Status	Single
Nationality	Indian
Place of Birth	Chelechuvadu, Idukki (Dist.), Kerala (State), India
Permanent Address	S/o (Late) P. M. Sebastian, Porimattathil House, Chelechuvadu P.O., Idukki – 685 602, Kerala (State), India. Tel.: +91 4862 237 554
Hobbies	Farming, Music, Football and Cricket

WORK EXPERIENCE

Period	*Position Held*	*Institution*
June 2003 –Till Date	Senior Research Fellow	Central Salt and Marine Chemicals research Institute Bhavnagar, India
Nov. 2000 – June 2003	Research Fellow	Central Salt and Marine Chemicals research Institute Bhavnagar, India
Oct. 1999 - Nov 2000	Chemist	Ronuk Industries Ltd. Mumbai, India.

AWARDS / ACHIEVEMENTS

1. (Late) Dr. P. S. Mene Best Patent Award, *Central Salt and Marine Chemicals Research Institute*, *Bhavnagar,* 2004.
2. Senior Research Fellowship, *Council of Scientific and Industrial Research (CSIR)*, *New Delhi,* 2003.
3. Prof. Sitaram Iyer Award, for scoring highest marks in II B.Sc. Chemistry in first sitting, *Sacred Heart College, Thevara,* 1996.
4. Rani Memorial Award, for Scoring Highest marks in IXth standard, *St. George's High School, Vazhathope North*, 1991.

LIST OF PUBLICATIONS

1. Catalytic Epoxidation of Styrene with Molecular Oxygen Using Cobalt Exchanged Zeolite X having Alkali and Alkaline Earth Metal Promoters
   Jince Sebastian and Raksh Vir Jasra, *Communicated*
2. Sorption of Nitrogen and Argon in Silver Exchanged Zeolites
   Jince Sebastian and Raksh Vir Jasra, *Physical Chemistry Chemical Physics*, in revision
3. Pore Size Engineering of Zeolite A for the Size/Shape Selective Molecular Separation
   C. D. Chudasama, **Jince Sebastian** and Raksh Vir Jasra, *Industrial Engineering and Chemistry Research*, in press.
4. Adsorption of Nitrogen, Oxygen and Argon in Transition and Rare Earth Ion Exchanged Zeolites A and X
   Raksh Vir Jasra, **Jince Sebastian**, and C. D. Chudasama, *Adsorption Science and Technology, Proceedings of the 3rd Pacific Basin conference*, World Scientific Publications, Singapore, 2003, 334-338.
5. Anomalous Adsorption of Nitrogen and Argon in Silver Exchanged Zeolite A
   Jince Sebastian and Raksh Vir Jasra, *Chemical Communications*, 2003, 267-268.

LIST OF PATENTS GRANTED / FILED

1. Process for the Preparation of a Molecular Sieve Adsorbent for Selectively Adsorbing Nitrogen and Argon from a Gaseous Mixture with Oxygen
   Jince Sebastian and Raksh Vir Jasra, *U. S. Pat. No. 6,572,838, PCT Pat. No. WO 03/080236A1, U. K Pat. No. GB 2386889A, Japanese Pat. No. JP2003275582*, 2003.
2. Process for the Preparation of a Molecular Sieve Adsorbent for the Size / Shape Selective Separation of Air
   Raksh Vir Jasra, C.D. Chudasama and **Jince Sebastian,** *U.S. Pat. Published Application No. 20040192537*, Dated 30 September 2004, *PCT International Application*, March 2003.
3. Process for the Preparation of a Molecular Sieve Adsorbent for the Adsorptive Dehydration of Alcohols
   Raksh Vir Jasra, **Jince Sebastian** and C. D. Chudasama, *U. S. Pat. Application No. 10/726,748*, Dated 2 December 2003, *International Application PCT / IB 03 / 05324*, Dated 24 November 2003.

LIST OF PAPERS PRESENTED

1. Sorption of Nitrogen, Oxygen and Argon on Silver Exchanged Zeolite A
   Jince Sebastian and Raksh Vir Jasra, *First Indo-US Joint Conference '04*, Bombay, India, Dec. 2004. (*Accepted for the presentation)*
2. Anomalous Adsorption of Nitrogen and Argon on Silver Exchanged Zeolites
   Jince Sebastian and Raksh Vir Jasra, *3rd All Gujarat Research Scholars Meet*, M. S. University of Baroda, Baroda, India, Feb. 2003.
3. New Adsorbents for Oxygen, Nitrogen and Argon Separation
   Raksh Vir Jasra, C. D. Chudasama and **Jince Sebastian**, *Korean- Indo Seminar on Adsorption Technology*, KIER, Korea, Nov. 2002.
4. Surface Modification and Pore Size Engineering of Zeolites for Developing O_2, N_2 and Ar Selective Adsorbents.
   Jince Sebastian, C. D. Chudasama, B. Tyagi and Raksh Vir Jasra, *Modern Trends in Inorganic Chemistry MTIC-IX*, I.A.C.S., Kolkata, India, Dec. 2001.